# FLOW AND ACOUSTIC CHARACTERISTICS OF SUPERSONIC JETS WITH CROSS-WIRE

by

SREEJITH.R.B



DEPARTMENT OF AEROSPACE ENGINEERING
INDIAN INSTITUTE OF TECHNOLOGY KANPUR

April, 2000

# FLOW AND ACOUSTIC CHARACTERISTICS
# OF
# SUPERSONIC JETS WITH CROSS-WIRE

*A Thesis Submitted in Partial Fulfillment of the Requirements*
*For the Degree of*

**MASTER OF TECHNOLOGY**

by


**SREEJITH. R.B**



**Department of Aerospace Engineering**
**Indian Institute of Technology Kanpur, India**

**April, 2000**

# CERTIFICATE

It is certified that the work contained in the thesis entitled **"FLOW AND ACOUSTIC CHARACTERISTICS OF SUPERSONIC JETS WITH CROSS-WIRE"** by Sreejith.R.B, has been carried out under my supervision and that this work has not been submitted elsewhere for a degree.

April 25, 2000

Prof. E Rathakrishnan
Department of Aerospace Engineering
Indian Institute of Technology Kanpur

**To**

**My Beloved Parents**

# ACKNOWLEDGMENT

I record my deep sense of gratitude to Prof. E. Rathakrishnan for his exemplary supervision, complete support, unlimited freedom, constant encouragement, immense patience, and benevolence. It was a privilege to be associated with him, which was a rich, memorable and cherishing experience.

I must acknowledge with lot of gratitude, the spontaneous assistance and co-operation extended by Mr. Sharad Chauhan, Mr. Suresh Mishra and Mr. Shishupal Singh of High Speed Aerodynamics Laboratory, Dept. Aerospace Engineering.

I thank Mr. S.S. Chauhan, Incharge, Aerospace workshop for fabricating the models of my work.

Prof. S.A. Khan's infectious cheerfulness was always refreshing and talking to him lightened the drudgery of the work.

Mr. Jayant Vishnu's [M.Tech student] relaxing presence and humour enlivened the lab atmosphere.

My thanks are also due to my friends especially Dr. David Joseph, Tony Thomas, Shibu, Gibu, Gireesh Sreedhar, Sunup Sam Mathew, Roshan, Lalmoni and Marimuthu who helped me in various ways and at various stages.

I want to thank my local guardian, Mr. Gopalakrishnan and family members for literally providing me a home away from home.

The blessing of my parents, the love and encouragement of my brother and the good wishes of other family members especially Mr. Pushparajan have been an invaluable source of inspiration for me.

Sreejith R. B

# CONTENT

# Abstract

This work provides a unique, detailed investigation of aerodynamics and acoustics of supersonic jets from axisymmetric nozzles, with passive control in the form of cross-wire positioned at the nozzle exit. The performance of such passive control is important in missile and launch vehicle engine application for jet mixing enhancement and noise suppression. In contrast to most prior experimental studies on passive control where the control geometry was limited to the boundary layer thickness at the nozzle exit, the present work takes the passive control right upto the nozzle centre. Information on decay, growth and noise suppression characteristics for three supersonic jets are presented. The parameters included in the study are the jet Mach number, level of expansion at nozzle exit and cross-wire diameter. The combination of parameters that produced the best mixing and noise suppression characteristics has been studied in detail. The present results show that the passive control in the form of cross-wire that produces the maximum mixing (fastest jet decay) also exhibits the lowest jet noise. When cases having control and no control were compared, one found that noise suppression achieved with control is significant. The noise suppression dependent on the mixing was apparent at all Mach number of the study. The above observations are justified by noting that the level of underexpansion and the shock strength in the jet core are strong factors in determining the radiated noise.

# Nomenclature

| | |
|---|---|
| ADC | Analog to Digital Converter |
| D | Nozzle exit diameter |
| DAQ | Data Acquisition |
| M | Nozzle exit Mach number |
| NPR | Nozzle Pressure Ratio (Po/Pa) |
| OASPL | Overall Sound Pressure Level in dB |
| P | Centreline pitot pressure |
| Pa | Ambient pressure |
| Po | Stagnation pressure in the settling chamber |
| PRV | Pressure Regulating Valve |
| PSI | Pressure System Inc. |
| X | Co-ordinate perpendicular to nozzle exit plane |
| Y | Co-ordinate parallel to the wire |
| Z | Co-ordinate normal to the wire |

# Chapter 1

## 1.1 Introduction

**Jets** are free shear flows driven by the momentum introduced at the exit of, usually, a nozzle or an orifice. Jet flow plays a central role in research aimed at improving our understanding of the fundamental physics of turbulent shear flows in general. Over the last 20 years there has been a sustained endeavour for proper understanding of free turbulent shear flows; the class of flows to which jets belong. This is owing to the extensive nature of applicability; from household appliances to high-tech rockets. High speed jets find application in numerous engineering fields like, aircraft, rocket and missile exhausts, propulsive systems of aircraft (eg. combustion chambers) and thrust augmenting ejectors.

### 1.1.1 Jet Control

The diverse nature of applicability of jets demand that they be made suitable for their specific applications by controlling them. Control may be defined as the ability to modify the flow characteristics in such a way as to achieve better engineering efficiency, technological ease, economy, adherence to standards etc. Jet controls may be broadly classified into active and passive controls. In active control, an auxiliary power source (like microjets, acoustic excitation) is used to control the jet characteristics. The other method, termed passive control does not require any additional energy for achieving control. Both active and passive control mainly aim at modifying the flow and acoustic characteristics of jets to result in enhanced mixing and reduced noise.

### 1.1.2 Flow Control

Jet flows are an important part of various mixing devices and propulsive systems, wherein enhanced rates of mixing or thrust augmentation is desirable. The jet decay is an important phenomenon. A rapid jet decay implies faster mixing. A typical jet-velocity decay pattern associated with the correctly expanded and "shock dominated" (incorrectly expanded) jets are shown schematically in Fig. 1.1. In combustion chambers with space constraint, the entire mixing

process has to be completed within a short distance. In certain other cases, a jet might be required to entrain more ambient mass. This feature becomes more important for fighter aircraft where faster mixing of hot gases with ambient cold air causes a rapid jet decay, this rapid decay of jet plume makes the detection of jet more difficult for the infrared sensors commonly used in surface-to-air and air-to-air missiles. This helps in increasing the stealth capabilities of fighter aircraft.

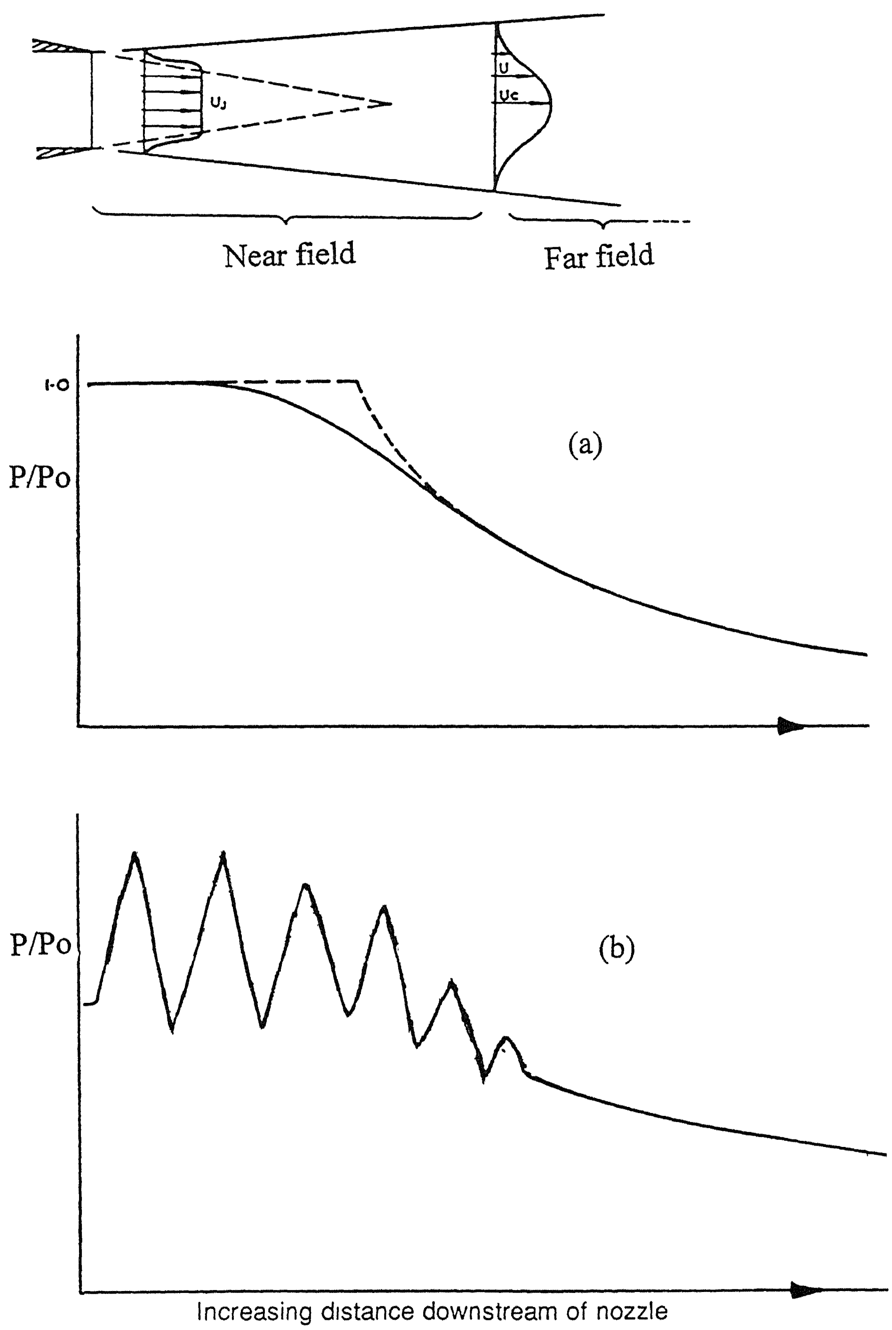


Figure 1.1 Velocity decay rate in correctly expanded (a) and underexpanded (b) shock dominated jets

### 1.1.3 Jet Noise and its Control

The expression "jet noise" has become part of the international language, and is usually taken to mean the noise of jet-powered aircraft. However, strictly speaking, it covers only those sources associated with the mixing process between the exhaust flow of the engine and atmosphere, and those components associated with the shock system in an incorrectly expanded jet of supercritical velocity.

The origins and spectral characteristics of the jet mixing and shock associated noise are illustrated in Fig. 1.2. For jets operating in the subcritical regime (i.e. with an exhaust velocity less than the local speed of the sound), the mixing noise is the only component to be generated. In the case of the supercritical jet, shock-associated noise appears as a superimposed secondary source of a largely broadband nature. However, so-called screech tones have been observed in engine exhaust tests and are often a common feature of experimental work on cold model jets. The mechanisms that generate both screech and broadband shock-associated noise have to do with the expansion shock.

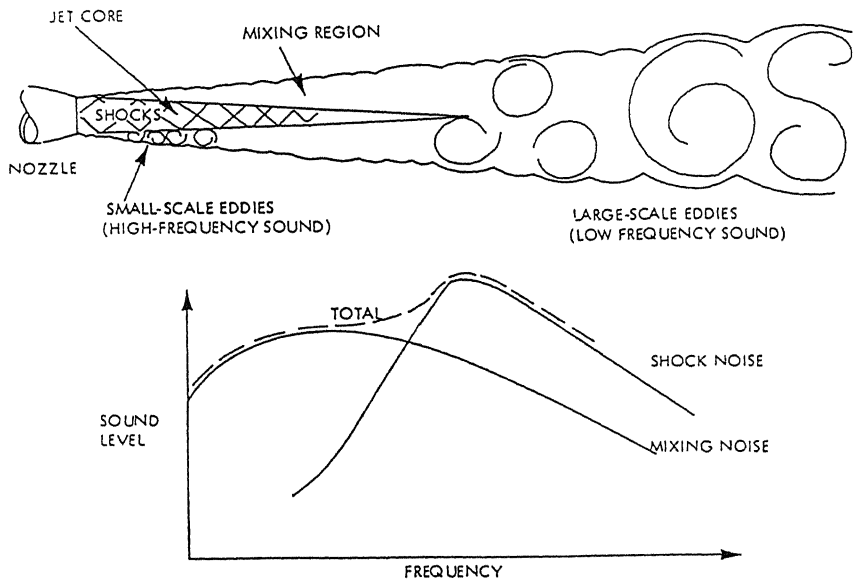


Figure 1.2 Origin of shock and mixing noise components of jet noise spectrum.

The first generation of pure jets and, to a large extent, the low-bypass-ratio engines that succeded them, all had extremely high exhaust velocities which caused high levels of jet noise. The jet velocity could not be reduced, since it was controlled by the thrust requirement via the available total airflow, and jet noise had to be reduced by other approaches. These took the form of mechanical devices aimed at modifying the aerodynamic structure of the mixing process and controlling the energy dissipated as noise.

## 1.2 Passive Control of Jets

Among the two main types of jet control, passive controls are mostly desired not only because no external power source is required, but since in some cases the engineer is left with no other option. Passive control methods use geometrical modifications which alter the flow structure. Some commonly used passive control methods are shown in Fig. 1.3. These methods mostly aim at disturbing the boundary layer at nozzle exit to achieve the desired flow behavior. Particularly, the grooves or tabs at the jet exit trip the boundary layer developing inside the nozzle. This drastically influences the shear layer growth, and the flow behavior, thus providing lot of scope for passive control.

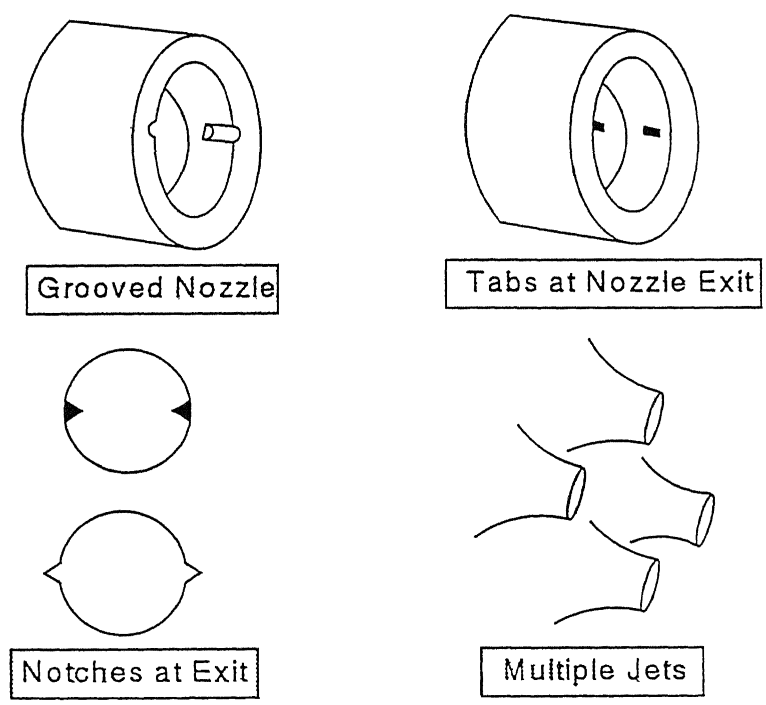


Figure 1.3 Some commonly used passive control methods for jets.

## 1.3 Aim of the Present Investigation

The present investigation is primarily aimed at evaluating the efficacy of cross-wire as a passive control technique employed to modify the mixing and acoustic characteristics of correctly and incorrectly expanded supersonic jets. The effect of cross-wire diameter on jet decay characteristics also investigated. Actual acoustic level studies were carried out.

# Chapter 2

## Review of Literature

In this chapter, free jets are described; the mechanism underlying their behavior, and their consequences are discussed. The descriptions of subsonic and incorrectly expanded jets are done separately for clarity.

## 2.1 Free Jets

Free jet can be defined as a pressure driven unrestricted flow of a fluid into a quiescent ambience. Since a fluid boundary cannot sustain a pressure difference across it, the jet boundary is a free shear layer in which static pressure is constant throughout. The boundary layer at the exit of a nozzle develops as a free shear layer, mixing with the ambient fluid thereby entraining the ambient fluid into the jet stream. Thus, the mass flow at any cross section of the jet progressively increases along the downstream direction. Hence, to conserve momentum the centreline velocity decreases with downstream distance. Many textbooks [1-3] have been dedicated to jet flows, fully, or in part, starting from the monograph of Abramovich in 1936. The ultimate aim of the jet researchers has been the achievement of mixing enhancement and noise suppression.

## 2.2 Subsonic Jets

The structure of a free jet and zones into which the flow regimes may be classified are given in Fig.2.1 [4] The flow velocity resembles that of a top-hat at the exit (assuming boundary layer at the exit is thin enough) and the exit velocity is preserved upto some axial distance. When the fluid at the periphery of the jet comes in contact with the ambient fluid, the shear due to their difference in velocity causes the peripheral layer (shear layer) to roll up into a vortical structure which, during the process of roll up, scoops ambient mass into itself. This phenomenon causes mass addition into the jet with axial distance and is called entrainment. The exit velocity is preserved within a region

close to the nozzle exit. This region is known as the potential core in a correctly expanded jet (subsonic jets are always correctly expanded). In the core region, the annulus surrounding the core witnesses vigorous mixing and large scale vortex action. The velocity profile thus gradually becomes smoother with jet propagation. The region downstream of the core is the transition region, characterized by mixing of the stream with the entrained ambient mass. The large structures of the upstream region break down into the smaller structures in the process of transit and thus promote small scale mixing. A self-similar behaviour is achieved further downstream, namely the fully developed region.

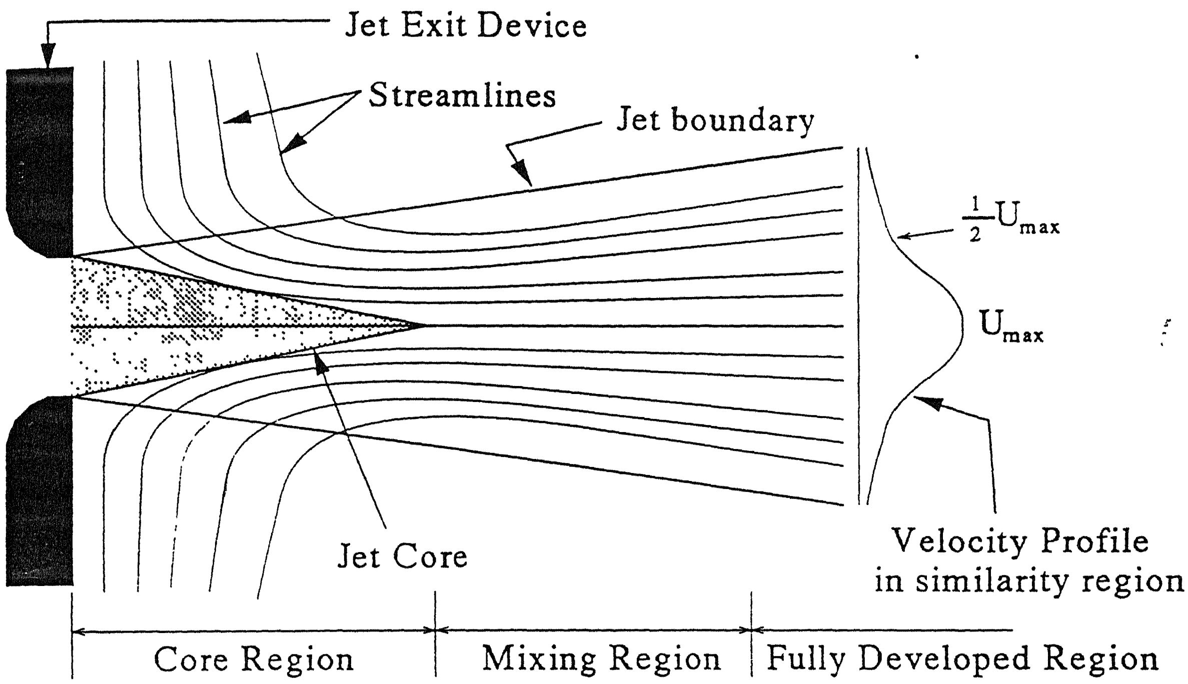


Figure 2.1. Schematic of a subsonic jet flow and zones within.

### 2.2.1 Evolution of Vortical Structures

The boundary layer leaving the nozzle/slot rolls up into a vortical structure which has the shape directed by the nozzle/slot geometry. These vortical structures are basically unstable. This is because, the advection velocity of a local segment of a curved vortex filament is along its binormal (i.e. normal to the plane of the segment, and is proportional to its curvature) [5]. Thus, in a non-circular vortex ring, e.g. elliptic vortex ring, the

segment with larger curvature moves faster than a segment with a smaller curvature. Thus, non-circular vortical structures do not remain in a plane, and also, continuously deform, which results in a change in the cross-sectional shape as they move downstream. For example in elliptic or rectangular jets, the major diameter becomes minor diameter and vice-versa as the jet expands. This is the well known phenomenon of *axis switching*.

## 2.3 Mixing Enhancement by Non-Circular Jets

Improving the mixing helps in achieving thrust augmentation, heat transfer promotion, augmentation of combustion efficiency, etc. While coherent structures are beneficial in enhancing large scale mixing, they prevent fine scale (molecular) mixing, particularly during the initial vortex development process [6]. Among the several passive control techniques used, non-circular geometries were recognized to be very effective in producing both small and large scale mixing. Results have showed that the presence of sharp corners in these geometries significantly increases the small-scale turbulence intensity at the corners relative to the flat segments of the nozzle. It was also pointed out that while coherent structures can be generated at the flat sides only small scale turbulent flow emanated from the corners [7,8,9]. This small-scale turbulence was found to be generated by axial or streamwise vortices in the corners inside the nozzle, and augmented by strong vortex bending by the highly curved flow at the corners. The vortex bending and the self-induction process also increases the spreading rate of the jet at the flat sides.

## 2.4 Incorrectly Expanded Jets

If the jet pressure ratio is increased beyond the critical (i.e. that at which a sonic exit velocity is first attained) a marked change takes place in the flow and also in the nature of the sound it produces. The flow is then 'choked', this condition causes a difference in the static pressure of the jet flow at the nozzle exit and the ambient pressure of the surroundings. This mismatch of pressure triggers the pressure equalizing mechanisms containing shocks and expansion fans. When the pressure at the nozzle exit is more than the ambient pressure, the flow is potentially capable of further expansion. In other words, the flow is said to be underexpanded. This leads to the formation of expansion fans at the nozzle lip, which get reflected as weak compression waves, and coalesce to form oblique

shocks. The intercepting shock (barrel shock) is an oblique shock behind which the flow is still supersonic but at a lower Mach number than the flow in the core of the jet. When the degree of underexpansion is high, the oblique shocks are terminated with a normal shock, popularly known as the Mach disc. The schematic of the underexpanded shock system is given in Fig. 2.2. Thus, until the pressure equilibrium is attained, the shocks and expansion fans bounce back and forth in the plume, giving rise to the shock cell pattern.

Powell [10,11] was the first to study the underexpanded jet noise. Powel found that the shock-associated noise is related to acoustic feedback loops. According to Powel [10], as the disturbances created at the nozzle lip passed through the third or fourth shock-cell, strong interaction takes place with the oblique shocks resulting in the emission of intense acoustic waves. Glass [12] suggested that disturbing the shock-cell structure or making it weaker might reduce the effect of acoustic feedback. He also found that the rate of spread could be increased by nearly 50% by this acoustic feedback. Krothapalli et al. [13] experimentally investigated the role of screech tones in the mixing of an underexpanded jet issuing from a rectangular nozzle of moderate aspect ratio. They concluded that the self-excitation of the jet results in higher spread rate. Rice and Raman [14] experimentally studied the influence of nozzle exit geometry on jet mixing and noise production for a series of beveled rectangular nozzles operating at supersonic jet velocities. They observed that the beveled geometries provided screech noise reduction for underexpanded jets.

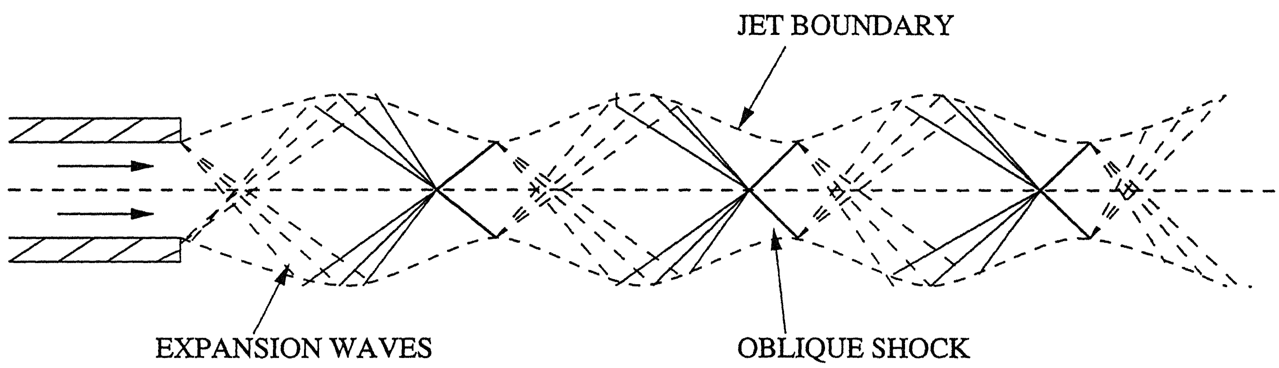


Figure 2.2 Structure of the underexpanded jet.

When the jet exit pressure is less than the ambient pressure the jet is said to be overexpanded. The flow tries to attain the ambient pressure; this takes place across an oblique shock attached to the nozzle exit outside the duct, as shown in the Fig. 2.3[15]. These days overexpanded jets has assumed greater importance as more and more launch vehicles are using overexpanded jet for their mission. India's very own GSLV is going to use overexpanded jets.

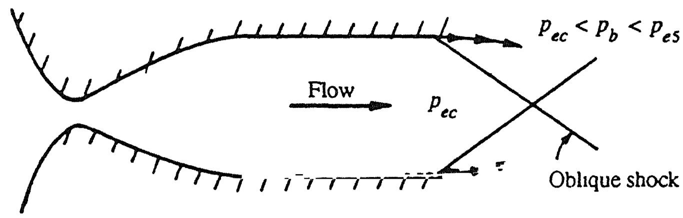


Figure 2.3. Oblique shock at the exit of an overexpanded jet.

## 2.5 Jet Noise

Noise is an inevitable consequence of jets, and in general all turbulent flows. Whenever there is relative motion between fluids, or between a fluid and a solid, noise is generated. Noise in jets depend on the speed of the jet, temperature, turbulence levels, shear layer dynamics, observer angle, etc. Hence, it will be convenient to discuss jet noise after classifying it. Jet noise can be classified into the following major types (Fig. 2.4):

- Turbulent mixing noise
- Broadband shock-associated noise
- Screech tones

The amount of importance associated with jet noise control can be felt by looking at the vast quantum of knowledge available on jet noise. Lighthill [16] and Ffowcs Williams [17] and Crighton [18] reviewed the theories on subsonic jet noise. The first review of supersonic jet noise was done by Tam [19]. In his inspiring review, Tam discusses the noise sources in supersonic jets and methods and models developed for predicting them.

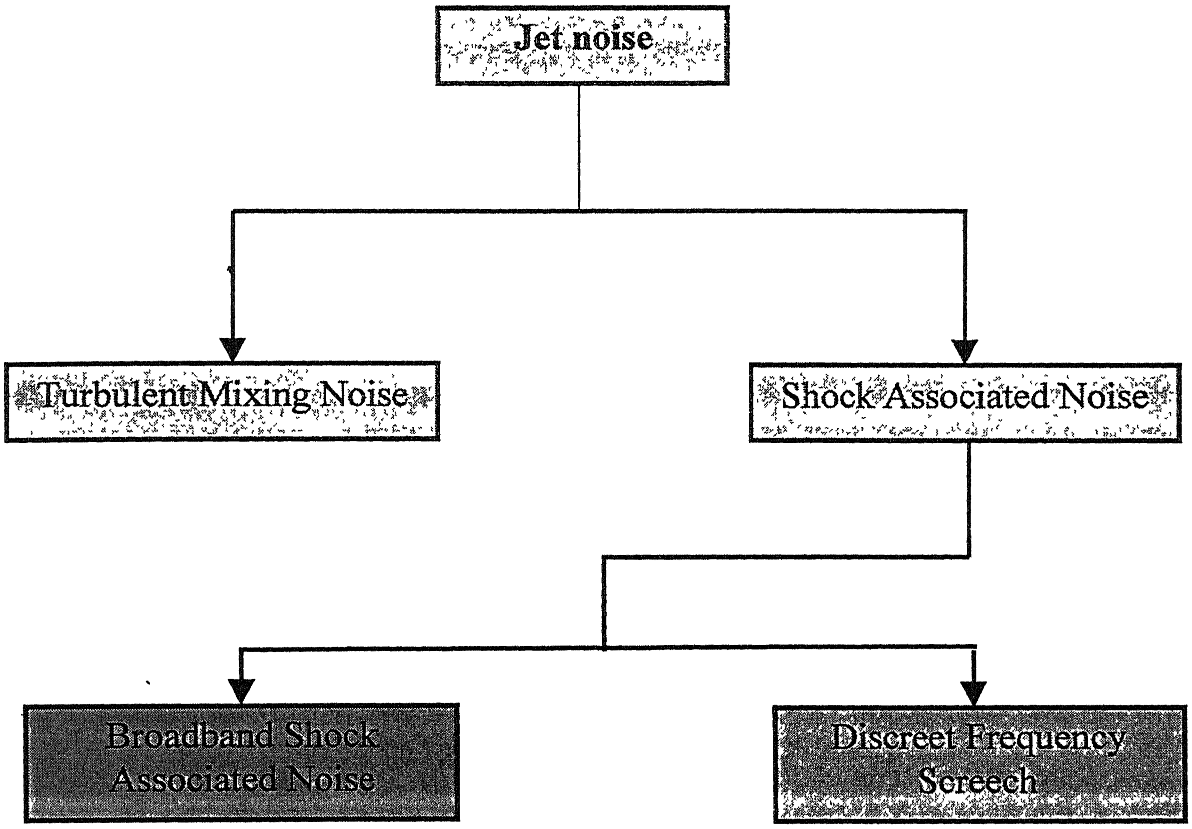


Figure 2.4. Taxonomy of Jet Noise.

### 2.5.1 Turbulent Mixing Noise

As mentioned earlier, the large-scale structures grow in size as they move forward, thus setting up intense activity in the circumferential region of the jet. Thus, the kinetic energy of the main flow is continuously extracted by the large structures and converted into "turbulence energy". It is these turbulent shear stresses of the fluctuating velocities, which were shown to be the source of sound by Lighthill [20] in his celebrated acoustic analogy. Since the noise is produced due to the exchange of momentum of the jet and the ambient fluid (i.e., mixing) by turbulent action, it is termed as turbulent mixing noise. Lighthill's order of magnitude analysis revealed that the total acoustic power emitted from a jet is proportional to the eighth power of the jet Mach number. Strictly, this is valid only at low Mach numbers. At high Mach numbers, the acoustic power emitted varies cubically as the Mach number [21].

Now, it is generally accepted that turbulent flows contain both fine-grained and large-scale turbulent structures. Both structures are capable of generating noise. The quantum and quality of the noise they produce largely depend on the jet Mach number and temperature. The convection Mach number plays an important role, being the relevant parameter. In subsonic jets, it is subsonic unless the jet is very hot. Hence, the large-scale structures convect slowly, and thus are ineffective noise generators. The dominant part of the subsonic noise is produced by the fine-scale or small-scale turbulence. Turbulent mixing noise of supersonic jets [19,22] are directive at 45 to 60 degrees measured from upstream jet axis. Noise measured here is dominated by a single broadband peak. The noise sources are two-fold: the background noise generated by the fine-scale turbulence and the dominant part of the noise generated by the large-scale turbulent structures. Overall noise radiation from jet increases with temperature. Tam and Chen [23] proposed a stochastic wave model theory for the turbulent mixing noise from supersonic jets. Apart from these studies, excitation studies have contributed to the understanding of the noise generating turbulent structures.

### 2.5.2 Shock-Associated Noise

Jet noise receives additional component in the form of shock-associated noise, when the jet plume contains shocks. The noise component with discrete frequencies is commonly called as the *screech tone*, and the other component is broadband, usually termed as the broadband shock-associated noise. The presence of these two shock components makes the supersonic jet rich in spectral and directional characteristics. In supersonic jets, and high temperature jets, the large turbulence structures propagate downstream at supersonic Mach numbers relative to the velocity of sound propagating in the upstream direction. As a result, they are capable of producing intense Mach wave radiation. Hence, large structures, or instability waves are the dominant sources in supersonic jet noise [24]. Tanna [25] obtained high quality data of broadband shock-associated noise over a wide range of parameters. Tam and Tanna [26] investigated theoretically and experimentally the broadband shock-associated noise. They proposed that the broadband shock noise is generated by the weak interaction between the downstream propagating large-scale structures and the quasi-periodic shock-cell structure of the jet. By using simple

analytical models to represent the large-scale structures and the shock-cell they derived a noise intensity scaling formula. The relationship between the instability waves and noise of supersonic jets was examined by Tam et al. [27]. Their analysis revealed that the highest sound pressure level of the far-field noise occurs at a direction and frequency that closely match the Mach wave radiation direction and the frequency of the most amplified instability wave of the jet.

### 2.5.3 Screech

The jet screech noise is a result of the large-scale coherent structures in the jet shear layer interacting with the shock cells, generating fluctuating pressures that propagate upstream. As they travel upstream, they couple with the shear layer causing amplification of the coherent structure in the shear layer and resulting in a feedback process. When the phase relationship between the downstream traveling coherent structures in the shear layer and the upstream traveling pressure waves is matched, high amplitude tones of discrete frequency are generated. These are called screech tones. When a jet emits strong screech tones, the jet flow undergoes strong oscillations. Observation reveals that two types of jet motion can occur: toroidal mode oscillations and helical/flapping mode oscillations. The superposition of an equal amount of left and right helical mode oscillations creates a flapping mode [19]. At certain Mach number the jet emits more than one screech tone. At low Mach numbers, the screech tones are associated with the toroidal mode. As Mach number increases, there is a switch over to the flapping/helical mode. The intensity of screech tones decreases with increase in temperature. Screech intensity depends on the nozzle lip thickness.

Tam *et al.* [28] examined the relationship between the broadband shock-associated noise and screech tones. Based on their analysis they concluded that the screech tone frequency is dictated by the weakest link of the feedback loop. It is the weakest link that relates the spectral characteristics of screech tone to those of broadband shock-associated noise. Tam *et al.* [29] thoroughly investigated the screech tones from bevelled rectangular nozzles. Their results further strengthen the wave-guide mode concept of the shock-cell structure and the weakest link feedback theory of jet screech.

## 2.6 Jets from Nozzles with Tabs

A tab is a small protrusion into the flow which produces a counter-rotating streamwise vortex pair that can affect the jet flow development significantly. The streamwise vortices usually have a long life and, once introduced in the flow, tend to persist over tens of nozzle exit diameters downstream. This is in contrast to azimuthal vortical structures that are more energetic but have a shorter life span. The generation mechanism of the streamwise vortex pairs by the tabs and their effect on the entrainment and spreading of free jets have been discussed in [30]

In a continuing effort to increase mixing in free shear flows, vortex generators in the form of tabs have been investigated by several researchers in recent years. Bradbury and Khadam [31] were the first to study in detail the effect of tabs on axisymmetric jet flows. They found that the tabs or small protrusion in the jet flow at the nozzle exit can significantly increase the jet spread. They reported reduction in jet core length from 6D to 3D, where D is the nozzle exit diameter. Zaman et. al. [32] and Ahuja et. al. [33] carried out a systematic study of jet mixing enhancement with tabs and found that the tabs can increase the jet mixing not only at low speed condition but enhance the mixing at high speed and high temperature conditions also. Ahuja [33] studied a round jet flow at Mach number 1.12 and total temperature 684 K. He found that the potential core length of the jet can be reduced from 6D to less than 2D by using two diametrically opposite tabs. He also concluded that, the tabs can reduce low-frequency noise up to 5 to 6 dB. Most of the investigators have focused their attention on the application of tabs to the overall mixing enhancement performance of tabs and jet noise reduction. However, it was in 1993 that, Zaman et. al. [32] carried out an extensive flow visualization study using laser sheet and cigar smoke illumination and pressure measurements to understand the physics of vortex generation by tabs. They conjectured that the jet distortion introduced by a tab is due to the generation of streamwise vortices. They postulated the generation of these vortices to the presence of two types of sources, the details of which can be found in their paper [32]. In the study of the effect of tab on turbulent boundary layer, Coretta et al [34] also found that a tab generates a pair of counter rotating streamwise vortices which stimulate a strong ejection of boundary layer flow into the high speed flow, thereby resulting in a very rapid cross-stream mixing and a significantly thickened turbulent boundary layer.

From the above discussions, it is evident that tabs are identified as a passive mechanism with potential to enhance jet mixing and attenuate jet noise. As we know, a jet is a continuous flow of fluid issuing from a nozzle (or orifice) into a medium of lower speed fluid (or medium at rest). As the jet fluid travels further away from its origin, it slows down due to the mixing with the ambient fluid. The interaction between the jet and the ambient fluid forms the mixing layer or the shear layer. As the primary structures or ring vortices roll-up and move downstream they grow in size due to the entrainment of ambient fluid. The resulting jet decay is proportional to the velocity gradient across the shear layer and is a strong function of the distance downstream of the jet exit. Liepmann and Gharib [35] have shown that streamwise vorticity drastically alters the mass entrainment of a jet, and efficiency of this vorticity in entraining fluid increases relative to that of azimuthal vorticity as the jet evolves downstream. From jet noise point of view, alteration of the coherent structures of the jet can produce a significant reduction in far-field noise or can change the directivity or spectral characteristics of the noise field.

Amongst the factors studied, jet nozzle boundary layer thickness, jet nozzle turbulence level and nozzle convergence were the least significant in the jet development. It was found that the insertion of rectangular tabs into the jet in the nozzle exit perimeter, produced large changes in the jet development as indicated by the faster decay of centreline mean velocity. The effect is more pronounced in a jet with only two tabs than it is in one with four or six or eight tabs.

It has been observed that there is significant reduction in overall sound pressure levels in the case of underexpanded flows due to faster jet decay. The reduction of core length finds useful applications in the aerodynamics of VTOL aircrafts. Recent study by Navin Kumar Singh and Rathakrishnan [36] have shown that the argument that the projection of tabs beyond the boundary layer thickness is ineffective, presented by Zaman at al [37], is not true and the tabs can extend upto the radius in the case of circular nozzle. Therefore, in the present study, instead of tabs, a cross-wire (wire running across a diameter) has been used as a passive control to enhance the jet mixing and core length reduction.

# Chapter 3

## Experimental Setup and Procedure

This chapter gives an overview of the test facility, describes the experimental arrangements, the measurement carried out and the various tools developed for the same. The uncertainty in the measurement is mentioned for all the measurements carried out. This chapter also briefly discusses the anechoic chamber in which noise measurements were carried out and calibration of the instruments used for the measurements.

## 3.1 The Test Facility

The experiments were conducted in the jet test facility at the High Speed Aerodynamics Laboratory, Indian Institute of Technology, Kanpur, India. The layout of the laboratory is shown in figure 3.1. The test facility consists of (1) compressor, (2) storage tanks and (3) jet test facility.

A two-stage reciprocating compressor, capable of delivering 360 cfm of air at a pressure of 500 psig is being used in this laboratory. The compressor is driven by a 150 hp 3-Ph induction motor. A cooling water circuit, driven by an independent pump, cools the compressed air through an inter-cooler. The compressed air is then passed through a pre-filter consisting of porous stone candles; to remove solid contaminates like rust particles and oil droplets. An activated carbon filter is further used for finer filtering. The compressed air is dried in a dual-tower semi-automatic silica gel dryer. While one tower is in use, a portion of the dried air is heated and used to reactivate the other. A diaphragm type back pressure valve operated by pressure relief pilot, permits the dryer to operate at 500 psig, while the pressure in the storage tanks builds up from atmospheric to storage pressure. The compressed is stored in three tanks, having a total capacity of 3000 $ft^3$ at 300 psig.

The air enters the settling chamber through a tunnel section with a gate valve followed by a pressure regulating valve (PRV), a mixing length of 3 inch diameter.

The settling chamber is connected to the mixing length by a wide-angle diffuser. The flow is further conditioned inside the settling chamber by closely meshed grids meant for minimizing turbulence. The settling chamber is a constant area circular section of 300 mm inner diameter and 600 mm length. The test model is fixed at the end of the settling chamber with O-ring sealing to avoid leakage. A photograph of the test facility along with the traversing system and instruments is shown in Figure 3.2.

## 3.2 Experimental Models and Measurement Procedure

The experimental models tested in the present investigation are shown in figure.3.3. Convergent-divergent (CD) nozzles made of brass were used for the present study. For Mach number 1.79, the nozzle exit diameter was 12 mm. The cross-wire used were made of copper of 0.8 mm diameter. The geometric blockage due to cross-wire is defined as the ratio of projected area of cross-wire intruding the flow to the nozzle exit area. For cross-wire with diameter 0.8 mm, blockage area ratio is (12 x 0.8)/(3.14 x 6 x 6)= 0.084 or 8.4 %. For Mach numbers 1.6 and 2.0, the nozzle exit diameters were 11.18 mm and 13.0 mm, respectively. The same wire diameter was used for this cases also. The corresponding blockages were 9.1 % and 7.89 % for Mach number 1.6 and 2.0, respectively.

The flow measurements include pitot pressure survey along the (geometric) centreline of the jet for the Mach numbers (1.6, 1.8 and 2.0), at correct and incorrectly expanded flow conditions. For the spread and entrainment analysis, pitot pressure was measured at points on rectangular grids in the X-Y, X-Z and Y-Z planes. A typical grid consisted of 100 to 350 points depending on the axial location. For example, the jet width is small at the exit plane, and hence, lesser number of points are sufficient to obtain the cross-sectional structure. As the jet grows in size along the axial direction, the number of points required to get the cross-sectional structure would be more. In circular and tabbed/grooved jet the symmetry about the axis was used, and hence measurements were made only on one half of the plane. These data also yielded the cross-sectional iso-baric contours.

The pitot pressure probe is mounted on a three-dimensional traverse (see Fig.3.2), for the pitot pressure surveys conducted over the entire flow field. The traverse has six degrees of freedom, which also includes a probe-yawing mechanism. The traverse has a spatial resolution of 0.1 mm. in all the three dimensions. The pitot

probe used, had an inner diameter of 0.4 mm. and outer diameter of 0.6 mm. Pitot pressure measurements prove to be important in high speed supersonic jets, where the flow regime is shock dominated. As mentioned by Rice and Raman [14], supersonic flows pose considerable measurement problems in using hot-wire or hot-film anemometry. To avoid these difficulties one can measure the raw total pressure, i.e., the total pressure downstream of the bow shock standing ahead of the pitot tube in supersonic flow.

### 3.3.1 Instrumentation for Pressure Measurements

The pitot pressure sensed by the probe was measured using a PSI model 9010 16-channel pressure transducer (interfaced with a PC386). The model 9010 transducer is capable of measuring pressures up to 300 psig, which is approximately 20 atm. The software provided by the manufacturer was used to interface the transducer with a computer. The user-friendly menu-driven software acquires data, and shows the pressure readings from all the 16 channels simultaneously in a window type display on the computer screen. The software can be used to choose the units of pressure from a list of available units, perform a rezero/full calibration, etc. The transducer also has a facility to choose the number of samples to be averaged, by means of dip-switch settings. The accuracy of the transducer (after rezero calibration) is specified to be ± 0.15% full scale. A view of the pressure transducer and computer is shown in figure 3.4. The settling chamber pressure was similarly displayed on the computer display using one of the 16 channels of the PSI 9010 transducer. The pressure measurements are accurate within ±1.8%. The stagnation pressure was maintained with an accuracy of ±0.1%. The maximum uncertainty in the pitot pressure data was estimated to be ±3.5% [40].

### 3.3.2 Noise Measurement Setup

The cases most often encountered in acoustics is the free-field, the diffuse (or reverberant) field, and the closed coupler. The free-field is, in principle, an infinite, empty (except for the medium and the source) space, with no reflections. Here, the waves are allowed to radiate freely in all directions without reflections. In practice, the free-field is implemented in anechoic (*without echo*) chambers, where all walls have been made nearly 100% absorptive. The diffuse field is obtained in a

reverberation room where all walls have been made, in principle, 100 % reflective. At the same time, the walls are made nonparallel and the result is a sound field with sound waves in all directions. The closed coupler is a small chamber, with dimensions small compared to the wavelength of the sound. A special case of this is the standing wave tube. This is a tube with a diameter smaller than the wavelength and with a sound source in one end.

Experiments in acoustics require free-field conditions for ensuring reliable results, which are impossible to obtain in enclosures with sound-reflecting surfaces. The enclosure, which simulates a free-field environment, is the anechoic chamber. The purpose of this enclosure is threefold:

- Firstly, to satisfy the requirement of providing a free field, that is, keeping the echo as minimum as possible.
- Secondly to reduce noise from external sources (outside the enclosure).
- Lastly to reduce noise transmitted through the walls of the chamber, enabling experiments involving high sound pressure levels to be conducted inside the chamber without causing annoyance to people outside the lab.

### 3.3.3 Anechoic Chamber

In jet noise experiments, free-field conditions become very essential for scaling laws to be derived, which would enable a comparison of results obtained at different power settings (e.g., model and full-scale jets).

The anechoic chambers used for experiments in jet acoustics are different from those used for purely acoustic or electronics experiments like for example, calibration of a microphone. Jet experiments involve mass flow through the chamber, and since jets entrain ambient fluid, it is necessary to provide ventilation for mass entrainment. Similarly, ventilation should be provided for the passage of jet mass outside the enclosure.

The present construction is a highly simplified arrangement for producing a near free-field condition to carry out jet noise studies, taking advantage of the flexibility of allowing a larger cut-off frequency for high-speed jet noise studies. This is because high-speed jets contain most of their energy in the higher frequencies. The corrugated foam was mounted on an iron mesh, to which they were stitched. This

three-layered arrangement was done on all walls of the anechoic chamber except the floor. Corrugated foam blocks were used to cover the floor area. The chamber has two openings; one to accommodate a small portion of the stagnation chamber and the traversing system, and other to permit mass flow outside the chamber. During the noise measurements, all reflecting surfaces inside the chamber (e.g., face of settling chamber, traverse, etc.) were covered with 15 mm or 5 mm poly-urethane foam to minimize sound reflection. A view of the anechoic chamber is shown in figure 3.5.

The calibrations of anechoic chambers require rigorous procedures and appropriate instrumentation. Hence, the procedure adopted here should only be considered rudimentary. The anechoic chamber was calibrated by verifying the abidance to the inverse square law. The overall sound level was measured along a straight line at $90^{\circ}$ to the jet axis with the microphone pointed just ahead of the jet center. The calibration curve thus obtained is shown in Fig. 3.6 (bottom Fig. 3.6 shows the curve in conventional logarithmic plot). The points shown in these figures are measured values and straight lines show theoretical curves. For anechoic conditions, the experimental region must be chosen where the points in the calibration curve are parallel to the theoretical curves. It is observed from the figures that, this condition is satisfied after 16 diameters within 0.5 dB. Thus, the measurement locations were chosen beyond 16 diameters, for ensuring near-free-field conditions.

For the determination of cut-off frequency, monotone generators were not available. Since turbulent jet noise has a broadband spectrum, the 1/3 octave filter was used to overcome this limitation. The frequency characteristics of the chamber were determined by repeating the above procedure, now for obtaining the 1/3-octave spectrum. This enables checking the agreement with inverse square law of each frequency band. Figure 3.7 shows the deviation from inverse square law of each frequency band. Here too, experimental lines must be parallel to theoretical curves for assuring anechoic properties. This condition is satisfied for frequencies above 630 Hz. Thus, the chamber is believed to have a cut-off frequency of 630 Hz.

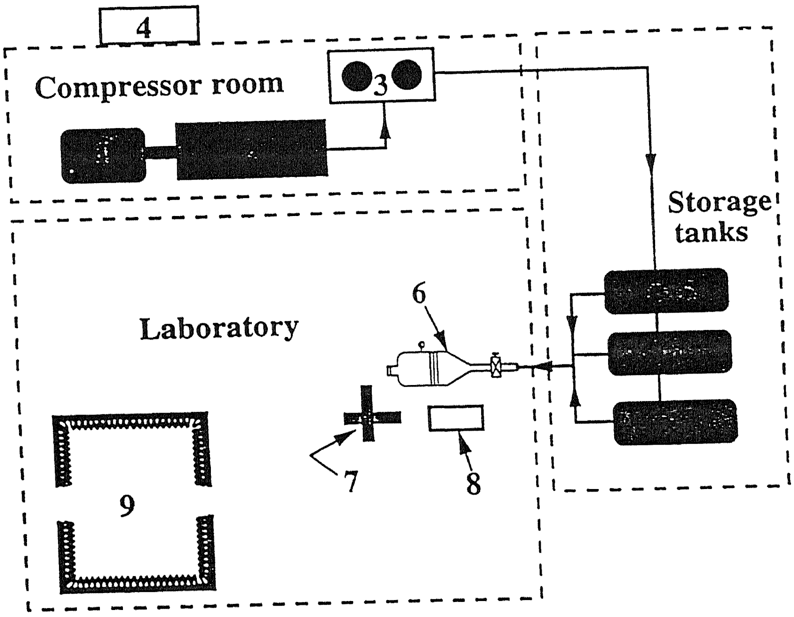


1. 150 hp induction motor
2. Ingersoll Rand 2 stage Reciprocating compressor
3. Activated Charcoal Filter and Silica Gel dryer units
4. Water cooling unit
5. Storage tanks
6. Jet test facility
7. Traversing system
8. Instrumentation desk
9. Movable Anechoic chamber

Figure 3.1 Layout of the Laboratory.

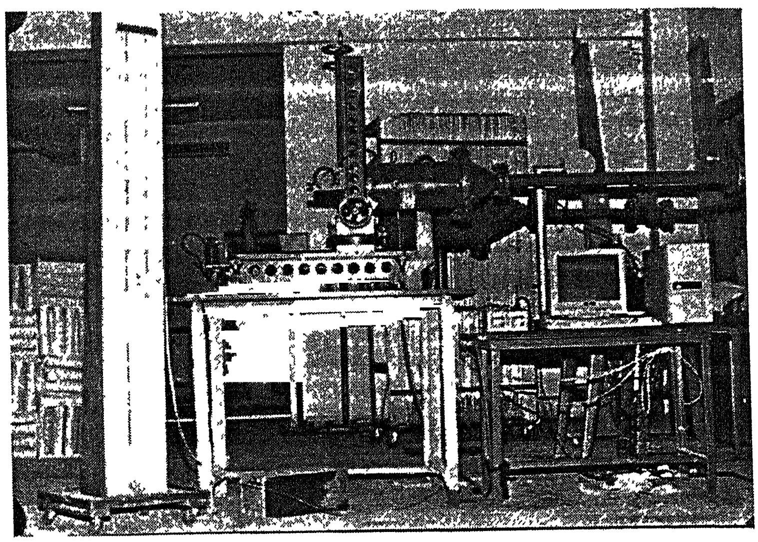

Figure 3.2 A view of the Jet Test Facility

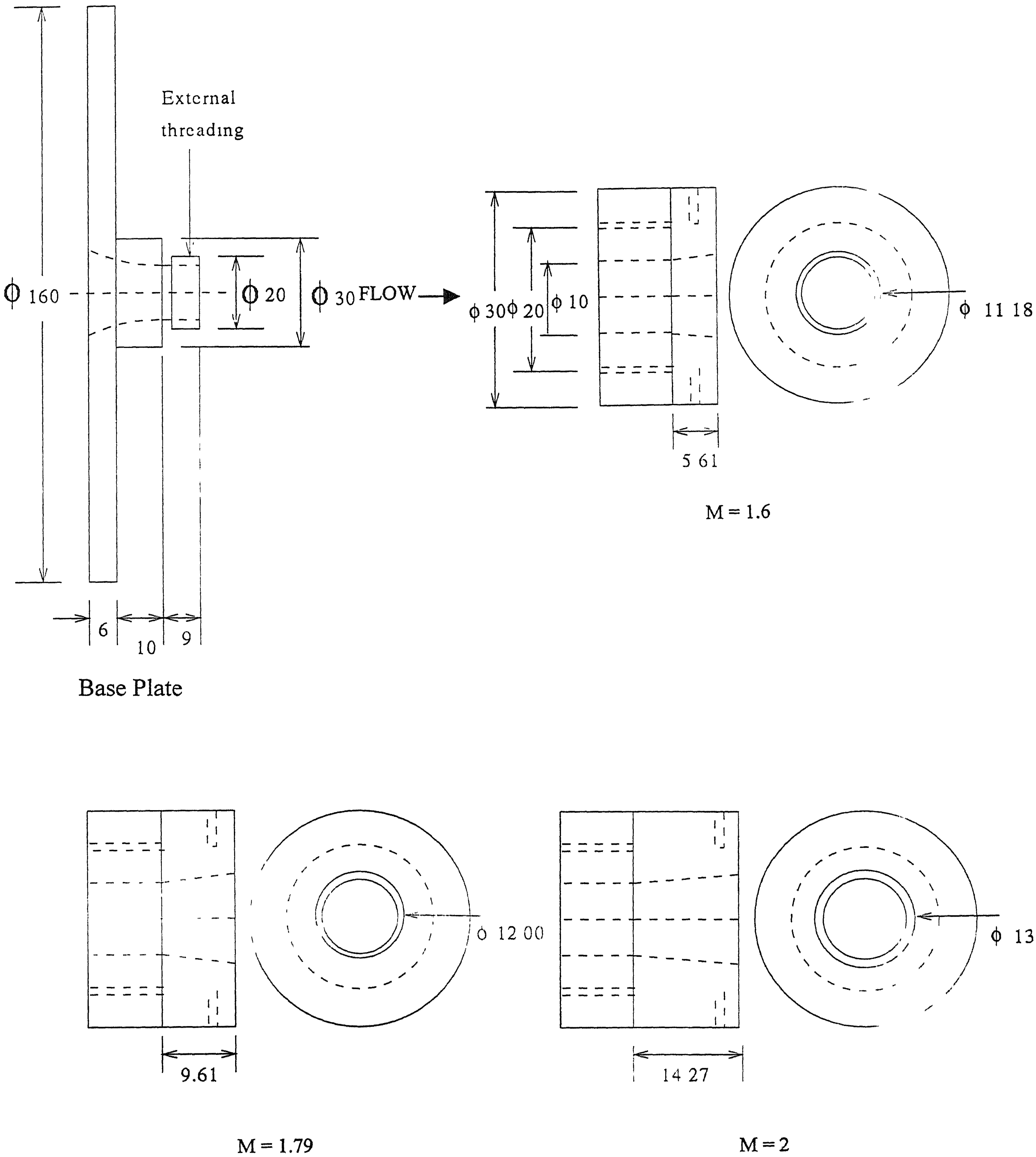


ALL DIMENSIONS ARE IN MM

Figure 3.3 Model Drawings

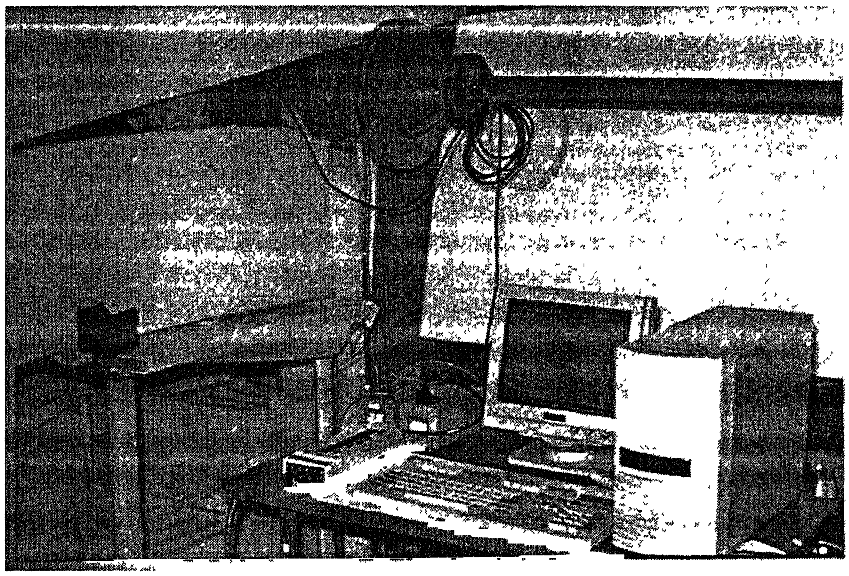

Figure 3.4 Pressure Measurement Setup

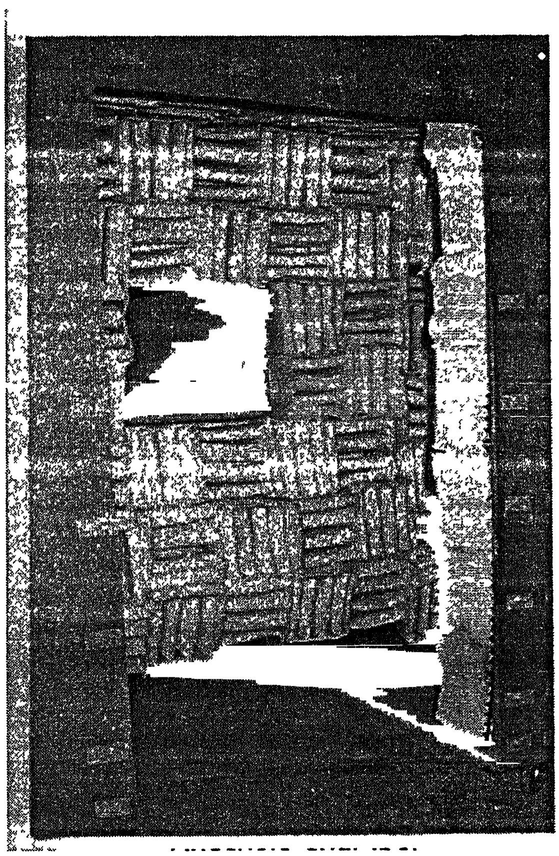

Figure 3.5 Anechoic Chamber

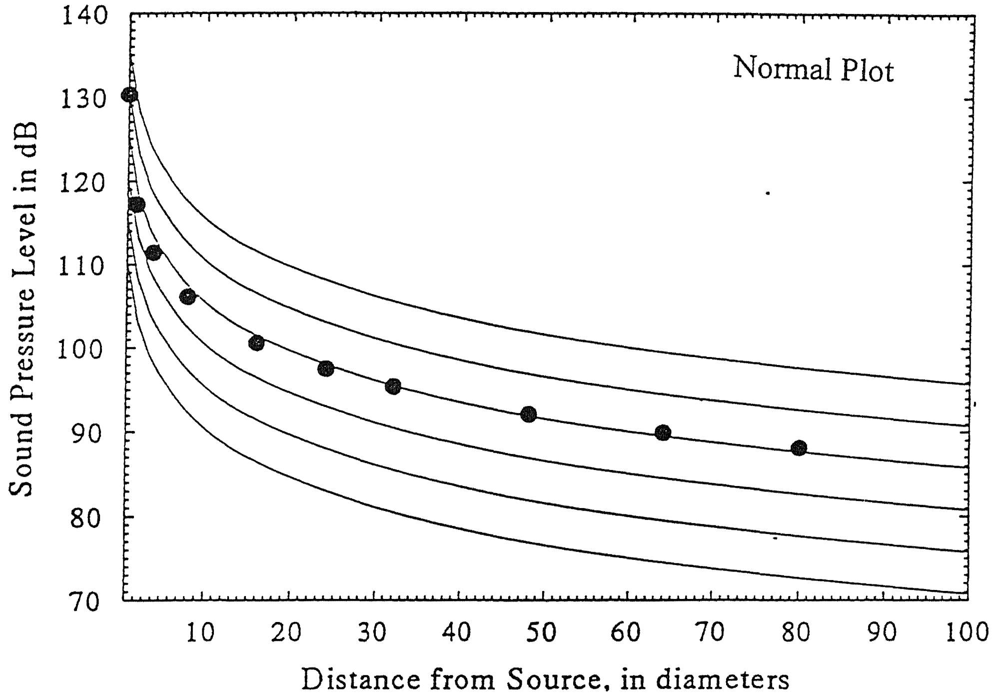


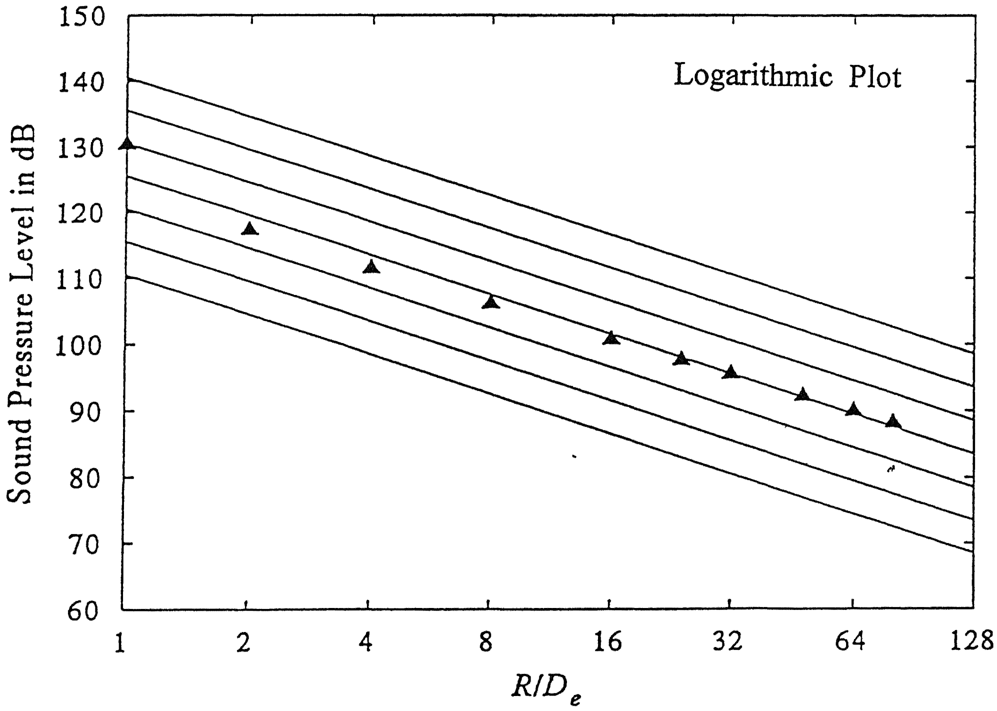


Figure 3.6 Inverse Square Law calibration of Anechoic chamber.

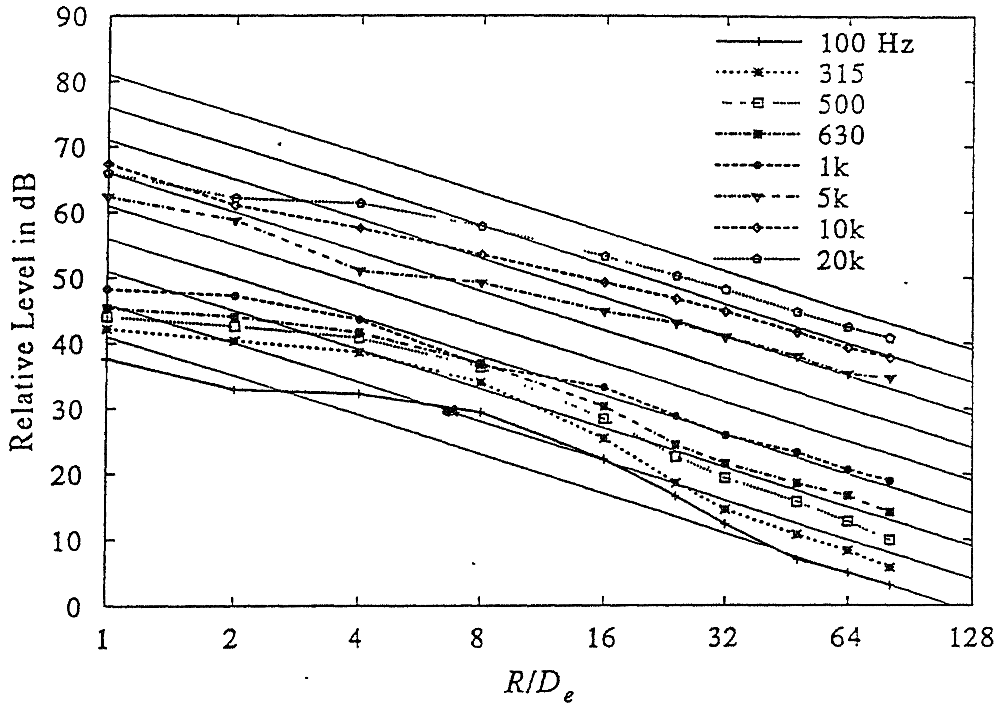


Figure 3.7 Deviation from inverse square law for various frequency bands.

## 3.4 Acoustic Instruments

From the wave equation it is clear that the full acoustic field can in principle be described from only pressure measurements. This means all other acoustic parameters can be derived from pressure measurements and, in practice, pressure is often the only parameter measured.

A sound level meter is the principal instrument for general noise measurement. The indication on a sound level meter (aside from weighting considerations) indicates the sound pressure, P, as a level referenced to 0.00002 Pa.

Sound Pressure Level = 20 x log (P/0.00002) dB

If there are two sound sources producing X dB and Y dB in a room, then the total sound level is a logarithmic sum of the two sound sources i.e.,

Combined sound level = 10 x log $(10^{(X/10)} + 10^{(Y/10)})$

The sound level meter can be functionally divided into four parts: microphone and preamplifier, C-weighting filter, rms detector and display, as shown below

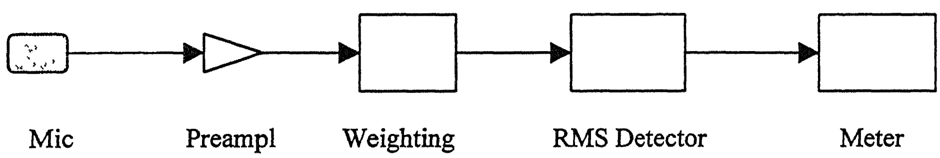


FUNCTIONAL PARTS OF A SOUND LEVEL METER

The absolute transducers for acoustic measurements are the condenser type microphones. For acoustic measurements, they are proved to be the best with respect to temperature stability, long term stability and insensitivity to rough handling.

### 3.4.1 Condenser Microphones

Basically the condenser microphone consists of five elements: protection grid, microphone casing, diaphragm, backplate and insulator, as shown in the figure 3.8. The diaphragm and the backplate form the parallel plates of an air capacitor. The capacitor is polarized with a charge from an external voltage supply (externally polarized type) or by an electric charge injected directly into an insulating material on the backplate (pre-polarized type). When the sound pressure in the sound field

fluctuates, the distances between the diaphragm and the backplate will change, and consequently change the capacitance of the diaphragm/backplate capacitor. As the charge on the capacitor is kept constant, the change in capacitance will generate an output voltage on the output terminal of the microphone.

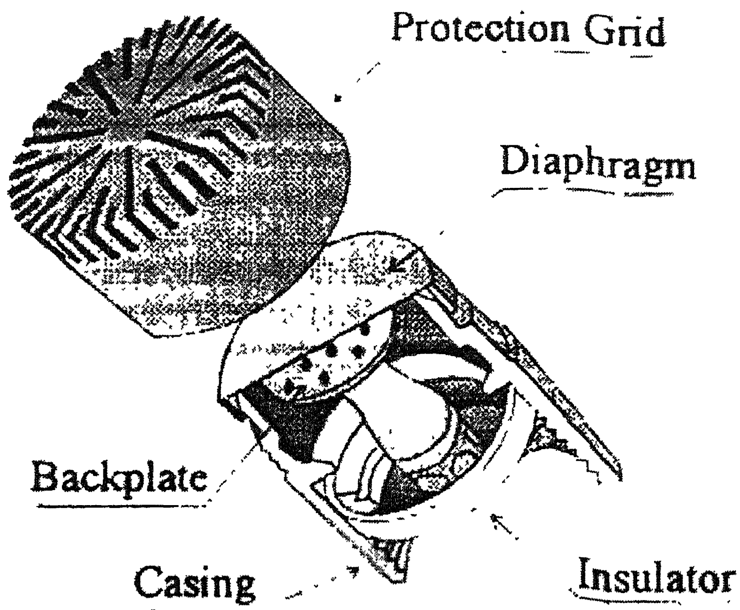


Fig 3.8 Basic elements of a measurement microphone

The condenser microphones can be classified into the free-field microphones, the pressure microphones, and the random incidence microphones based on their design features. The *free-field microphone* is designed to essentially measure the sound pressure as it existed before the microphone was introduced into the sound field. At higher frequencies, the presence of the microphone, in the sound field itself, will change the sound pressure. In general, the sound pressure around the microphone cartridge will increase due to reflections and diffraction. The free-field microphone is designed so that the frequency characteristics compensate for this pressure increase. The resulting output of the free-field microphone is a signal proportional to the sound pressure as it existed before the microphone was introduced into the sound field. The free-field microphone should always be pointed towards the sound source (0° incidence).

The pre-amplifier converts the high-impedance output signal from the microphone to a low-impedance signal, but has in itself no or even negative voltage amplification. The signal from the preamplifier is then passed through a C-weighting filter.

The signal from the weighting filter is subsequently passed through an exponential rms detector, with a time constant of either 125 ms ("fast") or 1 s ("slow"). These time constants simulate the behavior of the human ear when subjected to time-varying signals. Especially when the duration of the sound stimuli to the human ear becomes short (e.g., around 200 ms), the sound is subjectively judged as being lower compared to the same sound heard continuously. The same effect is obtained using the "fast" averaging time.

In the present study the jet noise was measured using a Larson Davis model 800B precision integrating sound level meter with a 1/8 inch B & K type 4138 condenser microphone. This microphone is certified to have a flat response in the range 10 Hz to 50 Hz within ± 1 dB, and 6.5 Hz to 140 kHz within ± 2 dB. The microphone was calibrated using a CA 250 precision acoustic calibrator. This acoustic calibrator gives a uniform monotone of 250 Hz at 114 dB (Reference. 20 μPa). The accuracy of the noise measurement, according to the manufacturer's specification is ± 0.3 dB. The sound level meter has an amplitude range of –10 dB to 140 dB, in five user selectable ranges of 60 dB dynamic range. Three standard weighting networks; A, C and Linear weightings are available. Throughout the present work C-weighting was used. The instrument gives output signal in both AC and DC form. The AC output follows all signal-conditioning circuits including the band pass filters. The AC output can be used to drive the inputs of external signal analyzers such as FFTs. Full scale output is approximately 1.0 Vac. The DC output voltage is 50 mV/dB and the full-scale output is 3.2 Vdc. The sound pressure was measured in fast mode. All sound pressure levels are referred to 20 μPa.

The microphone signal was fed to the connector box of the PCI-MIO-16E-1 Data acquisition card, through a BNC cable from the AC output port of the sound level meter. The AC output port gives the conditioned signal in the form of AC voltage. Full scale (of the sound level meter setting) corresponds to 1 Vac. The B & K model 4138 1/8 inch microphone has a frequency response upto 140 kHz, but the

microphone preamplifier (which connects the microphone and the sound level meter) has a response of only 65 kHz.

## 3.5 Data Acquisition and Analysis

### 3.5.1 Data Acquisition

In the present study a software tool was developed for acquiring the noise samples at desired sampling rate and store the samples on the hard disk in a binary format. The basic elements of a typical PC-based DAQ system comprises of

- Transducers
- Signal conditioning
- DAQ hardware
- Personal computer
- Software

The basic function of a transducer is to sense a physical phenomenon and provide the electrical signal that the DAQ system can measure. In the present case sound level meter was used as transducer and the electrical signals produced are proportional to the physical parameter we are monitoring.

The electrical signals generated by the transducers must be optimized for the input range of the DAQ board. Signal conditioning accessories can amplify low-level signals, and then isolate and filter them for more accurate measurements. In addition, some transducers require voltage or current excitation to generate a voltage output. In the present case all the signal conditioning was done inside the sound level meter.

### 3.5.2 DAQ hardware

The basic Analog Input considerations are

- Number of channels
- Sampling rate
- Resolution
- Input range

**Number of Channels** - The number of analog channel inputs will be specified for both single-ended and differential inputs on boards that have both types of inputs. Single-ended inputs are all referenced to a common ground point. These inputs are typically used when the input signals are high level (greater than 1 V), the leads from the signal source to the analog input hardware are short (less than 15 ft), and all input signals share a common ground reference. If the signals do not meet these criteria, one should use differential inputs. With differential inputs, each input has its own ground reference. Noise errors are reduced because the common-mode noise picked up by the leads is canceled out.

**Sampling Rate** – This parameter determines how often conversions can take place. A faster sampling rate acquires more points in a given time and can therefore often form a better representation of the original signal. For example, audio signals converted to electrical signals by a microphone commonly have frequency components up to 20 kHz. To properly digitize this signal for analysis, the Nyquist sampling theorem stipulates that the sampling rate must be more than twice the rate of the maximum frequency component to be detected. Hence, a DAQ board with a sampling rate greater than 40 kilocycles/s is needed to properly acquire this signal.

**Multiplexing** – A common technique employed for measuring several signals with a single ADC is multiplexing. The ADC samples from one channel, switches to the next channel, samples it, switches to the next channel, and so on. Because the same ADC is sampling many channels instead of one, the effective rate of each individual channel is inversely proportional to the number of channels sampled.

**Resolution** – The number of bits that the ADC uses to represent the analog signal is the resolution. The higher the resolution, the higher the number of divisions the range is broken into, and therefore, the smaller the detectable voltage change. A 12-bit converter divides the analog range into 4096 divisions. By increasing the resolution to 16 bits, however, the number of codes from the ADC increases from 4096 to 65,536, and one can therefore obtain an extremely accurate digital representation of the analog signal if the rest of the analog input circuitry is designed properly. But in the present study the resolution of the ADC is 12 bit.

**Range** – Range refers to the minimum and maximum voltage levels that the ADC can quantize. The multifunction DAQ boards offer selectable ranges so that the board is configurable to handle a variety of different voltage levels. With this flexibility, one

can match the signal range to that of the ADC to take best advantage of the resolution available to accurately measure the signal.

The range, resolution, and gain available on a DAQ board determine the smallest detectable change in voltage. This change in voltage represents 1 LSB (Least Significant Bit) of the digital value, and is often called the code width. The ideal code width is found by dividing the voltage range by the gain times two raised to the order of bits in the resolution.

In the present case the resolution of the DAQ board is 12 bit, has a voltage range of 0 to 5V and gain of 2. Ideal code width is given by

$$5/2 * 2^{12} = 0.61\ \mu V$$

Therefore, the theoretical resolution of one bit in the digitized value is 0.61 μV.

### 3.5.3 Software

The software required for the sampling was developed using the application tool LabVIEW. In this software we can select the number of channels, sampling rate, buffer size and the minimum number of scans to write at a time on the hard disk. In addition to the above we can supply the user header, which we can use --for identification of the sampling parameters during the analysis. The front panel and the block diagram of the program are shown in figures 3.9 and 3.10.

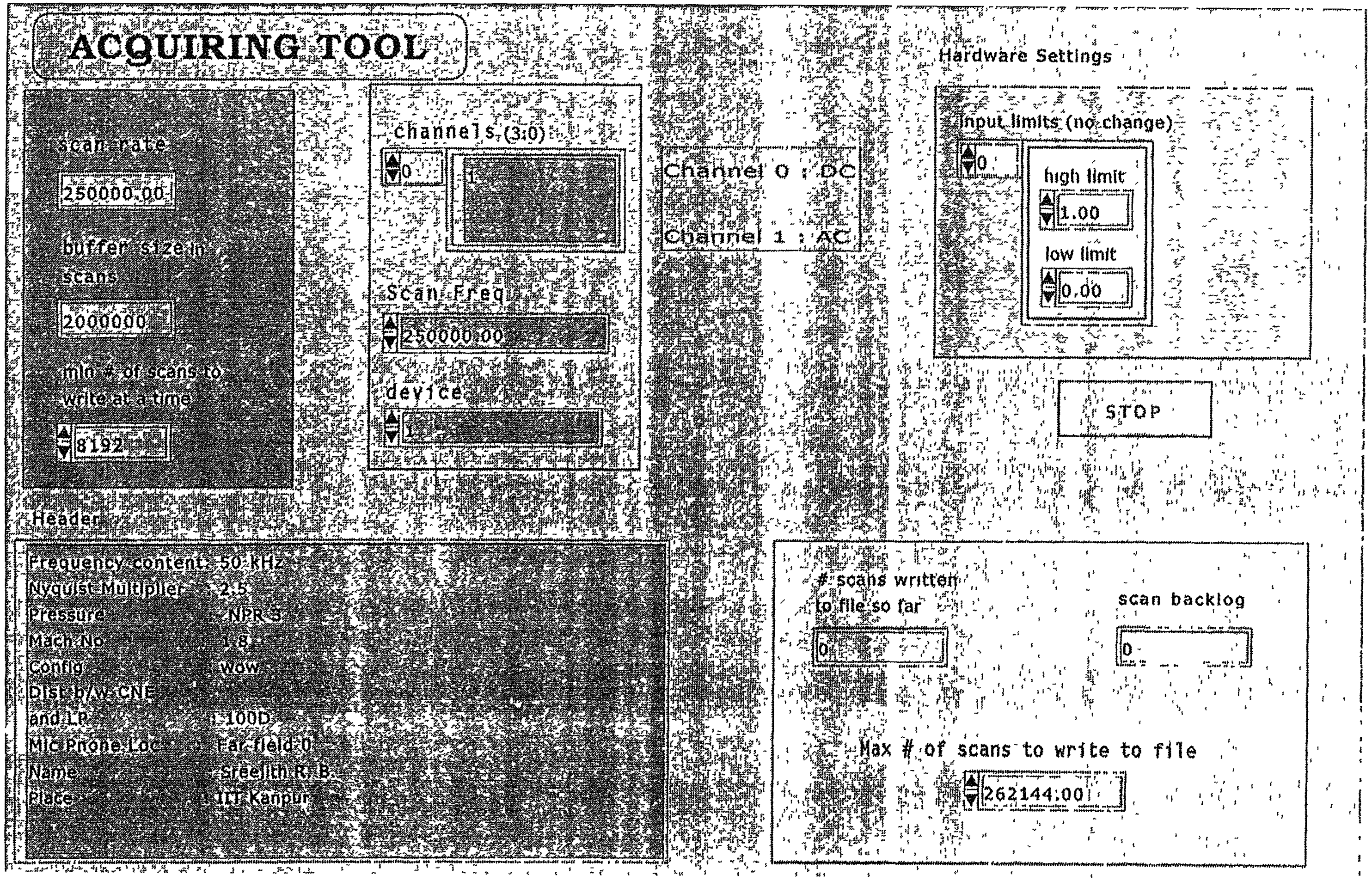


Figure 3.9 Front panel of the Acquiring tool.

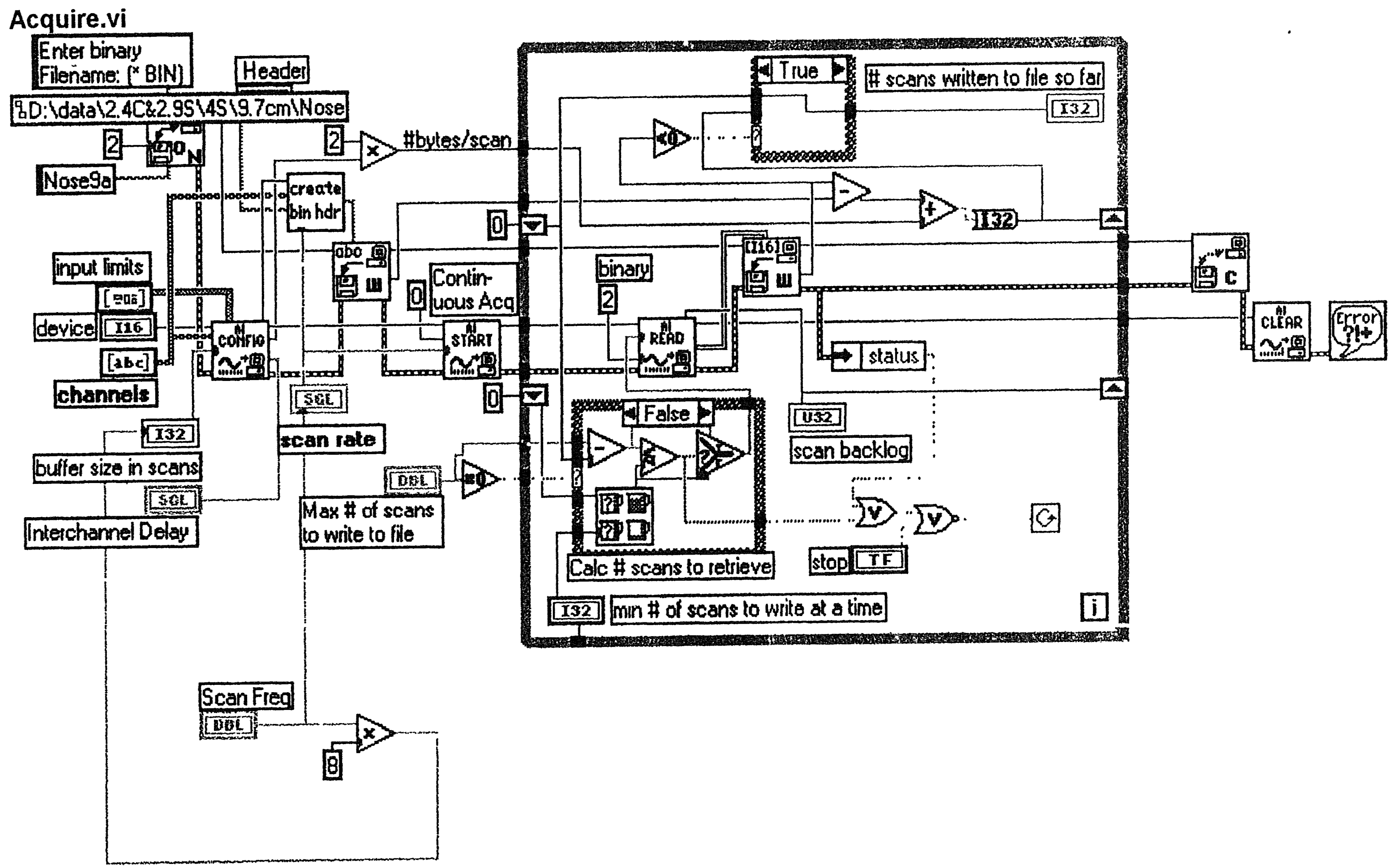


Figure 3.10 Block diagram of the Acquiring tool.

### 3.5.4 Analysis

The samples obtained from a DAQ board constitutes the time domain representation of the signal, i.e., amplitude of the signal at the instant of time during which it had been sampled. But we want to know the frequency content of a signal rather than the amplitude of the individual samples. The representation of signal in terms of its individual component is known as the frequency domain representation of the signal. This signal is used because a signal of interest is buried in the noise and because the signal of interest is easily identified in the frequency domain. Based on frequency information, digital filtering can remove the noise from the signal. The Fourier transform is one of the most powerful signal analysis tools, particularly in acoustics.

The Fourier transform maps time domain functions into frequency domain representations and is defined as

$$X(f) = F\{x(t)\} = \int_{-\infty}^{\infty} x(t) e^{-j2\pi ft}\, dt \qquad 1$$

where x (t) is the time domain signal, and

X (f) is its Fourier Transform.

Similarly, the *discrete Fourier transform* (DFT) maps discrete-time sequences into discrete-frequency representations and is given by

$$X_k = \sum_{i=0}^{n-1} x_i e^{-j2\pi ik/n} \qquad 2$$

for k=0,1,2,.......,n-1

where x is the input sequence,

X is its DFT, and

n is the number of samples in both the discrete-time and the discrete-frequency domains.

Direct implementation of the DFT, equation 2, requires approximately $n^2$ complex operations. However, computationally efficient algorithms can require as little as $n\log_2(n)$ operations. These algorithms are called *Fast Fourier transforms* (FFTs).

From the definition of the DFT, equation 2, the Fourier transform of any sequence x, whether it is real or complex, always results in a complex output sequence X of the form

$$F\{x\} = X = X_{\mathrm{Re}} + jX_{\mathrm{Im}} = \mathrm{Re}\{X\} + j\,\mathrm{Im}\{X\} \tag{3}$$

An inherent DFT property is

$$X_{n-i} = X_{-i}, \tag{4}$$

Which means that the (n-i)$^{th}$ element of X contains the result of the $-i^{th}$ harmonic. Furthermore, if x is real, the i$^{th}$ harmonic and the $-i^{th}$ harmonic are complex conjugates

$$X_{n-i} = X_{-i} = X_i^* \tag{5}$$

Consequently,

$$\mathrm{Re}\{X_i\} = \mathrm{Re}\{X_{n-i}\} \tag{6}$$

$$\mathrm{Im}\{X_i\} = -\mathrm{Im}\{X_{n-i}\} \tag{7}$$

These symmetrical Fourier properties of real sequences are referred to as conjugate symmetric (equation 5), symmetric or even symmetric (equation 6), and anti-symmetric or odd-symmetric (equation 7).

FFT-based measurement requires digitization of a continuous signal. According to the Nyquist Criterion, the sampling frequency, $F_s$, must be at least twice the maximum frequency component in the signal. If this criterion is violated, a phenomenon known as aliasing occurs. Figure shown below shows an adequately sampled signal and an undersampled signal. In the undersampled case, the result is an aliased signal that appears to be at a lower frequency than the actual signal.

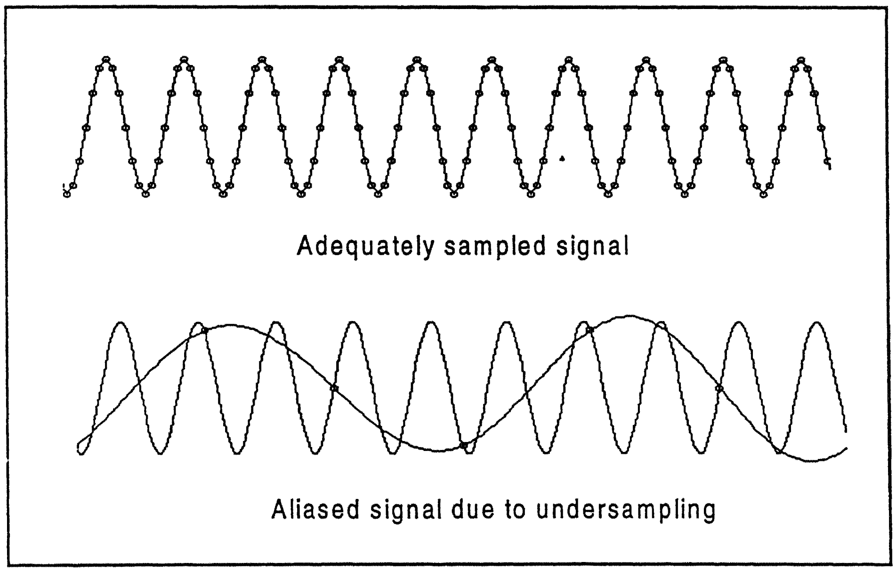


Adequate and Inadequate Signal Sampling

When the Nyquist Criterion is violated, frequency components above half the sampling frequency appear as frequency components below half the sampling frequency, resulting in an erroneous representation of the signal.

The basic computations for analyzing signals include converting from a two-sided power spectrum to a single-sided power spectrum, adjusting frequency resolution and graphing the spectrum, using the FFT, and converting power and amplitude into logarithmic units.

Most real-world frequency analysis instruments display only the positive half of the frequency spectrum because the spectrum of a real-world signal is symmetrical around DC. Thus, the negative frequency information is redundant.

In a two-sided spectrum, for each frequency other than DC, half of the energy is displayed at the positive frequency, and half of the energy is displayed at the negative frequency. Therefore, to convert from a two-sided spectrum to a single-sided spectrum, discard the second half of the array and multiply every frequency point except for DC by two.

The frequency range and resolution on the x-axis of a spectrum plot depend on the sampling rate and the number of points acquired. The number of frequency points equals to

N/2

Where $N$ is the number of points in the acquired time-domain signal. The first frequency line is at 0 Hz, that is, DC. The last frequency line is at

$$\frac{F_s}{2} - \frac{F_s}{N}$$

Where $F_s$ are the frequency at which the acquired time-domain signal was sampled. The frequency lines occur at $\Delta f$ intervals where

$$\Delta f = \frac{F_s}{N}$$

Frequency lines can also be referred to as frequency bins or FFT bins because you can think of an FFT as a set of parallel filters of bandwidth Δf centered at each frequency increment from DC to

$$\frac{F_s}{2} - \frac{F_s}{N}$$

Alternatively you can compute Δf as

$$\Delta f = \frac{1}{N * \Delta t}$$

Where Δt is the sampling period. Thus $N$ * Δt is the length of the time record containing the acquired time-domain signal.

The computations for the frequency axis demonstrate that your sampling frequency determines the frequency range or bandwidth of your spectrum, and that for a given sampling frequency, the number of points acquired in the time-domain signal record determine your resolution frequency. To increase your frequency resolution for a given frequency range, increase the number of points acquired at the same sampling frequency.

Most often, amplitude or power spectrums are shown in the logarithmic unit decibel (dB). Using this unit of measure, it is easy to view wide dynamic ranges; that is, it is easy to see small signal components in the presence of large ones. The decibel is a unit of ratio and is computed as follows.

Power in dB = 10 $\log_{10}$(Measured Power/Reference power)

Use the following equation to compute the ratio in decibels from amplitude values.

Amplitude in dB = 20 $\log_{10}$ (Measured Amplitude/Reference Amplitude)

When using amplitude or power as the amplitude-squared of the same signal, the resultant decibel level will be exactly the same. Multiplying the decibel ratio by two is equivalent to having a squared ratio. Therefore, you obtain the same decibel level and display regardless of whether you use the amplitude or power spectrum. As shown in the preceding equations for power and amplitude, you must supply a reference for a measure in decibels. This reference then corresponds to the 0 dB level. Several conventions are used. A common convention is to use the reference 1 Vrms

for amplitude or 1 Vrms squared for power, yielding a unit in dBV or dBVrms. In this case, 1 Vrms corresponds to 0 dB.

In the present study a software has been developed for obtaining the frequency spectrum of the acquired acoustic samples. Before we are running the program we have to supply certain parameters like sampling frequency, number of scans to read at a time, lower cutoff and higher cutoff of the band pass filter. The front panel and program of the software are shown in figures 3.11 and 3.12.

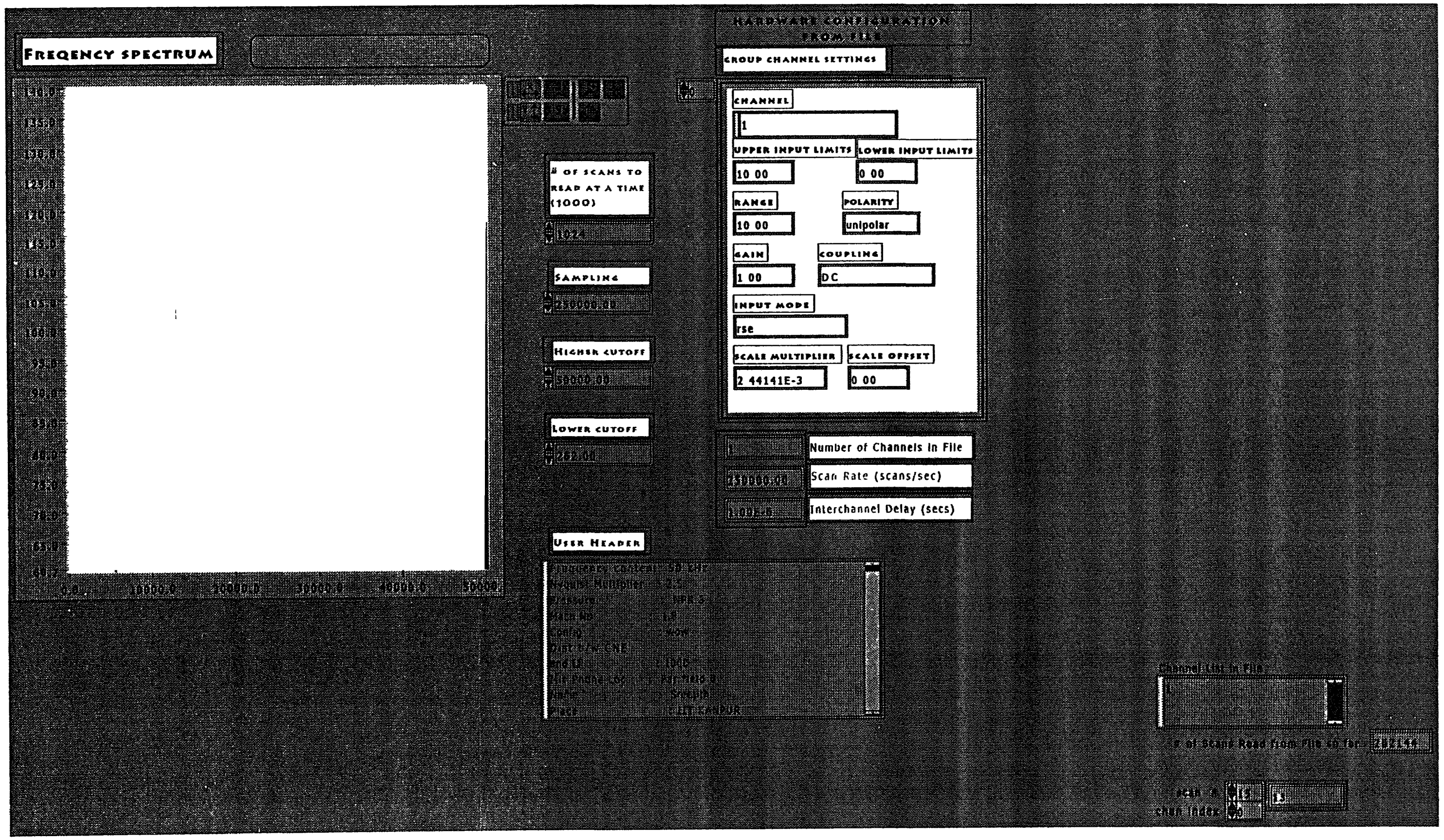


Figure 3.11 Front panel of the Analysis tool.

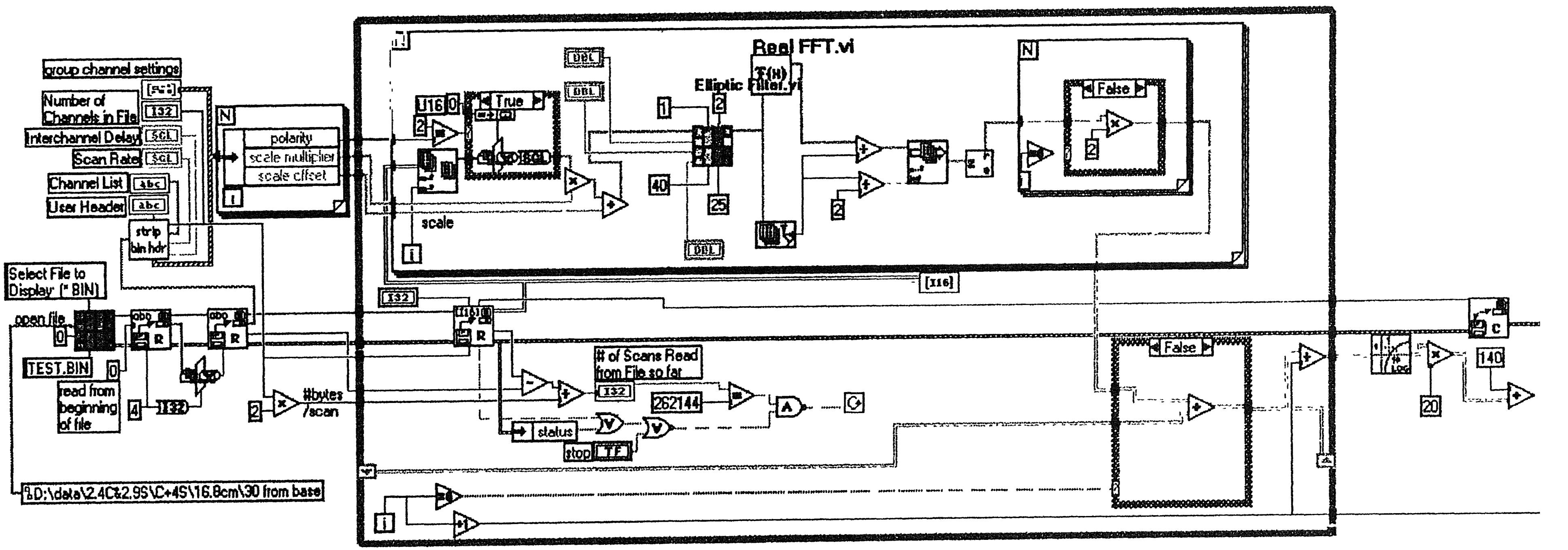


Figure 3.12 Block diagram of the Analysis tool.

## 3.6 Acoustic Measurements

The acoustic measurements were made at two locations; in the nozzle exit plane and far-field. In the nozzle exit plane the microphone was positioned at 30D radial distance. For far-field case acoustic data was acquired at radial distance of 100D in the azimuthal plane, with the microphone tip positioned at 30 degree orientation to the jet axis, as shown in figure 3.13. For both the cases acoustic data were acquired in two planes, namely along the wire and normal to the wire.

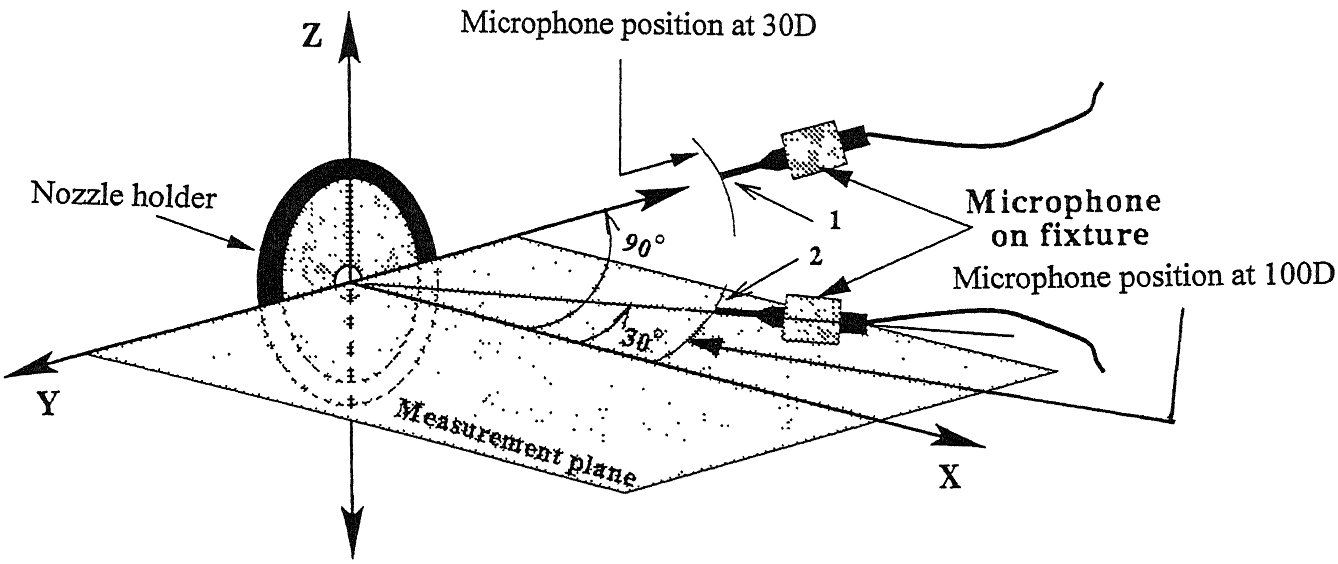


**Measurement Locations: 1. $90^{0}$ to jet axis (jet exit plane)**
**2. $30^{0}$ to jet axis**

Figure 3.13 Apparatus used for acoustic measurements and positions of the microphone.

## 3.7 Experimental Precautions

In addition to the measures taken to minimize errors, like linearity checks, rezero calibrations, etc., the following precautions were observed during the experiments.

- The vertical and horizontal alignment of the settling chamber was ensured.
- Care was exercised in the alignment of the models, to ensure proper positioning of the measurement planes.

- The nearest wall is 150 diameters. Hence, wall effects are negligible.
- The pressure lines and the settling chamber ports were ensured to be leak free.
- During the experiments, the stagnation pressure reading was constantly monitored.
- The positioning of the microphone was carried out with the help of spirit level to get the $0^{\circ}$ incidence.
- During the noise measurements, the exposed metallic parts inside the measurement enclosure were wrapped with thin sheet of polyurethane foam, to minimize reflections. This was done for the traverse, settling chamber parts, etc.
- The noise measurements were carried out during nights, when ambient noise level is minimum.

# Chapter 4

# Results and Discussion

As discussed in the previous chapters the aim of the study is to investigate the effect of a passive control in the form of a cross-wire on jet aerodynamic and acoustic characteristics of supersonic jets from axi-symmetric convergent-divergent nozzles. The Mach number of the present investigation are 1.6, 1.79 and 2. These Mach numbers were specifically chosen to study the cross-wire effect on jets which are screech prone (Mach 1.6 and 1.79 jets) and jets without screech. Another aspect of interest on jet control is the control effectiveness in adverse pressure gradient. To achieve this goal the nozzle pressure ratio considered where such that the jets generated were of the type underexpanded, correctly expanded and overexpanded, exhibiting favorable pressure gradient and adverse pressure gradient under underexpanded and overexpanded conditions, respectively. The nozzle pressure ratio (NPR) tested were 2,4,6,8 and the corresponding NPR for correct expansion for Mach number 1.6 and 1,79. The tested NPRs for Mach 2 were 4, 7.82 and 9.

## 4.1 Characteristics of Mach 1.6 Jet

### 4.1.1 Centreline Decay for Mach 1.6 Jet

The jet centreline decay is a measure of jet mixing[38]. Therefore, to investigate the effect of cross-wire on jet mixing the measured pitot pressure (P) along the jet axis is non-dimensionalised with the settling chamber pressure (Po) and plotted as a function of non-dimensionalised axial distance, X/D, in figures 4.1 to 4.5

Centreline decay for NPR 2 (which corresponds to an overexpansion) is given in figure 4.1 for the cases of jets with wire and without wire. From these results it is seen that, the jet core has only mild shocks when there is no wire. Also, the initial shock is

weaker than that with wire. After the core the jet without wire experiences a faster decay compared to the jet with wire. However, for the wired jet the initial shock is much stronger and the other cells after the first shock cell does not posses shocks of significant strength. But the decay after the core is slower for this case. It should be noted that all the above mentioned differences in the jet behavior are taking place within 10D axial distance. Beyond 10D jets from nozzles with wire and without wire are behaving almost similar. It is well established that, weakening the shocks in the jet core will result in reduction of shock associated noise, hence reduction in the over all jet noise. Therefore, weakening of shocks in the core by the presence of wire can result in jet noise reduction. The faster decay of jet from the plain nozzle (without wire) is because before the core ends, the jet passes through a number of mild shocks, thereby resulting in a lower subsonic Mach number compared to the wired jet for which the core does not posses any shock of significant strength. It is seen that the jet with wire has a core shorter than the plain nozzle jet. The core has comedown marginally from 2.2D to 1.9D.

The centreline decay for NPR4 is given in figure 4.2. This is again an overexpanded jet. It is seen that the presence of wire results in significant reduction in shock strength and jet core reduction. It should be noted that, though NPR2 and NPR4 generate overexpanded jets, the level of overexpansion comes down with increase of NPR, i.e. with NPR increase the adverse pressure gradient comes down and the cross-wire becomes more effective in reducing the core length and weakening the shocks. These results agree well with the observation made by Samimy [30] that, passive control will be effective in favorable pressure gradient. Even though the above NPR increase from 2 to 4 does not give a favorable pressure gradient, the adverse pressure gradient level has comes down when NPR increased from 2 to 4 and hence the passive control became effective. For NPR4 the core has come down from 7.2D (plain) to 4.6D (with wire)

The centreline decay for NPR4.24 (correctly expanded jet) is shown in figure 4.3. For the plain nozzle, the core exhibits shocks of significant strength, even though at the nozzle exit there is no shock present for the correct expansion. This is because expansion fan is positioned at the nozzle exit and the flow accelerates a higher Mach number after the exit and the expansion waves getting reflected as compression waves from the jet

boundary coalesce to form shock at the jet axis and the shocks get reflected as expansion fan and the cycle repeats. Therefore, the initial shocks are weaker compared to some of the downstream shocks. When the wire is introduced, the shock in front of the wire results in significant reduction in total pressure and hence a much lower pressure at X/D = 0, compared to plain nozzle. The shocks were found to be very weak for the wired case and the core has come down from 9.2D to 6.3D. Here again the jet propagation is not influenced by the wire beyond 13D.

The centreline decay for underexpanded jets at NPR 6 is shown in figure 4.4. This is the case with favorable pressure gradient, since the jet is underexpanded. As reported by Zaman [32], Samimy [37] and Navinkumar and Rathakrishnan [36] the passive control results in significant core reduction. For plain nozzle large number of strong shocks are present in the core and the core extends upto 17D. Whereas, when the wire is introduced the core length comes down to 11D. Further, the number of shock cells are reduced and shocks become significantly weaker. Also, the effect of wire results in different decay than the plain nozzle even beyond 13D.

When the level of underexpansion increases the favorable pressure gradient also increases and the shocks in the core for the plain nozzle become stronger as seen from figure 4.5 for NPR 8. At this level of underexpansion also cross-wire results in considerable reduction of shock strength. But the core length reduction achieved is only marginally for this case. The jet decay with wire and without wire retain their identity as far as 30D.

To quantify the above results on core length reduction a parameter namely percentage reduction of core length is defined as

$$\boxed{\% \text{ Reduction} = \frac{\text{Core length without wire - Core length with wire}}{\text{Core length without wire}} \times 100}$$

has been used. The variation of percentage reduction in core length as a function of NPR for jet Mach number 1.6 is shown in figure 4.6. It is seen from this plot that, the cross-wire is effective in reducing the core length in the range of NPR from about 4 to 6. It is interesting to note that this range of NPR covers over-, correctly- and underexpanded

conditions for the jet and hence, the literature information namely, passive control will not be efficient under adverse pressure gradient and will be very efficient under favorable pressure gradient should be re-looked into.

From the above results, it is seen that the passive control in the form of cross-wire extending upto the nozzle centreline can reduce the core length and weaken the shocks in the core very efficiently for some combinations of Mach number and level of expansion. A closer look into the physical phenomenon taking place, when the wire is present, in the jet may explain the reason for this control achieved with cross-wire. Basically, when a cylinder is placed in a subsonic stream it will shed vortices alternatively. These vortices are streamwise in nature and can travel long distance compared to spanwise or azimuthal vortices. Therefore, the streamwise vortices can efficiently serve as a mixing enhancement mechanism for jets. This aspect is exploited for faster decay with passive control in subsonic jets. But in supersonic jets the core consist of a mixture of subsonic and supersonic Mach number zones. Further, when a passive control in the form of a cylindrical cross-wire, as in the present study, is introduced at the nozzle exit, a detached shock is positioned ahead of the wire. This makes the flow behind the shock as subsonic thereby rendering the wire to shed streamwise vortices as in the case of subsonic flow. However, these streamwise vortices shed by the cross-wire have to pass through the different Mach number zones before loosing their identity. This process will result in mixing enhancement. The mixing level will vary from place to place in the supersonic jet because of the subsonic and supersonic zones present. Nonetheless the mixing initiated by these streamwise vortices will result in significantly enhanced mixing of the supersonic jet, especially in the core region. This is the main cause for the shocks in the core to become weaker compared to the plain nozzle jet. The effectiveness of the cross-wire is strongly influenced by the level of expansion since the Mach number zones in the jet core strongly depends in the expansion level, i.e. the level of NPR.

### 4.1.2 Jet Flow Development for Mach 1.6 Jet

The above discussion in section 4.1.1, explaining the physics of streamwise vortices generation and their impact on jet mixing enhancement can be better understood by

studying isobaric contours of the jet field at different axial locations and NPRs. The isobars with wire and without wire for Mach number 1.6 are given in figures 4.7 to 4.32.

From fluid dynamics we know that, the streamlines will come closer as the Mach number comes down and vice-versa. figures 4.7 to 4.10 present the isobars for NPR 2 at different axial distances from X/D = 0 to 6. At X/D = 0 it is seen that, the introduction of the wire introduces a relatively low speed zone across the jet. As the jet moves downstream the low speed zone introduced gets bifurcated and forms two counter rotating zones towards the jet periphery. Because of this, the jet with cross-wire behaves like a noncircular jet, showing a tendency of axis switching, which is a well known phenomenon in jet mixing. An earlier axis switching implies a faster mixing. For NPR2 the axis switching with wire is taking place at about 6D as clearly seen from figure 4.10, whereas, for the plain nozzle case there is no tendency of axis switching. This validates the discussion for figure 4.1, indicating almost no shocks in the core.

The isobars for NPR 4 are given in figures 4.11 to 4.14. It is interesting to note that in this case the axis switching is taking place at X/D less than 1. This implies a very much enhanced jet mixing compared to NPR 2. This was reflected as a drastically reduced core length and significantly weakened shocks in the core, as seen in figure 4.2. The slower jet decay compared to the plain nozzle case (figure 4.2) is also evident from the larger jet width of the plain nozzle compared to the wired nozzle at X/D 5 and 6 as seen from figures 4.13 and 4.14.

The isobars for NPR4.24, correctly expanded case, are shown in figures 4.15 to 4.18. For this case also the jet axis switching is taking place at X/D less than 1. The observation of considerable reduction in core length and shocks strength is supported by these isobars. The faster decay of the jet after the core for the plain nozzle compared to the controlled nozzle is evident from these isobars.

The isobars for Mach number 1.6 jet at underexpanded condition with NPR6 are shown in figures 4.19 to 4.25. It is seen that, the jet is clean at the core portion for the plain nozzle, but low speed zones are introduced at the centreline when the wire is introduced. However, because of the favorable pressure gradient the jet travels faster and the axis switching is taking place at about 3D compared to less than 1D for the lower NPR cases. The streamwise vortices could not weaken the shock to the extend they could

able to do for the lower NPR cases (figures 4.1 to 4.3). However, the effect of the vortices introduced by the wire on core length reduction and shock weakening becomes better after the fourth cell, i.e. beyond 5D.

The isobars for NPR8 are presented in figures 4.26 to 4.32. Here again the axis switching is taking place at 3D and also the streamwise vortices introduced by the wire could able to have only marginal control over the shock strength and jet mixing in the near field.

From the above discussions, it is evident that the effectiveness of cross-wire strongly depends on the NPR rather than the favorable or adverse pressure gradients.

### 4.1.3 Acoustic Characteristics of Mach 1.6 Jet

As summarized by Tam [19], except for jet operating at correctly expanded condition the noise of a supersonic jet comprises three basic components-- the turbulent mixing noise, the broad band shock associated noise and screech tones. The appearance of screech tone is usually accompanied by its harmonics. Sometimes, even the fourth or fifth harmonics can be detected. The relative magnitudes of these noise intensity is a strong function of direction of observation. In the downstream direction of the jet turbulent mixing noise is the most dominant noise component. In the upstream direction the broadband shock associated noise is more intense. For circular jets the screech tones radiate primarily in the upstream direction.

As mentioned in the literature review, screech tones from supersonic jets were first observed by Powel [10,11]. Since then the phenomenon has been studied experimentally by a large number of investigators. It is found that the fundamental screech tones radiate primarily in the upstream direction, where as the principal direction of radiation of first harmonics is at 90 degree to the jet flow [39].

The turbulent mixing noise is from both the large scale turbulence structures and the fine-scale turbulence of the jet flow. The large scale turbulence structures generate the dominant part of the turbulent mixing noise. The fine-scale turbulence is responsible for the background noise.

Broadband shock associated noise and screech tones are generated only when a quasi-periodic shock cell structure is present in the jet core. It can be shown that the

quasi-periodicity of the shock cells plays a crucial role in defining the characteristics of both the broadband and discrete frequency shock noises. The shock cell structure in an imperfectly expanded supersonic jet is formed by oblique/normal shock and expansion fans. These shocks and expansion fans are generated at the nozzle lip because of the mismatch of the static pressures inside and outside the jet. For an underexpanded jet an oblique shock forms at the nozzle lip. The expansion fan or shock, once form, propagates across the jet flow until it impinges on the mixing layer on the other side. Since the flow outside the jet is stationary either a shock or an expansion fan is not allowed to that zone. The impinging shock or expansion fan is, therefore, reflected back into the jet field. The reflection process repeated many times downstream until the shock/expansion fan is dissipated by turbulence. These repeated reflections of the shock/expansion fans by the mixing layer of the jet give rise to quasi-periodic shock cells (cells are illustrated in figure2.2). From this point of view, the disturbances get trapped inside the jet by the mixing layer surrounding the jet column. In other words, one may consider the jet flow as behaving like a wave guide for the disturbances that form the shock cell.

One of the objectives of the present investigation is to study the effect of cross-wire on jet acoustics. To achieve this goal acoustic measurements were carried out at X/D = 0, R/D = 30, in the direction normal to the jet axis and at R/D = 100, 30 degrees to jet axis. At X/D = 0 the measurements were made at two directions, one with microphone along the wire and the second with microphone normal to the wire. For the second case(R/D = 100) also the cross-wire was aligned in the horizontal plane and in the vertical plane. The X/D = 0 measurement was meant for the effect of cross-wire on screech suppression and hence only the spectral content of the jet noise was measured, whereas, the far field measurement is meant for the quantitative investigation of the jet noise from nozzle with and without wire. Therefore, both OASPL and frequency spectra were measured for this case.

The frequency spectra for Mach number 1.6 jet at NPR 2 and X/D = 0 are presented in figures 4.33 to 4.35, respectively, for the cases of without wire and with wire, along the wire and normal to the wire. It is seen that the introduction of the wire resulted in reduction of shock associated noise as seen at frequency 5000 Hz for these

cases. Also, the fact that the jet noise is sensitive to the direction of measurement is evident from figures 4.34 and 4.35.

The jet noise (OASPL) and the corresponding spectra measured at R/D = 100 are presented in figures 4.175 and 4.36 to 4.38. From these results it is seen that, the jet noise has come down by nearly 2 dB when wire is introduced. This is mainly due to the reduction of shock associated noise owing to the weakening of the shocks by the cross-wire as seen from figure 4.1.

The frequency spectra at X/D = 0 for NPR 4 are shown in figures 4.39 to 4.41. For the plain nozzle, screech tones with four harmonics are seen in the spectrum. When the cross-wire is introduced, in the direction along the wire the screech is suppressed to a large extent and at low frequencies it is totally eliminated. In the direction normal to the wire also the screech is reduced to a single peak screech, also its amplitude has come down from 98 dB to about 90 dB. This is mainly due to the weakening of the shocks by the cross-wire as seen from figure 4.2.

The far field(R/D = 100) spectra for NPR4 are shown in figures 4.42 to 4.44. In this case the OASPL come down by 5 dB along the wire and 2.1 dB normal to the wire. For the plain nozzle screech tones with two frequencies are present. It is reduced to screech with single frequency in the wire plane and this resulted in nearly 5 dB reduction in jet noise. However, in the direction normal to the wire, there is no screech suppression, both the harmonics are prevailing with slight reduction in their amplitudes.

For the correctly expanded jet (NPR4.24, X/D = 0) as seen from figures 4.45 to 4.47, the spectra for plain nozzle as well as wired nozzle exhibit screech tones. For the plain nozzle four screech harmonics were seen. But along the wire the harmonics were reduced to two and also the amplitude of the screech tones come down significantly. However, normal to the wire even though the screech amplitudes have come down, the four harmonics present in the plain nozzle case is seen for this case also.

The far field (R/D = 100) spectra for correct expansion (NPR 4.24) are given in figures 4.48 to 4.50. For the plain nozzle two screech tones were present. The screech is suppressed to a large extent along the wire but normal to the wire though the shock associated noise is reduced marginally, the screech amplitude remains unaffected. For

this case an OASPL reduction of 4.5 dB along the wire and 2.1 dB normal to the wire were achieved as seen from figure 4.175.

The frequency spectra for NPR5 which corresponds to an underexpanded condition is shown for X/D = 0 in figures 4.51 to 4.53. The behavior for this NPR is slightly different from correctly expanded and overexpanded cases. For the plain nozzle three prominent screech frequencies were seen but when the wire is introduced the screech amplitude increased along the wire as well as normal to the wire. However, the dB content at other frequencies come down at low frequencies. Further, at high frequencies the noise level shows some increase when the wire is introduced.

The far field (R/D = 100) spectra for NPR5 are shown in figures 4.54 to 4.56. For the plain nozzle two screech tones are present also the shock associated noise content is significant. The introduction of wire brings down the screech amplitude from 109 dB to 98 dB along the wire. Also the shock associated and mixing noise is reduced significantly when the wire is introduced. This results in an OASPL reduction of 6.9 dB along the wire. Normal to the wire the screech frequencies are unaffected for the first two harmonics and also the third harmonic is seen. But the shock associated noise and mixing noise get reduced in this plane also. This results in an OASPL reduction of 4 dB.

### 4.1.4 Effect of Cross-wire Diameter

The cross-wire diameter was decided keeping the blockage limit less than 10 %. To have an idea about the effect of cross-wire diameter on aerodynamics and acoustic characteristics of the jet two diameters – 0.8 mm and 0.5 mm were tested. The 0.8 mm gives a blockage of 9.1 % (blockage = wire projected area normal to the jet axis / nozzle exit area) and 0.5 mm corresponds to 5.7 %. The jet centreline decay for NPR2 (overexpansion), NPR4.24 (correctly expanded) and NPRs 6 and 8 (underexpanded) for 0.8 mm and 0.5 mm wire are compared with the plain nozzle in figures 4.57 to 4.60. It is seen that excepting for NPR 2, the 0.8 mm wire results in significant core length reduction and shock strength weakening. Therefore for the rest of the investigation at Mach numbers 1.79 and 2, 0.8 mm wire was used for control.

## 4.2 Characteristics of Mach 1.79 Jet

### 4.2.1 Centreline Decay for Mach 1.79 Jet

The centreline decay of Mach number 1.79 jet at different levels of expansion are shown in figures 4.61 to 4.65. The decay for NPR2 shows no significant reduction in the core length excepting that the pressure level with wire is always lower than that without wire. This is because the presence of the wire generate a detached shock and the flow experiences considerable pressure loss due of the detached shock.

The centreline decay for NPR4 shown in figure 4.62 clearly shows that the shocks in the jet core have been made very weak by the wire. This reduction the shock strength can result in significant reduction of jet noise. The core length reduction achieved is not significant in this case even though the shocks get diffused.

The results for NPR 5.66, i.e. the correctly expanded case shows (figure 4.63) that the wire is effective in diffusing the shocks in the core and also the core length has comedown from 20.5D to 10.5D. The supersonic flow prevailing upto 20D for the plain nozzle as been brought down to just 10D when wire is introduced. This may be considered as a very good aerodynamic advantage in terms of mixing.

The centreline decay for NPR6 which is an underexpanded case is shown in figure 4.64. Here again the strong shocks in the plain nozzle core have been made significantly weaker with the wire introduction. Also, the core has come down from 13.2D to 9.8D.

The centreline decay for NPR8 again an underexpanded condition, is shown in figure 4.65. The strong shocks in the core have significantly diffused by the wire and the core has come down from nearly 11.2D to 10.2D.

The cross plot of percentage reduction of core length with NPR is shown in figure 4.66. It is interesting to note that, for the overexpanded case the core length reduction is not influenced by NPR. The maximum core length reduction is at correct expansion. For underexpanded condition also the core length reduction comes down with increase of NPR.

### 4.2.2 Jet Flow Development for Mach 1.79 Jet

The flow developments for jets from plain nozzle and nozzle with wire for Mach number 1.79 at NPR2 for different X/D from 0 to 30 are shown in figures 4.67 to 4.77, in the form of isobars. From these results it is evident that, compared to plain nozzle, for the wired nozzle mixing become active right from X/D = 0. As seen in figure 4.68, the mixing initiated by the wire at X/D = 0 has spread throughout the jet cross section as early as X/D = 1. Further as seen from the isobar in figure 4.70, the jet growth is substantial in all directions and hence there is no possibility of axis switching for this case in the near field. The mixing activity is hectic upto X/D = 30 and there seems to be some kind of axis switching around X/D = 30. The active mixing process prevailing throughout the jet cross section is the cause for shock strength diffusion in the jet core for the wired jets.

The isobar contours for jets from plain nozzle and wired nozzles for NPR4 at different X/D are compared in figures 4.78 to 4.82. At NPR4, the mixing initiated by the wire spreads faster compare to NPR2 as seen in the figure 4.78. At X/D = 1, it is seen from figure 4.78 that at the jet centre 90 % of the exit pressure for plain nozzle become 60 % for the wired nozzle. Also, there are different pressure levels across the wired jet. This can be regarded as an active mixing activity.

Figures 4.83 to 4.90 shows the isobars for correctly expanded jets at NPR5.66. Compared to NPR4, the isobars for the correctly expanded wired jet spreads faster. The plain nozzle growth is much slower compared to the wired nozzle. The wired jet behaves like an elliptical jet and exhibits an axis switching at X/D = 15. Whereas, the growth of the plain nozzle jet is much slower. This rapid growth of the wired jet resulted in drastic reduction in the core length, as seen from figure 4.63.

The isobars for underexpanded jet at NPR6 are shown in figures 4.91 to 4.96. It is interesting to see that, the mixing initiated by the wire in the horizontal plane at the jet axis is pushed to the jet periphery even at X/D = 0. So this makes the advantage we can derive with the wire introduction gets reduced, i.e. inspite of the wire introduction the mixing growth is taking place from the jet periphery to the axis as in the case of plain nozzle, because of this even though the wire makes the jet to behave like a non-circular

jet, the advantage derived is not much as in the case of correctly expanded jet. For this case also there is an axis switching around 15D.

The isobars for underexpanded jet with NPR8 are given in figures 4.97 to 4.104. Here again the introduction of wire makes the jet to behave something similar to NPR6 and an axis switching is experiences somewhere between X/D = 15 to 20.

### 4.2.3 Acoustic Characteristics of Mach 1.79 Jet

The results of the acoustic measurement made for Mach number 1.79 jet at X/D = 0, R/D = 30 and at R/D = 100 and 30 degree orientation are discussed in this section. The results presented in this section are for overexpanded condition. The frequency spectra for plain nozzle and along the wire and normal to wire at X/D = 0 and NPR2 are presented in figures 4.105 to 4.107. It is seen from these results that, the introduction of the wire results in increase of amplitude of shock associated noise both along and normal to the wire compared to the plain nozzle. A probable reason for this may be that the detached shock generated by the wire is contributing to the shock associated noise. However, from the spectral content it is evident that the introduction of wire results in reduction of overall sound pressure level.

The frequency spectra for NPR2 at R/D = 100, for plain nozzle and wired nozzle are shown in figures 4.108 to 4.110. For the plain nozzle case there is a screech at around 6kHz frequency. The amplitude peak seen at 47 kHz frequency may be due to some flow separation at the nozzle exit. The introduction of the wire reduces the screech amplitude from 90 dB to about 82 dB, as seen from figure 4.109, along the wire. However, the amplitude peak at the higher frequency has gone up by 5 dB. The spectrum normal to the wire shows that the screech is completely suppressed in this direction, however, the shock associated noise has taken a wider band of frequency. As seen from these spectra, the introduction of wire resulted in an OASPL reduction of 4.8 dB along the wire and 8.9 dB normal to the wire, which is a substantial reduction.

Similar results for NPR3 are presented in figures 4.111 to 4.113 for X/D = 0. It is interesting to note that, the screech present for the plain nozzle is completely suppressed by the wire introduction. Also, there is a significant reduction in the amplitude at all frequency levels when wire is introduced.

The frequency spectra for R/D =100 at NPR3 are shown in figures 4.114 to 4.116. For the plain nozzle there are two screech harmonics and significant broadband shock noise. The introduction of wire completely eliminates the screech and even the shock associated noise amplitude gets reduced significantly. Because of these effect an OASPL reduction of 8.9 dB along the wire and 9 dB normal to the wire were achieved.

The frequency spectra for X/D = 0 and NPR4 for Mach number 1.79 jet (figures 4.117 to 4.119) exhibits screech tones with four harmonics for the plain nozzle. When wire is introduced the screech tone amplitude is reduced significantly along the wire and to some extent normal to the wire. This reduction in screech tone amplitude is reflected in the form of reduction in OASPL in the far field. The spectra of far field noise at R/D = 100 and NPR4 for this jet are given in figures 4.120 to 4.122. In the far field also introduction of wire suppresses the screech amplitude along the wire but normal to the wire the screech tones are not affected by the wire. However, the introduction of the wire results in an OASPL reduction of 5.2 dB along the wire and 3.5 dB normal to the wire, as shown in figure 4.176.

Similar results at NPR5 are presented in figures 4.123 to 4.128. It is interesting to note that the introduction of wire increases the screech amplitude. However, the frequency band of shock associated noise become narrower with the introduction of the wire. This results in an OASPL reduction of 4.2 dB along the wire and 3.2 dB normal to the wire as shown in figure 4.176.

## 4.3 Characteristics of Mach 2 Jet

### 4.3.1 Centreline Decay for Mach 2 Jet

The centreline decay and flow development for three NPRs corresponding to overexpansion, correct expansion and underexpansion were studied for this jet. The centreline decay for NPR4, which is overexpanded condition, is shown in figure 4.129. It is seen that the shocks in the core have become weaker when the wire is introduced. However, the core length has marginally increased for the wired jet.

The centreline decay for correct expansion (NPR7.82) shows (figure 4.130) significant reduction of shock strength in the jet core due to the introduction of the wire. Here again the core length is not influenced much even though the shocks have been diffused by the wire.

For the underexpanded condition (NPR9), the centreline decay is shown in figure 4.131. For this case also it is seen that the shocks have been made very weak but the core seems to remain the same as that of the plain nozzle.

### 4.3.2 Flow Development for Mach 2 Jet

The isobars for the above discussed jets in section 4.3.1 are presented in figures 4.132 to 4.150.

For overexpanded with NPR4 it is seen that the streamwise vortices introduced by the wire at the central plane along a diameter at the nozzle exit move rapidly towards the jet boundary and results in an axis switching as early as at X/D =1. This rapid mixing introduced by the wire and spread throughout the jet field is responsible for the significant reduction of shock strength. After axis switching at X/D = 1 the wired jet grows like a noncircular jet as it moves downstream.

The isobars for the correctly expanded jet are given in figures 4.138 to 4.143. Unlike the overexpanded jet, the introduction of vortices by the cross-wire makes the jet to grow like a noncircular jet right from the nozzle exit. The streamwise vortices introduced at the central plane of the jet are quickly convected to the jet periphery and the mixing activities become rapid near the ends of the major axis, as seen in figure 4.138. For further downstream locations the jet continues to grow as an elliptical jet with mixing activities trying to occupy the entire cross section.

The isobars for the underexpanded condition (NPR9) are shown in figures 4.144 to 4.150. It is interesting to note that unlike other cases discussed the wired jet exhibits two distinct zones as though a twinjet is propagating after merging. This trend continues upto X/D = 3, after that it grows like an elliptical jet. The reason for this kind of behavior may be the following. The underexpanded jet is expanding rapidly away from the centreline because of the strong expansion fans positioned at the nozzle lip. Under this condition when the streamwise vortices were introduced by the wire, they are carried

away by the high inertia streams on either side of the wire moving away from it. Hence, the concentration of increased mixing activity at the extremities of the diameter normal to the wire.

### 4.3.3 Acoustic Characteristics of Mach 2 Jet

To investigate the effect of streamwise vortices introduced by the cross-wire on the acoustic characteristics of a jet which is at the limiting end of the screech prone Mach number, the noise measurements were made for Mach number 2 jet from nozzle with and without wire. Here again like in the case of Mach numbers 1.6 and 1.79 jets, the measurements were made for NPRs 2 to 5 only.

The frequency spectra at X/D = 0 are presented in figures 4.151 to 4.153 for NPR2. No screech tone is observed even for the plain nozzle. The introduction of the wire brings down the mixing noise amplitude at lower frequencies along the wire. However the amplitude of the mixing noise has been enhanced at all frequency levels normal to the wire. This is the direct effect of the convection of the streamwise vortices away from the wire in the direction normal to it.

The frequency spectra for R/D = 100 and NPR2 are given in figures 4.154 to 4.156. It is seen that the shock associated noise amplitude has come down significantly along the wire and marginally normal to the wire. An OASPL reduction of 3.2 dB along the wire and 2.1 dB normal to the wire has been experienced in this case, as shown in figure 4.177.

The frequency spectra at X/D = 0 and NPR3 shown in figures 4.157 to 4.159 exhibit a screech with three harmonics with the second harmonic being that with highest amplitude. The introduction of the wire suppresses the screech completely and the amplitudes at all frequency level come down along the wire, however normal to the wire the amplitudes go up.

The far field (R/D = 100) spectra at NPR3 shown in figures 4.160 to 4.162 shows that the amplitudes of both shock associated and mixing noise come down when wire is introduced. This results in an OASPL reduction of 4 dB along the wire and 4.5 dB normal to the wire, as shown in figure 4.177.

The frequency spectra at X/D = 0 for NPR4 shows four harmonics for the screech for the plain nozzle, as shown in figure 4. 163. Whereas, the screech is completely eliminated by the introduction of the wire as seen from figures 4.164 to 4.165. The carresponding frequency spectra for R/D = 100 shown in figures 4.166 to 4.168, shows a screech tone for the plain nozzle. Whereas, the screech is completely eliminated along the wire and screech amplitude is reduced from 102 dB to 88 dB normal to the wire. The amplitude of the shock associated noise also has been reduced significantly both along the wire and normal to the wire. This is because the shocks have been made significantly weaker by the wire as seen in figure 4.129. An OASPL reduction of 6.1 dB along the wire and 5.9 dB normal to the wire has been achieved for this case.

The frequency spectra for NPR4 at X/D = 0, shown in figures 4.169 to 4.171, show that for the plain nozzle there are three harmonics for the screech. The screech has been completely eliminated by the wire and the amplitudes have come down at all frequency levels along the wire but they have gone up significantly at all frequencies in the direction normal to the wire.

The frequency spectra for R/D = 100 and NPR5 are shown in figures 4.172 to 4.174. It is seen that, the introduction of the wire brings down the amplitude of both shock associated and mixing noises at all frequencies in the directions along and normal to the wire. For this case an OASPL reduction of 6 dB along the wire and 5 dB normal to the wire were achieved

# Chapter 5

## Conclusions

This investigation provided a detailed evaluation of the passive control in the form of cross-wire at nozzle exit on mixing and acoustic characteristics of Mach 1.6, 1.79 and 2 jets from convergent – divergent circular nozzles. The streamwise vortices introduced by the cross-wire was found to weaken the shocks in the jet core significantly. The controlled jets exhibited a drastic reduction in core length compared to uncontrolled jets as high as 48.8% reduction in core length was achieved for M=1.79 at NPR5.66. At all Mach numbers the mixing enhancement did exhibit a direct relationship to the noise suppression – i.e. better mixing did produce lower noise. The observation is explained by noting that the cross-wire suppressed the screech and promoted mixing, thereby resulting in reduced OASPL (Over all sound pressure level). Screech tones frequencies were altered and amplitude were significantly reduced by the presence of streamwise vortices across the jet at nozzle exit. The control in the form of cross-wire was found effective even for jets with adverse pressure gradient –overexpanded jets.

## Suggestions for further Work

1. The cross-wire tested in the present study is circular. Since it is meant for vortex generation, a flat wire may proved to be better than a circular one.
2. Similar studies with higher Mach number will be of use to many applications.
3. Similar studies with high temperature jet will be of use.
4. The directivity of jet noise will give better understanding of the control.

# Bibliography


[1] Abramovich G N, 1963,The Theory of Turbulent Jets.M.I.T.press,MA, USA

[2] Pai S, 1954, Fluid Dynamics of Jets. Van Nostrand, New York.

[3] Rajaratnam N, 1976, Turbulent Jets. Elsevier Sci. Publishing. Co. , Netherlands.

[4] Schlichting H, 1959, Boundary Layer Theory, McGraw Hill, New York.

[5] Batchelor G K, 1967, An Introduction to Fluid Mechanics. Cambridge University Press, England

[6] Gutmark E, Schadow K C, Parr T P, Hanson-Parr D M and Wilson K J, 1989, "Noncircular Jets in Combustion Systems", Experiments in Fluids, Vol. 7, pp. 248-258.

[7] Hussain F and Hussain H S 1991, "Elliptic Jets. Part-I: Characteristics of Unexcited and Excited Jets,"*Journal of Fluid Mechanics*, Vol. 233, pp. 439-482.

[8] Sforza M P Steiger M H and Trentacoste N 1966, "Studies in Three-Dimensional Viscous Jets,"*AIAA Journal*, Vol. 4, No. 5,pp. 800-806.

[9] Ho C M and Gutmark E 1987, "Vortex Introduction and Mass Entrainment in a Small-Aspect Ratio Elliptic Jet," *Journal of Fluid Mechanics*, Vol. 179, pp.383-405

[10] Powell A, 1953, "On the Mechanism of Choked Jet Noise", pps, Vol. 66 B, pp. 1039-1056.

[11] Powell A, 1953, "On the Noise Emanating from a Two-Dimensional Jet Above the Critical Pressure", The Aeronautical Quarterly, Vol. IV , pp. 103-122.

[12] Glass D R, 1968, "Effects of Acoustic Feedback on the Spread and Decay of Supersonic Jets", *AIAA Journal*, Vol. 6, No. 10, pp. 1890-1897.

[13] Krothapalli A Hsia Y Baganoff D and Karamcheti K 1986,"The Role of Screech Tones in Mixing of an Underexpanded Rectangular Jet", *Journal of Sound and Vibration*, Vol. 106, No. 1, pp. 119-143.

[14] Rice E J and Raman G, 1993, "Supersonic Jets from Beveled Rectangular Nozzles", ASME Paper 93-WA/NCA-26.

[15] Rathakrishnan E, 1995, Gas Dynamics, Prentice-Hall of India Pvt. Ltd., New Delhi.

[16] Lighthill M J 1963, "Jet Noise," *AIAA Journal*, Vol. 1, No. 7, pp. 1507-1517.

[17] Ffowcs Williams J E 1977, "Aeroacoustics", *Annual Review of Fluid Mechanics*, Vol. 9, pp 447-468.

[18] Crighton D G 1975, "Basic Principles of Aerodynamic Noise Generation," *Progress in Aerospace Sciences*, Vol. 16, pp. 31-96.

[19] Tam C K W 1995, "Supersonic Jet Noise," *Annual Review of Fluid Mechanics,* Vol. 27, pp. 17-43.

[20] Lighthill M J , 1952, "On Sound Generated Aerodynamically. I. General Theory," *Proc. Royal Soc. Of London*, Vol. A211. pp. 564-587.

[21] Dowling A P and Ffowcs Williams J E, 1983, *Sound and Sources of Sound.* Ellis Horwood Ltd., John Wiley and Sons.

[22] Tanna H K, 1977, "An Experimental Study of Jet Noise Part I : Turbulent Mixing Noise", *Journal of Sound and Vibration*, 50(3), pp. 405-428.

[23] Tam C K W and Chen P, 1994, "Turbulent Mixing Noise from Supersonic Jets", *AIAA Journal*, Vol. 32, No. 9, pp. 1774-1780.

[24] Tam C K W, 1975, "Supersonic Jet Noise Generated by Large-Scale Disturbances", *Journal of Sound and Vibration*, Vol. 38, pp. 51-79.

[25] Tanna H K, 1977, "An Experimental Study of Jet Noise : Shock Associated Noise", *Journal of Sound and Vibration*, 50(3), pp. 429-444.

[26] Tam C K W and Tanna H K, 1982, "Shock Associated Noise of Supersonic Jets from Convergent-Divergent Nozzles", *Journal of Sound and Vibration*, Vol. 81, No. 3, pp. 337-358.

[27] Tam C K W, Chen P and Seiner J M, 1992, "Relationship Between Instability Waves and Noise of High Speed Jets", *AIAA Journal*, Vol. 30, No. 7, pp. 1747-1752.

[28] Tam C K W, Seiner J M and Yu J C, 1986, "Proposed Relationship Between Broadband Shock Associated Noise and Screech Tones", *Journal of Sound and Vibration*, Vol. 110, pp. 309-321.

[29] Tam C K W , Shen H and Raman G, 1997, "Screech Tones of Supersonic Jets from Beveled Rectangular Nozzles", *AIAA Journal*, Vol. 35, No. 7, pp. 1119-1125.

[30] K.B.M.Q. Zaman, M.F. Reeder, and M. Samimy, ``Control of an axisymmetric jet using vortex generators," Phys. fluids A 6 p 778 (1993).

[31] L.J.S. Bradbury and A.H. Khadem, ``The distortion of a jet by tabs," *J. Fluid Mech.* Vol. 70, pp 801-813 (1975).

[32] K.B.M.Q. Zaman, "Streamwise vorticity generation and mixing enhancement in free jet by "Delta-Tabs," AIAA 93-3253 (1993).

[33] K.K. Ahuja, ``Mixing enhancement and jet noise reduction through tabs plus ejector," AIAA 93-4347 (1993).

[34] .W.J. Gretta and C.R. Smith, ``The flow structure and statistics of a passive mixing," *J. of Fluid Engineering.* Vol 115, p 255 (1993).

[35] . D. Liepmann and M. Gharib, ``The role of streamwise vorticity in the near-field entrainment of round jets," *J. of Fluid Mechanics*, Vol. 245, pp 643-668 (1992).

[36]Navin Kumar Singh and Rathakrishnan., `` Effect of Tab Geometry on Sonic Jet Characteristics" accepted in 22nd International Symposium on Space Technology and Science, Morioka, Japan, May 28-June 3, 2000.

[37] K.B.M.Q. Zaman, M.F. Reeder and M. Samimy, ``Control of an axisymmetric jet using vortex generators, "Phys. Fluid, Vol. 6, No. 2 p 778 (1994).

[38] K.B.M.Q. Zaman, M.F. Reeder and M. Samimy, ``Effect of Tab Geometry on the flow and noise field of an Axisymmetric jet", AIAA Journal,Vol.31,No.4,pp609-619(1993).

[39] Norum TD, "Screech Suppression in Supersonic Jets", AIAA Journal 21, pp235-240(1983)

[40] Rathakrishnan E, "Instrumentation, Measurements and Experiments in Fluids". Book to be published.

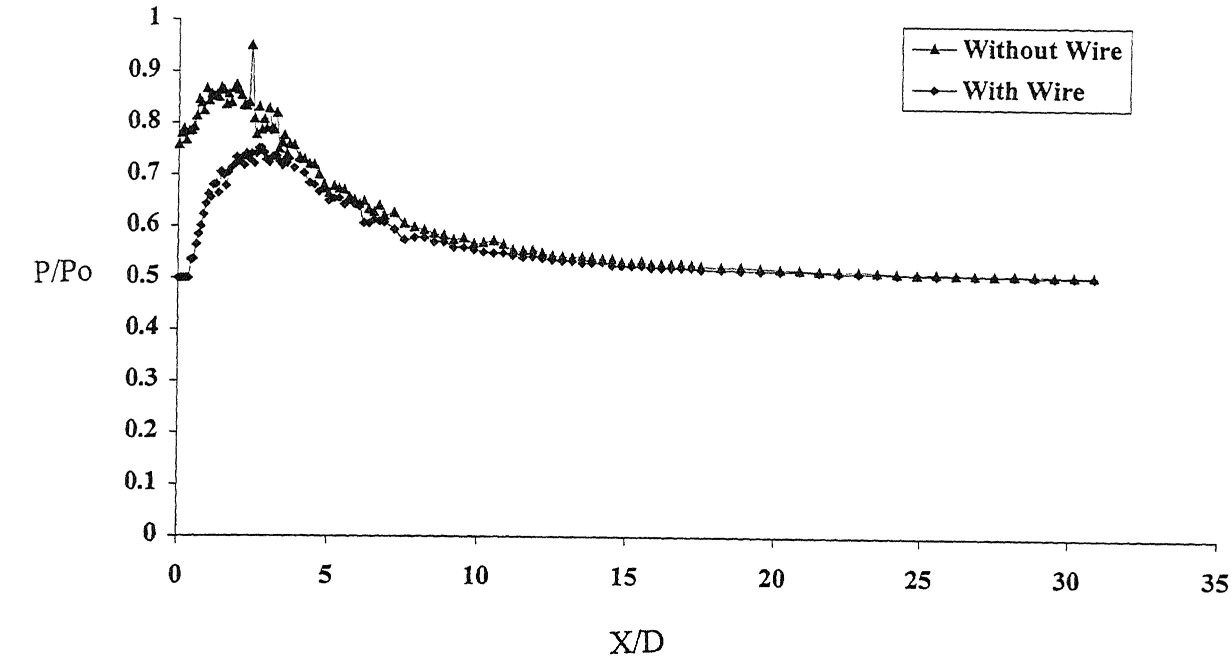


Figure 4.1 Centreline decay (M=1.6, NPR 2, Overexpansion)

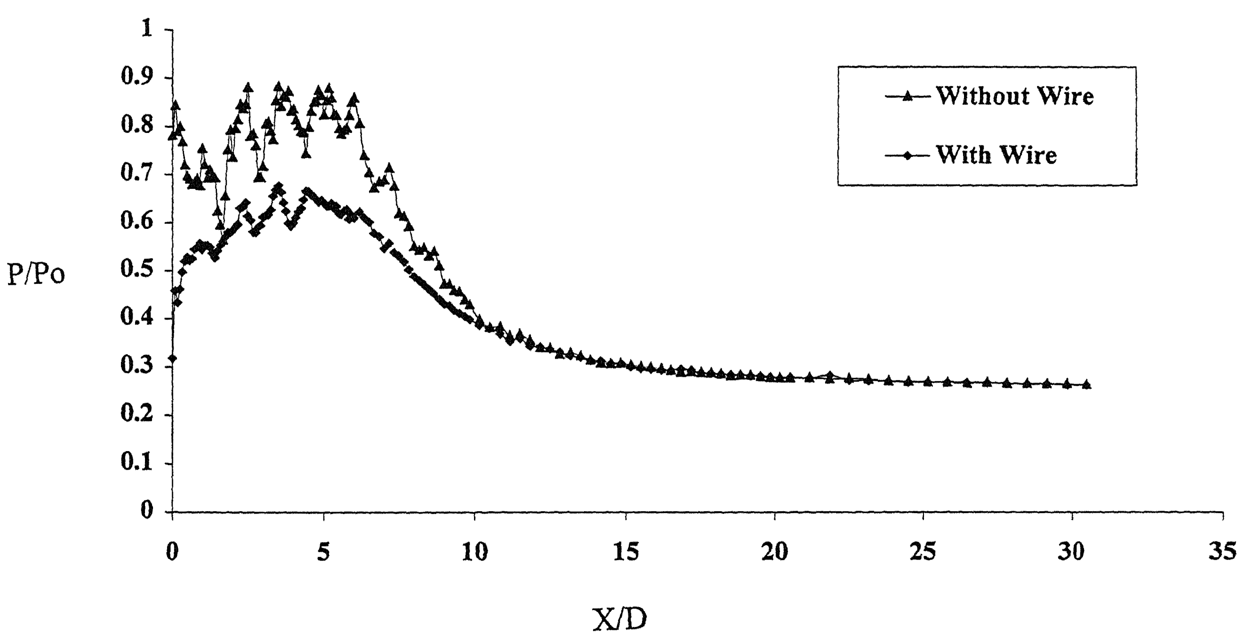


Figure 4.2 Centreline decay (M=1.6, NPR 4, Overexpansion)

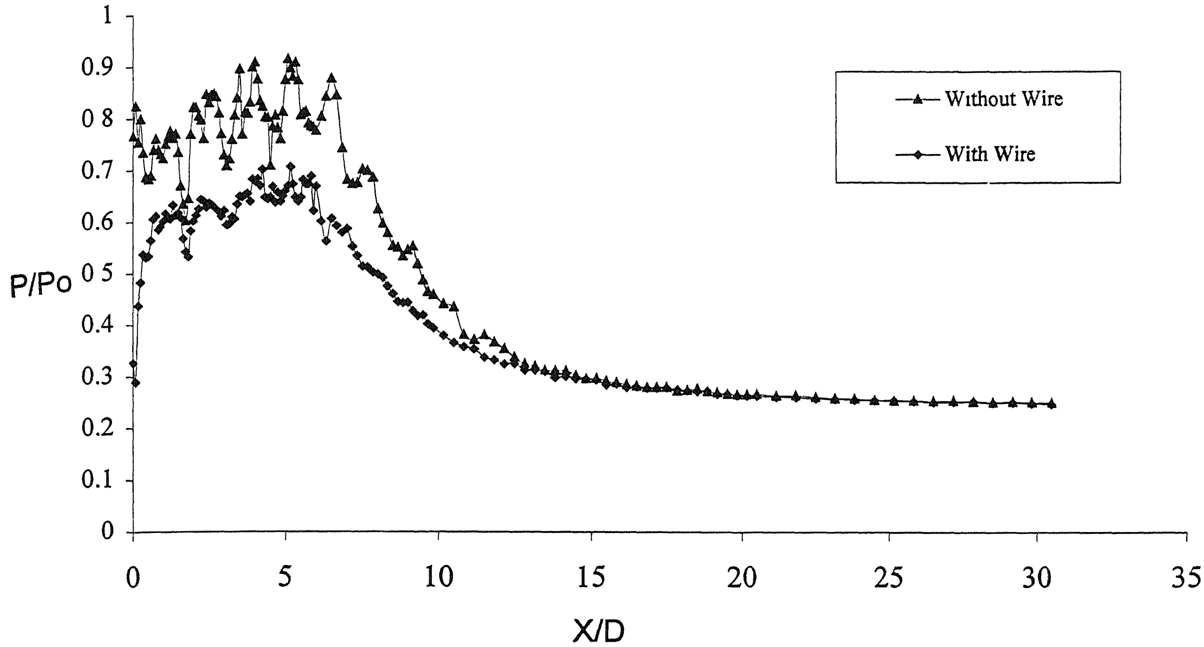


Figure 4.3 Centreline decay (M=1.6, NPR 4.24, Correct expansion)

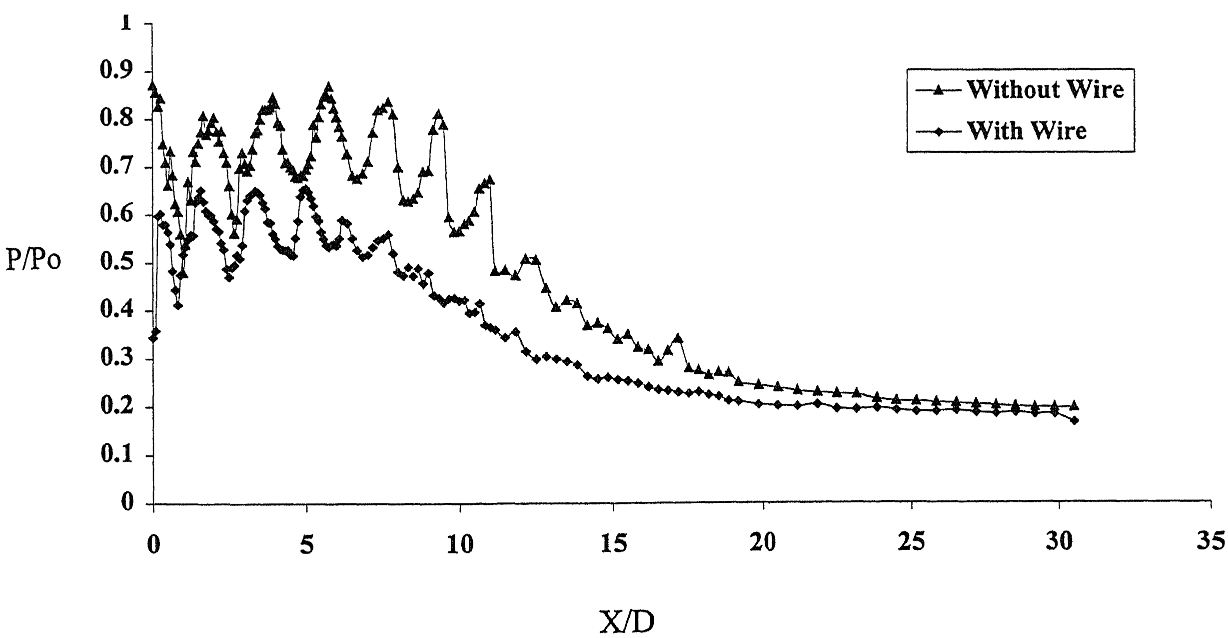


Figure 4.4 Centreline decay (M=1.6, NPR 6, Underexpansion)

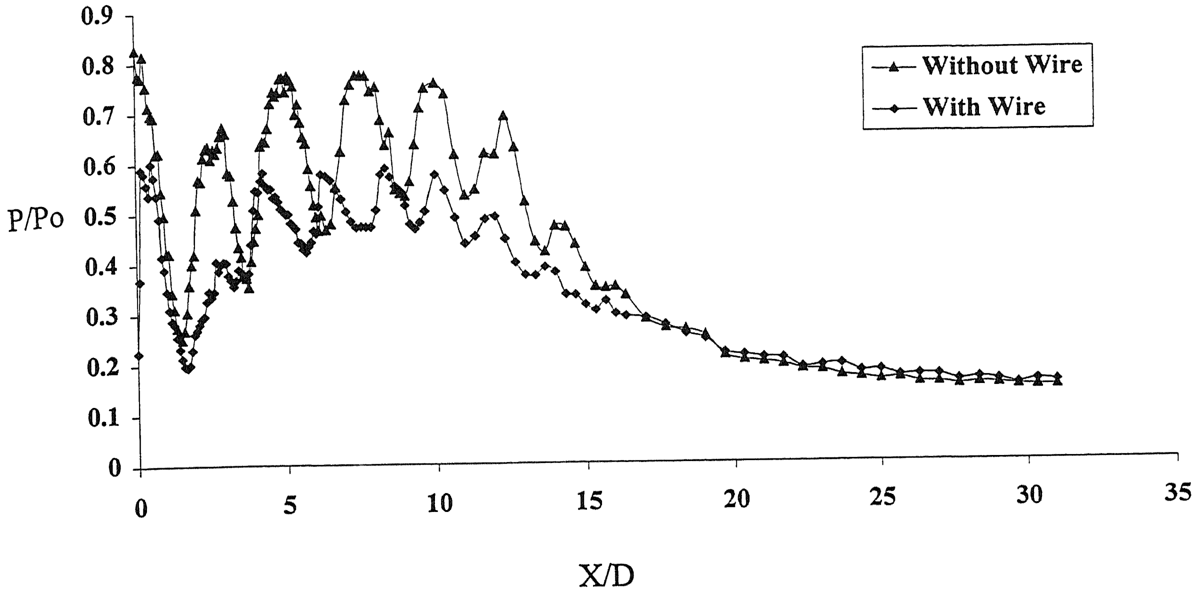


Figure 4.5 Centreline decay (M=1.6, NPR 8, Underexpansion)

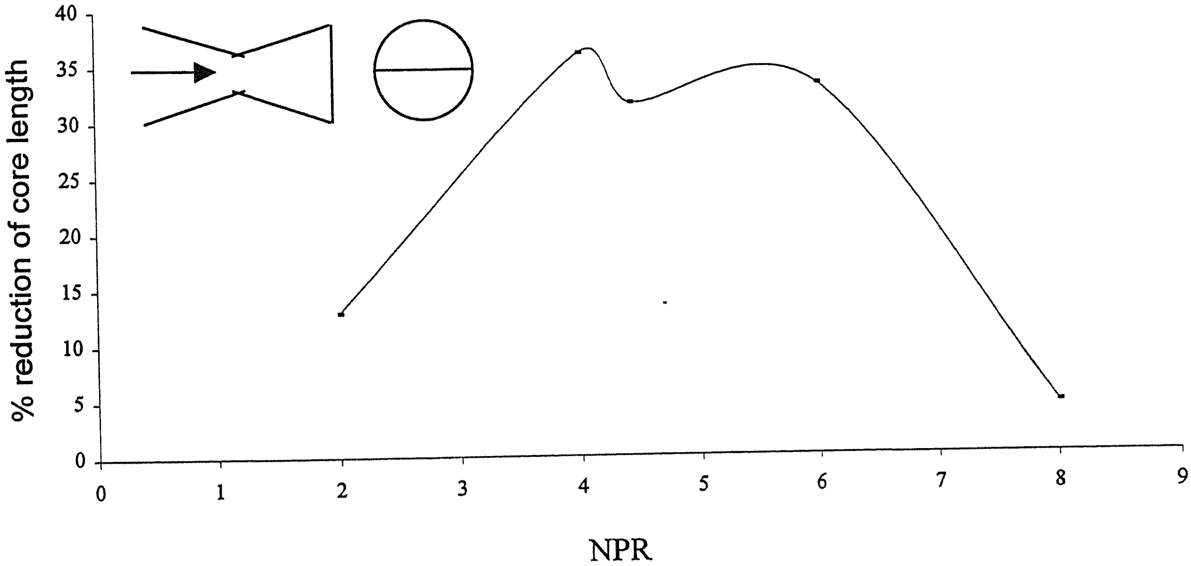


Figure 4.6 Percentage reduction in core length with NPR ( M=1.6)

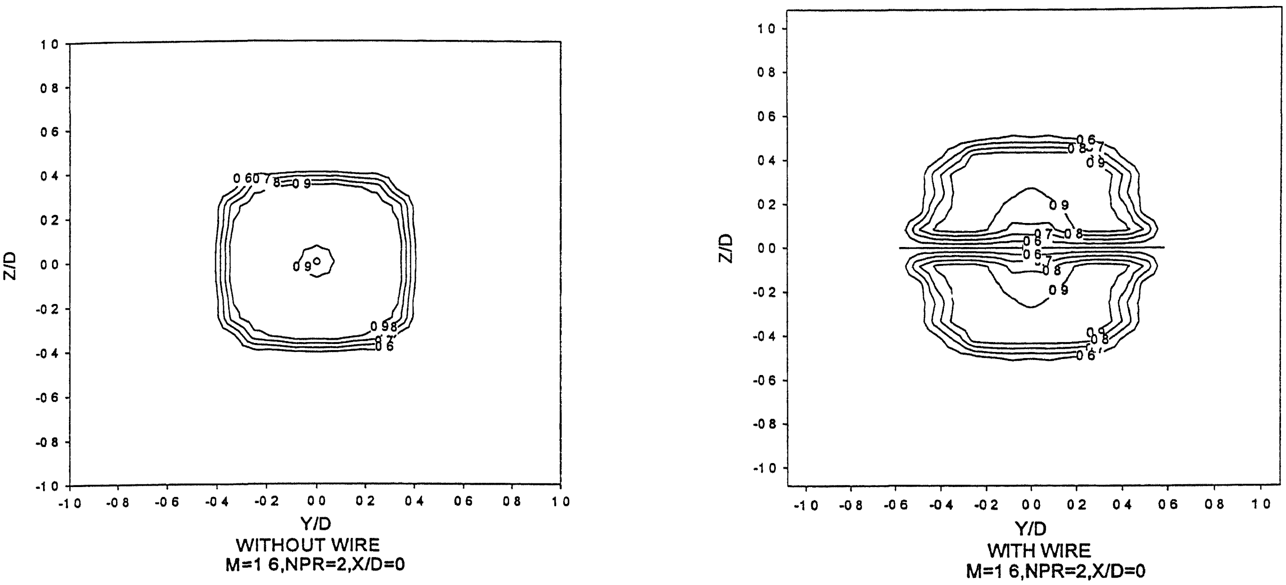


Figure 4.7

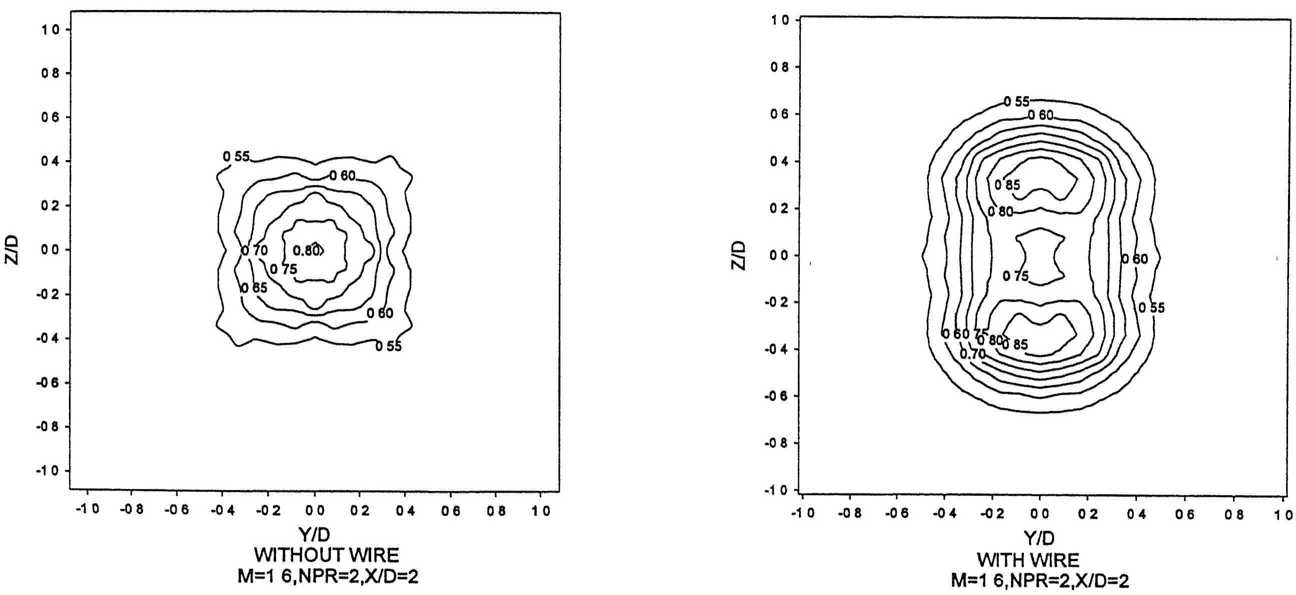


Figure 4.8

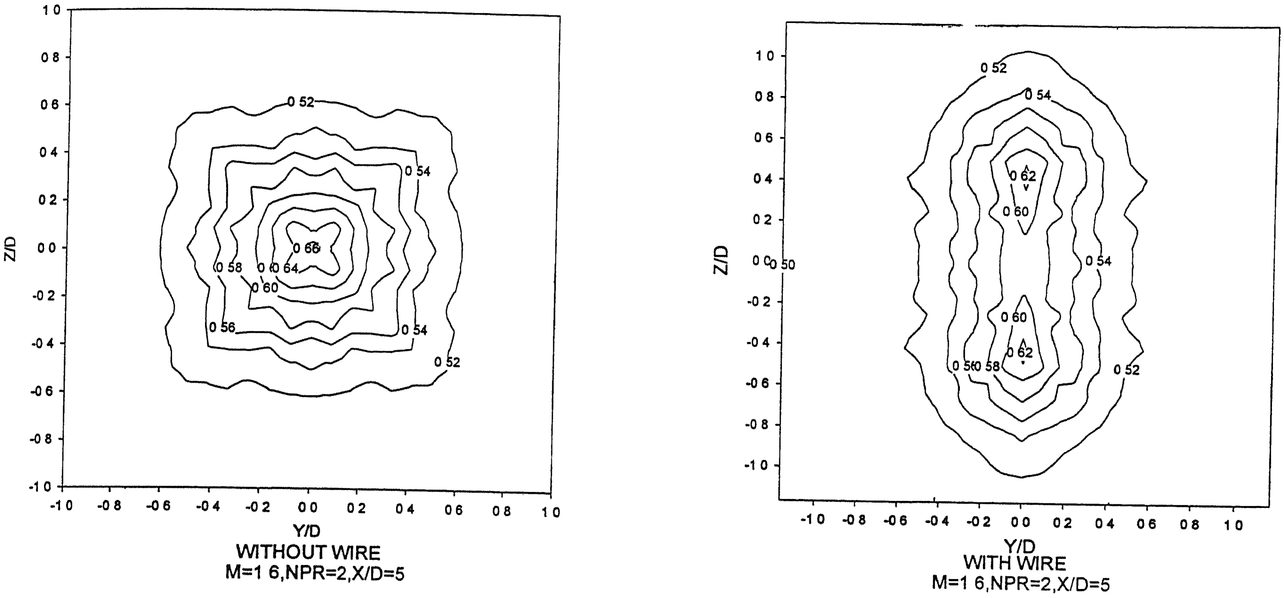


Figure 4.9

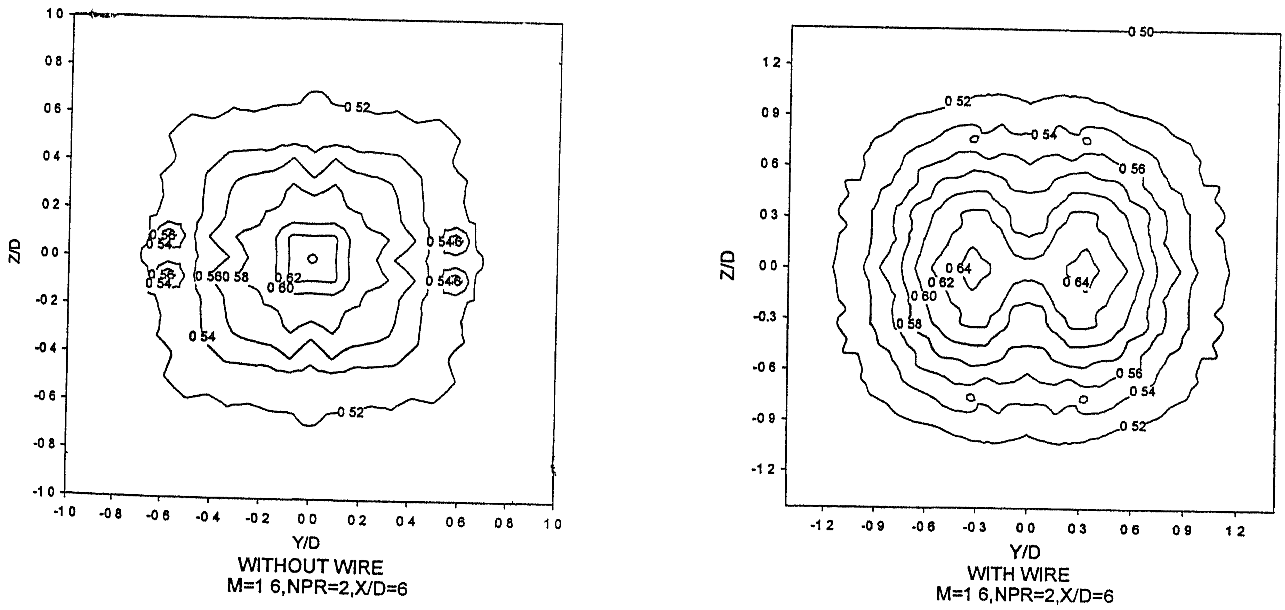


Figure 4.10

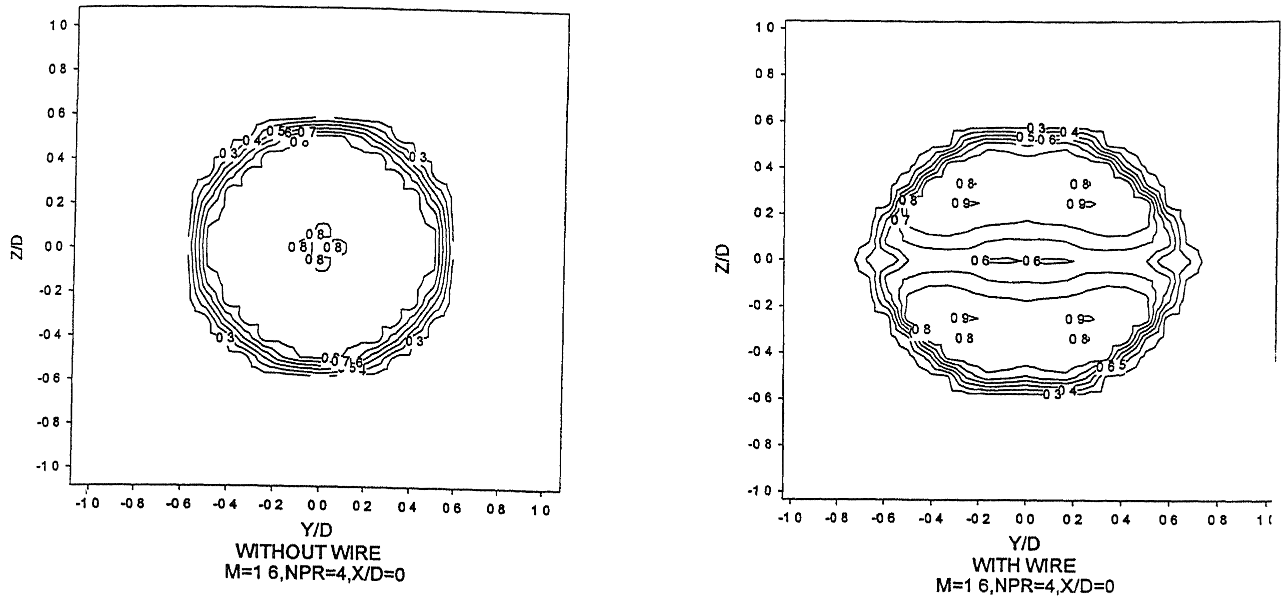


Figure 4.11

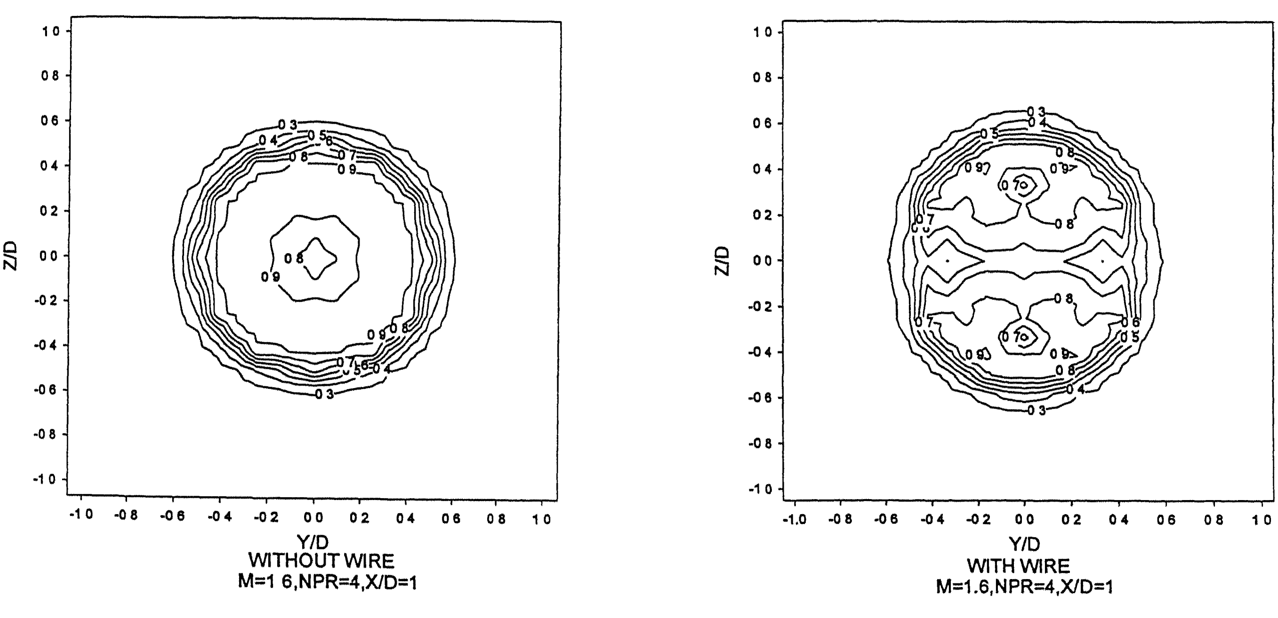


Figure 4.12

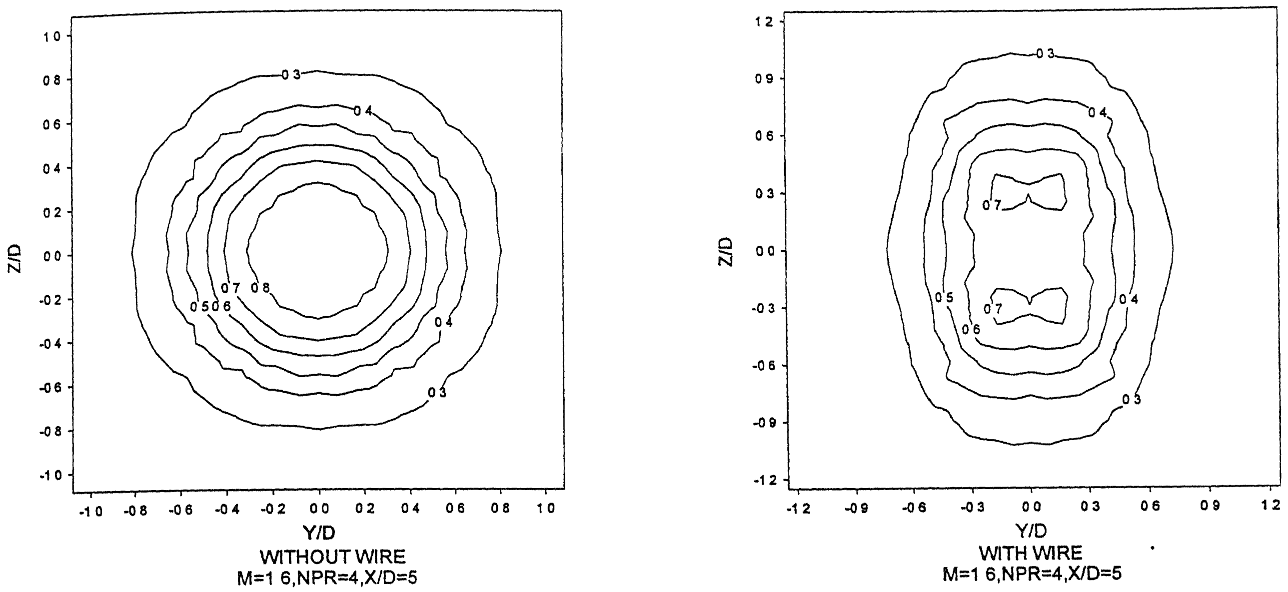


Figure 4.13

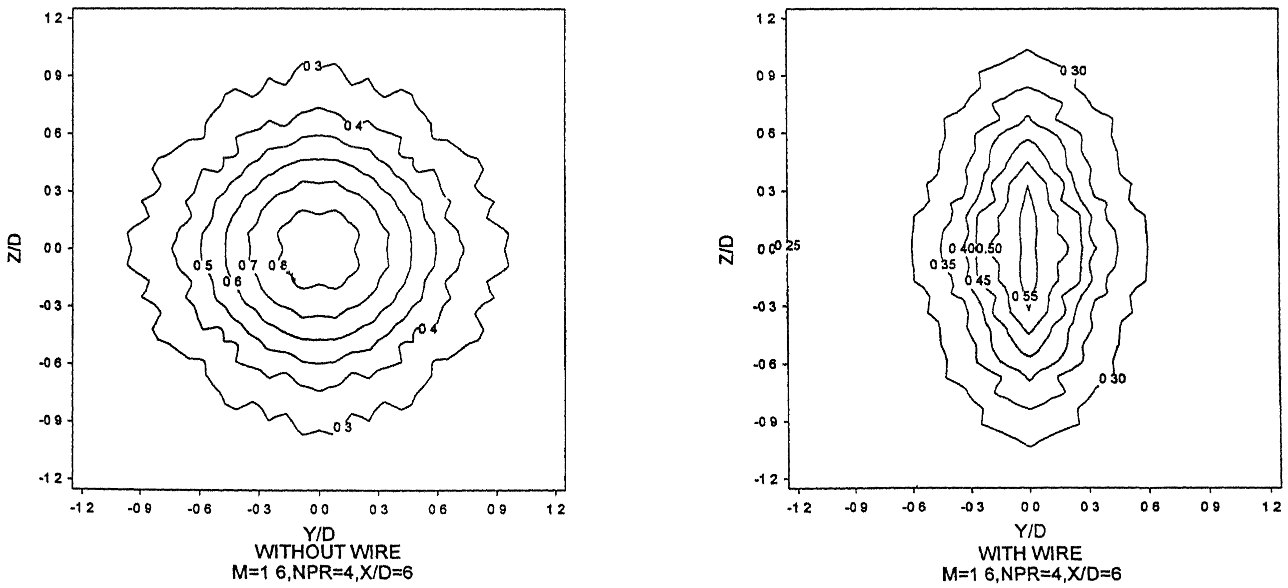


Figure 4.14

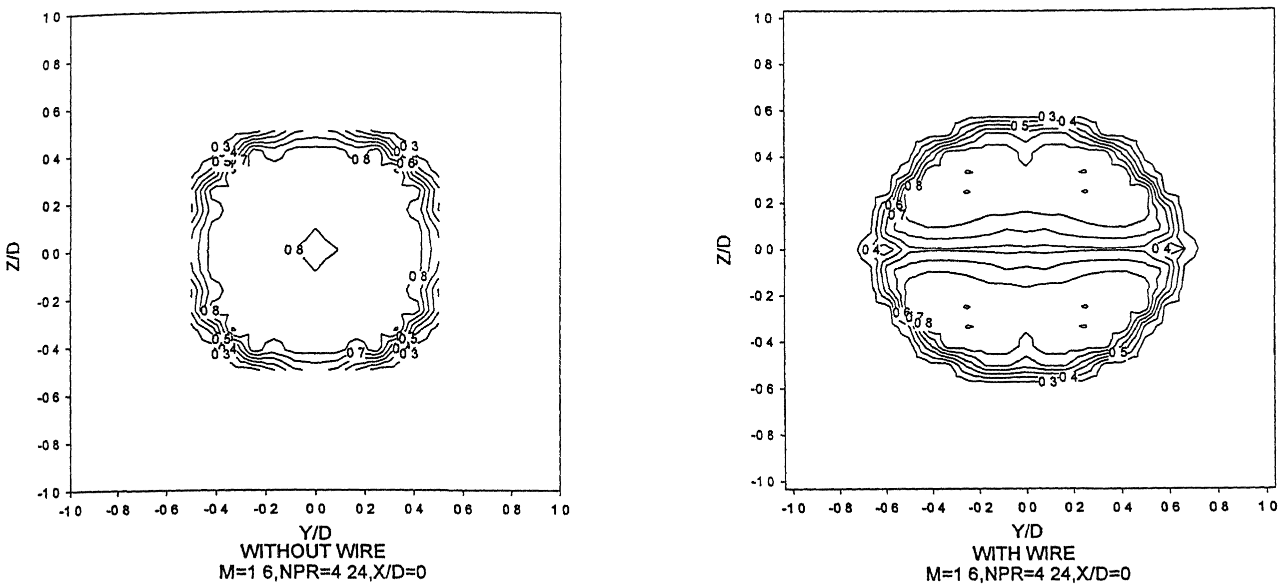


Figure 4.15

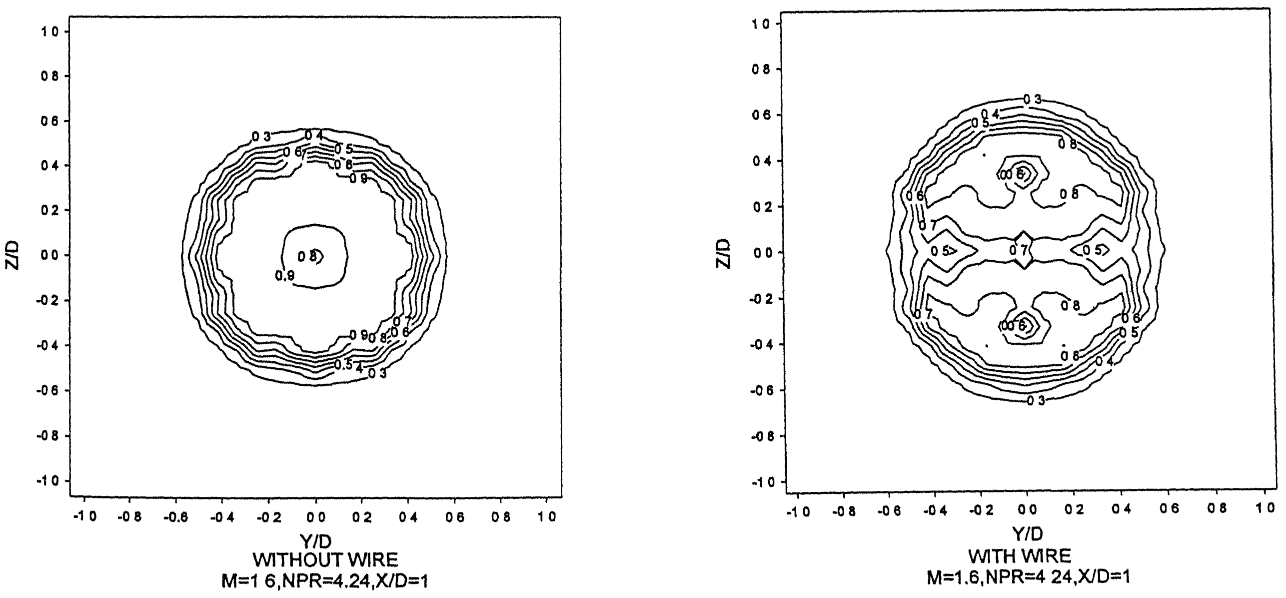


Figure 4.16

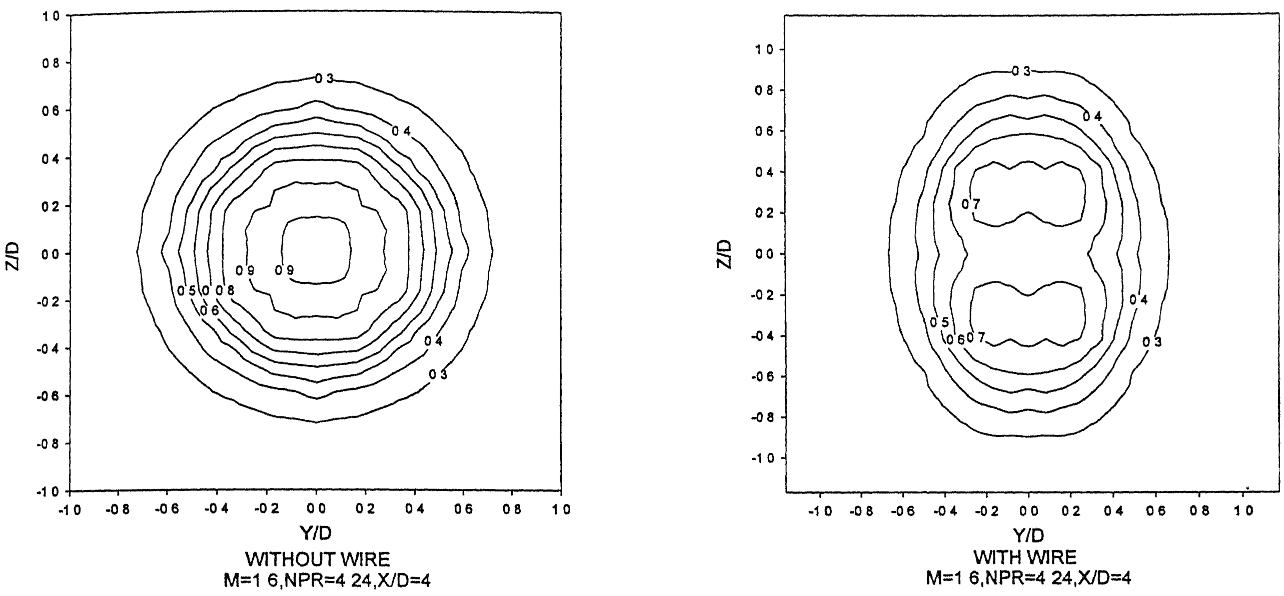


Figure 4.17

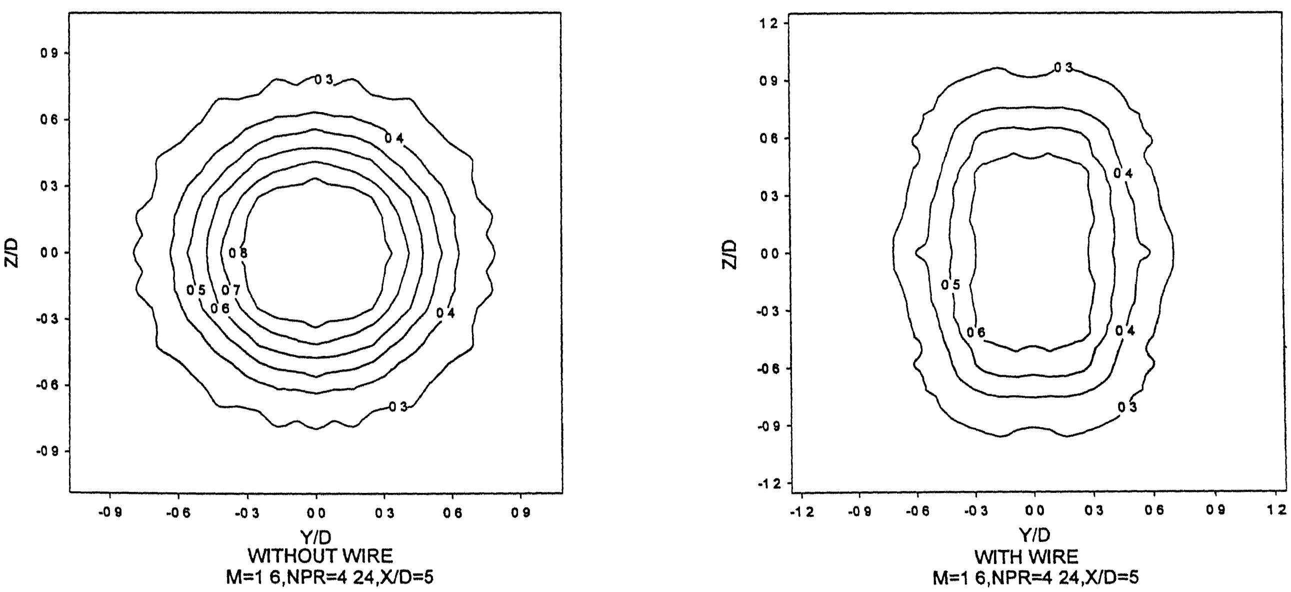


Figure 4.18

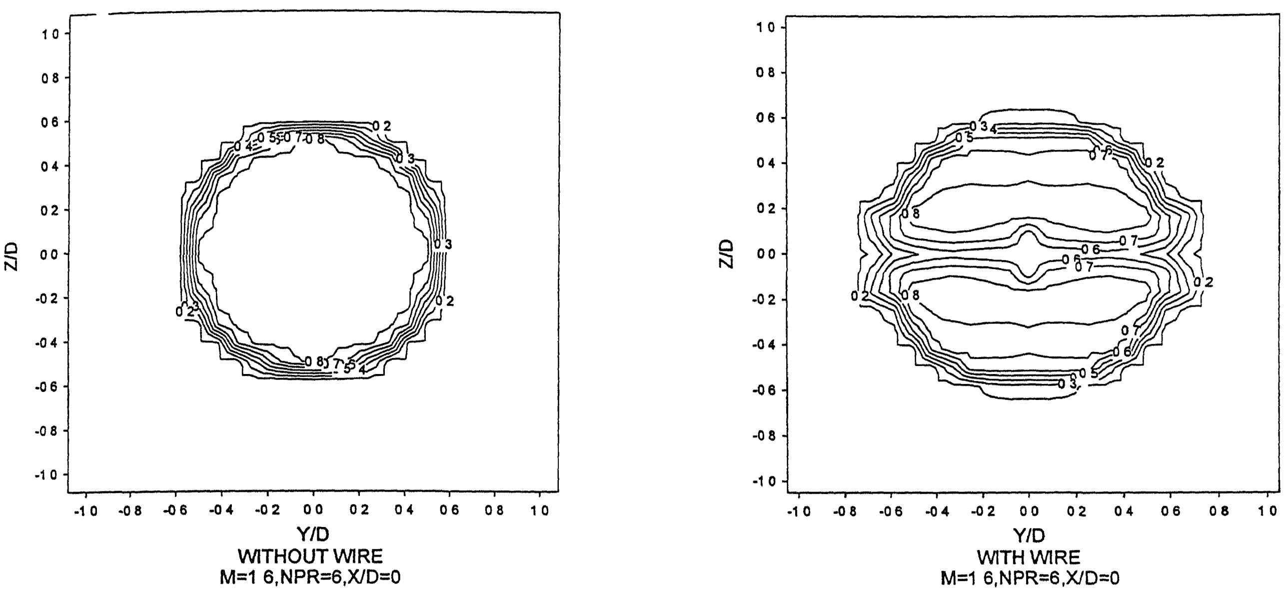


Figure 4.19

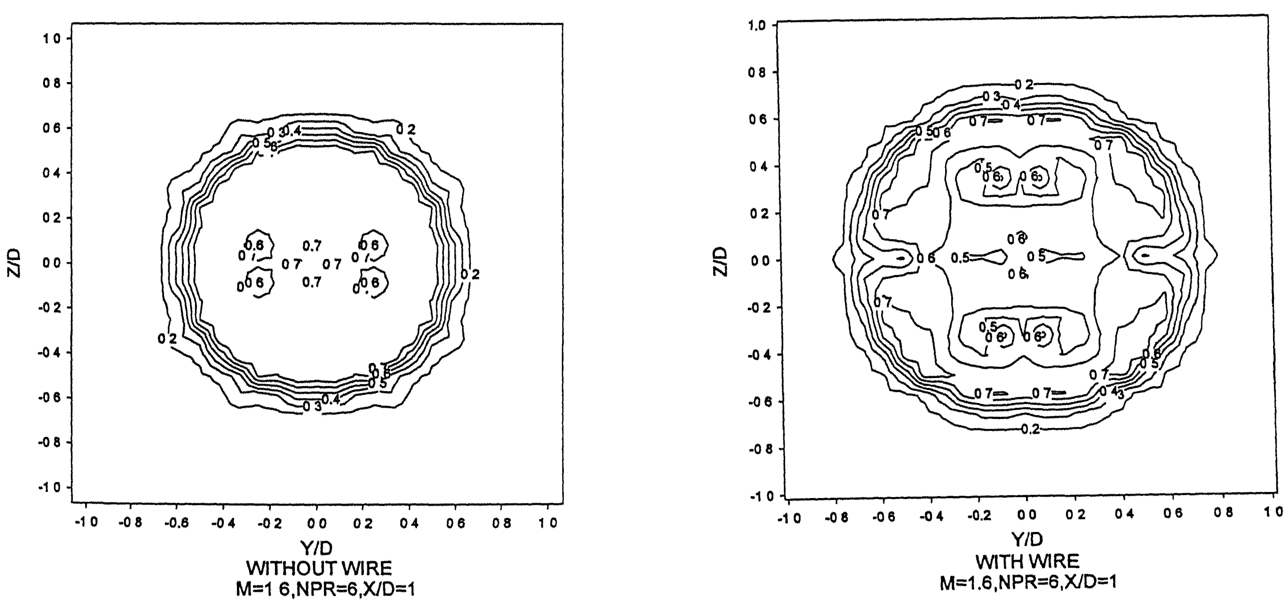


Figure 4.20

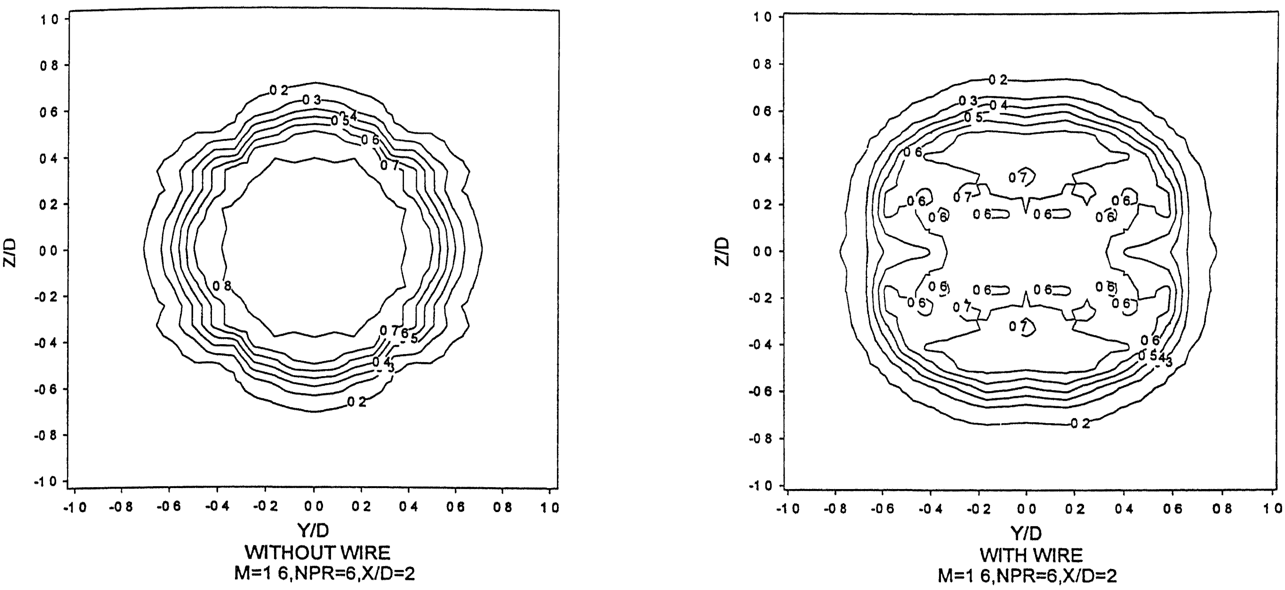


Figure 4.21

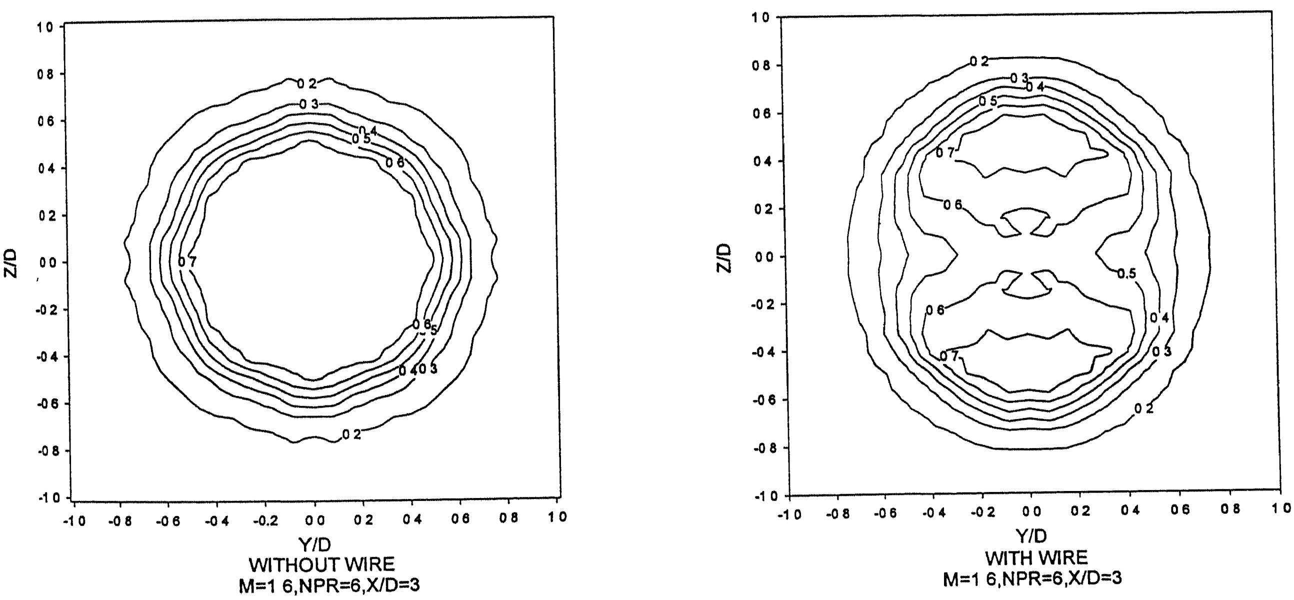


Figure 4.22

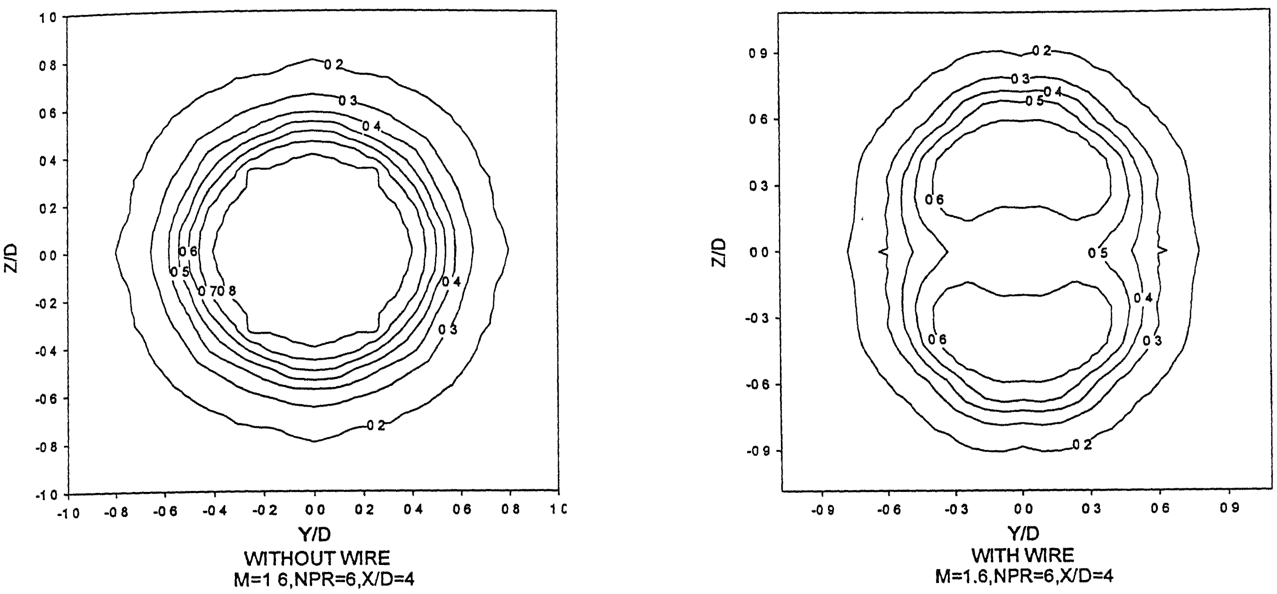


Figure 4.23

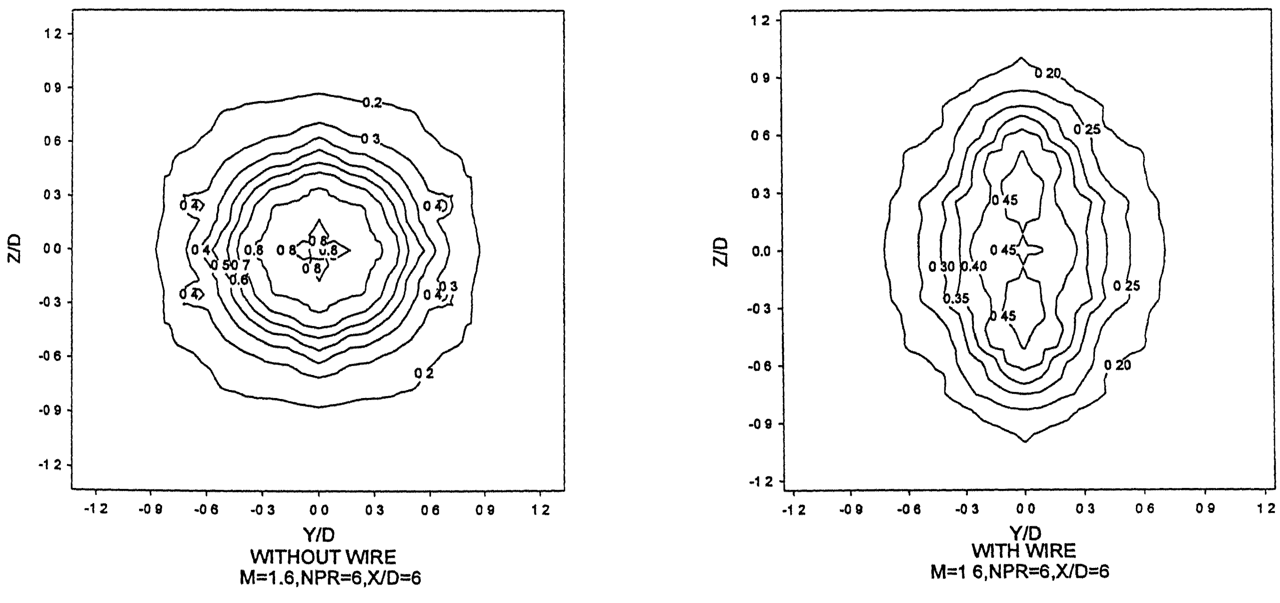


Figure 4.24

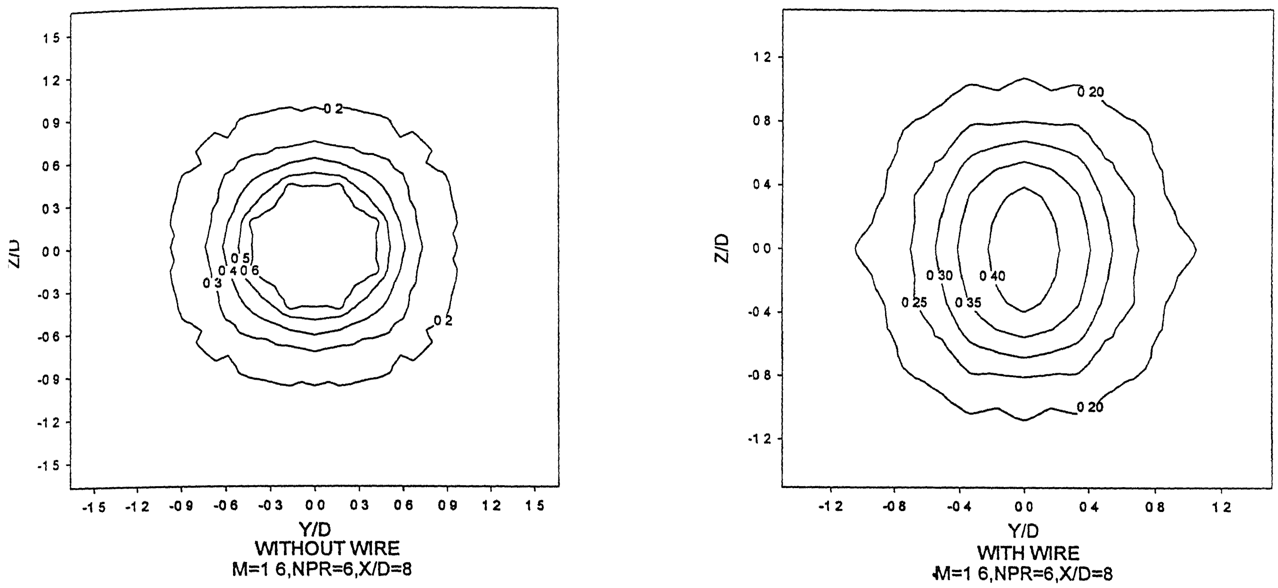


Figure 4.25

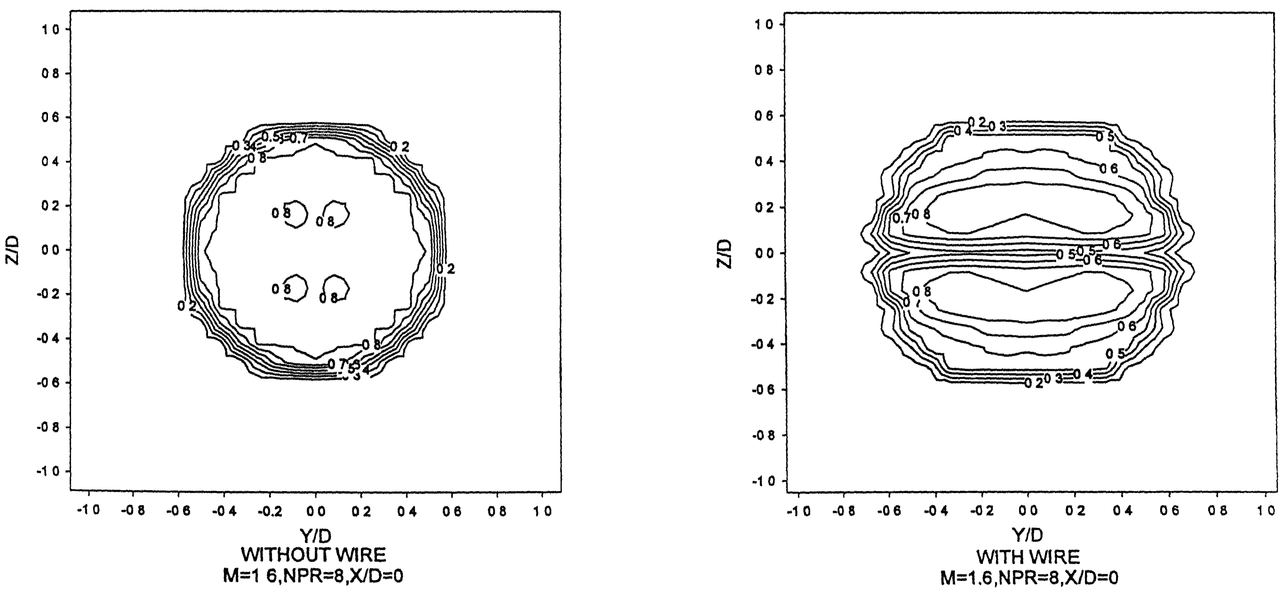


Figure 4.26

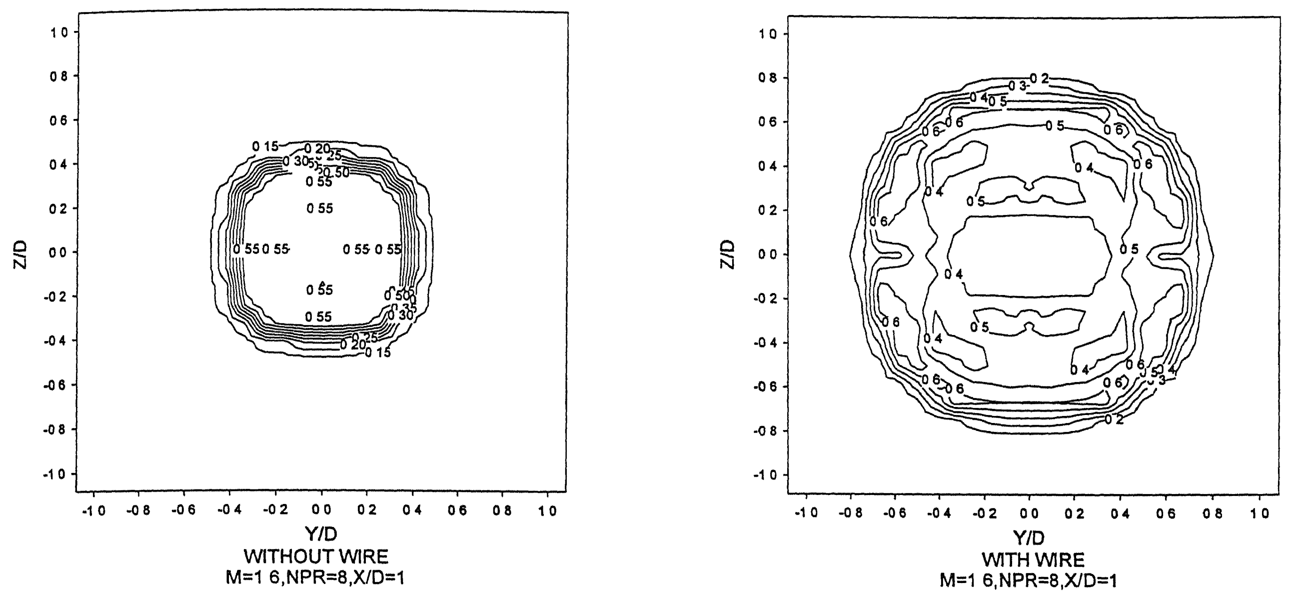


Figure 4.27

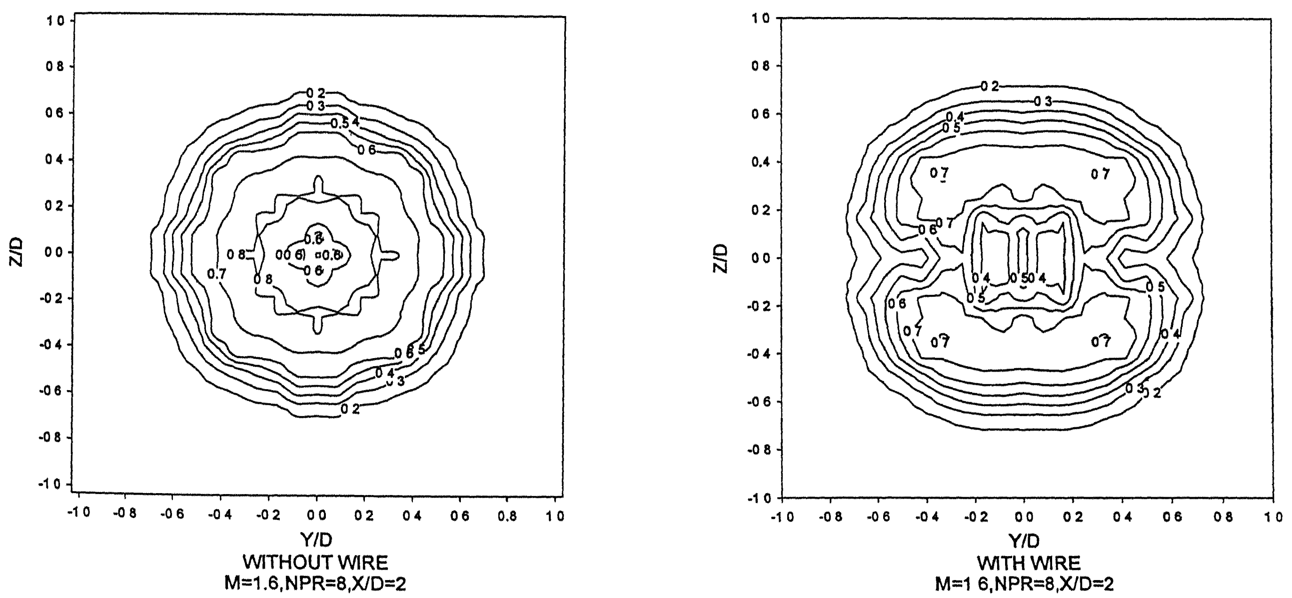


Figure 4.28

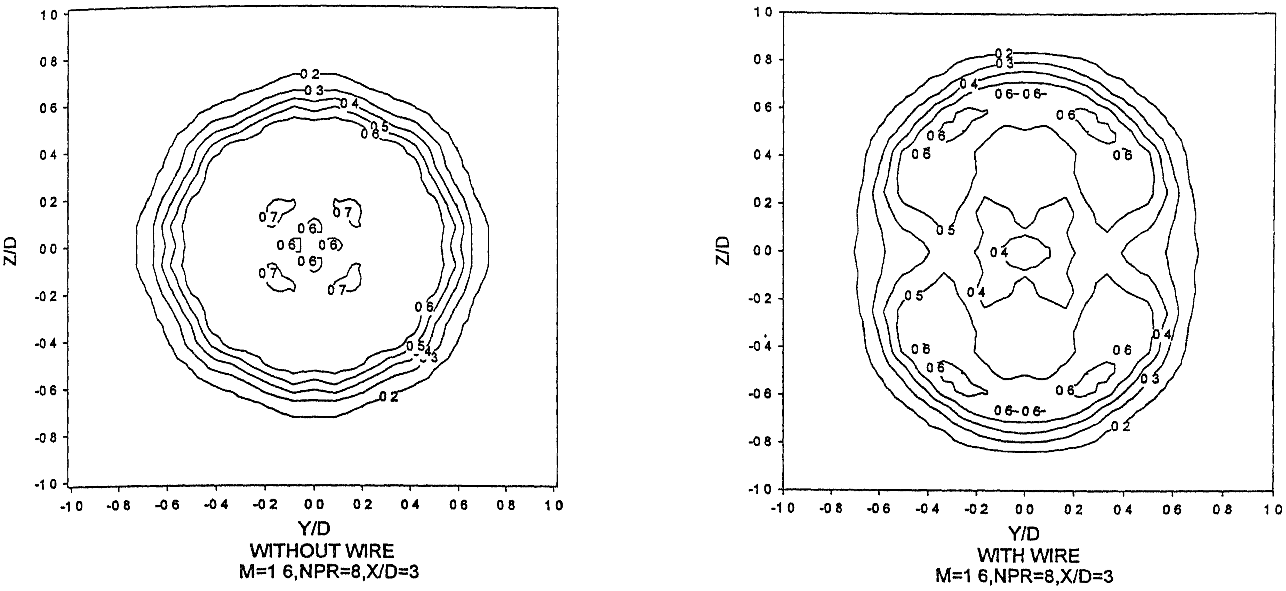


Figure 4.29

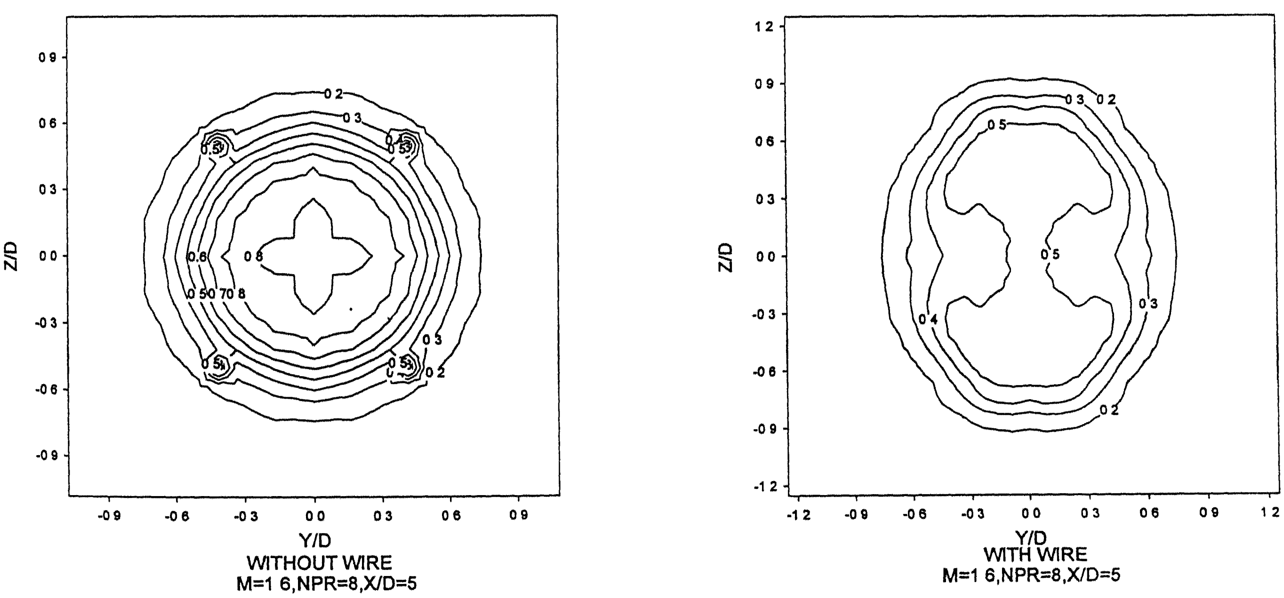


Figure 4.30

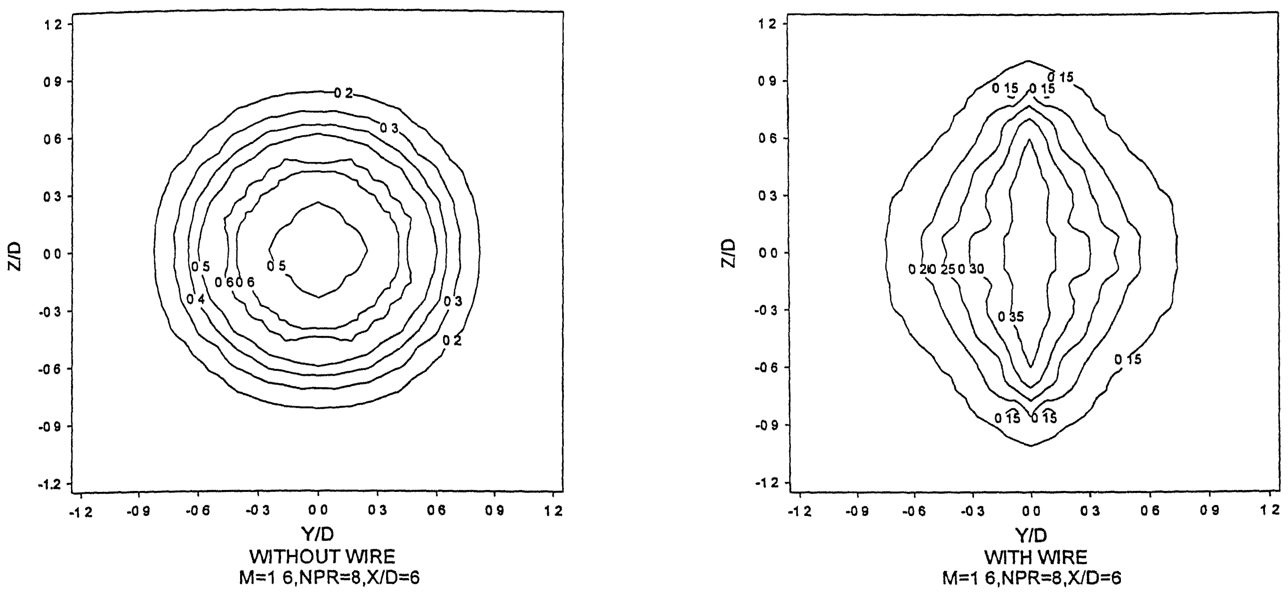


Figure 4.31

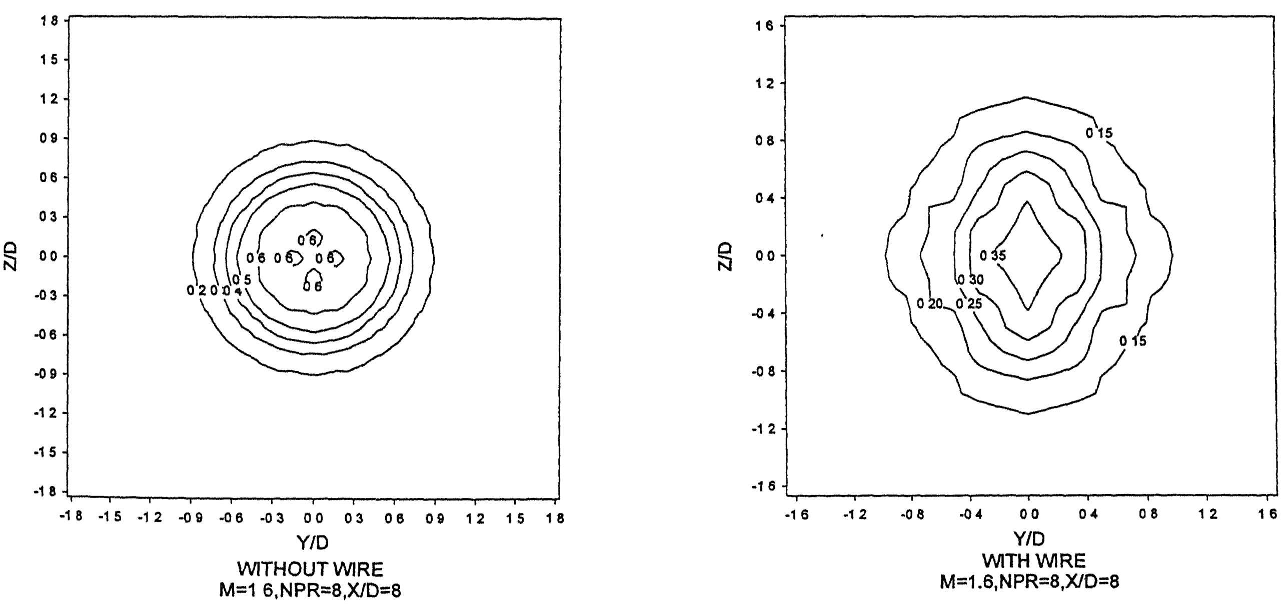


Figure 4.32

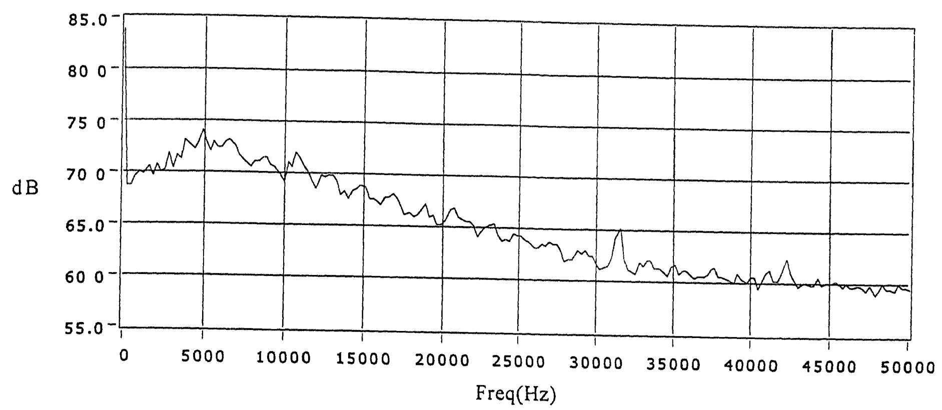


Figure 4.33 Frequency spectrum for M=1.6, NPR 2, X/D=0, R/D=30
Without wire

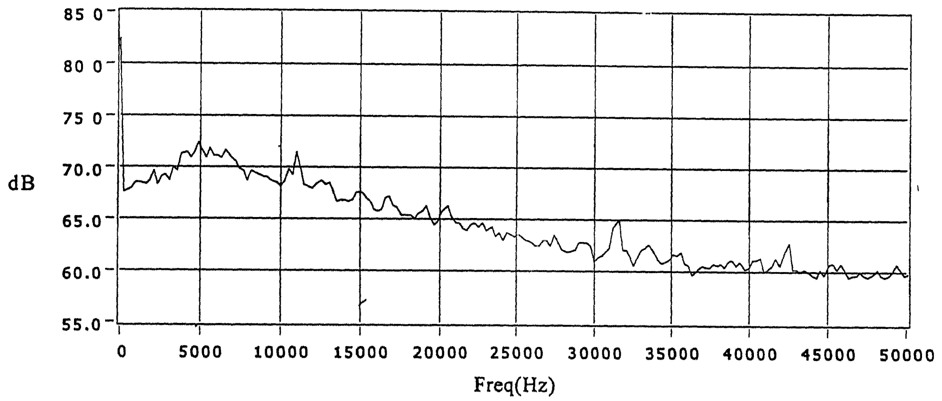


Figure 4.34 Frequency spectrum for M=1.6, NPR 2, X/D=0, R/D=30
along the wire

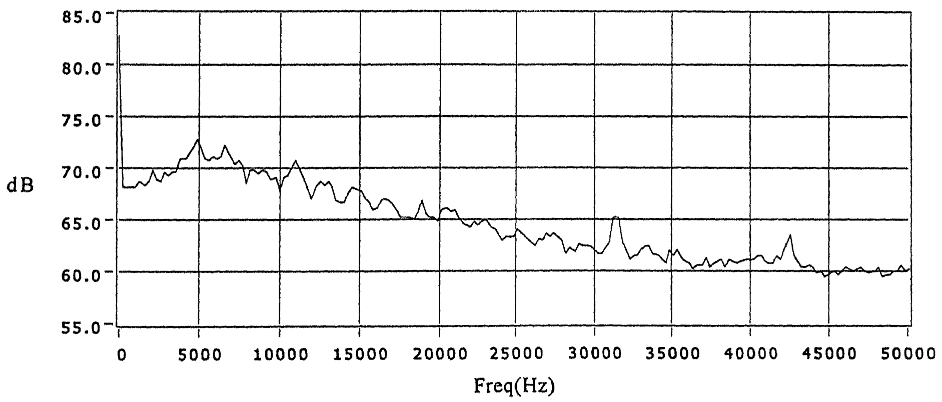


Figure 4.35 Frequency spectrum for M=1.6, NPR 2, X/D=0, R/D=30
normal to the wire

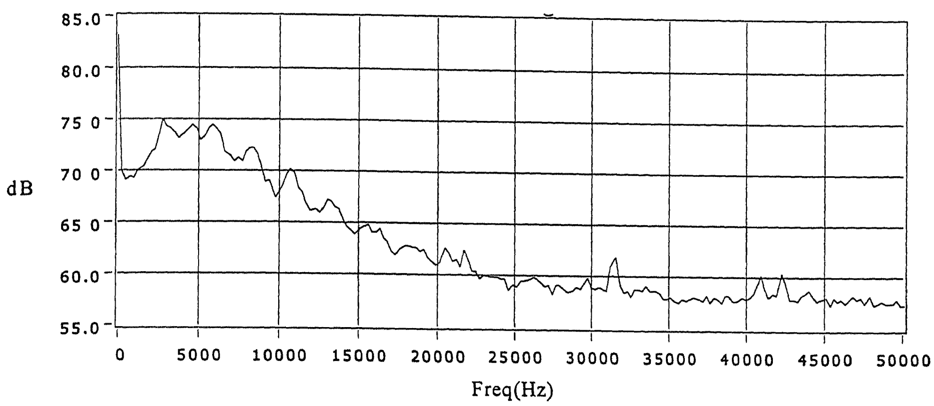


Figure 4.36 Frequency spectrum for M=1.6, NPR 2, R/D=100, θ =30 deg.
Without wire

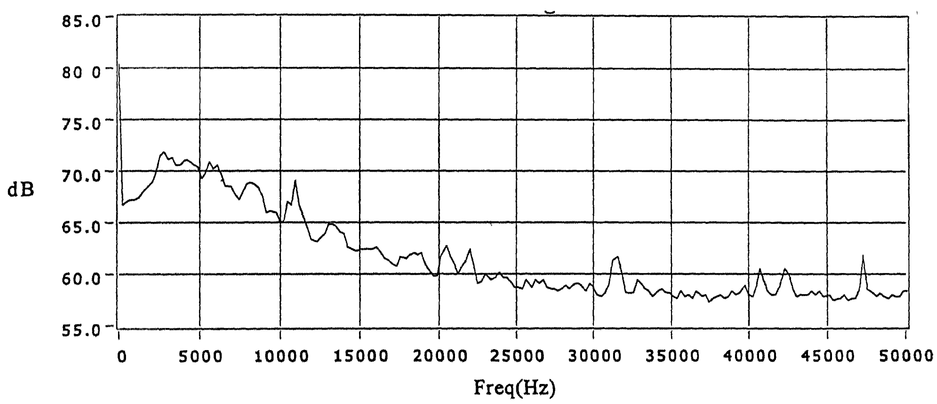


Figure 4.37 Frequency spectrum for M=1.6, NPR 2, R/D=100, θ =30 deg.
along the wire

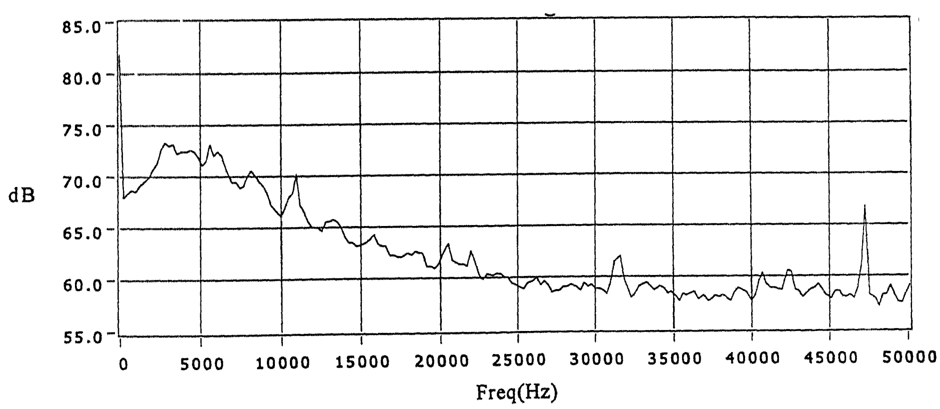


Figure 4.38 Frequency spectrum for M=1.6, NPR 2, R/D=100, θ =30 deg.
Normal to the wire

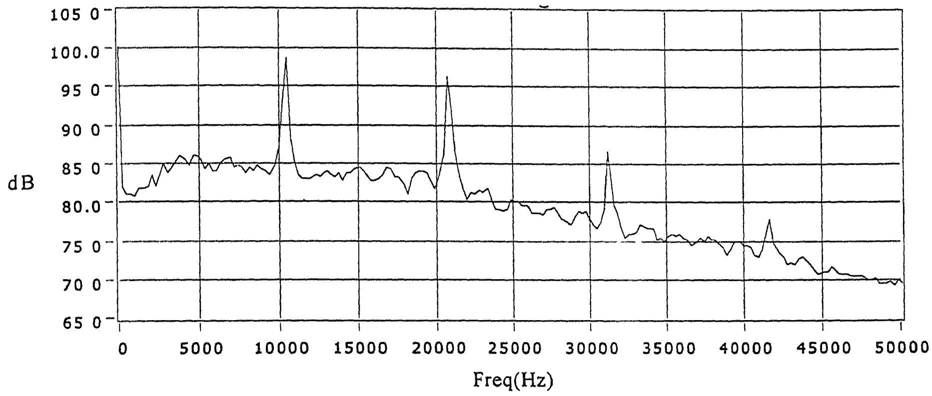


Figure 4.39 Frequency spectrum for M=1.6, NPR 4, X/D=0, R/D=30
Without wire

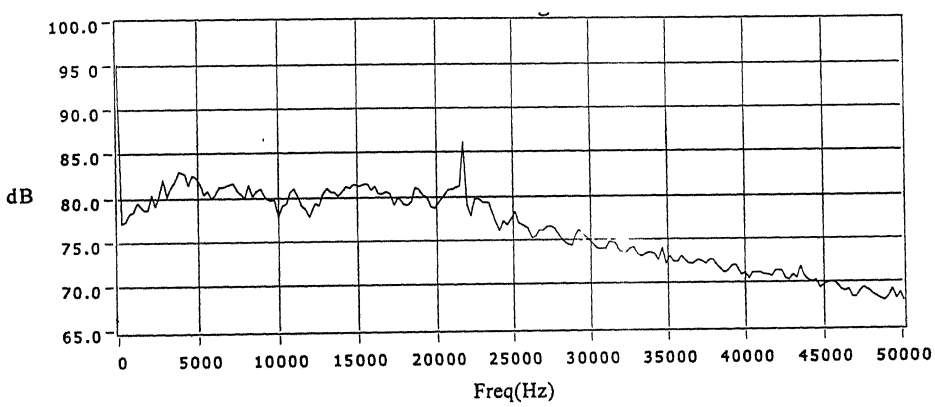


Figure 4.40 Frequency spectrum for M=1.6, NPR 4, X/D=0, R/D=30
along the wire

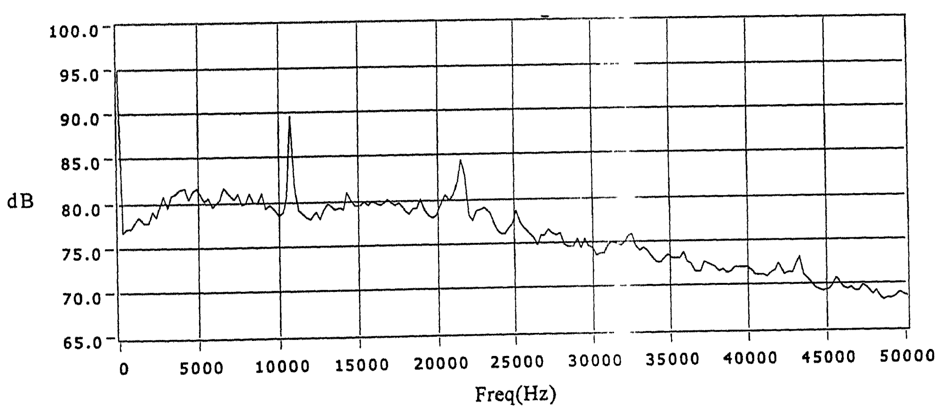


Figure 4.41 Frequency spectrum for M=1.6, NPR 4, X/D=0, R/D=30
normal to the wire

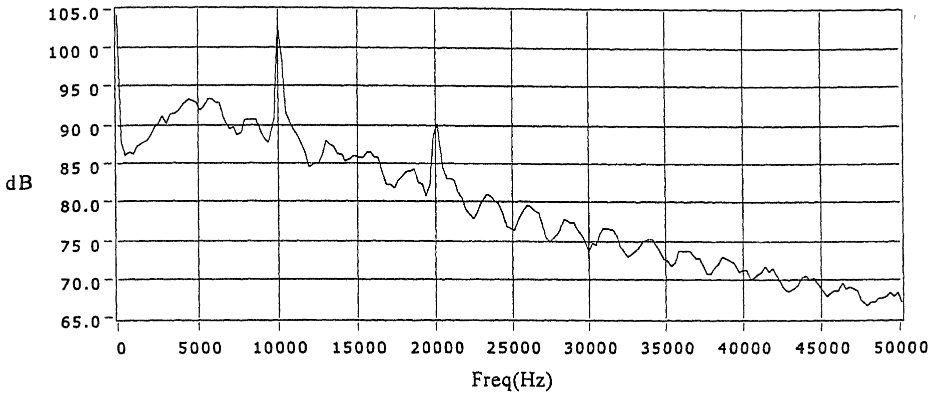


Figure 4.42 Frequency spectrum for M=1.6, NPR 4, R/D=100, θ =30 deg.
Without wire

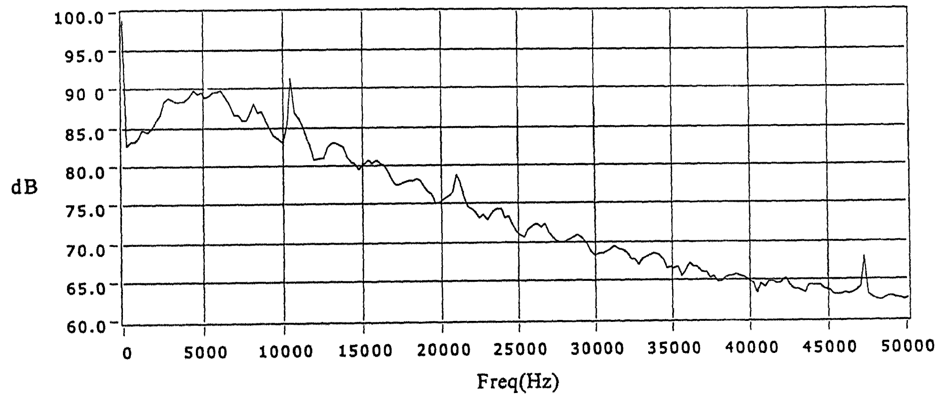


Figure 4.43 Frequency spectrum for M=1.6, NPR 4, R/D=100, θ =30 deg.
along the wire

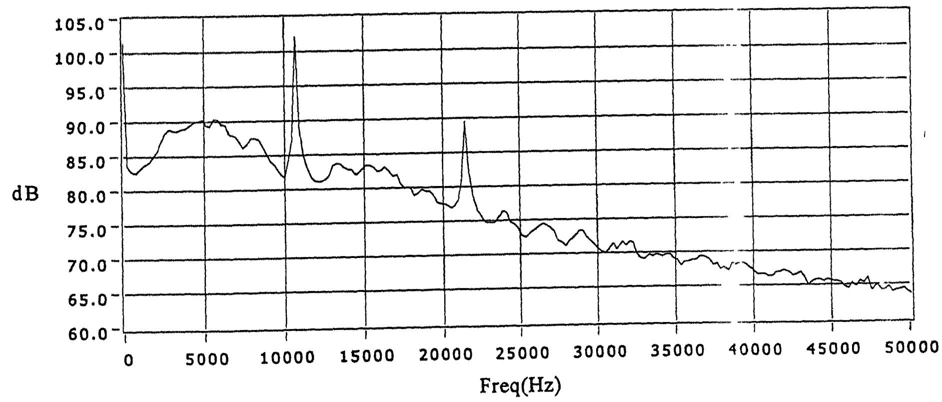


Figure 4.44 Frequency spectrum for M=1.6, NPR 4, R/D=100, θ =30 deg.
Normal to the wire

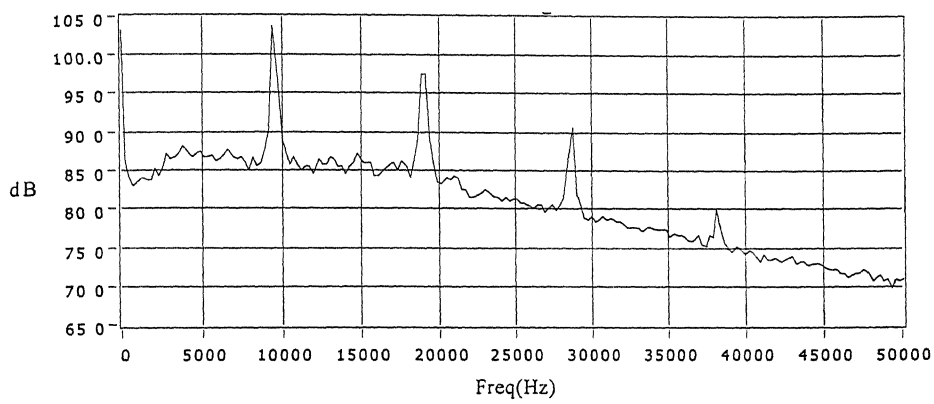


Figure 4.45 Frequency spectrum for M=1.6, NPR 4.24, X/D=0, R/D=30
Without wire

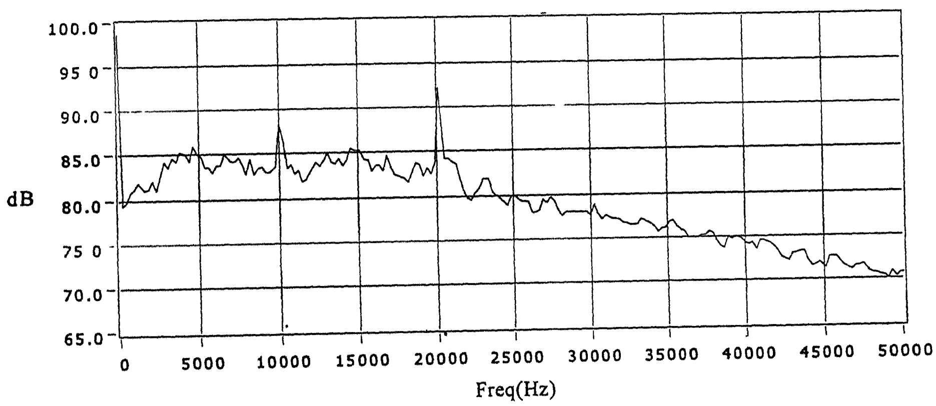


Figure 4.46 Frequency spectrum for M=1.6, NPR 4.24, X/D=0, R/D=30
along the wire

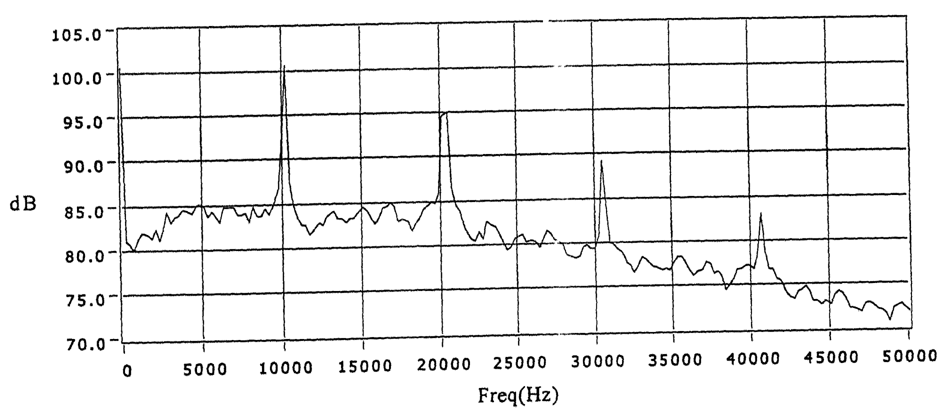


Figure 4.47 Frequency spectrum for M=1.6, NPR 4.24, X/D=0, R/D=30
normal to the wire

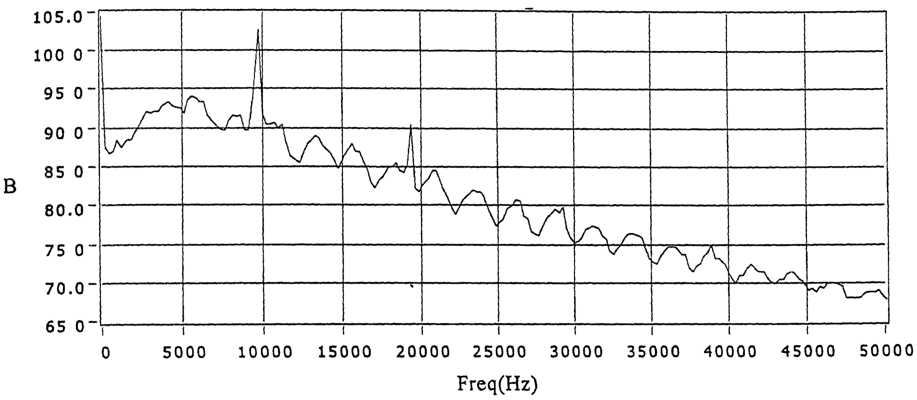


Figure 4.48 Frequency spectrum for M=1.6, NPR 4.24, R/D=100, θ =30 deg.
Without wire

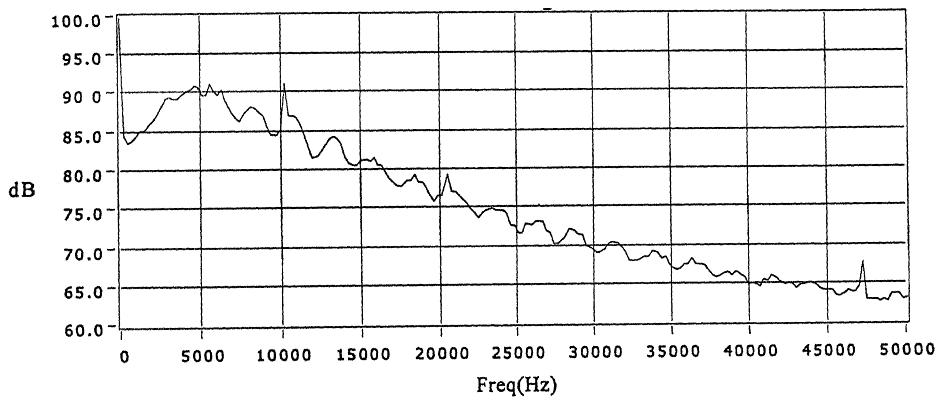


Figure 4.49 Frequency spectrum for M=1.6, NPR 4.24, R/D=100, θ =30 deg.
along the wire

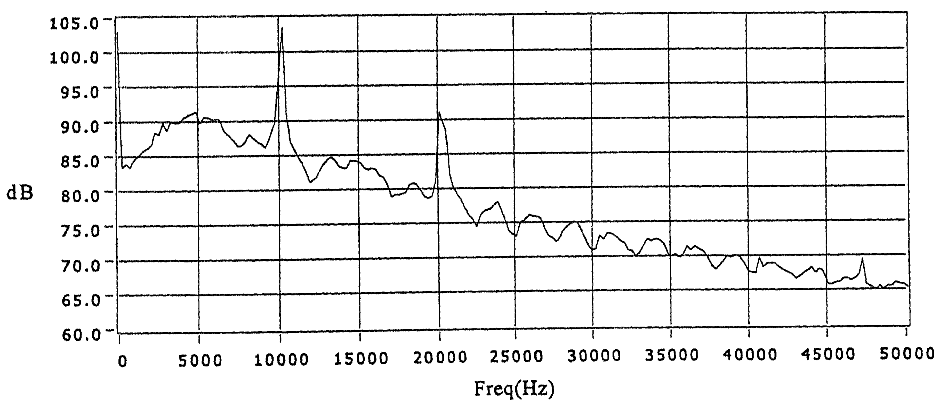


Figure 4.50 Frequency spectrum for M=1.6, NPR 4.24, R/D=100, θ =30 deg.
normal to the wire

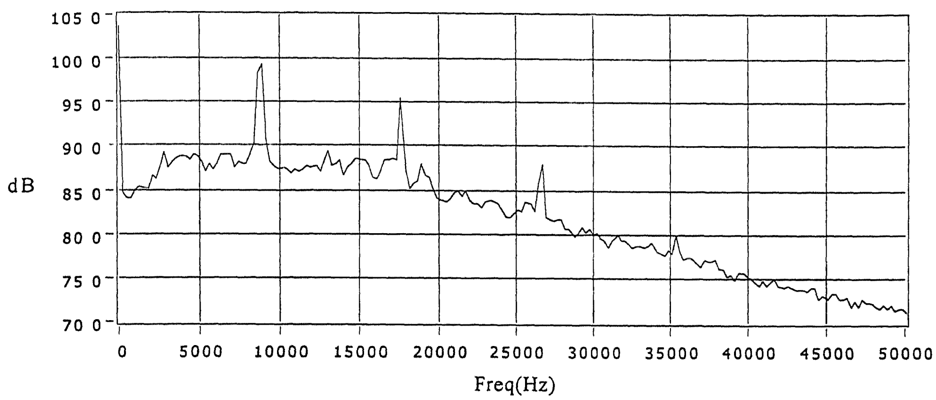


Figure 4.51 Frequency spectrum for M=1.6, NPR 5, X/D=0, R/D=30
Without wire

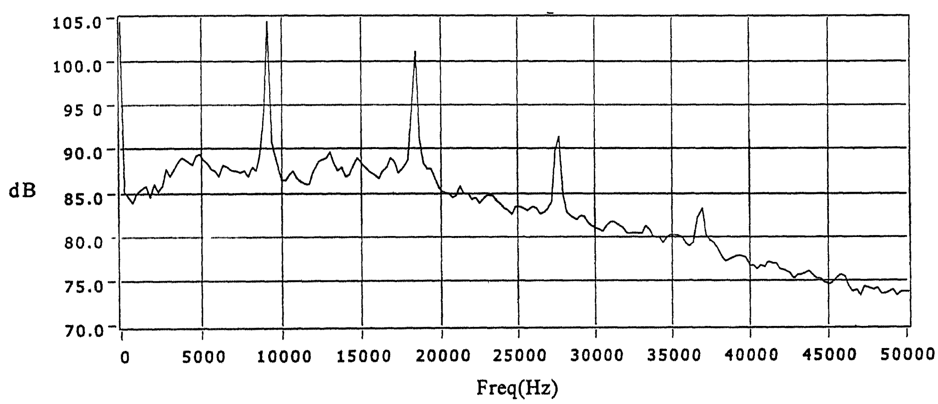


Figure 4.52 Frequency spectrum for M=1.6, NPR 5, X/D=0, R/D=30
along the wire

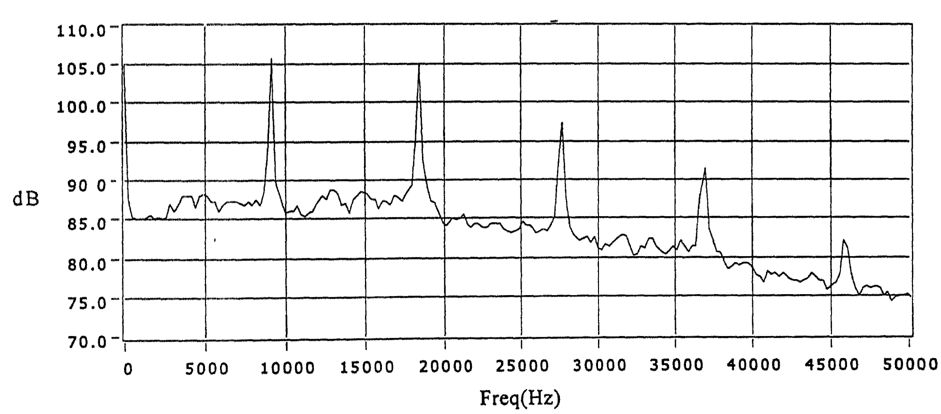


Figure 4.53 Frequency spectrum for M=1.6, NPR 5, X/D=0, R/D=30
normal to the wire

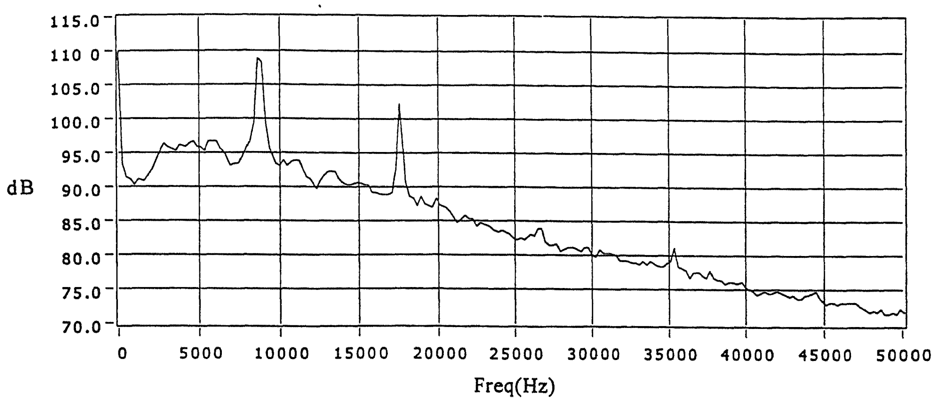


Figure 4.54 Frequency spectrum for M=1.6, NPR 5, R/D=100, θ =30 deg.
Without wire

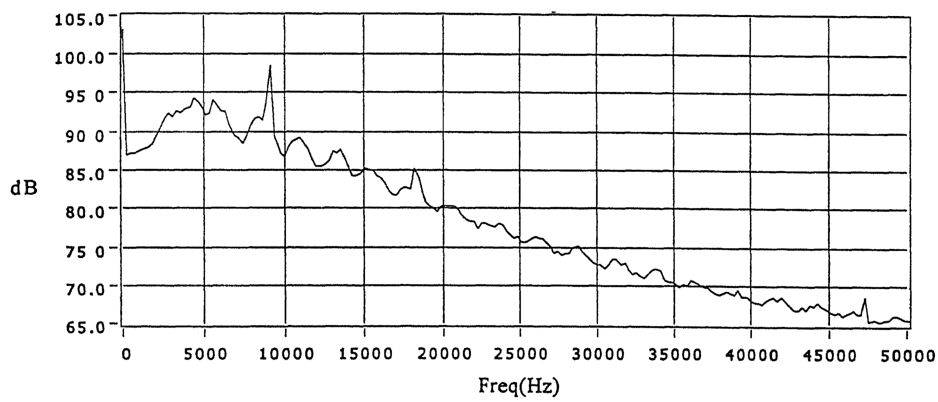


Figure 4.55 Frequency spectrum for M=1.6, NPR 5, R/D=100, θ =30 deg.
along the wire

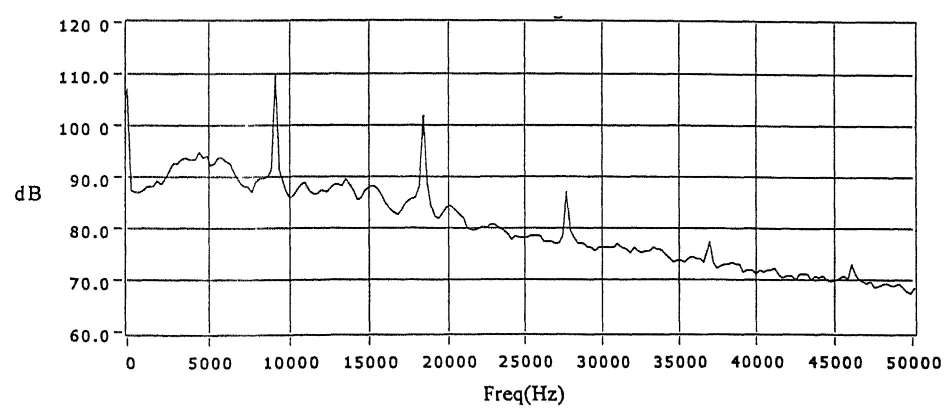


Figure 4.56 Frequency spectrum for M=1.6, NPR 5, R/D=100, θ =30 deg.
normal to the wire

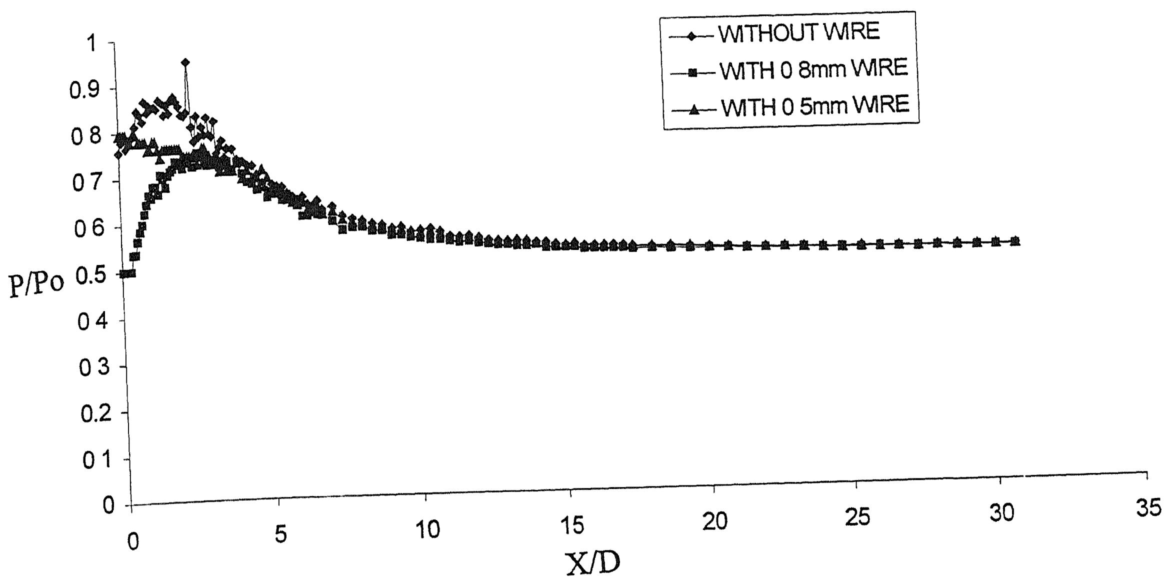


Figure 4.57 Effect of Cross-wire Diameter on Centreline decay(M=1.6,NPR 2)

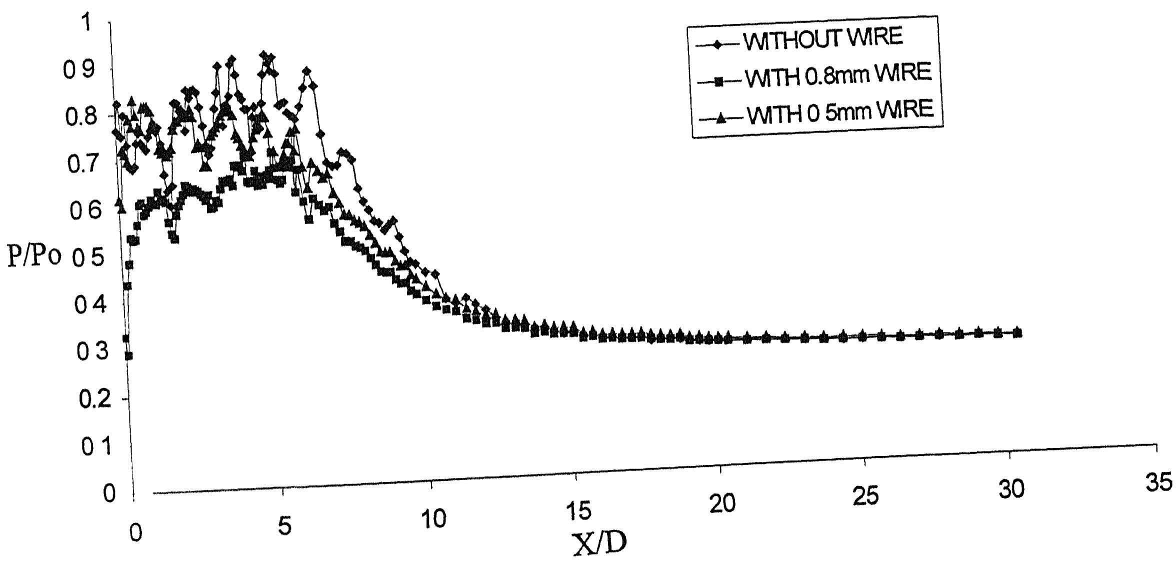


Figure 4.58 Effect of Cross-wire Diameter on Centreline decay(M=1.6,NPR 4.24)

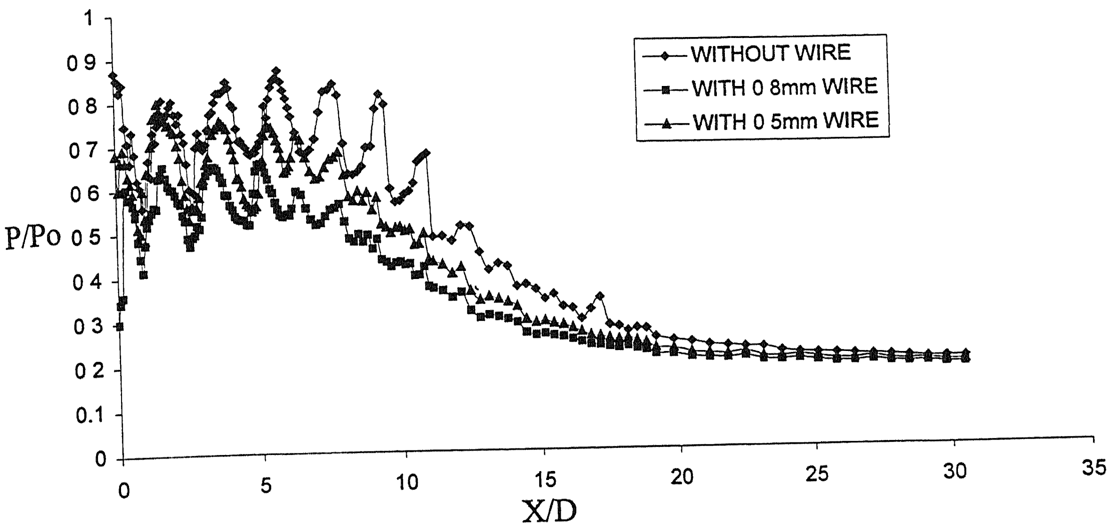


Figure 4.59 Effect of Cross-wire Diameter on Centreline decay(M=1.6,NPR 6)

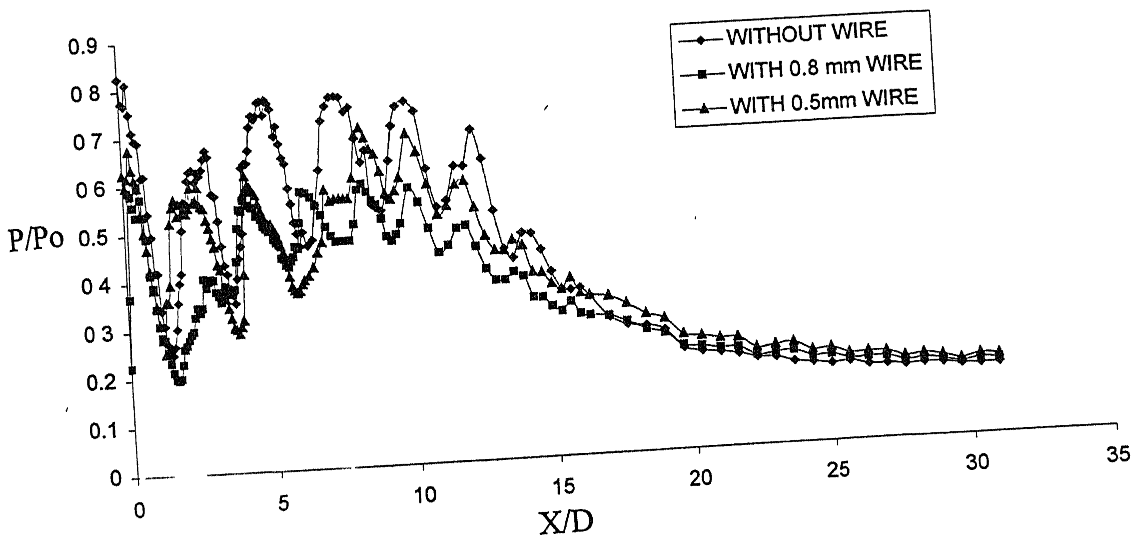


Figure 4.60 Effect of Cross-wire Diameter on Centreline decay(M=1.6,NPR 8)

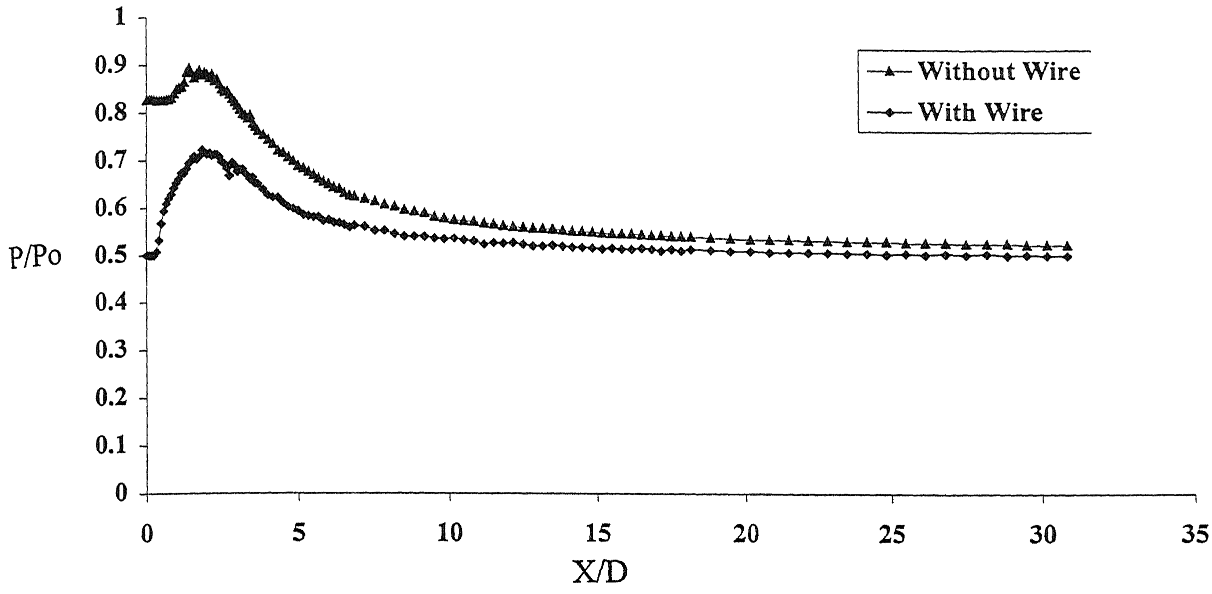


Figure 4.61 Centreline decay (M=1.79, NPR 2, Overexpansion)

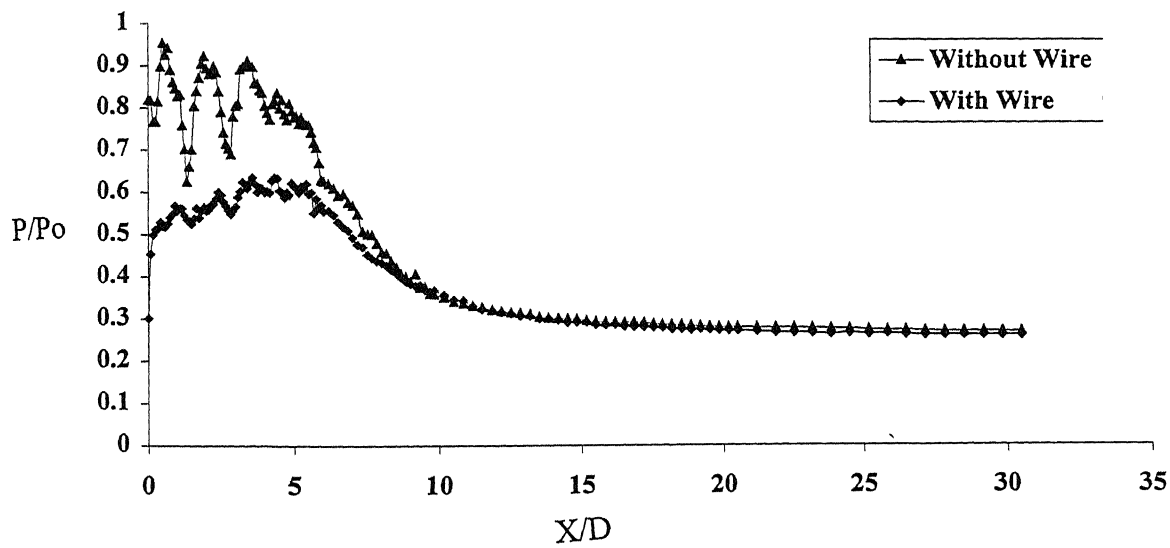


Figure 4.62 Centreline decay (M=1.79, NPR 4, Overexpansion)

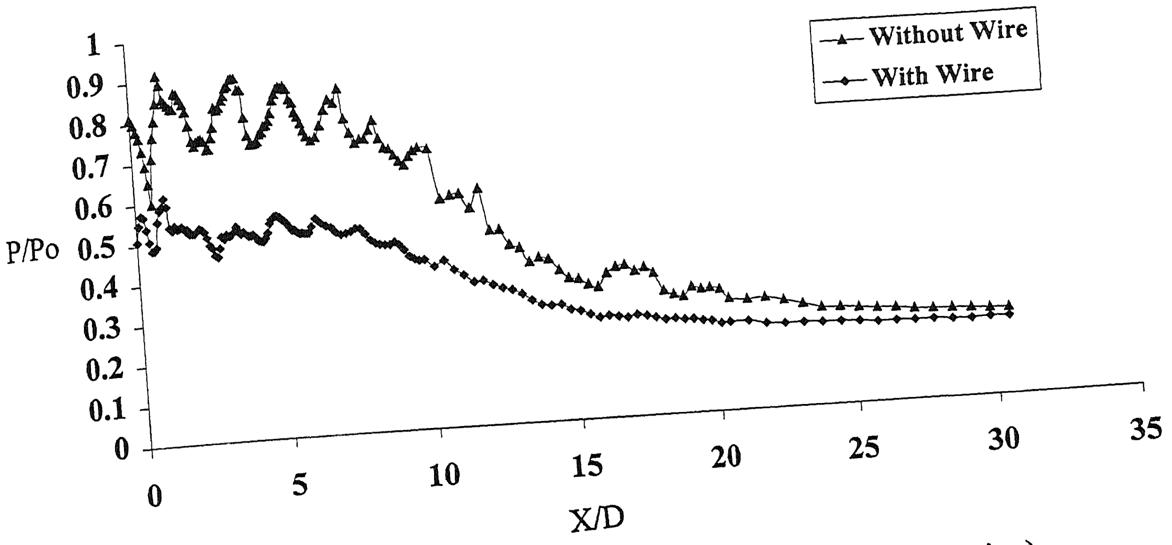


Figure 4.63 Centreline decay (M=1.79, NPR 5.66, Correct expansion)

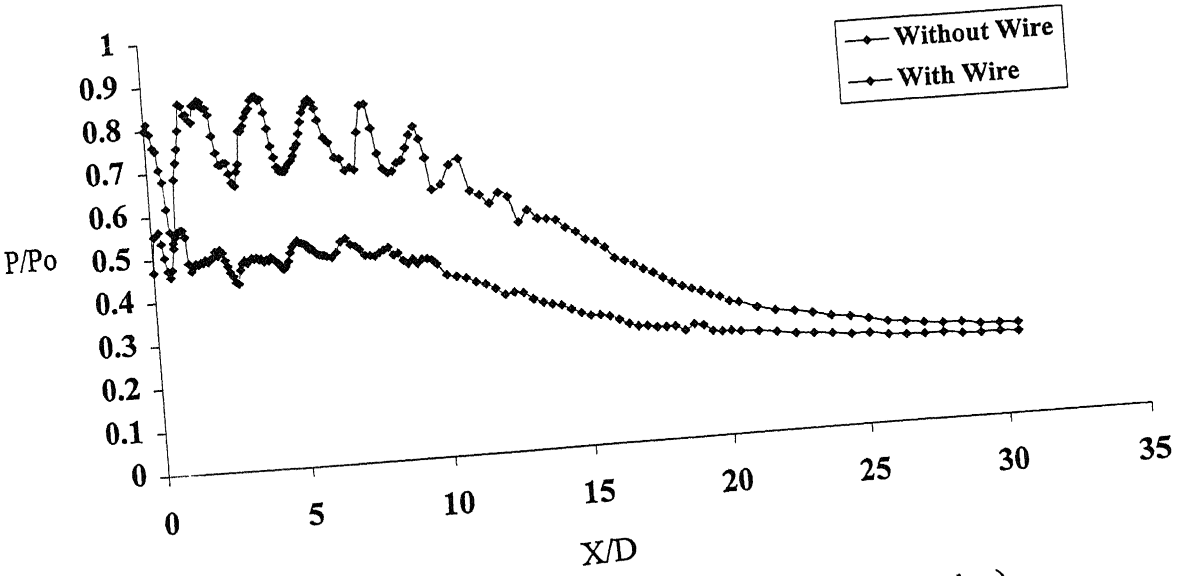


Figure 4.64 Centreline decay (M=1.79, NPR 6, Underexpansion)

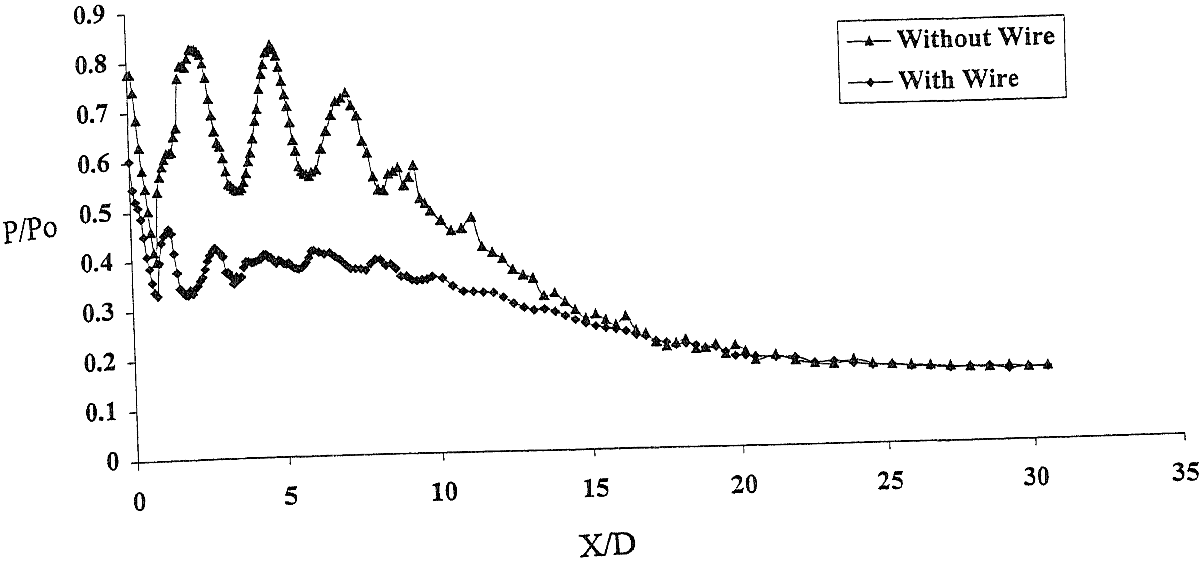


Figure 4.65 Centreline decay (M=1.79, NPR 8, Underexpansion)

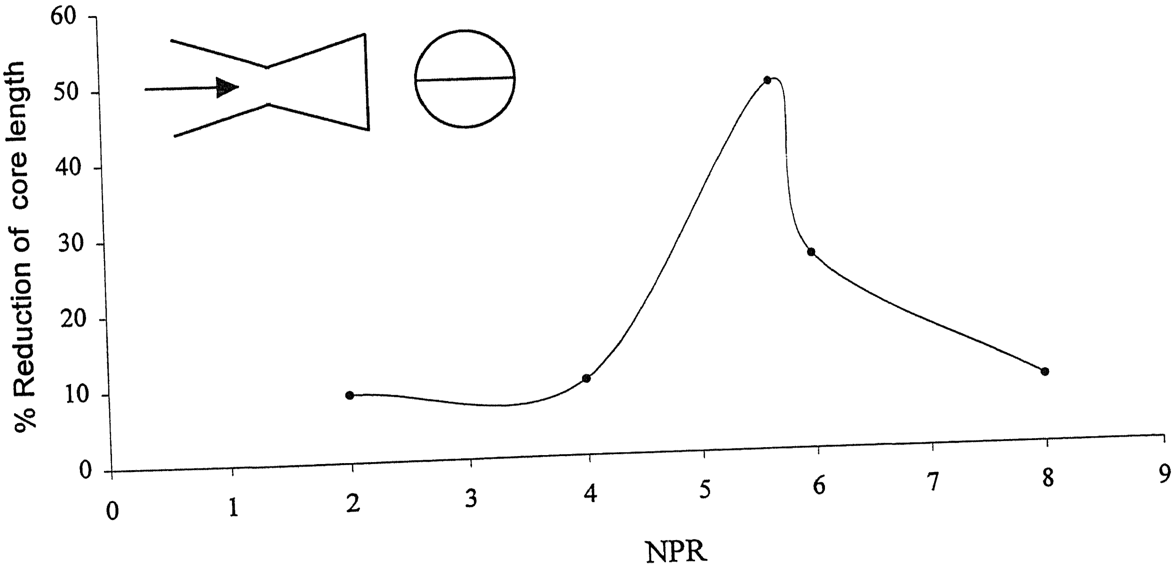


Figure 4.66 Percentage reduction in core length with NPR (M=1.79)

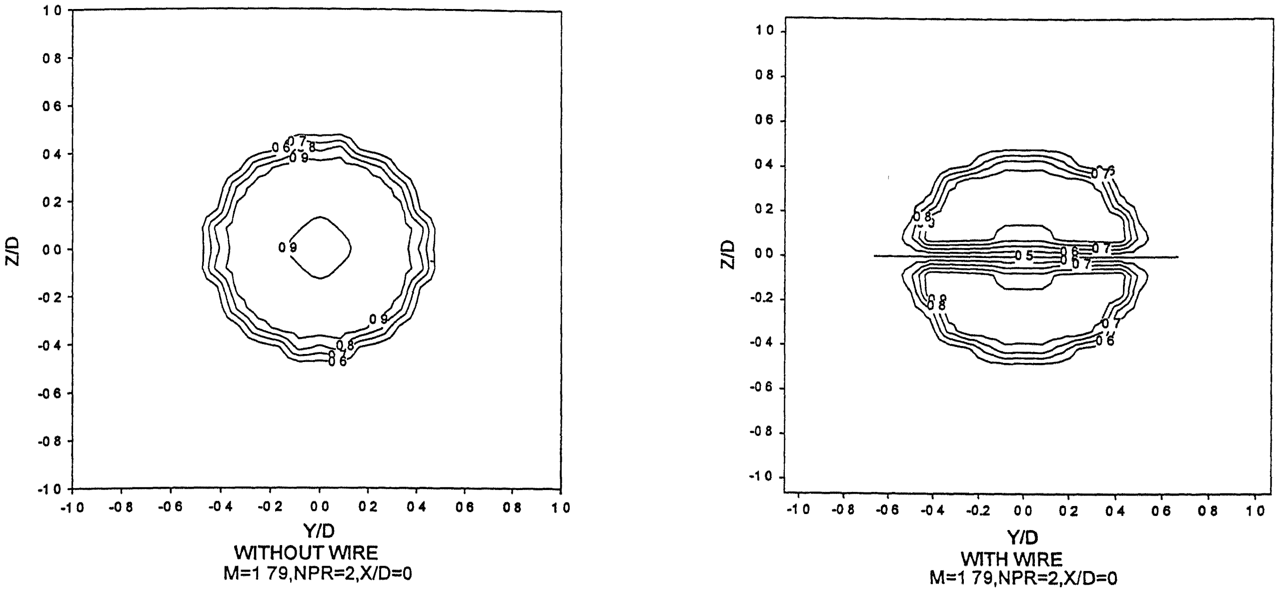


Figure 4.67

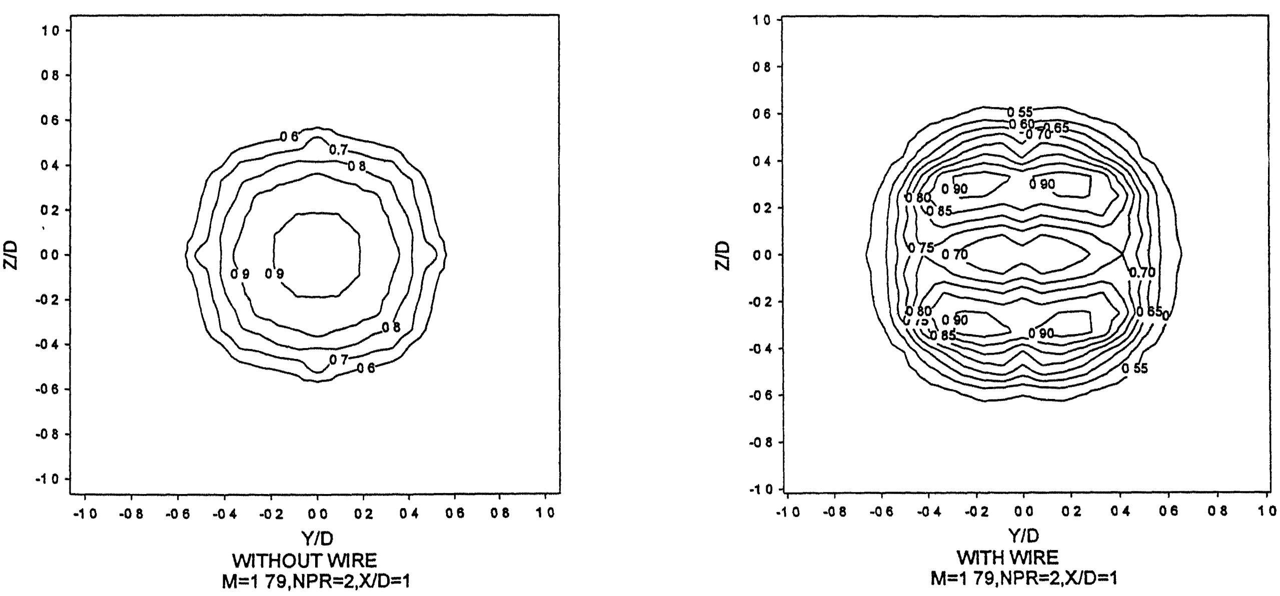


Figure 4.68

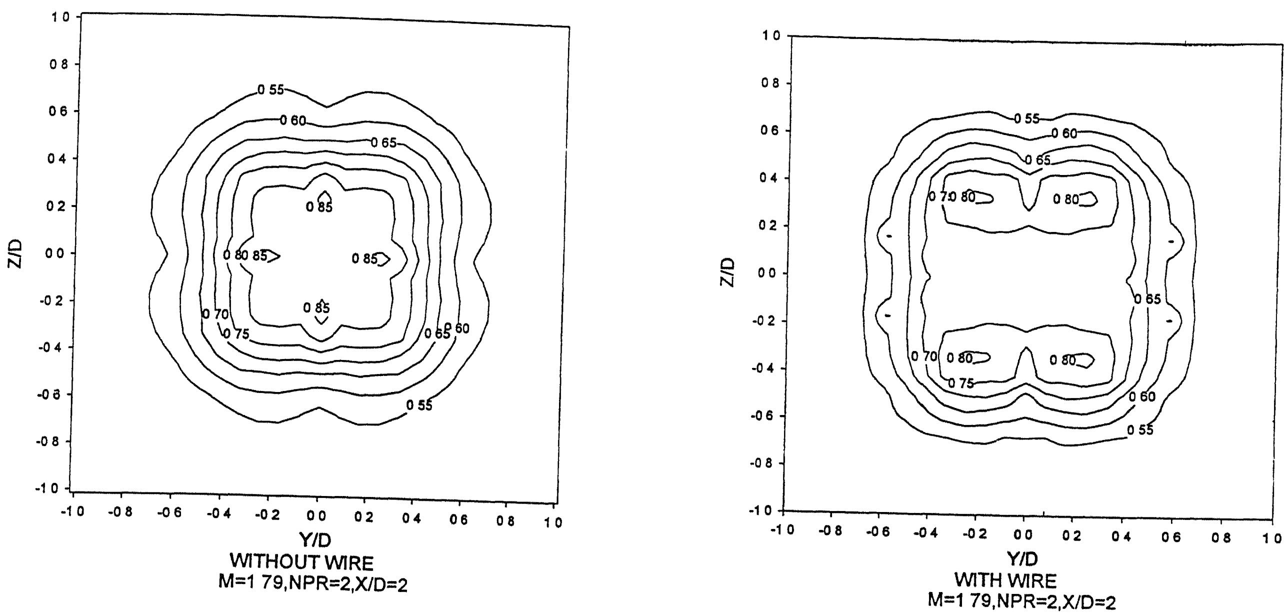


Figure 4.69

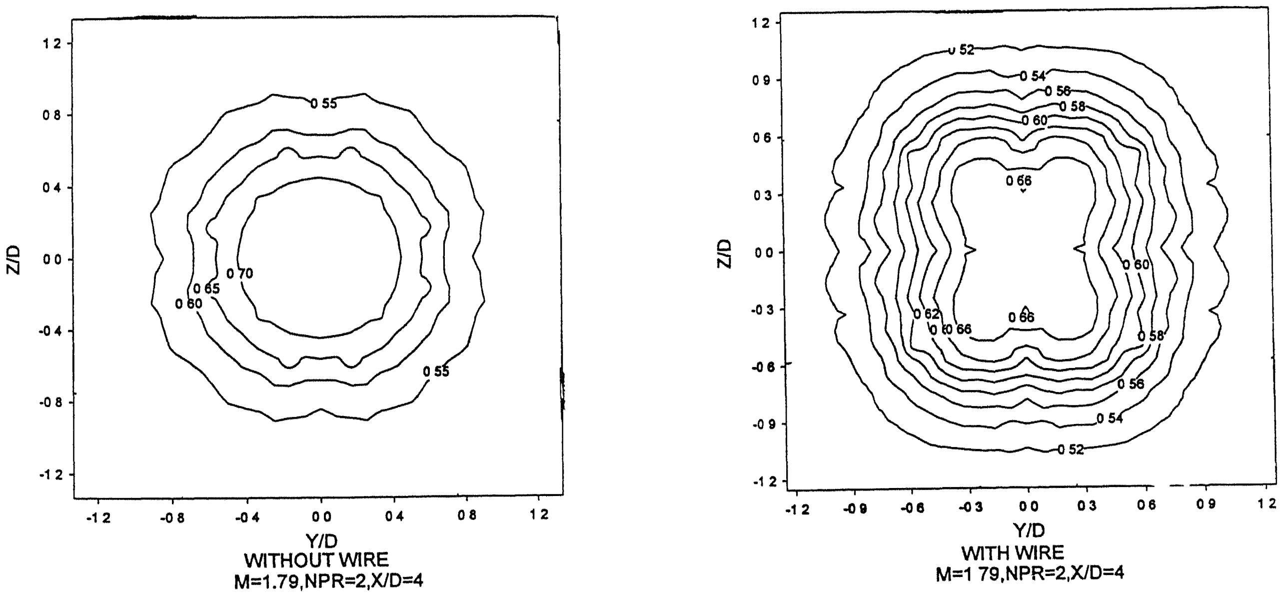


Figure 4.70

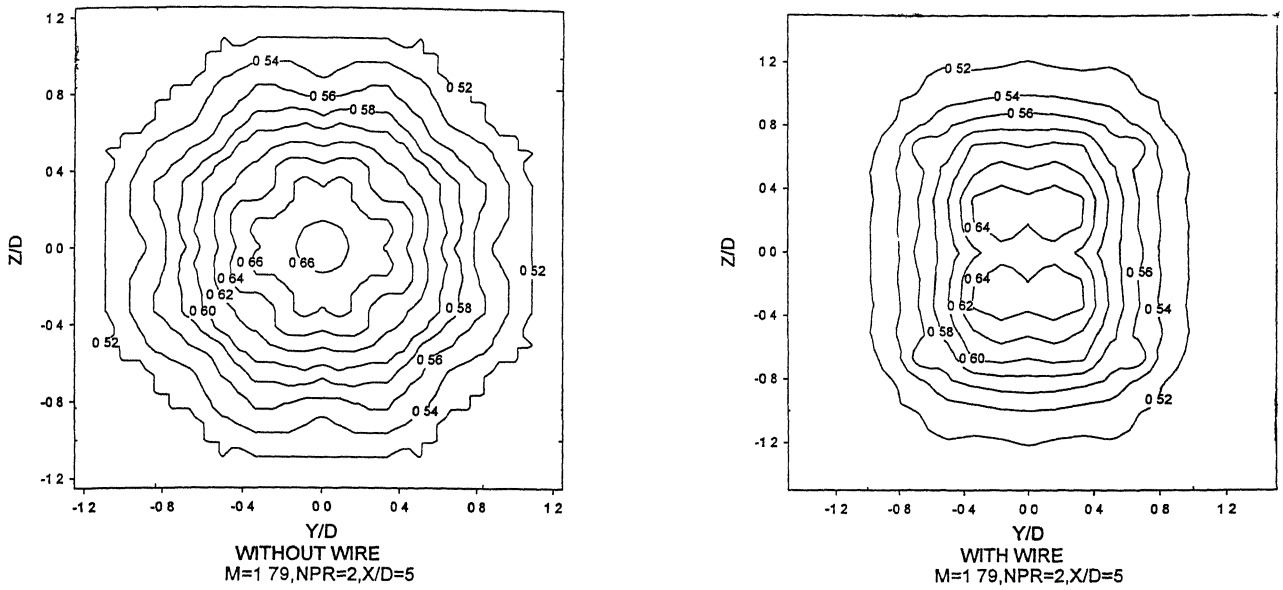


Figure 4.71

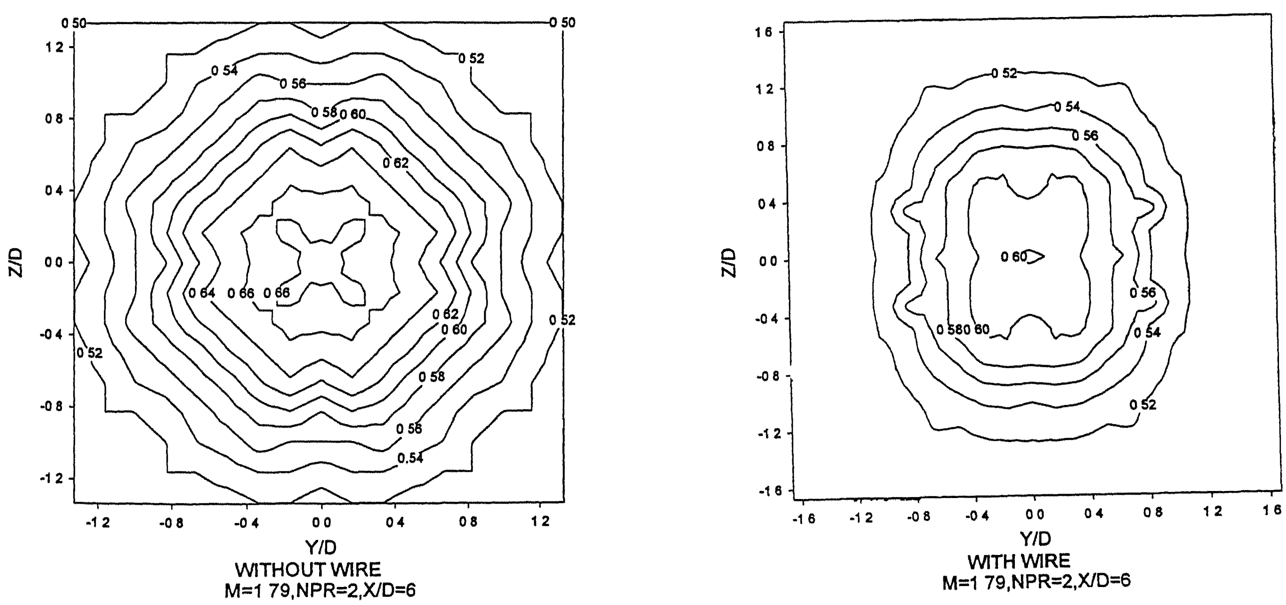


Figure 4.72

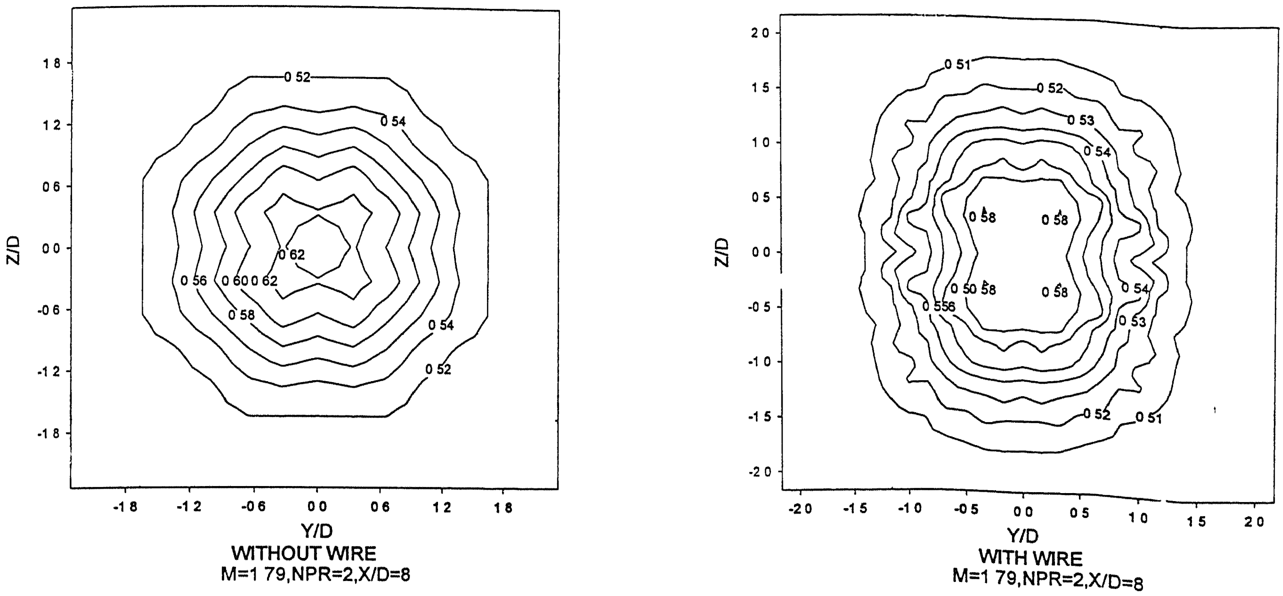


Figure 4.73

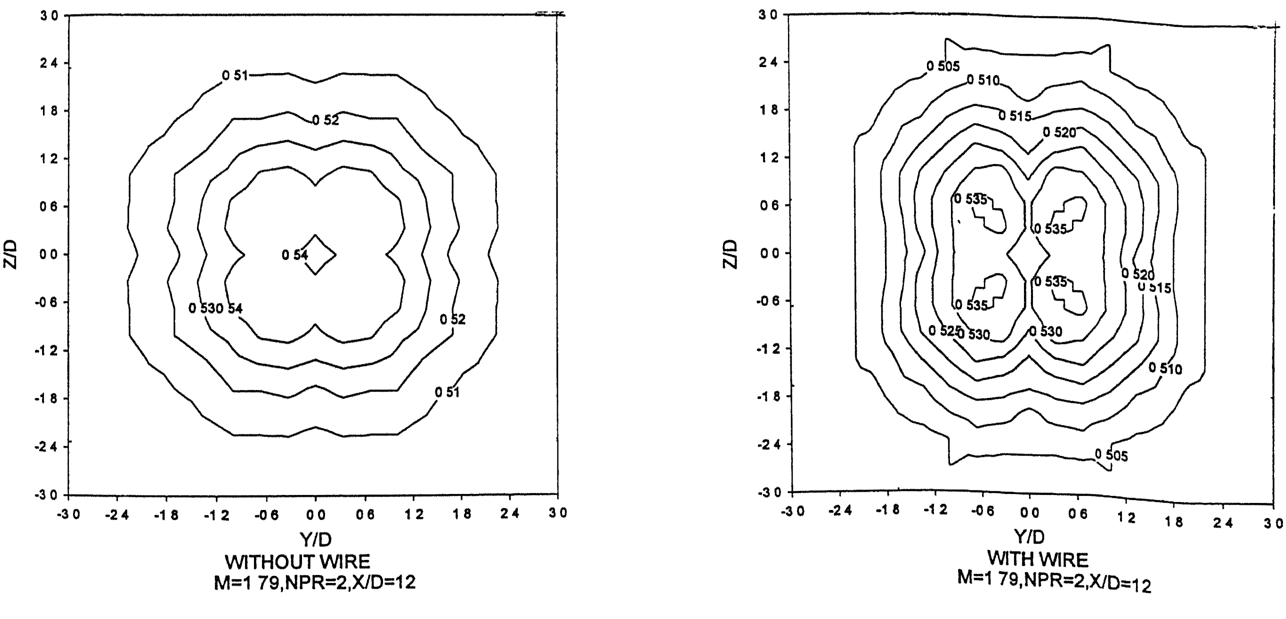


Figure 4.74

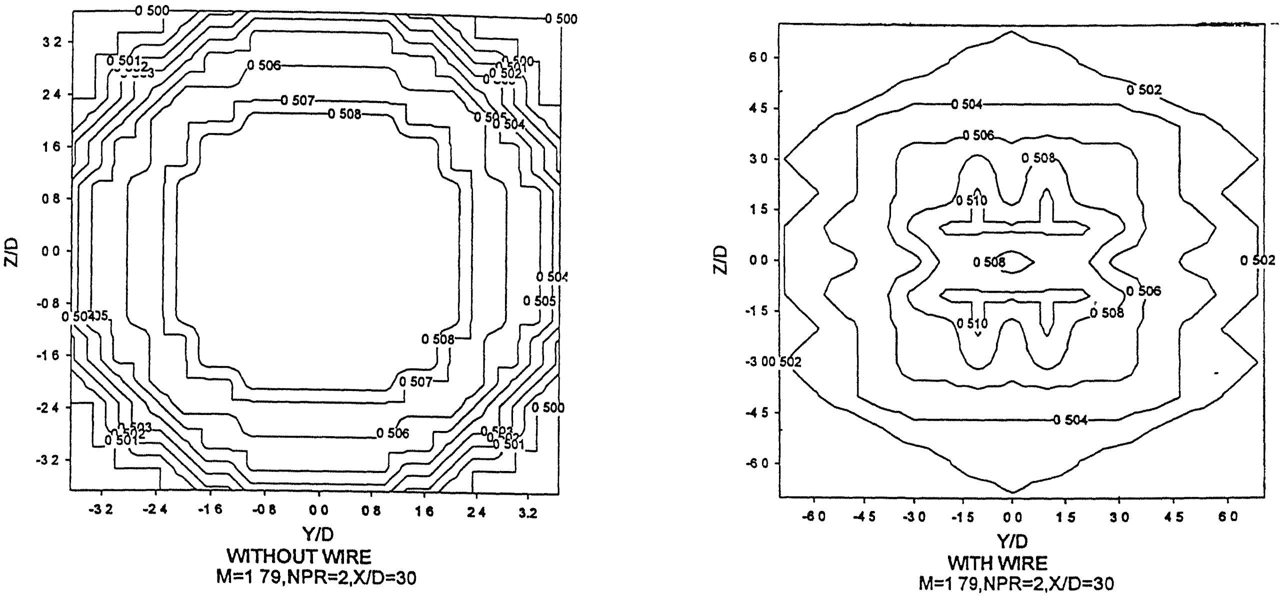


Figure 4.77

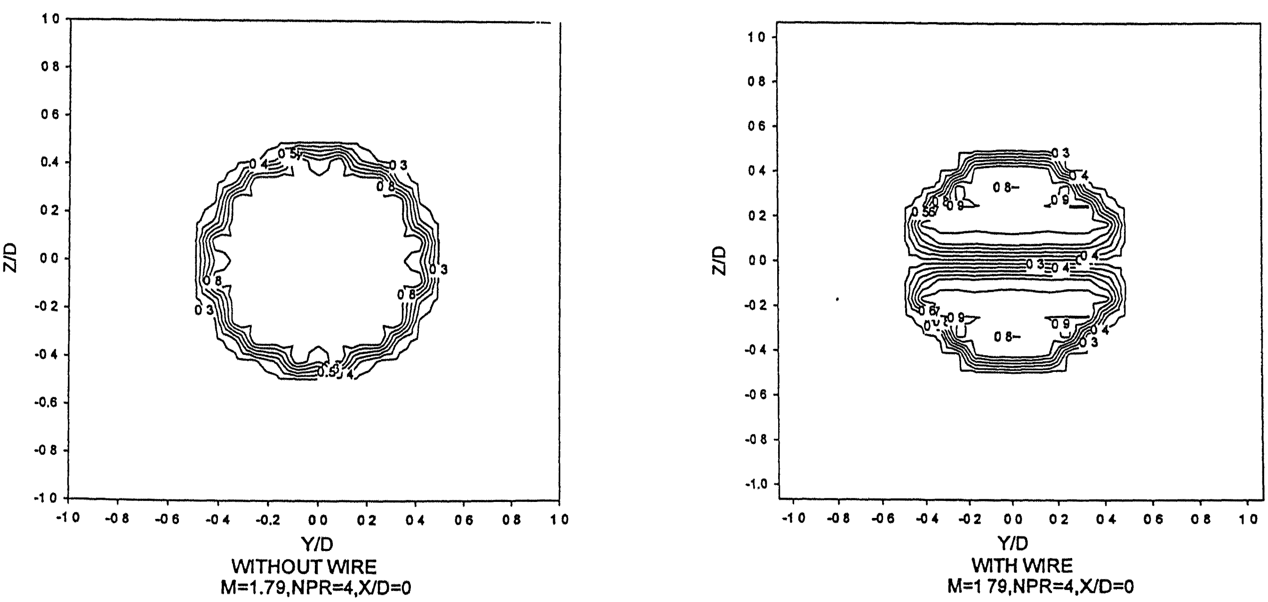


Figure 4.78

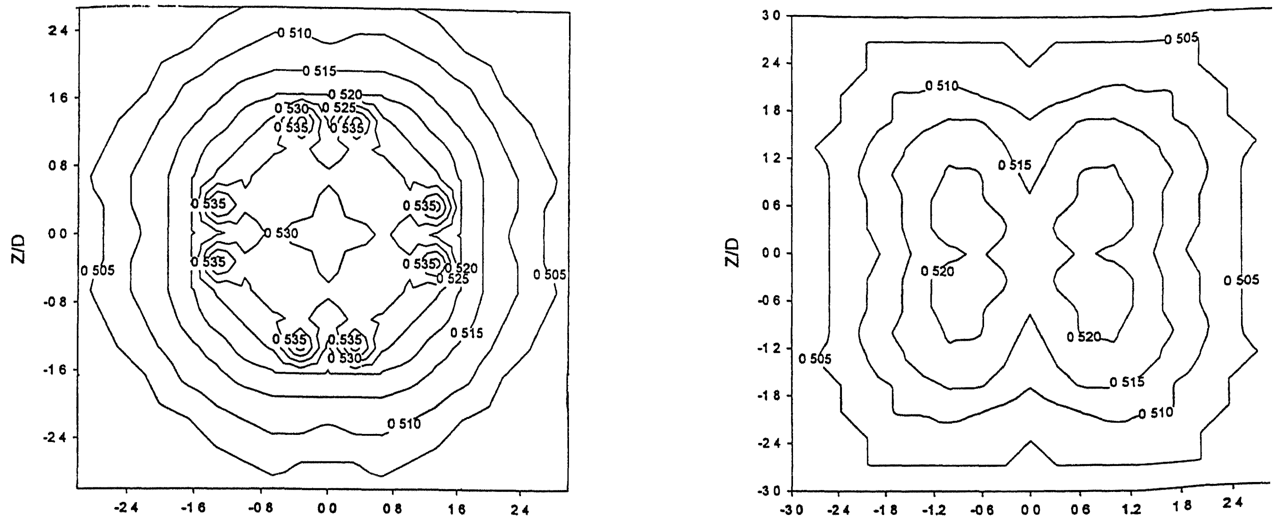


WITHOUT WIRE
M=1 79,NPR=2,X/D=15

WITH WIRE
M=1 79,NPR=2,X/D=15

Figure 4.75

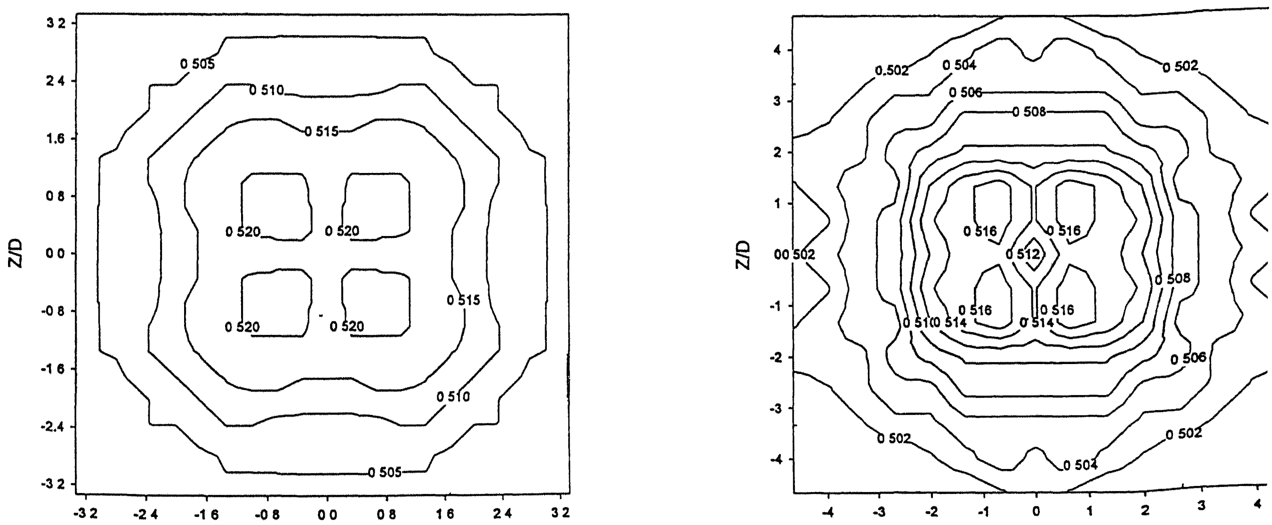


WITHOUT WIRE
M=1 79,NPR=2,X/D=20

WITH WIRE
M=1 79,NPR=2,X/D=20

Figure 4.76

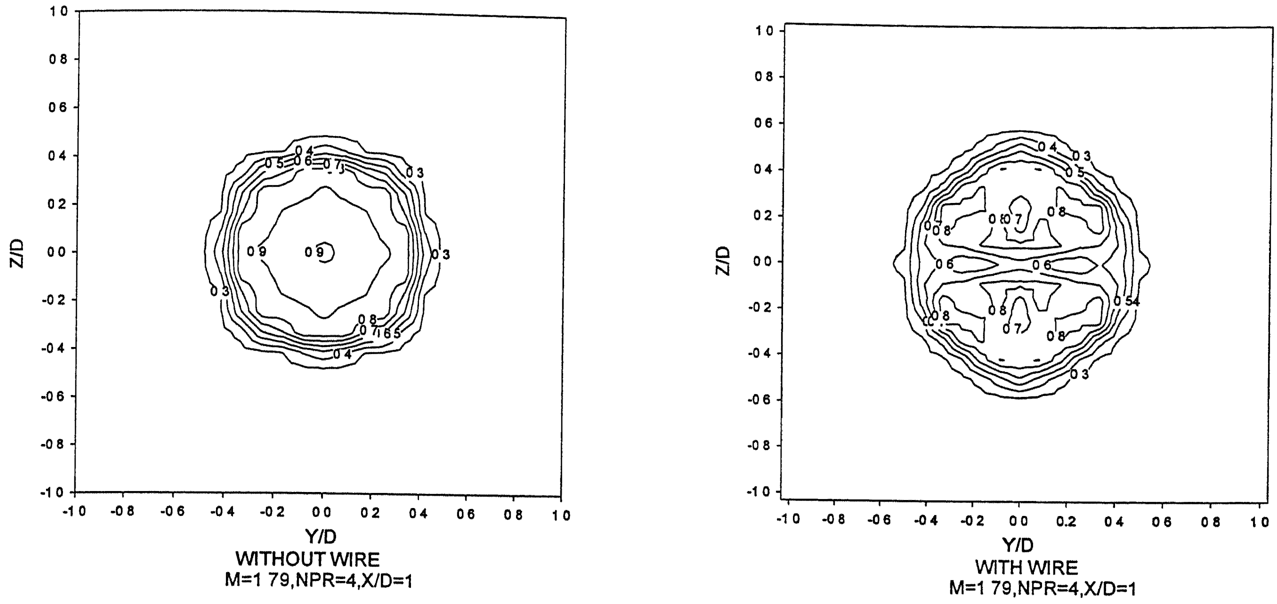


Figure 4.79

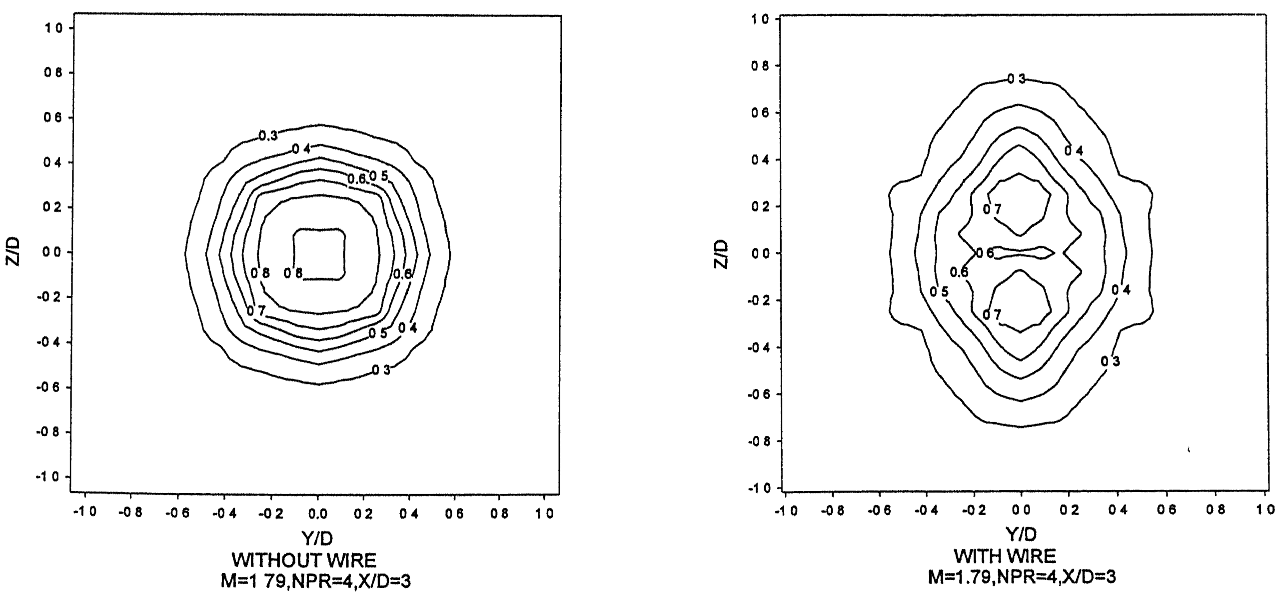


Figure 4.80

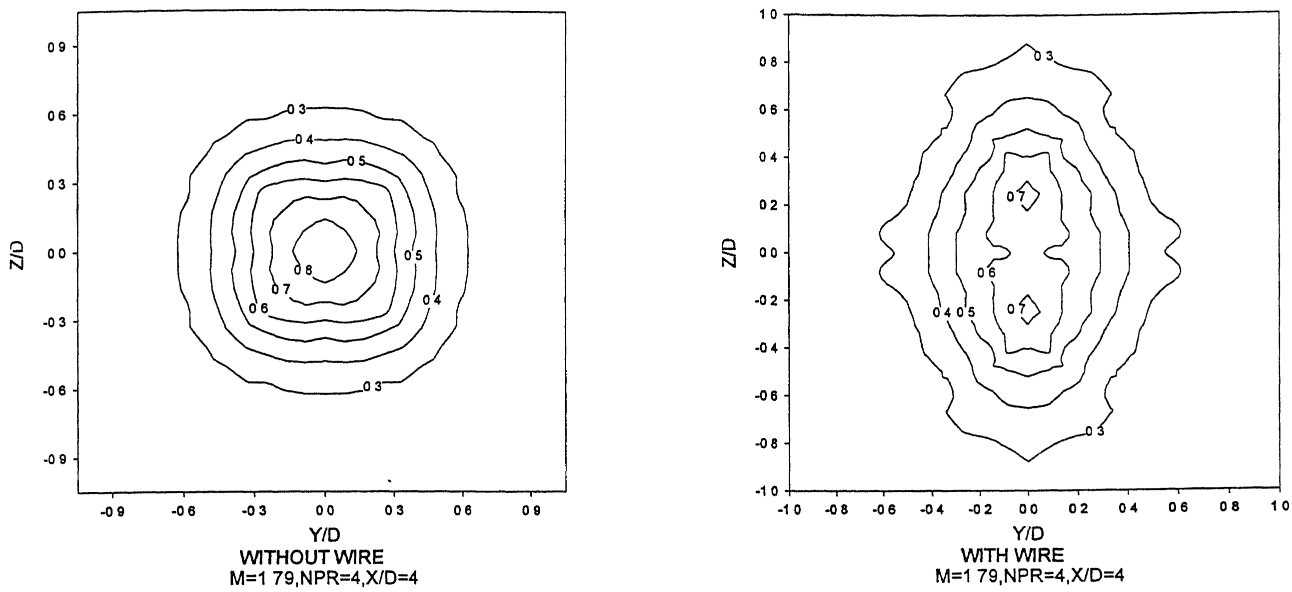


Figure 4.81

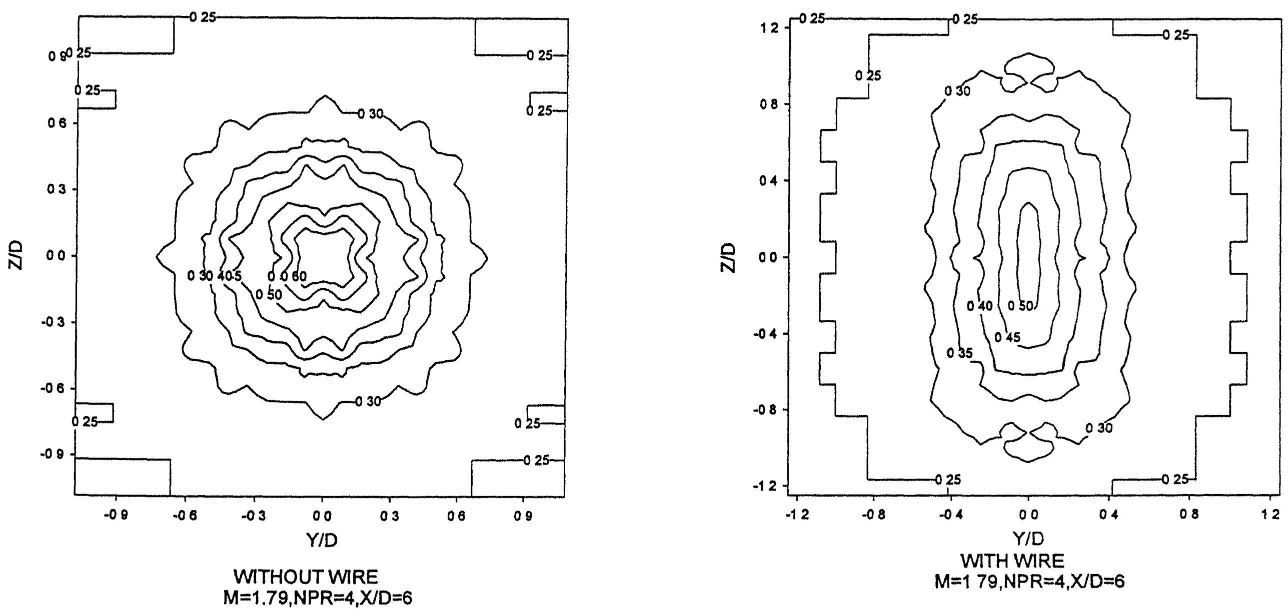


Figure 4.82

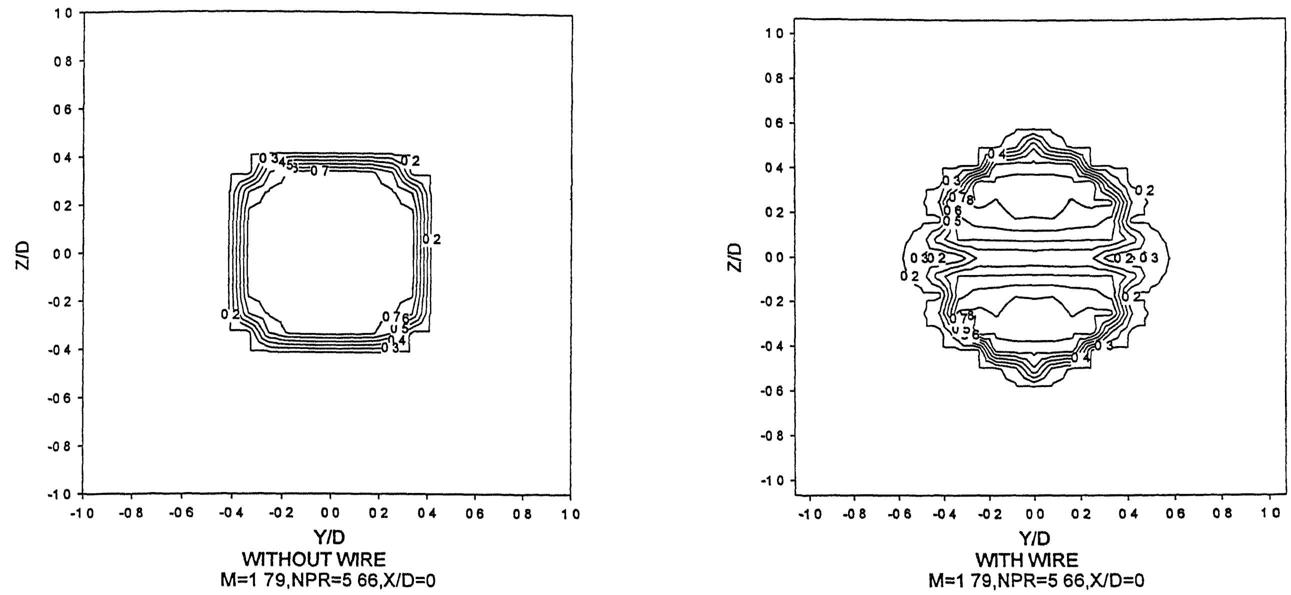


Figure 4.83

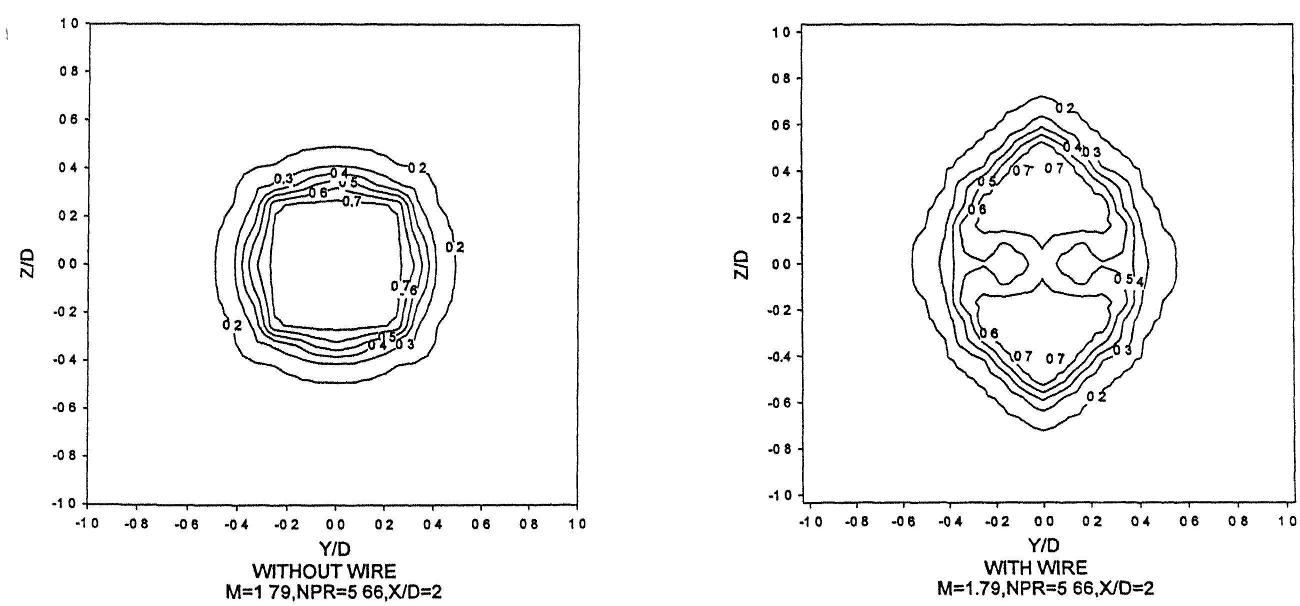


Figure 4.84

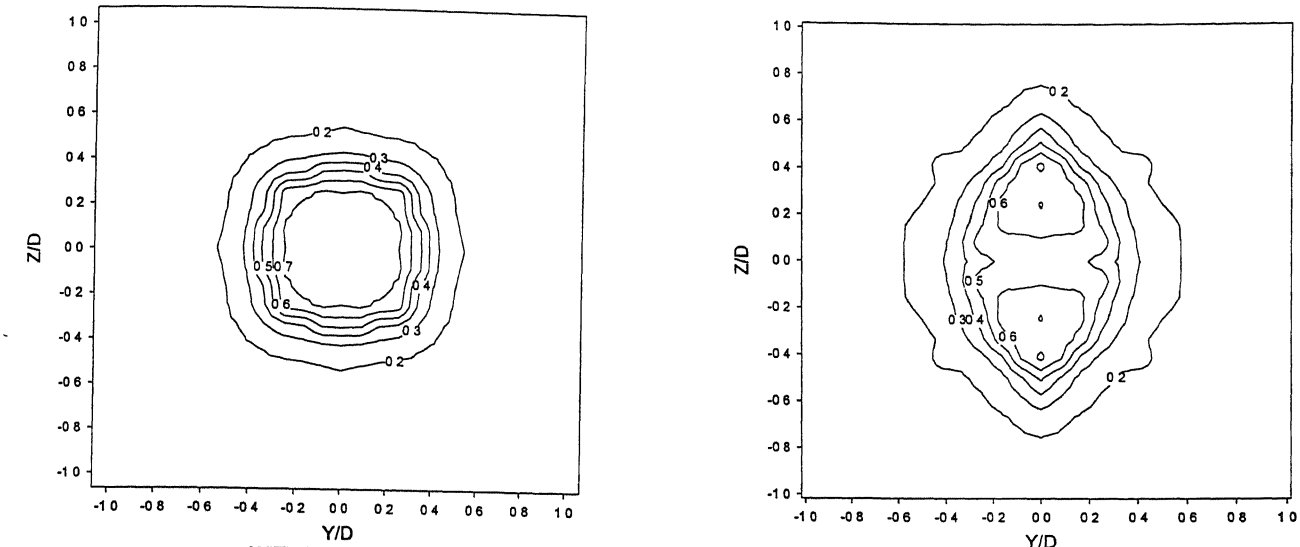


WITHOUT WIRE
M=1 79,NPR=5.66,X/D=3

WITH WIRE
M=1 79,NPR=5 66,X/D=3

Figure 4.85

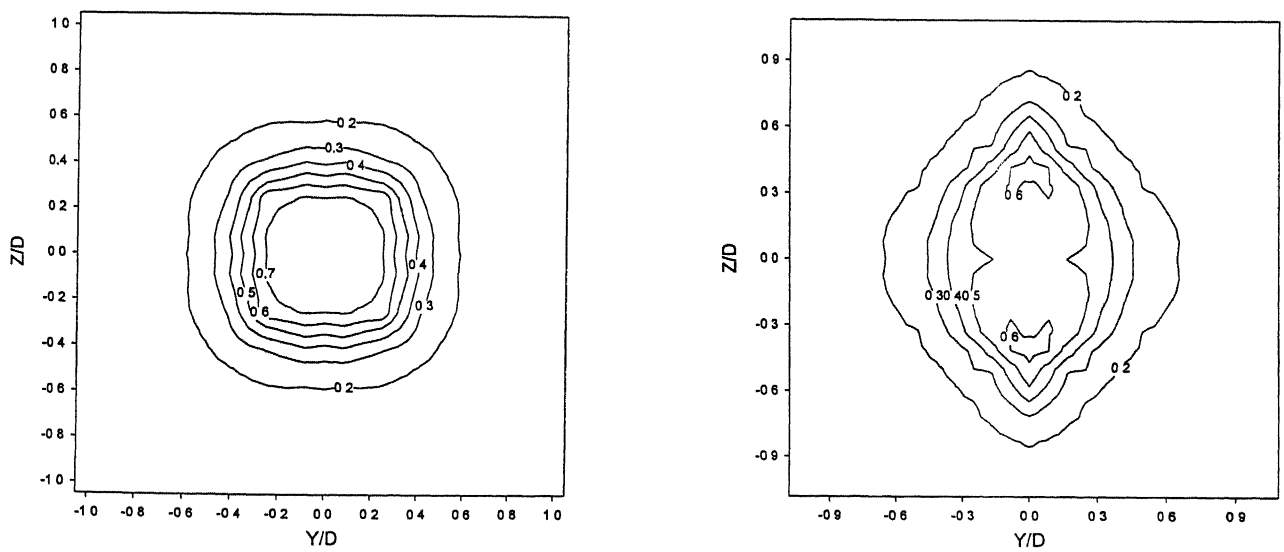


WITHOUT WIRE
M=1.79,NPR=5.66,X/D=4

WITH WIRE
M=1 79,NPR=5 66,X/D=4

Figure 4.86

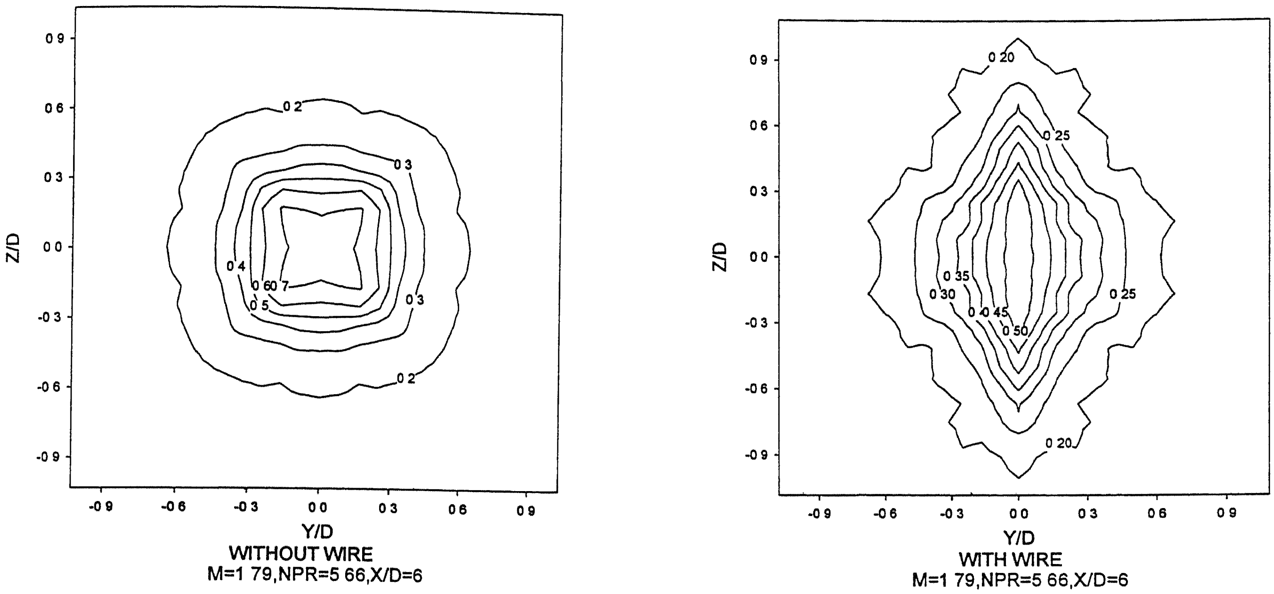


Figure 4.87

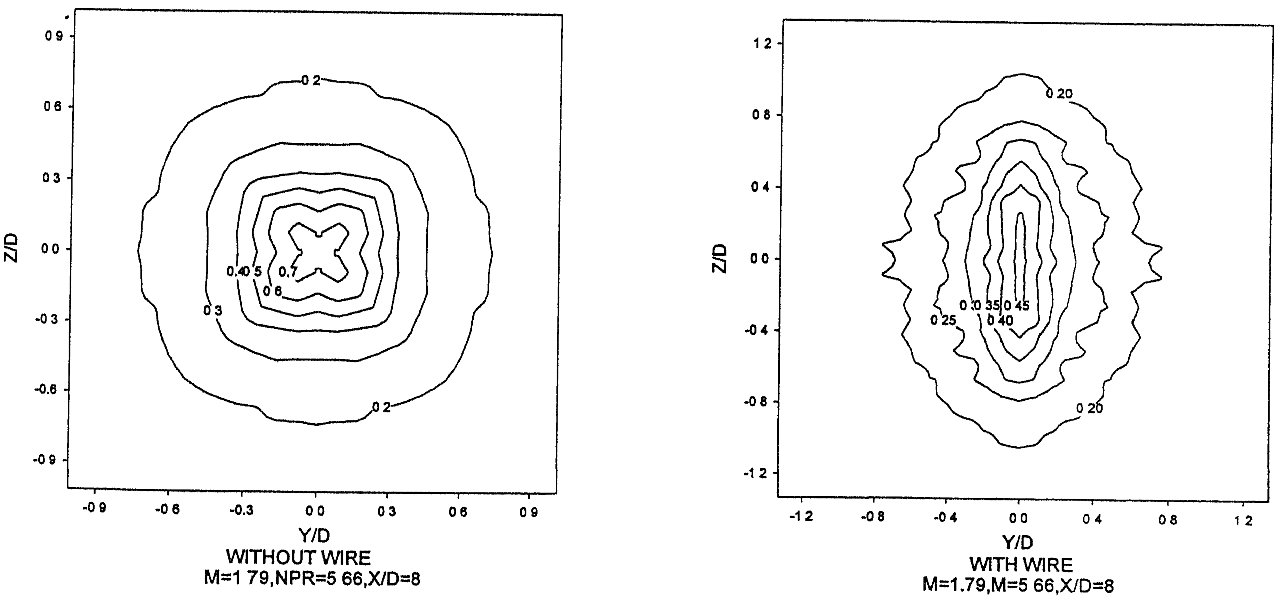


Figure 4.88

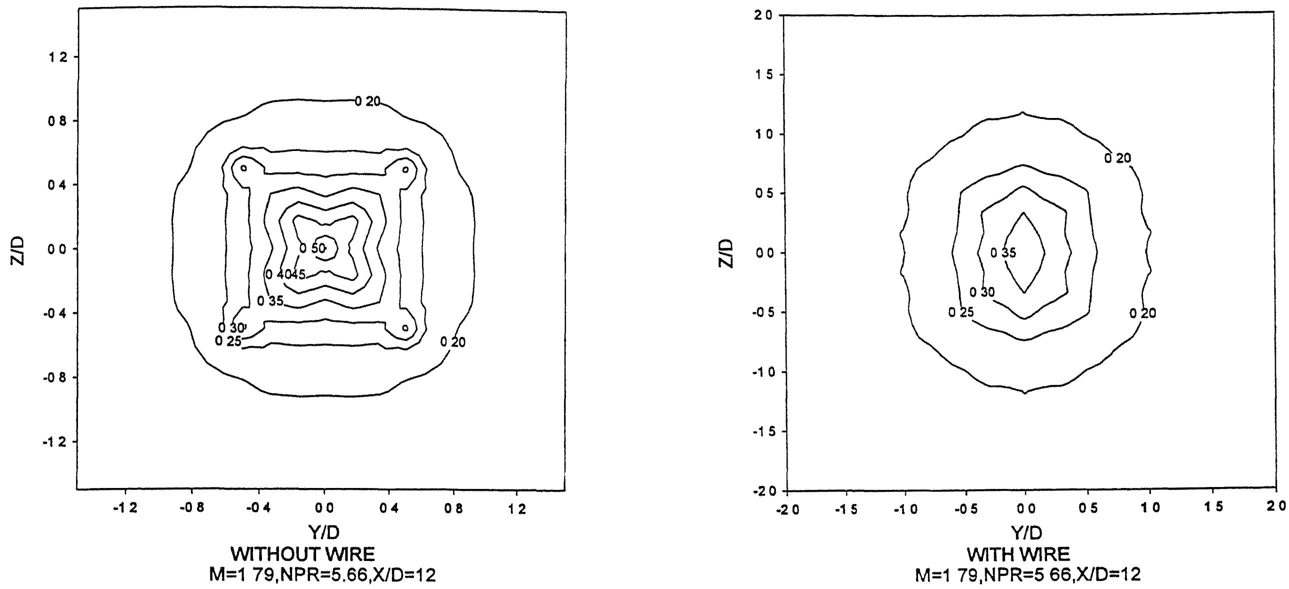


Figure 4.89

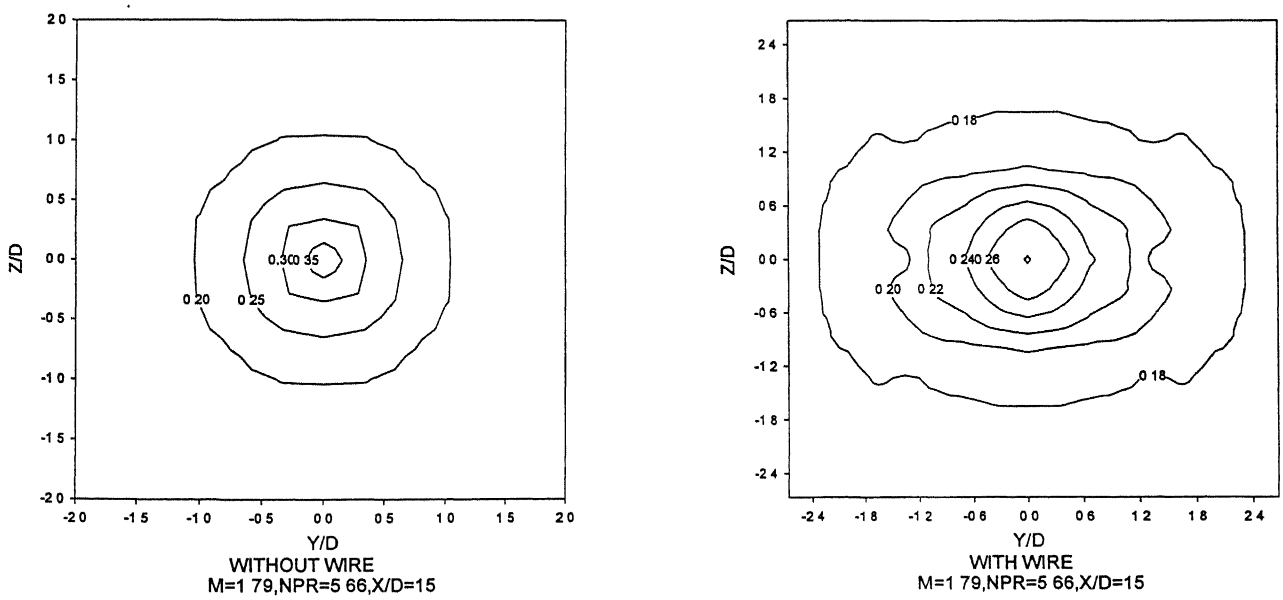


Figure 4.90

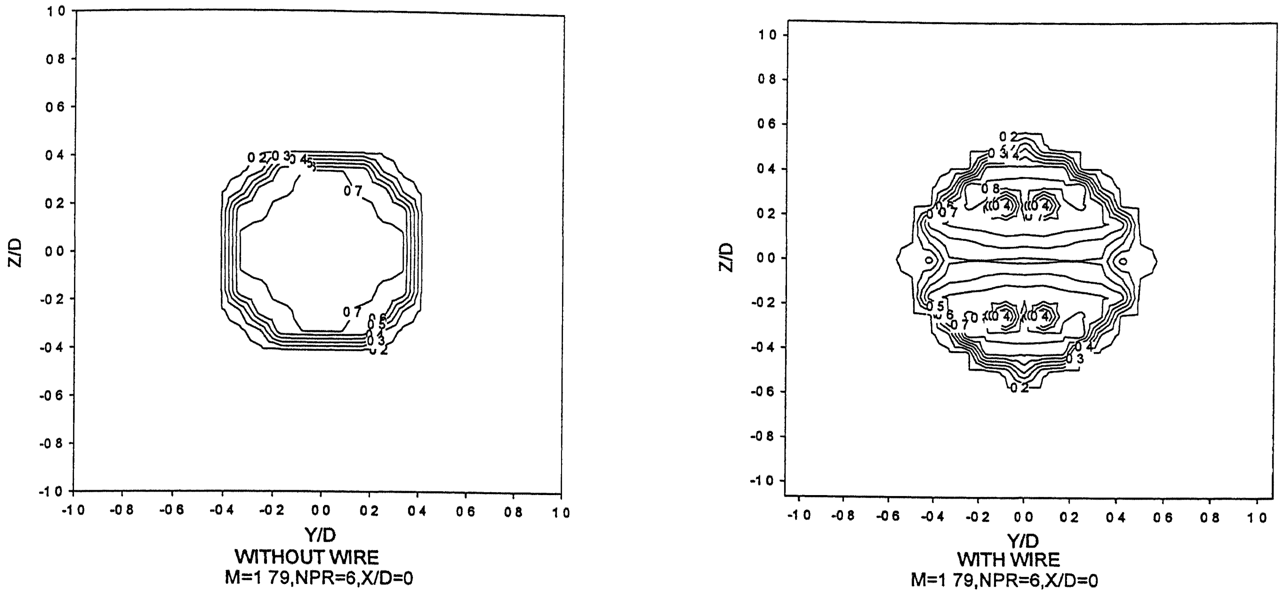


Figure 4.91

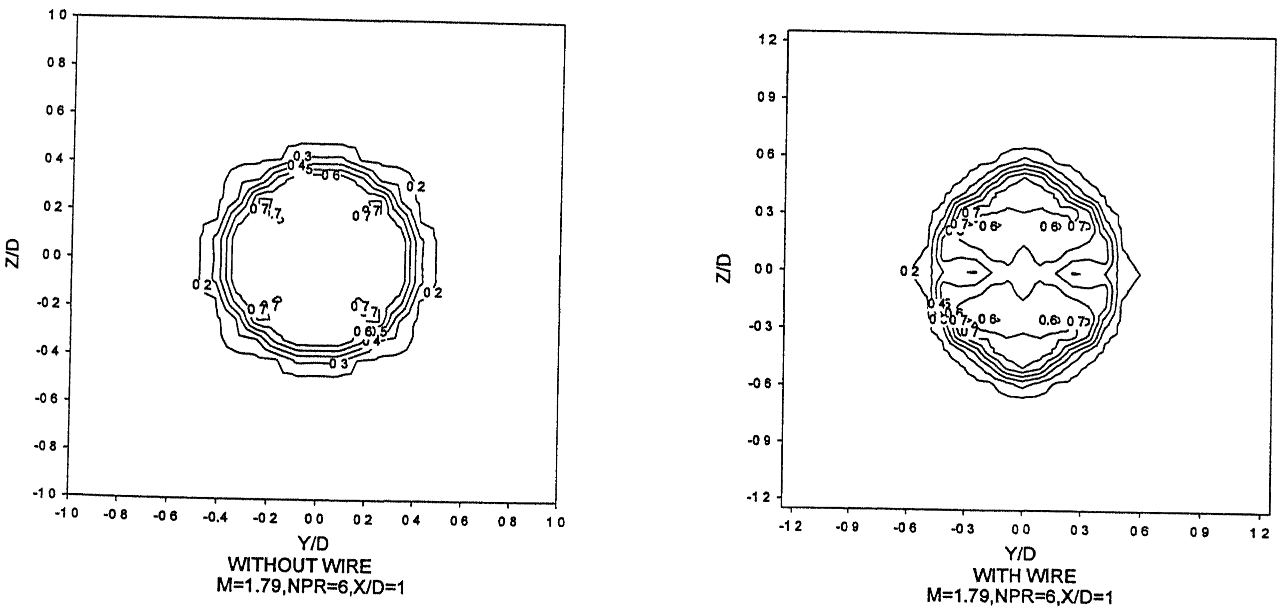


Figure 4.92

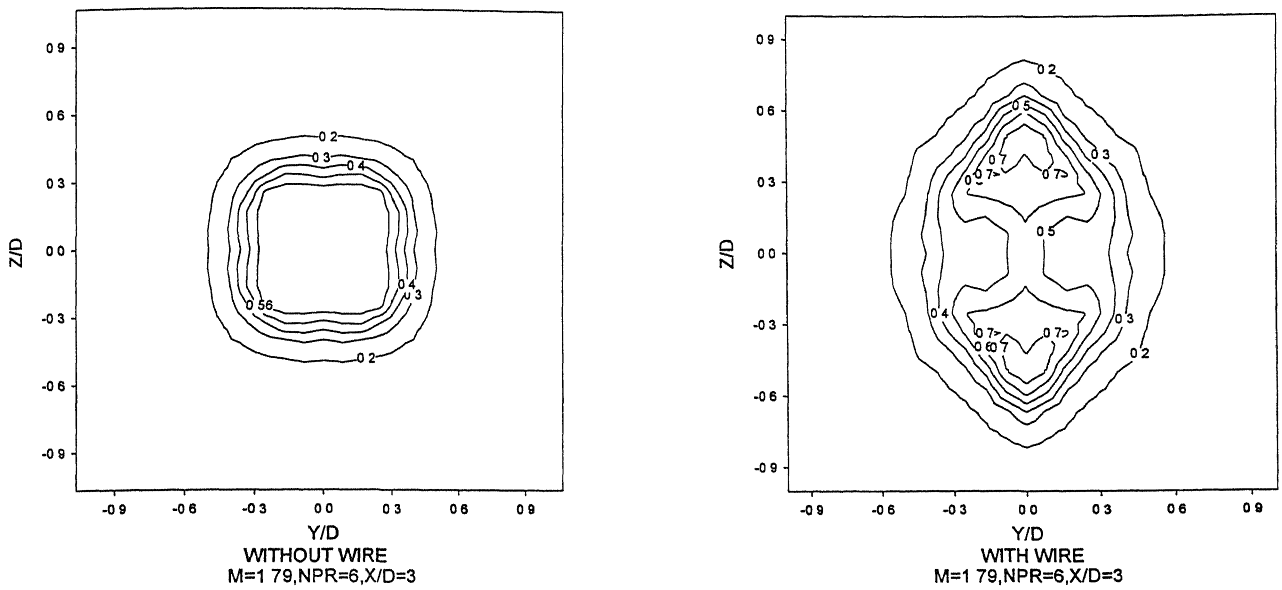


Figure 4.93

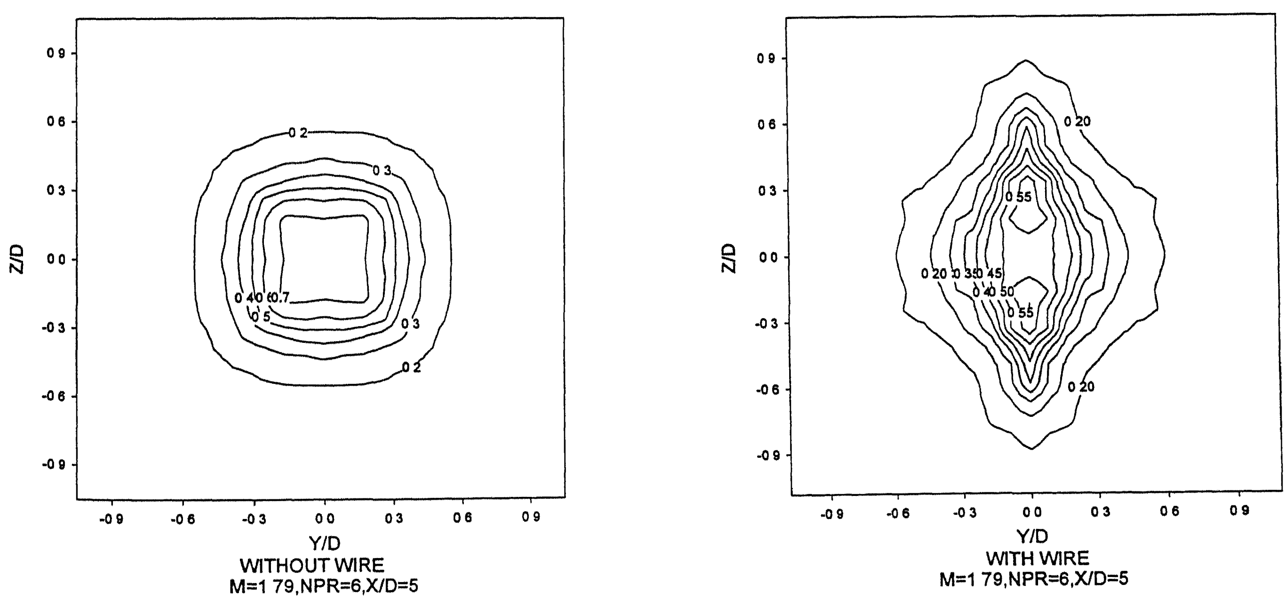


Figure 4.94

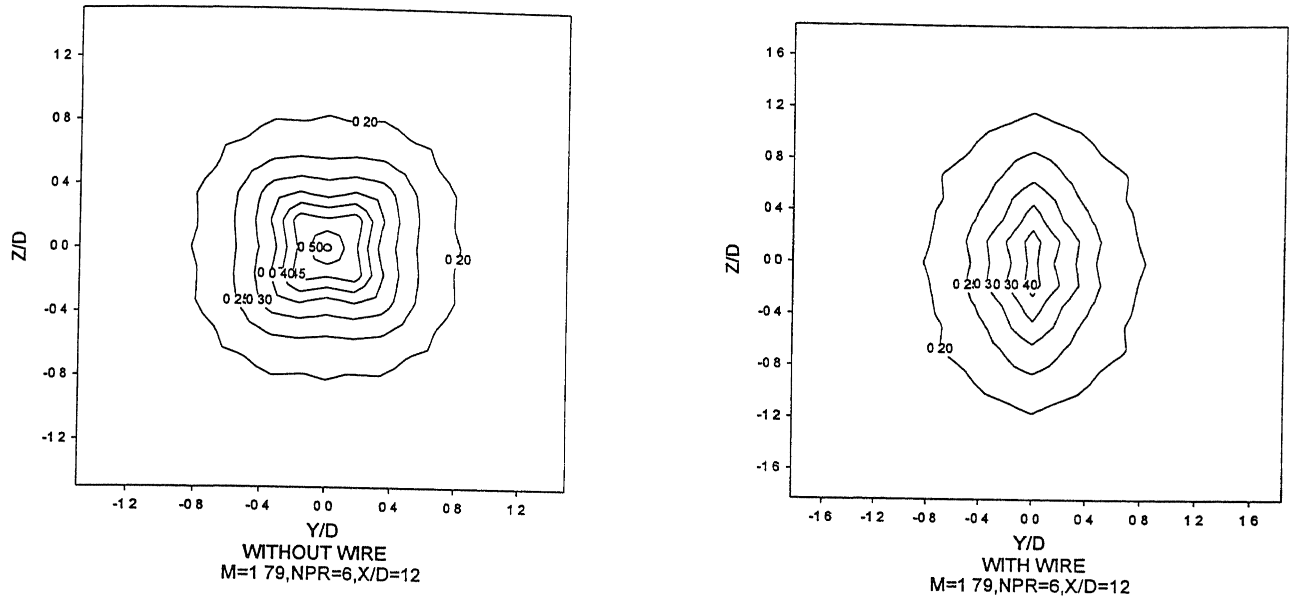


Figure 4.95

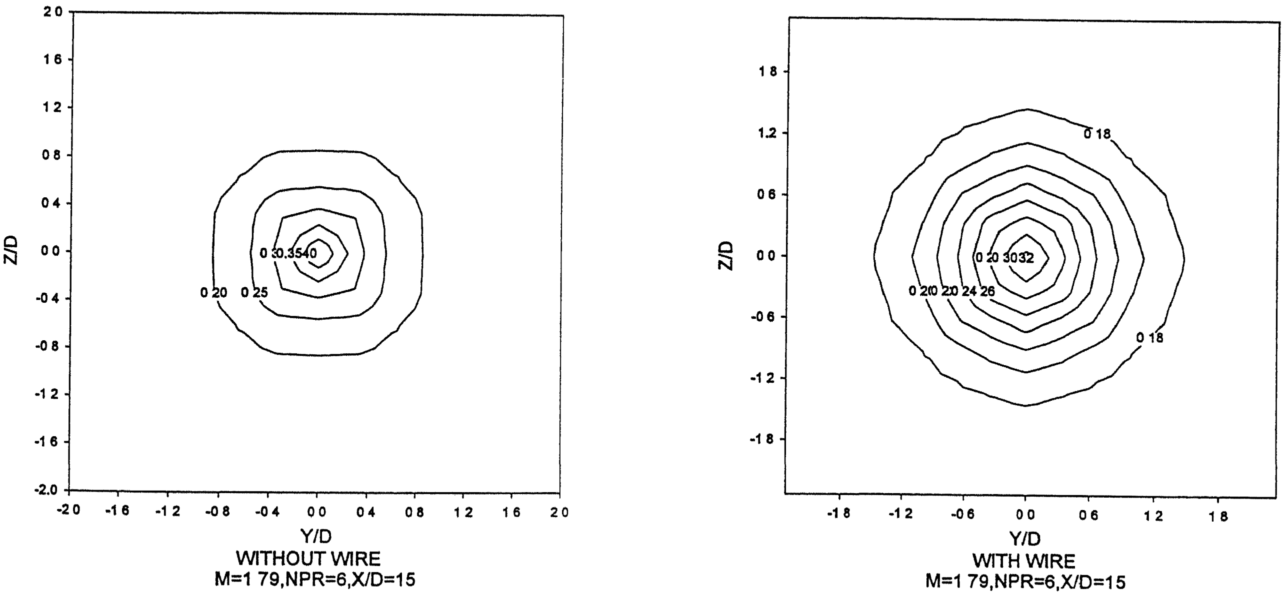


Figure 4.96

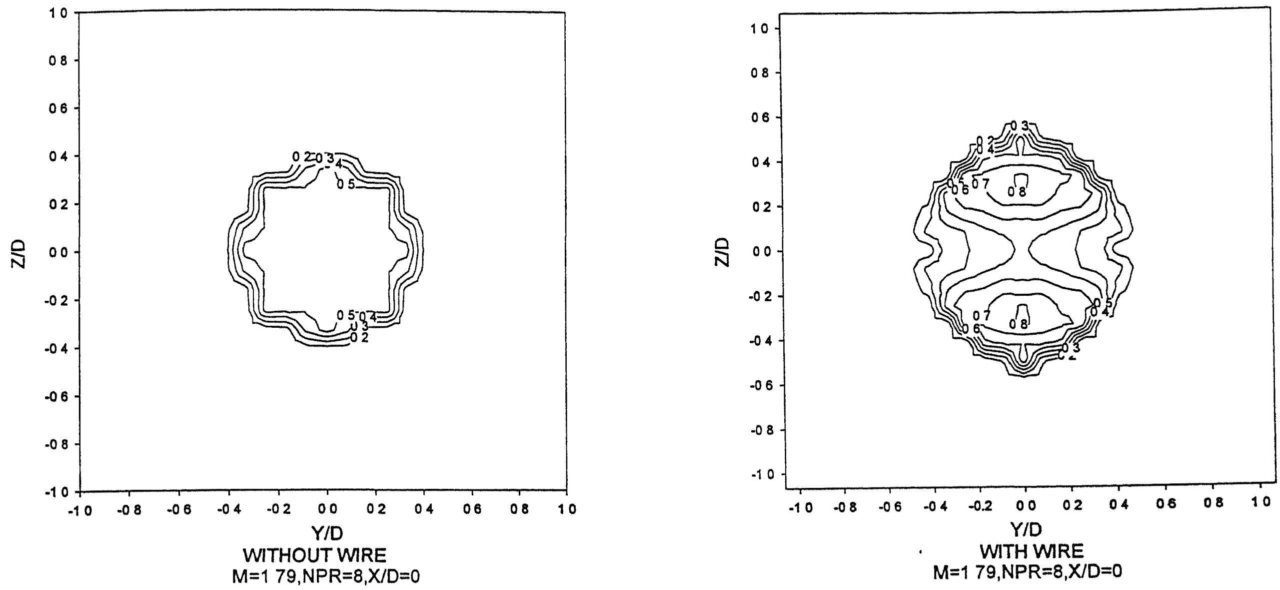


Figure 4.97

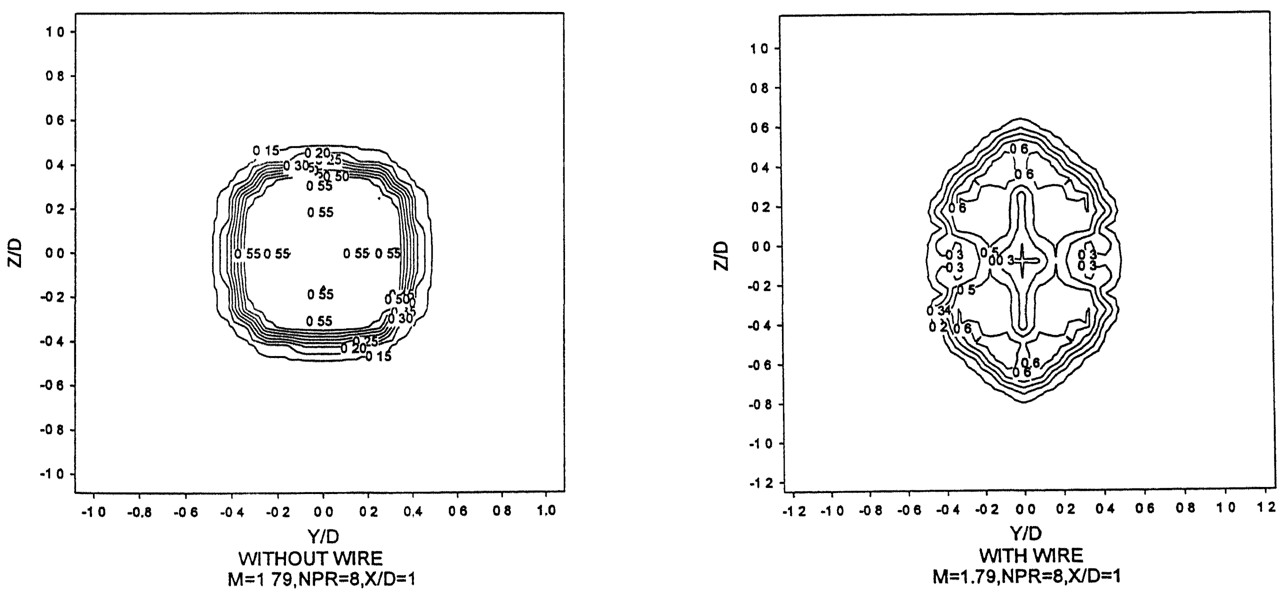


Figure 4.98

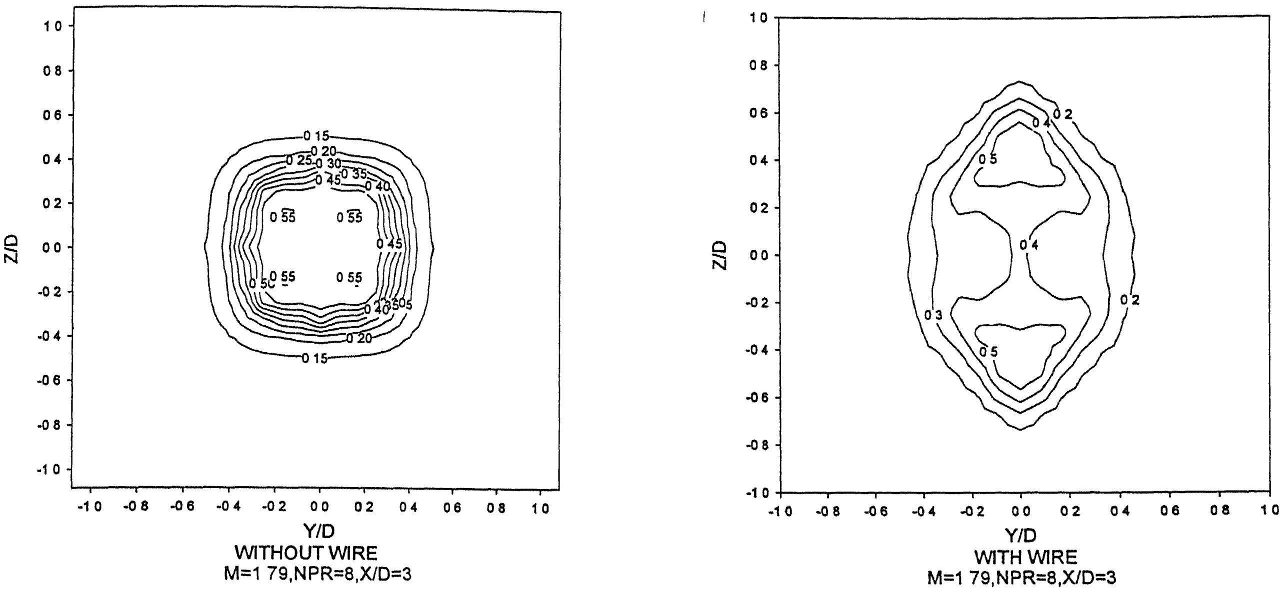


Figure 4.99

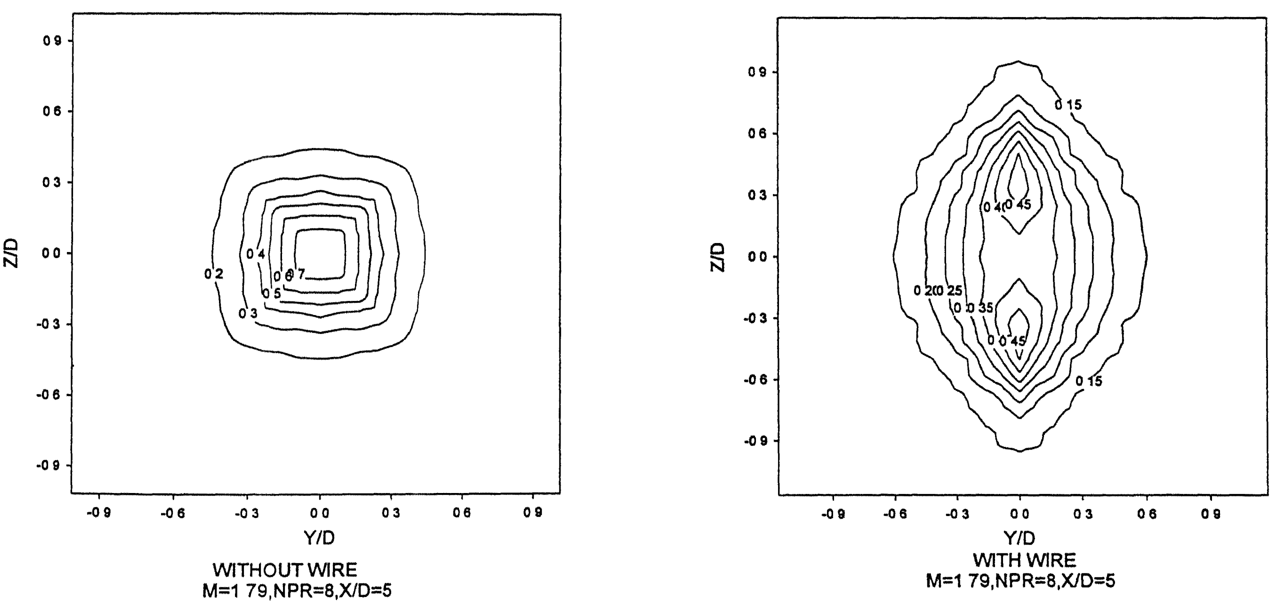


Figure 4.100

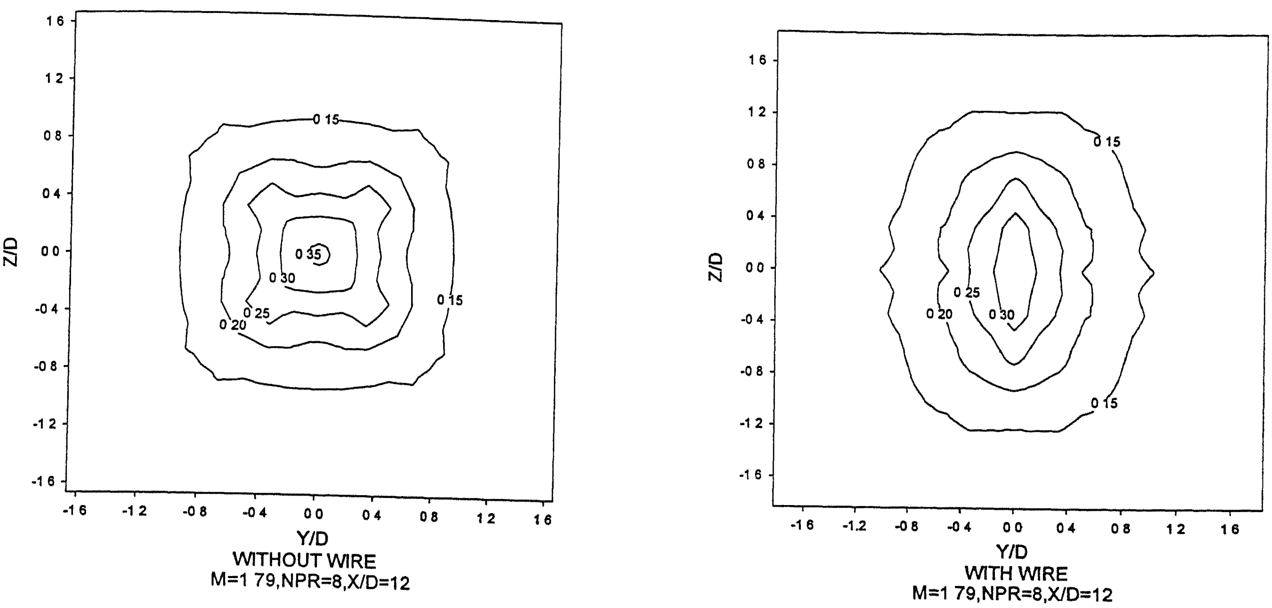


Figure 4.101

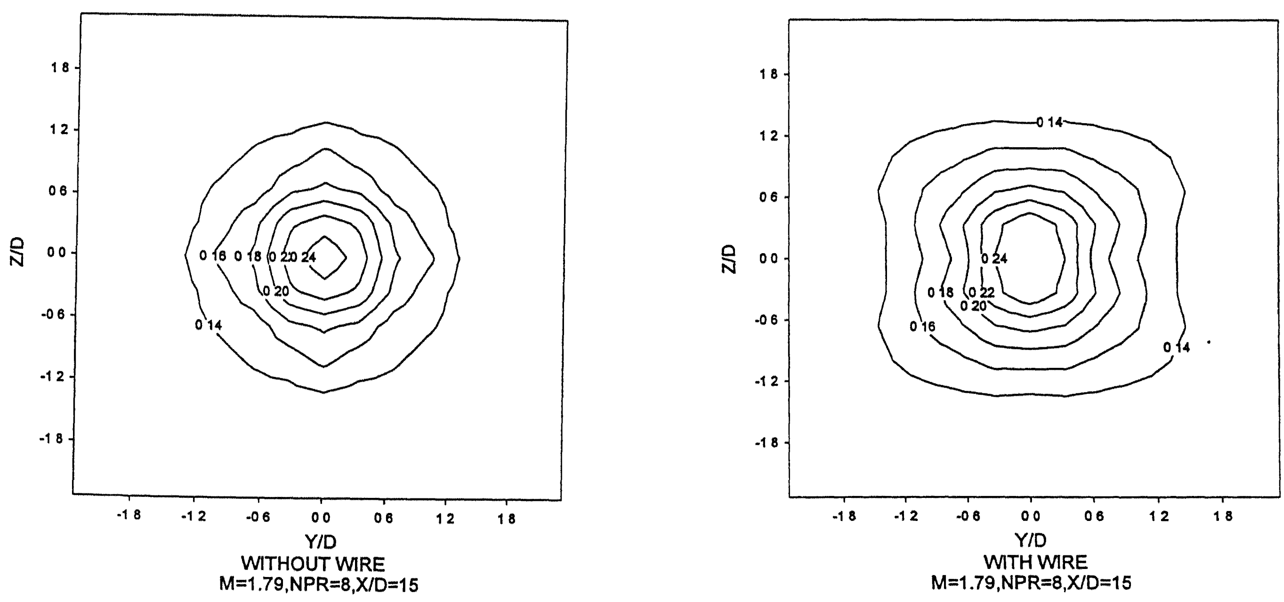


Figure 4.102

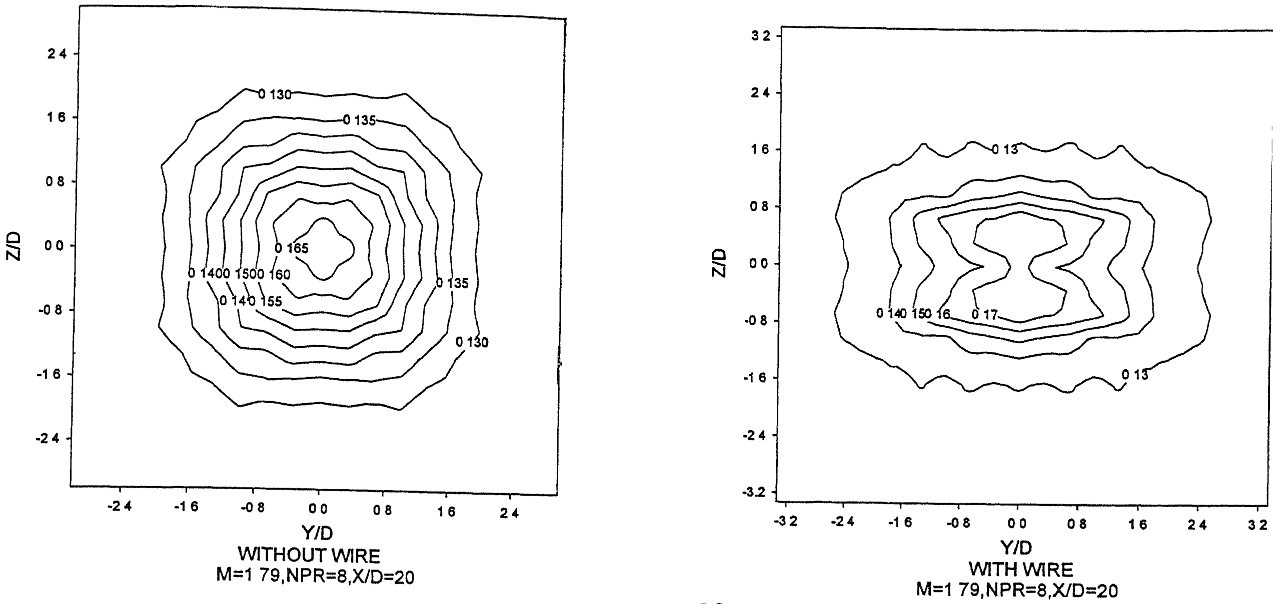


Figure 4.103

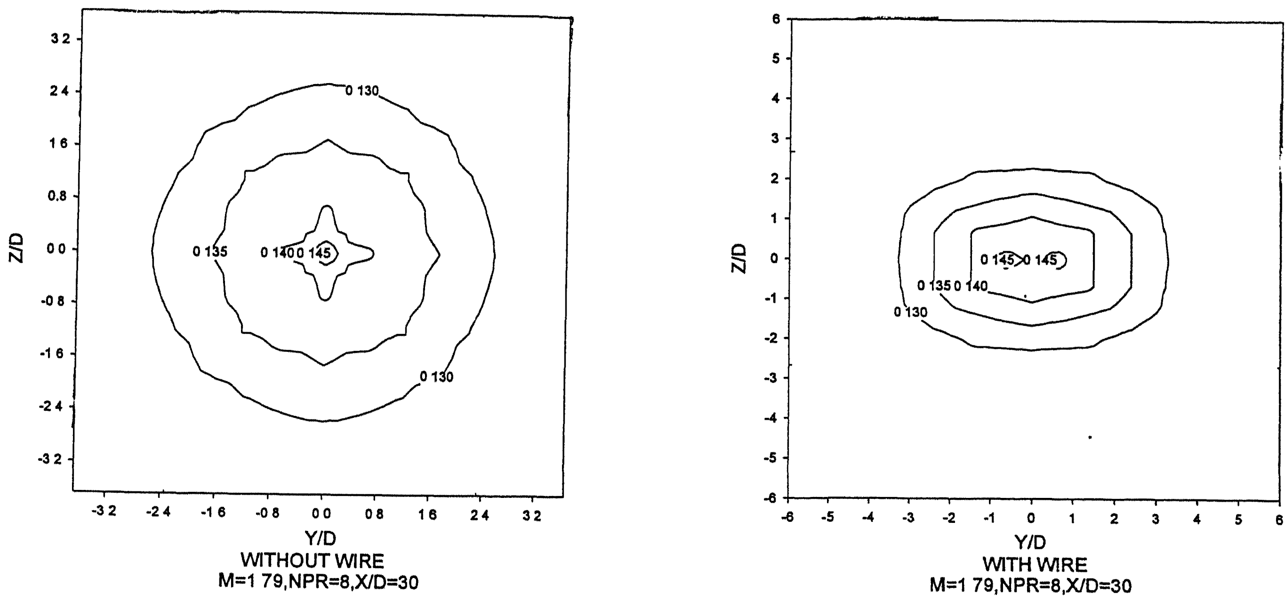


Figure 4.104

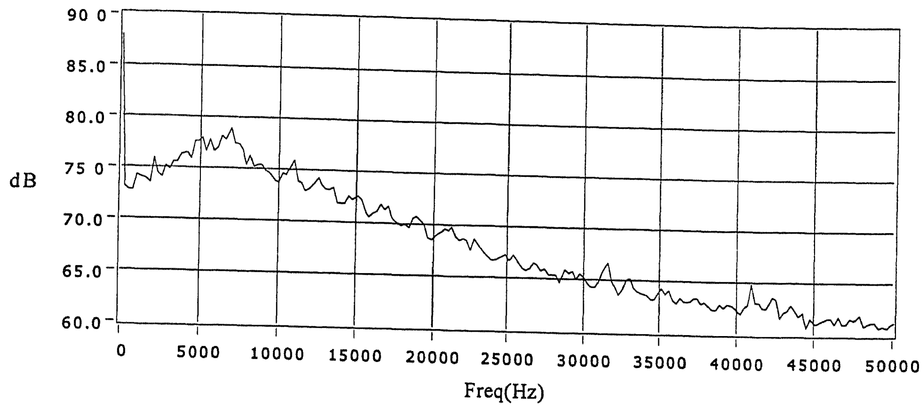


Figure 4.105 Frequency spectrum for M=1.79, NPR 2, X/D=0, R/D=30
Without wire

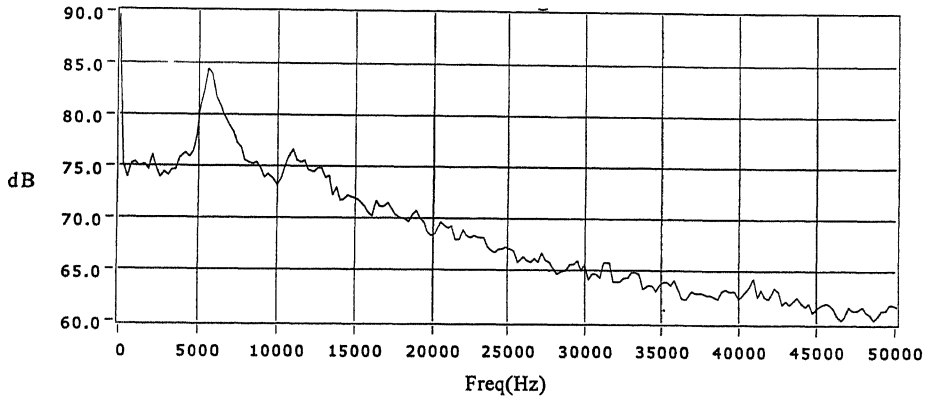


Figure 4.106 Frequency spectrum for M=1.79, NPR 2, X/D=0, R/D=30
along the wire

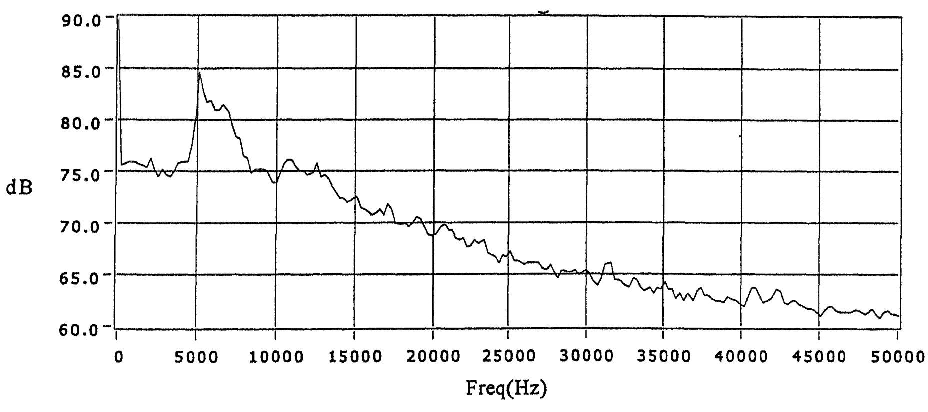


Figure 4.107 Frequency spectrum for M=1.79, NPR 2, X/D=0, R/D=30
normal to the wire

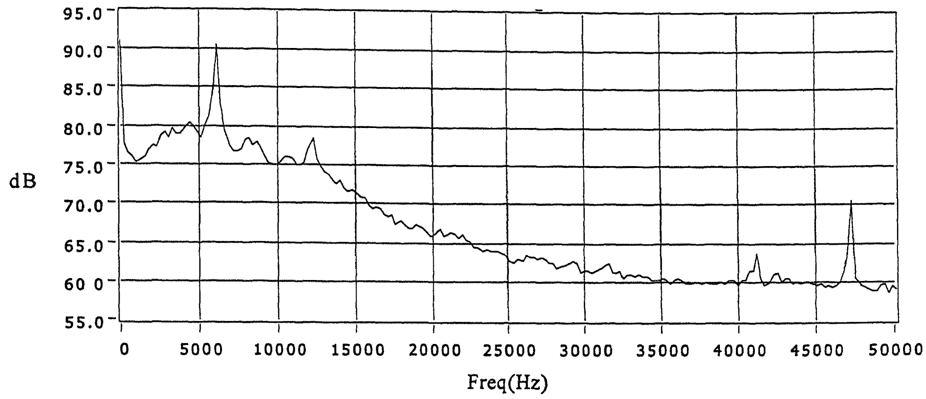


Figure 4.108 Frequency spectrum for M=1.79, NPR 2, R/D=100, θ =30 deg.
Without wire

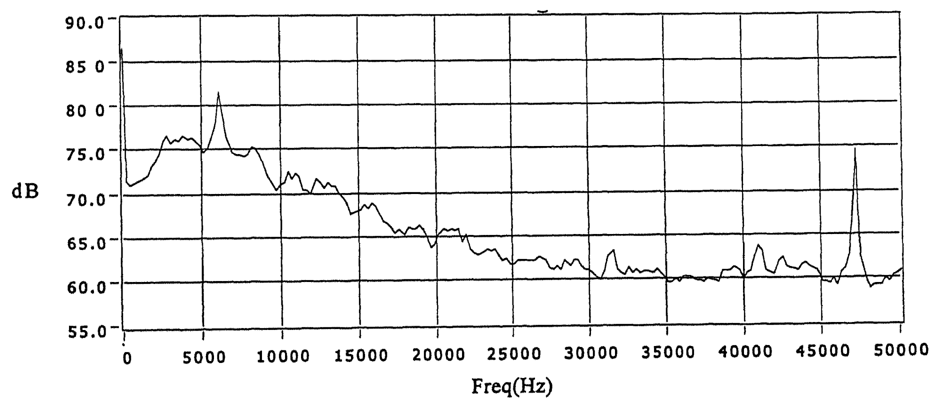


Figure 4.109 Frequency spectrum for M=1.79, NPR 2, R/D=100, θ =30 deg.
along the wire

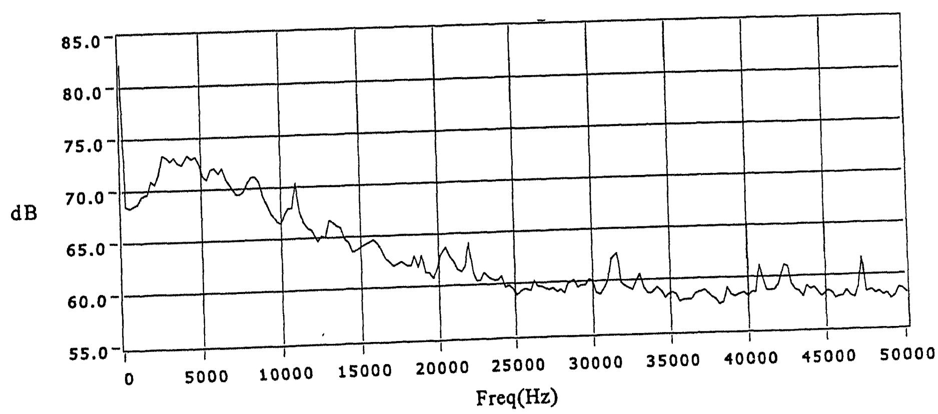


Figure 4.110 Frequency spectrum for M=1.79, NPR 2, R/D=100, θ =30 deg.
Normal to the wire

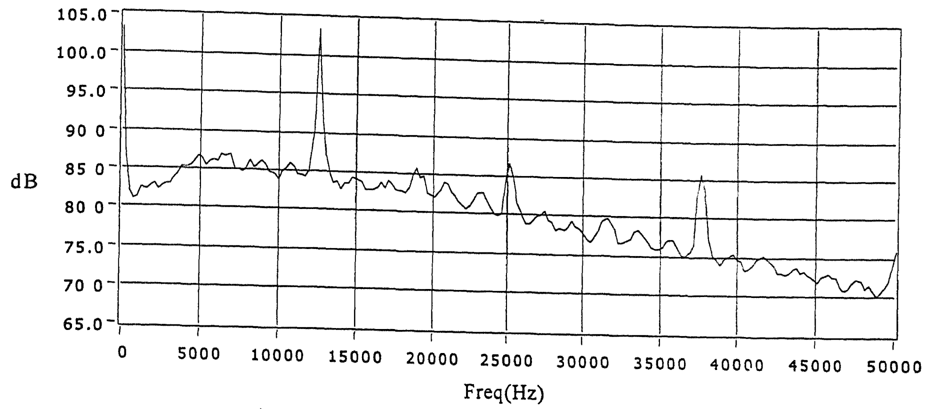


Figure 4.111 Frequency spectrum for M=1.79, NPR 3, X/D=0, R/D=30
Without wire

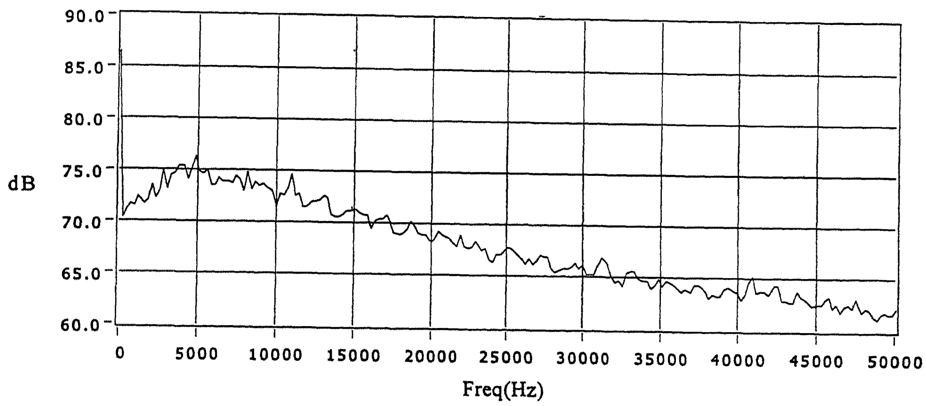


Figure 4.112 Frequency spectrum for M=1.79, NPR 3, X/D=0, R/D=30
along the wire

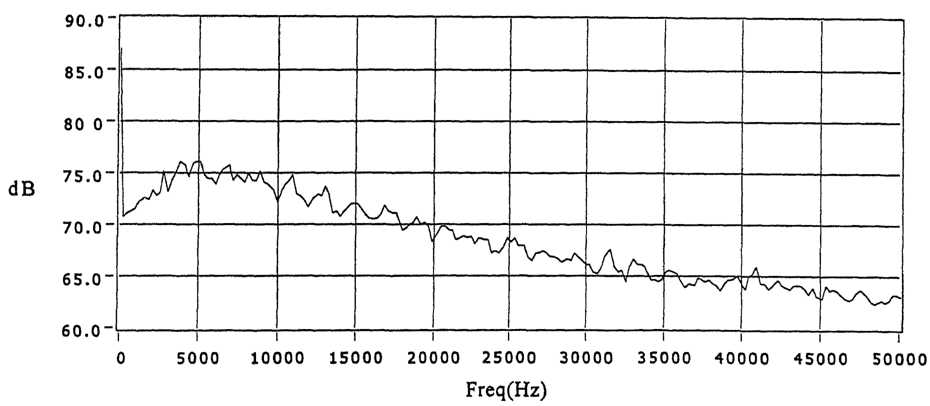


Figure 4.113 Frequency spectrum for M=1.79, NPR 3, X/D=0, R/D=30,
normal to the wire

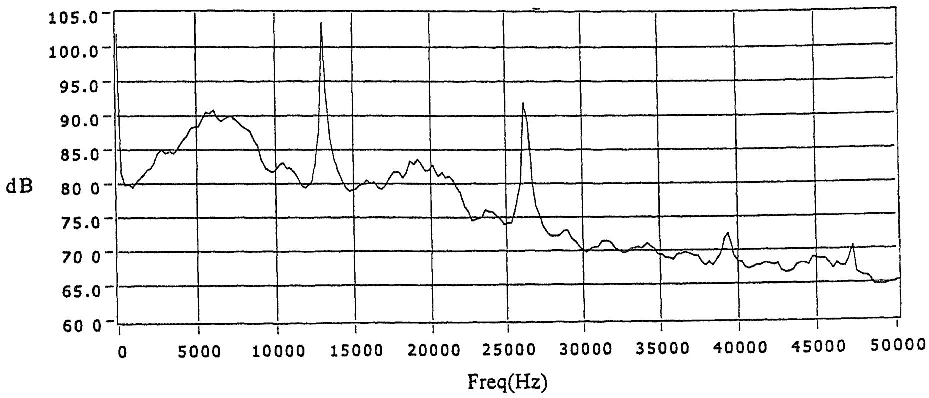


Figure 4.114 Frequency spectrum for M=1.79, NPR 3, R/D=100, θ =30 deg. Without wire

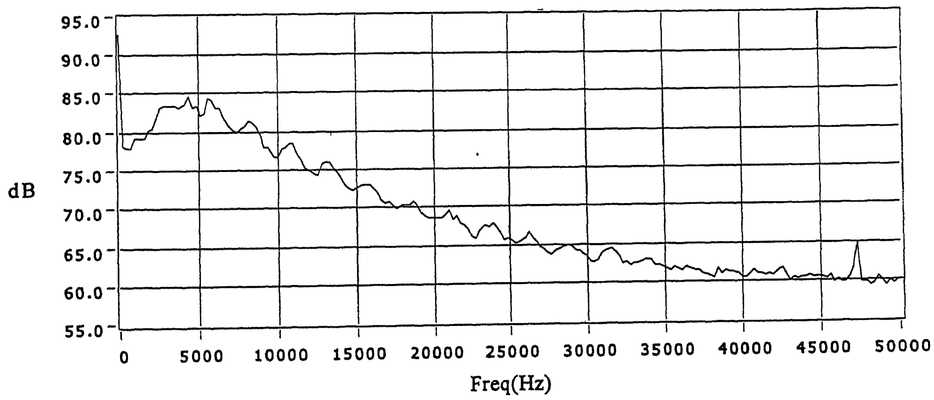


Figure 4.115 Frequency spectrum for M=1.79, NPR 3, R/D=100, θ =30 deg. along the wire

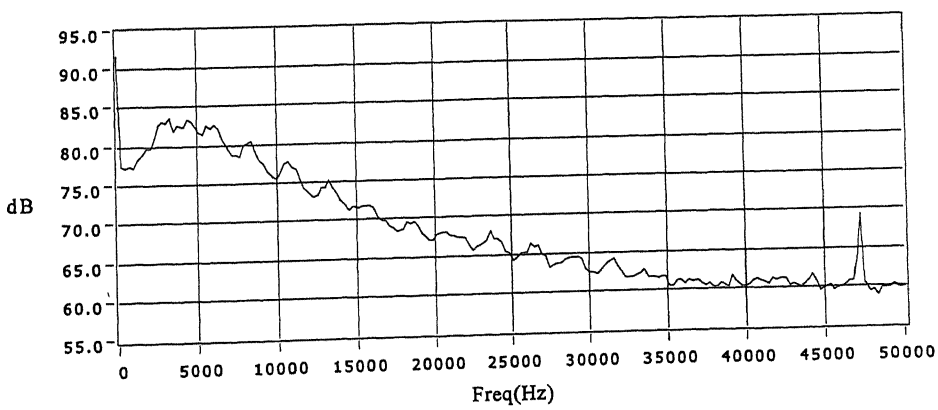


Figure 4.116 Frequency spectrum for M=1.79, NPR 3, R/D=100, θ =30 deg. Normal to the wire

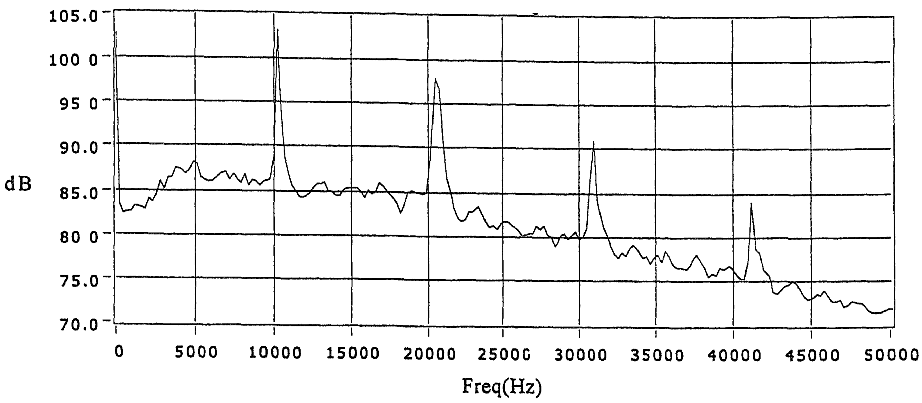


Figure 4.117 Frequency spectrum for M=1.79, NPR 4, X/D=0, R/D=30
Without wire

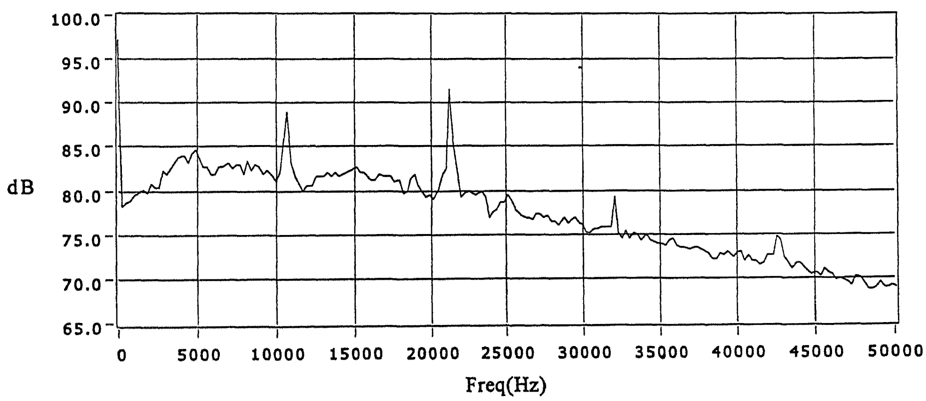


Figure 4.118 Frequency spectrum for M=1.79, NPR 4, X/D=0, R/D=30
along the wire

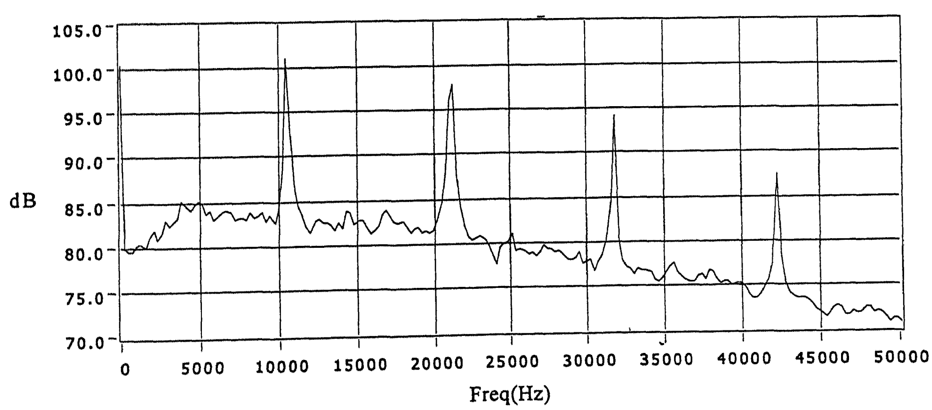


Figure 4.119 Frequency spectrum for M=1.79, NPR 4, X/D=0, R/D=30
normal to the wire

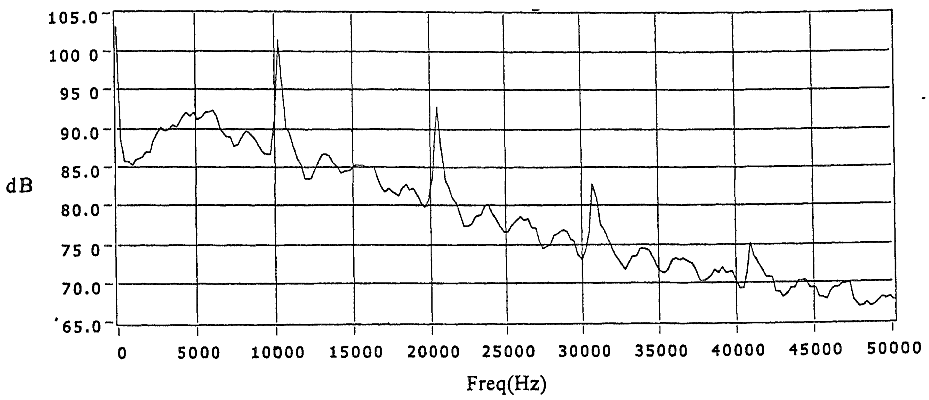


Figure 4.120 Frequency spectrum for M=1.79, NPR 4, R/D=100, θ =30 deg. Without wire

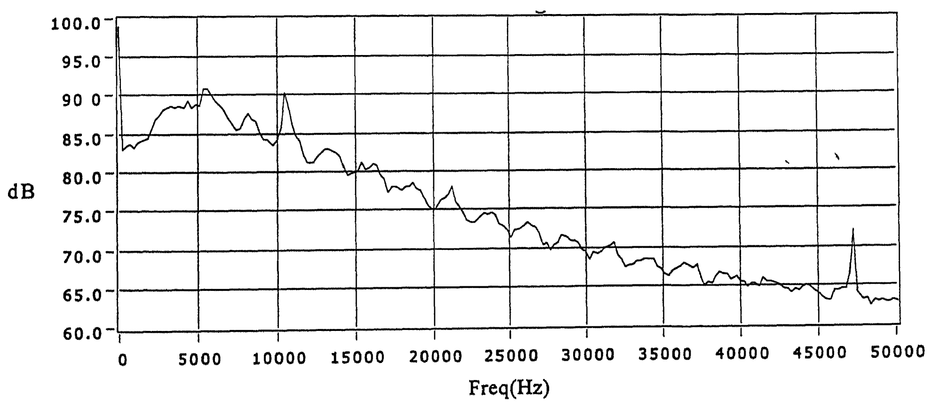


Figure 4.121 Frequency spectrum for M=1.79, NPR 4, R/D=100, θ =30 deg. along the wire

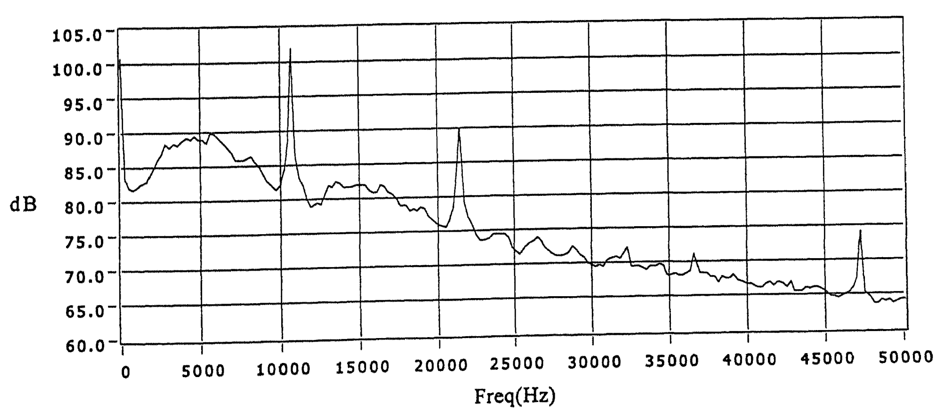


Figure 4.122 Frequency spectrum for M=1.79, NPR 4, R/D=100, θ =30 deg. normal to the wire

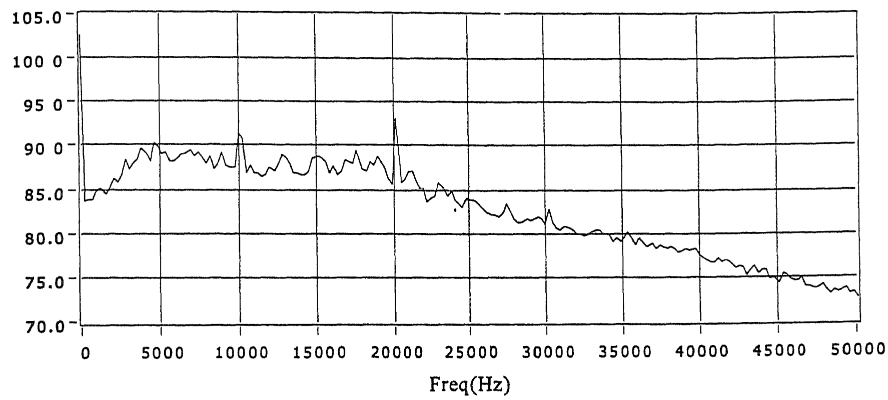


Figure 4.123 Frequency spectrum for M=1.79, NPR 5, X/D=0, R/D=30
Without wire

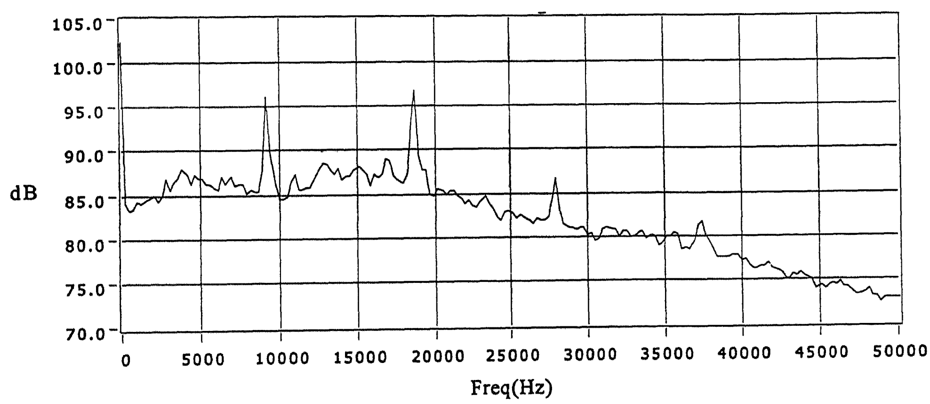


Figure 4.124 Frequency spectrum for M=1.79, NPR 5, X/D=0, R/D=30
along the wire

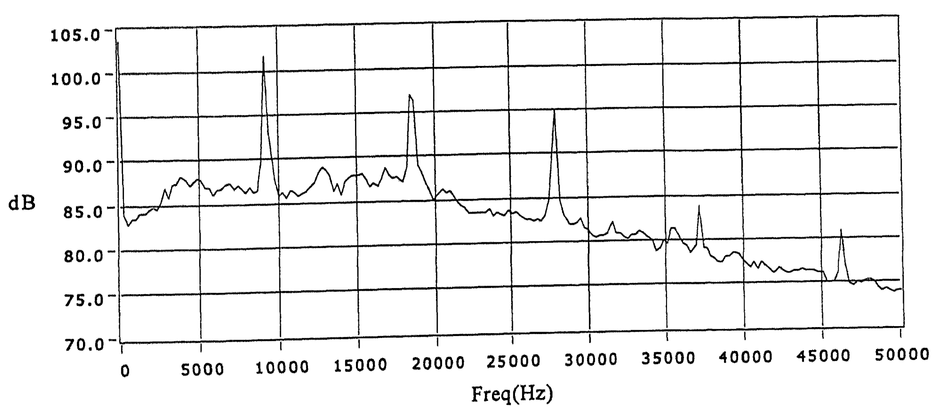


Figure 4.125 Frequency spectrum for M=1.79, NPR 5, X/D=0, R/D=30
normal to the wire

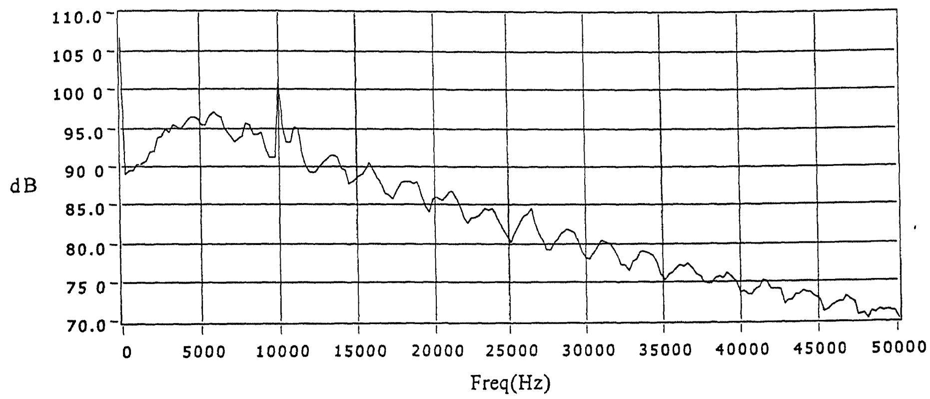


Figure 4.126 Frequency spectrum for M=1.79, NPR 5, R/D=100, θ =30 deg.
Without wire

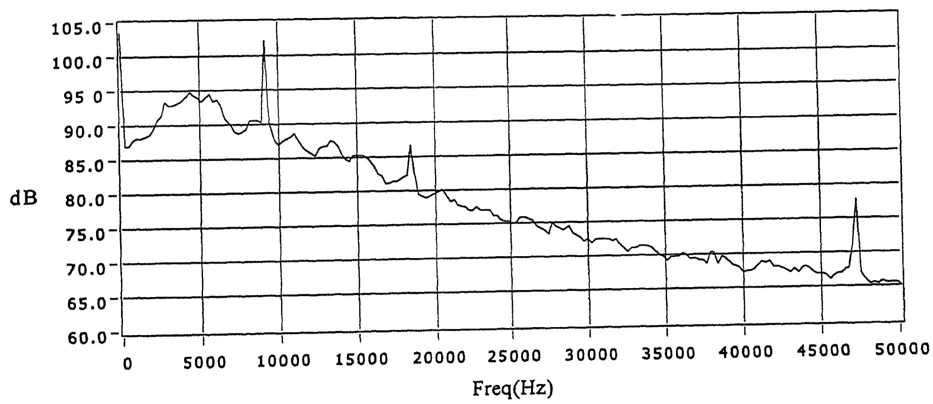


Figure 4.127 Frequency spectrum for M=1.79, NPR 5, R/D=100, θ =30 deg.
along the wire

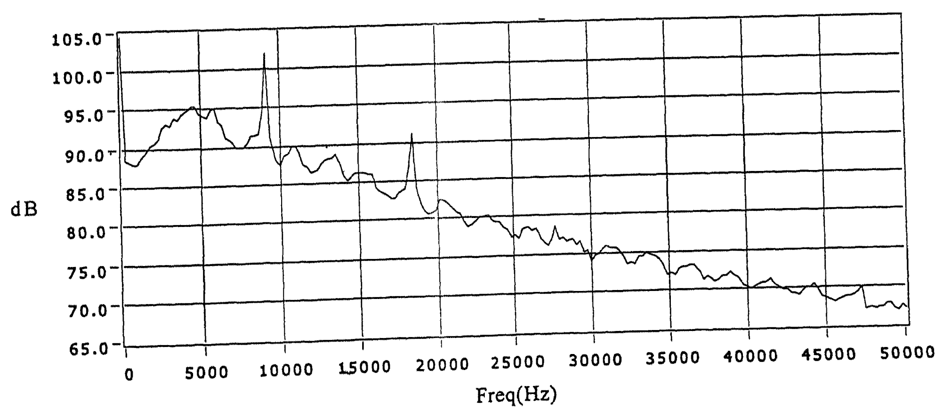


Figure 4.128 Frequency spectrum for M=1.79, NPR 5, R/D=100, θ =30 deg.
normal to the wire

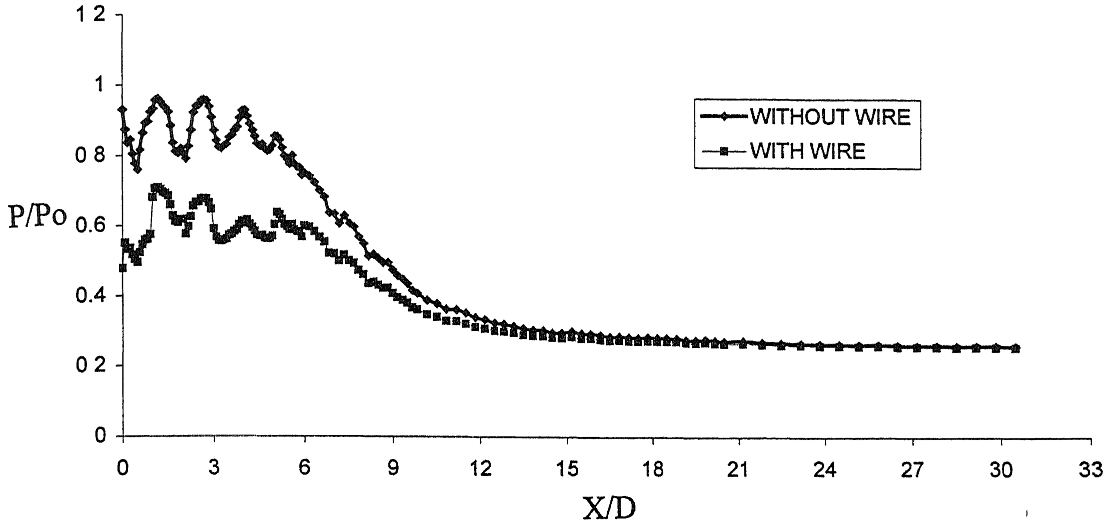


Figure 4.129 Centreline decay (M=2, NPR 4, Overexpansion)

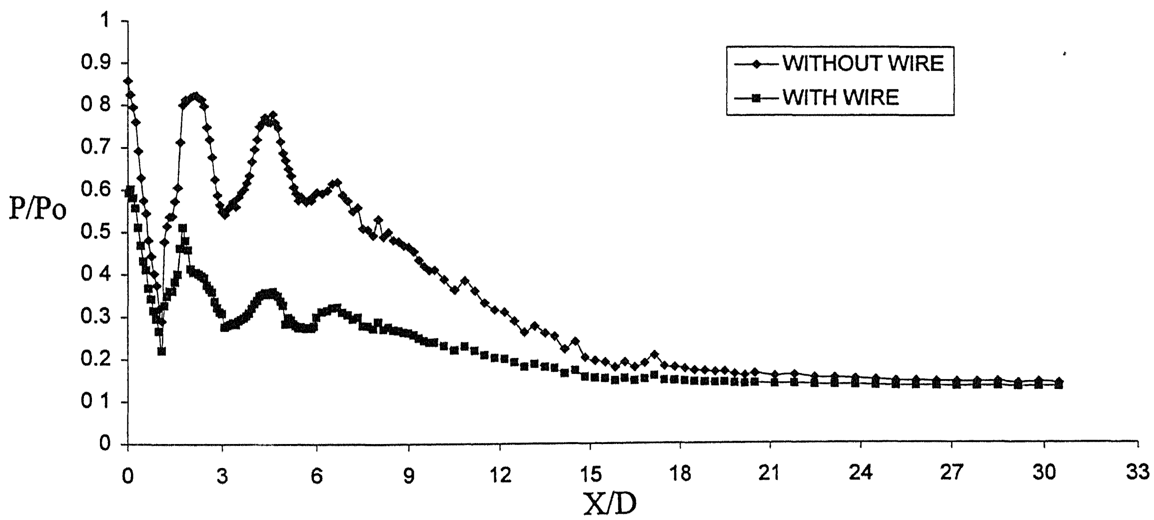


Figure 4.130 Centreline decay (M=2, NPR 7.82, Correct expansion)

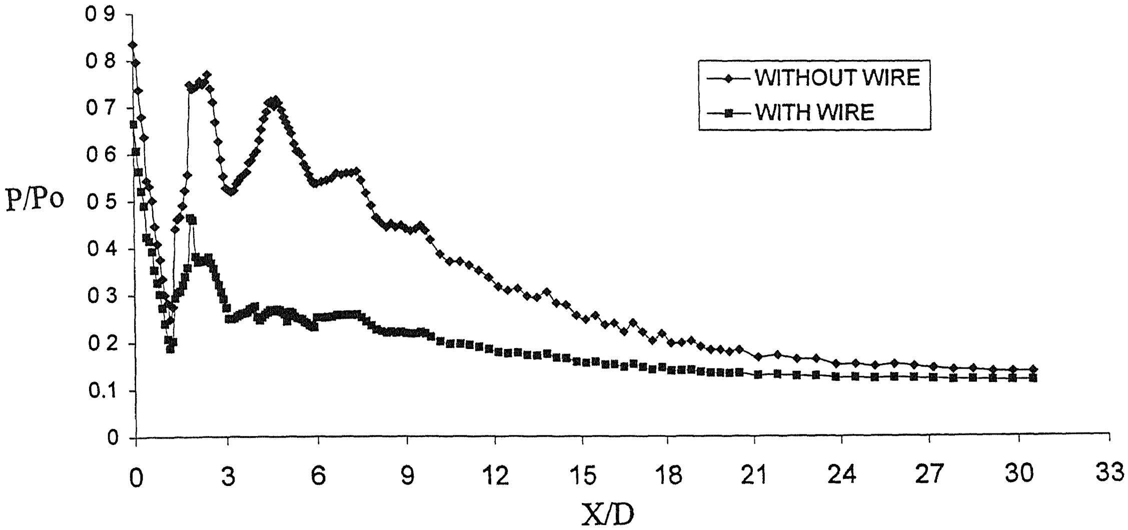


Figure 4.131 Centreline decay (M=2, NPR 9, Underexpansion)

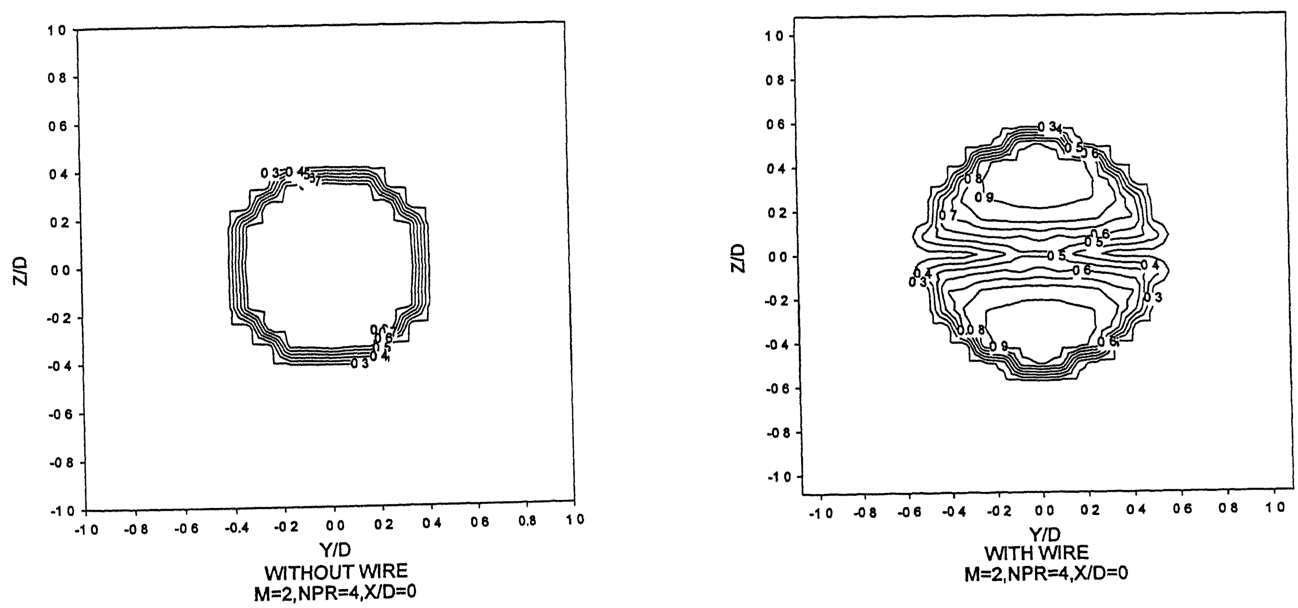


Figure 4.132

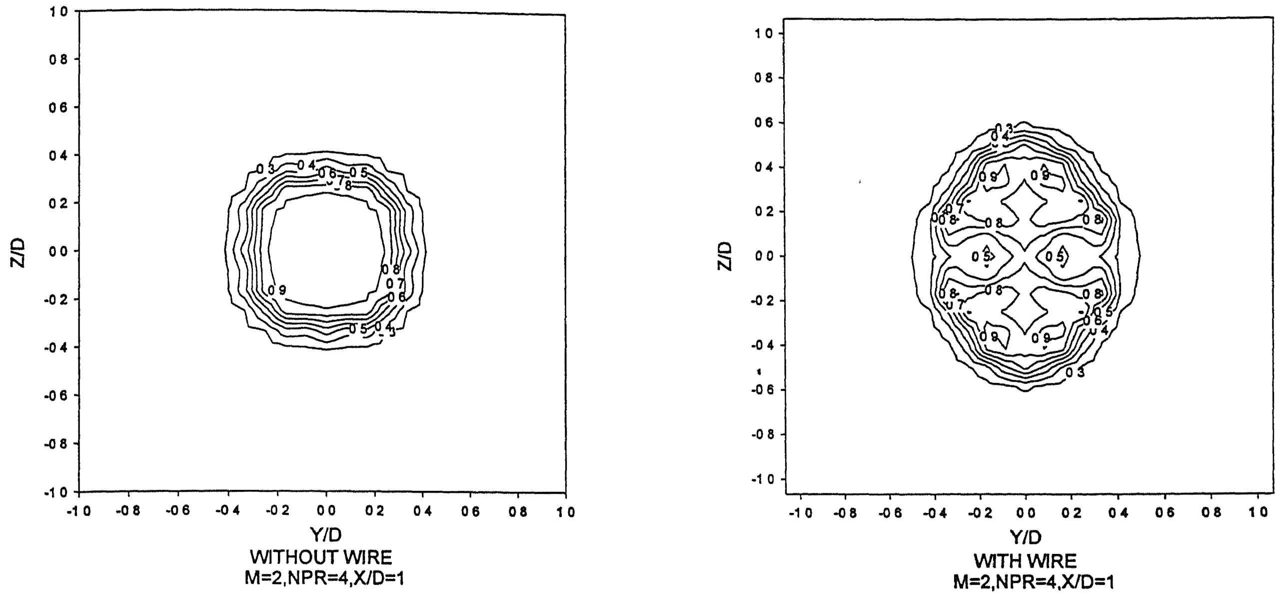


Figure 4.133

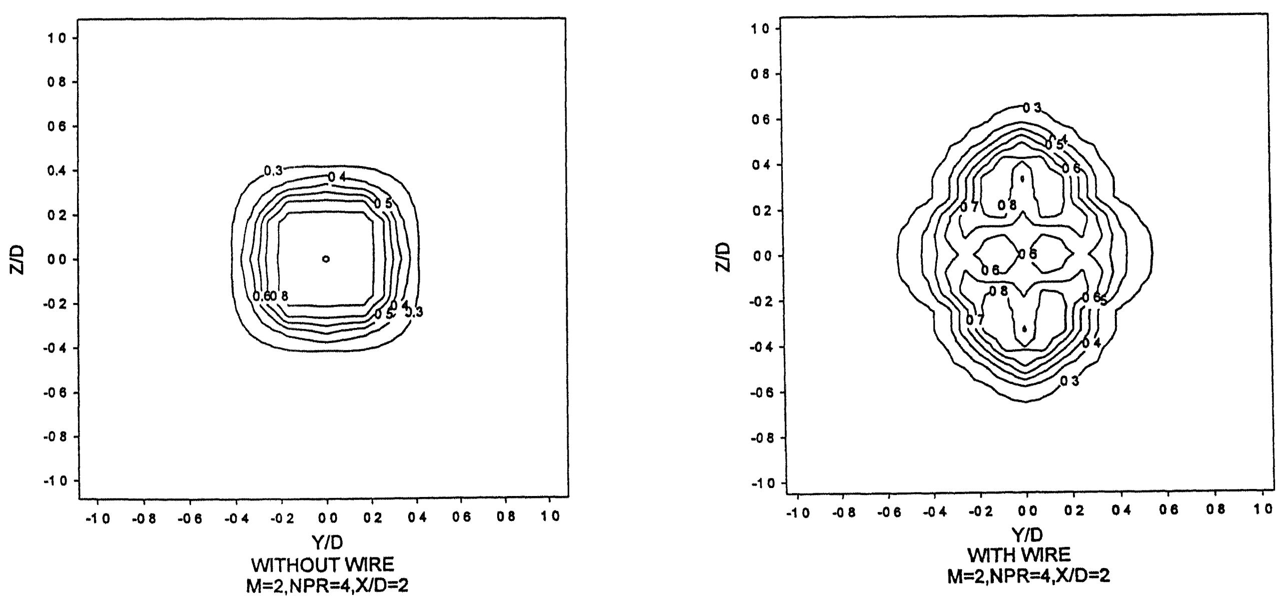


Figure 4.134

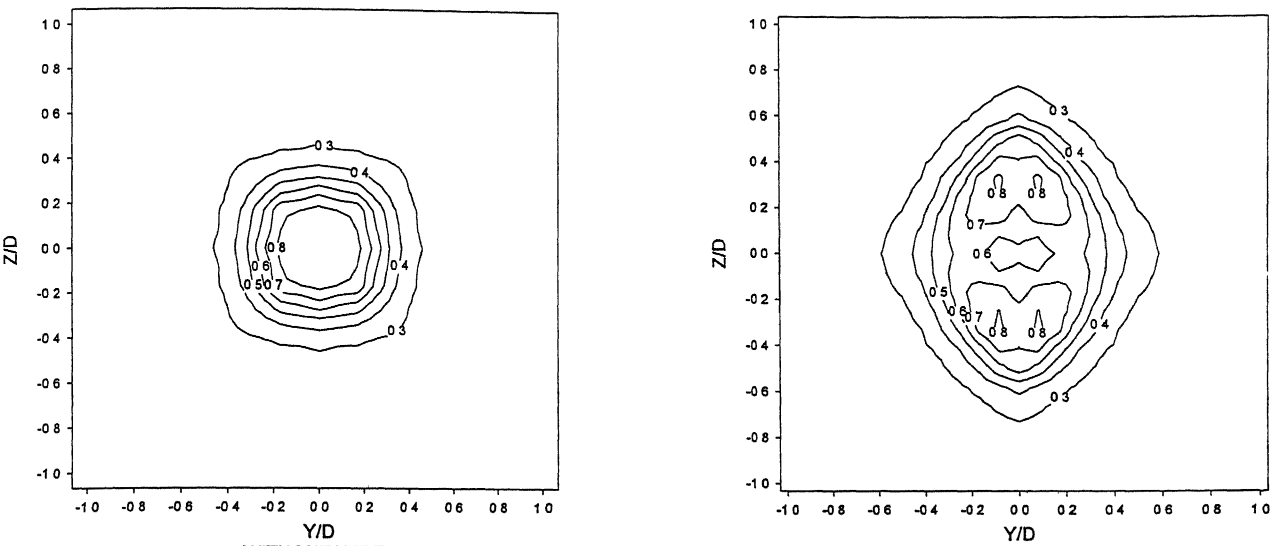


WITHOUT WIRE
M=2,NPR=4,X/D=3

WITH WIRE
M=2,NPR=4,X/D=3

Figure 4.135

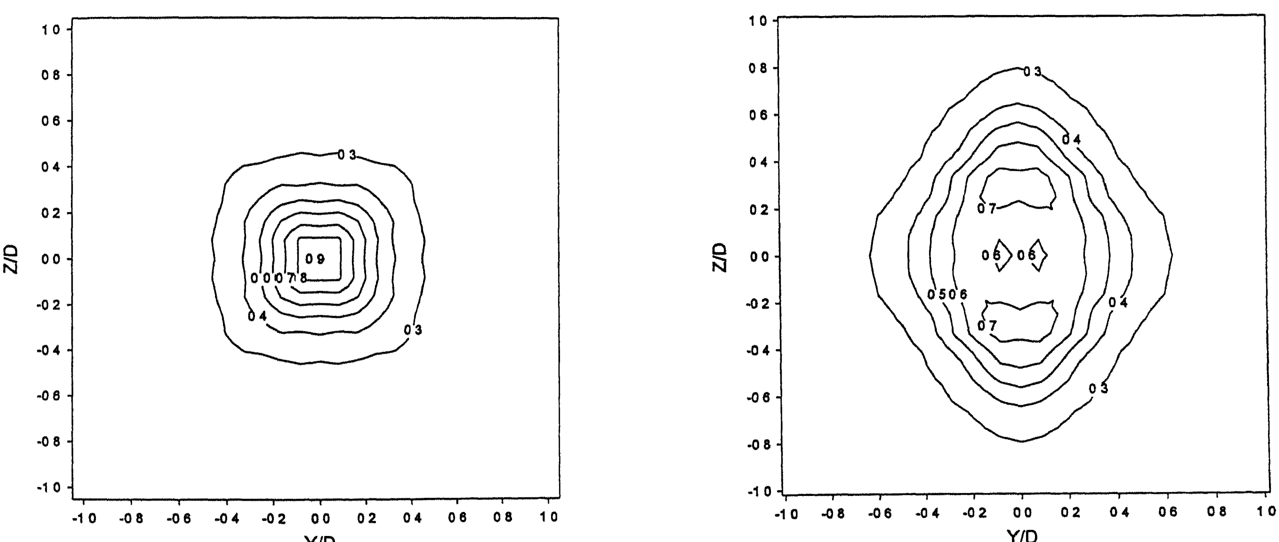


WITHOUT WIRE
M=2,NPR=4,X/D=4

WITH WIRE
M=2,NPR=4,X/D=4

Figure 4.136

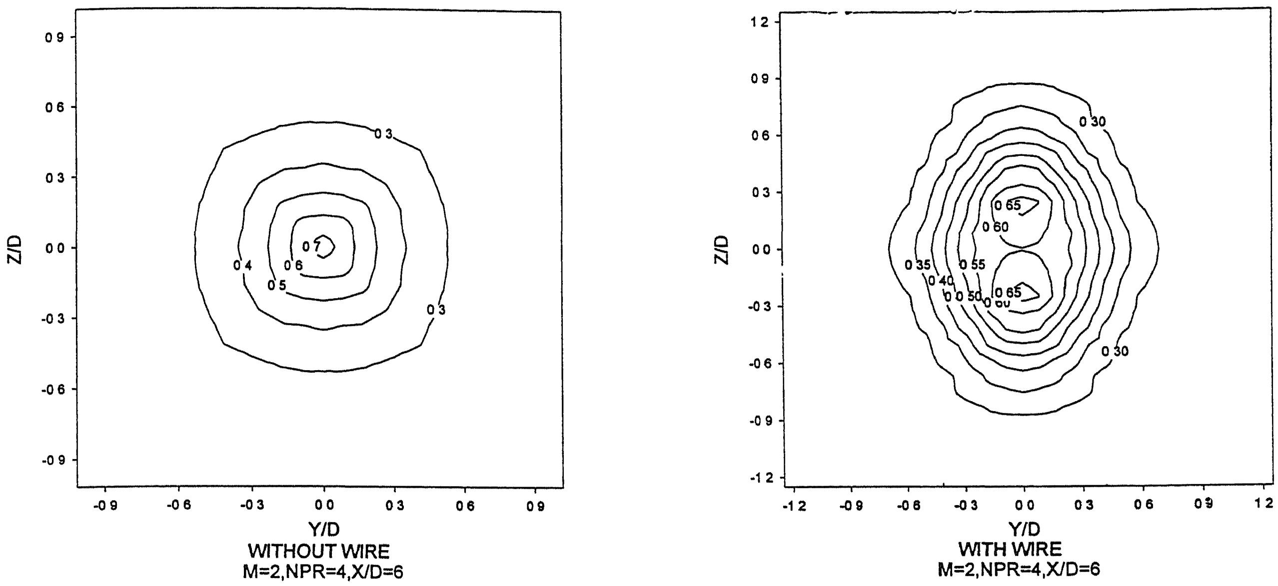


Figure 4.137

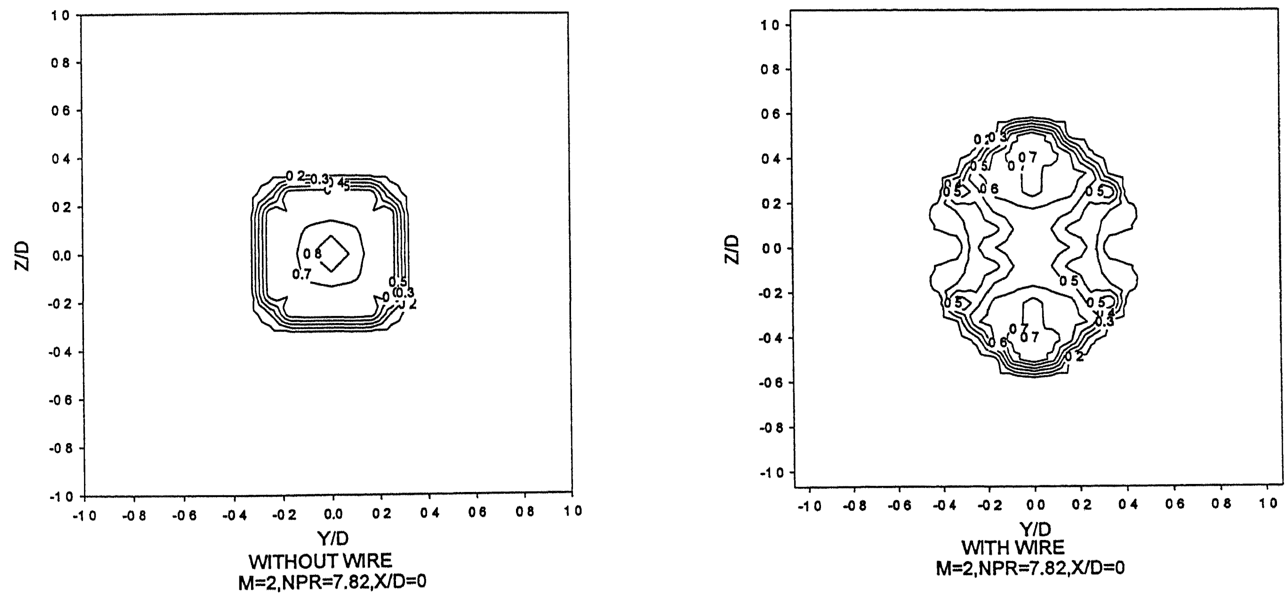


Figure 4.138

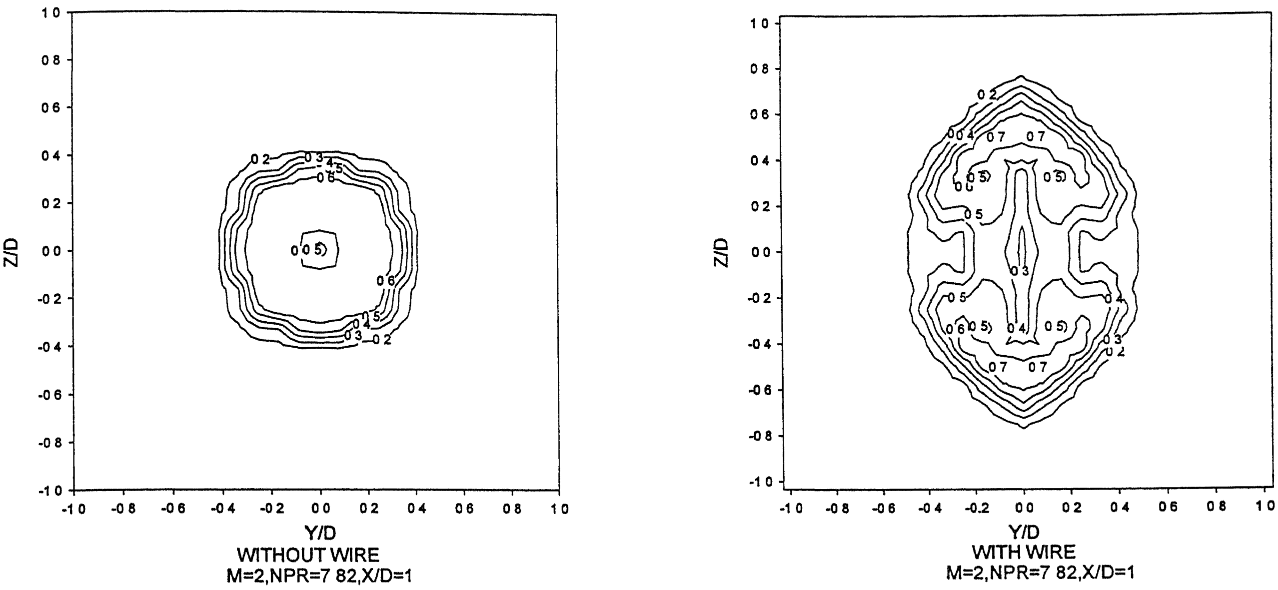


Figure 4.139

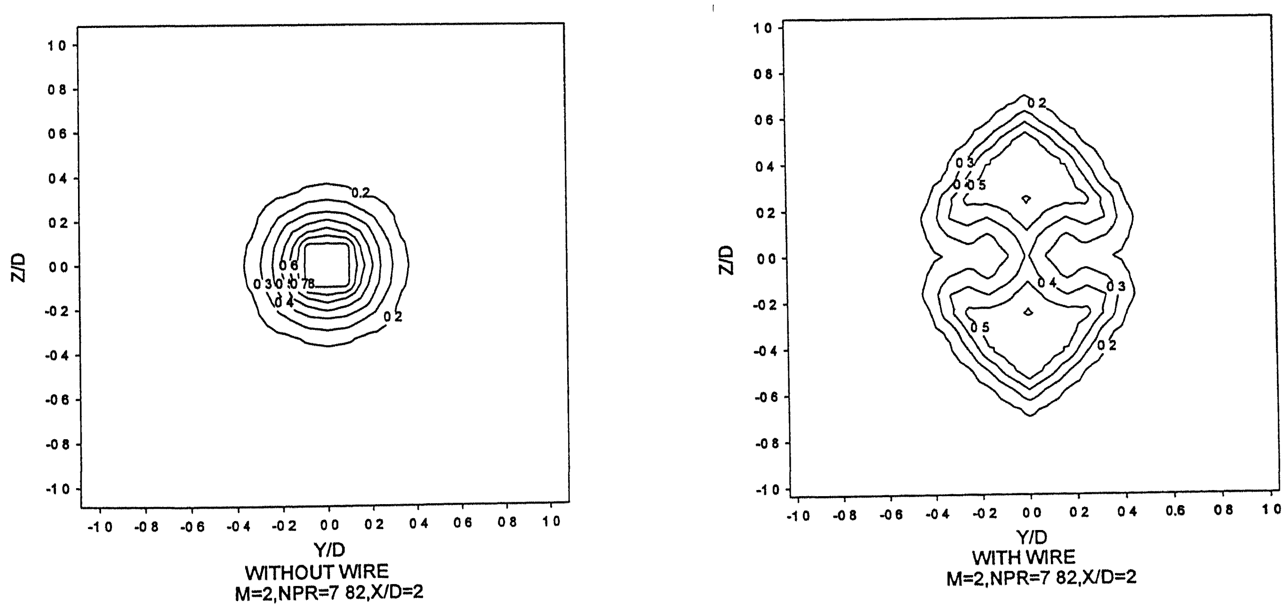


Figure 4.140

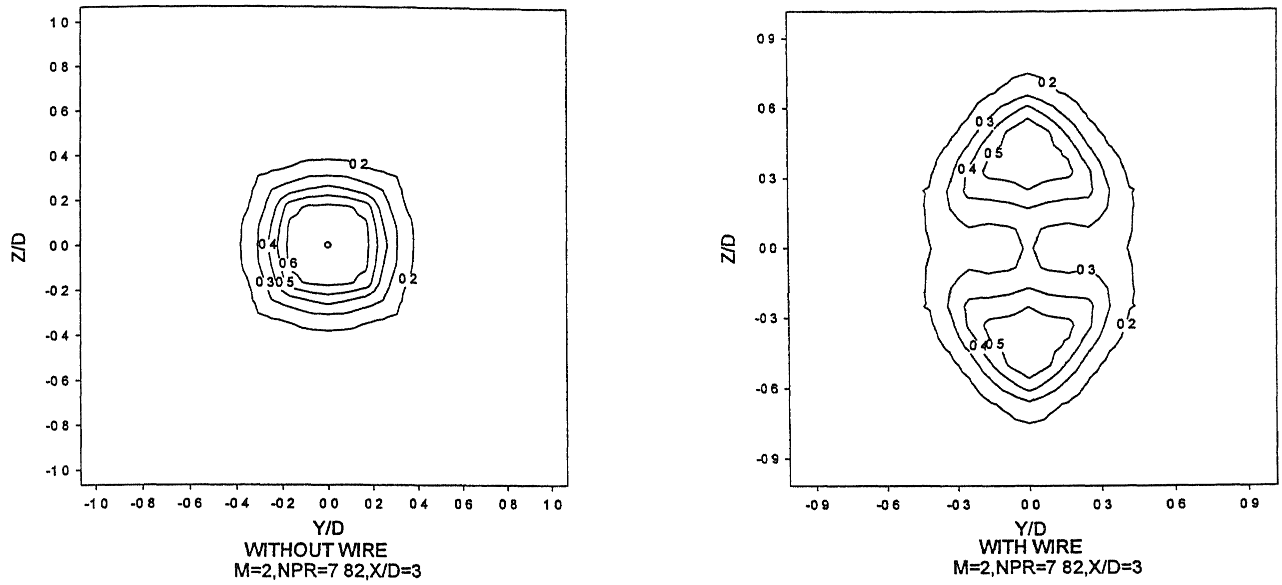


Figure 4.141

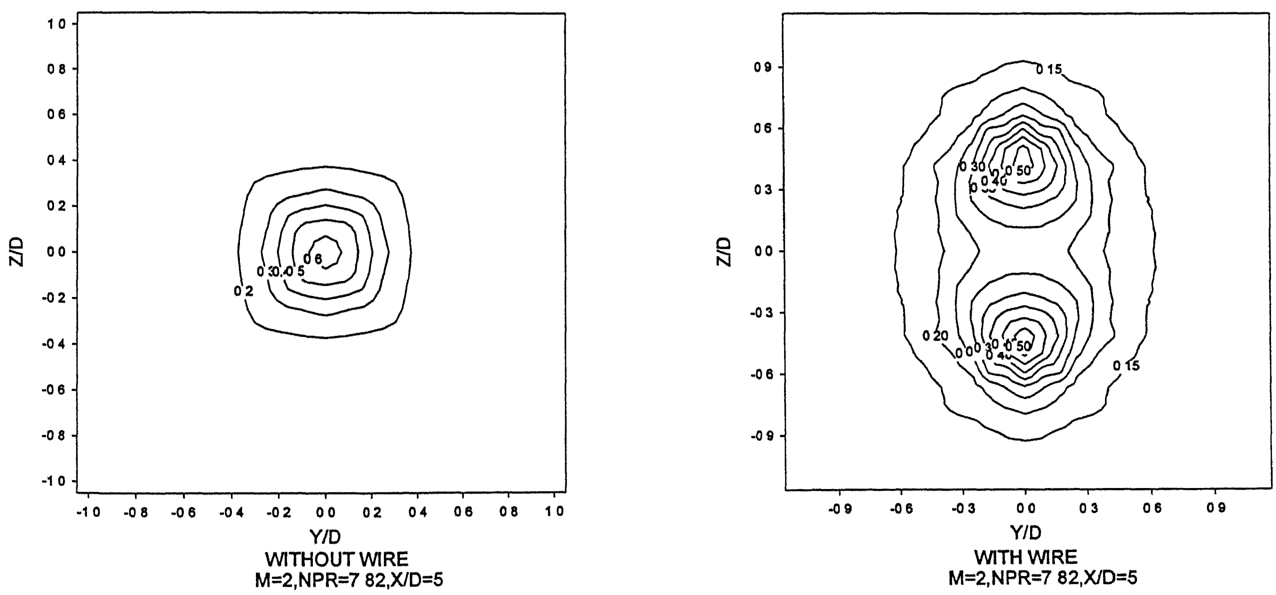


Figure 4.142

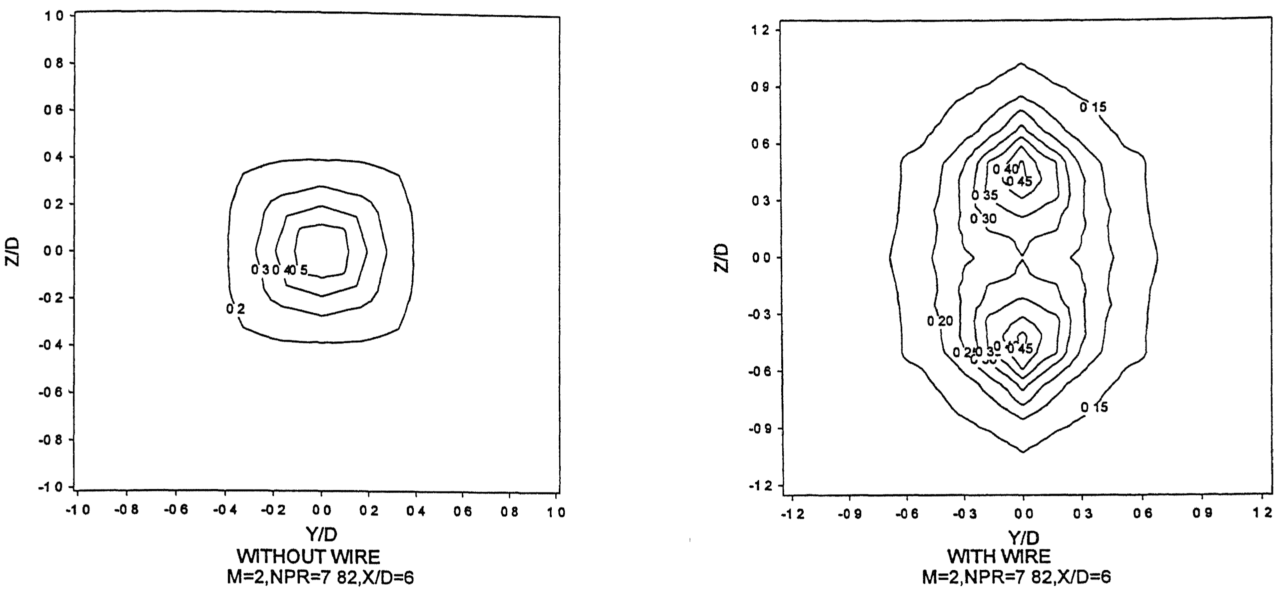


Figure 4.143

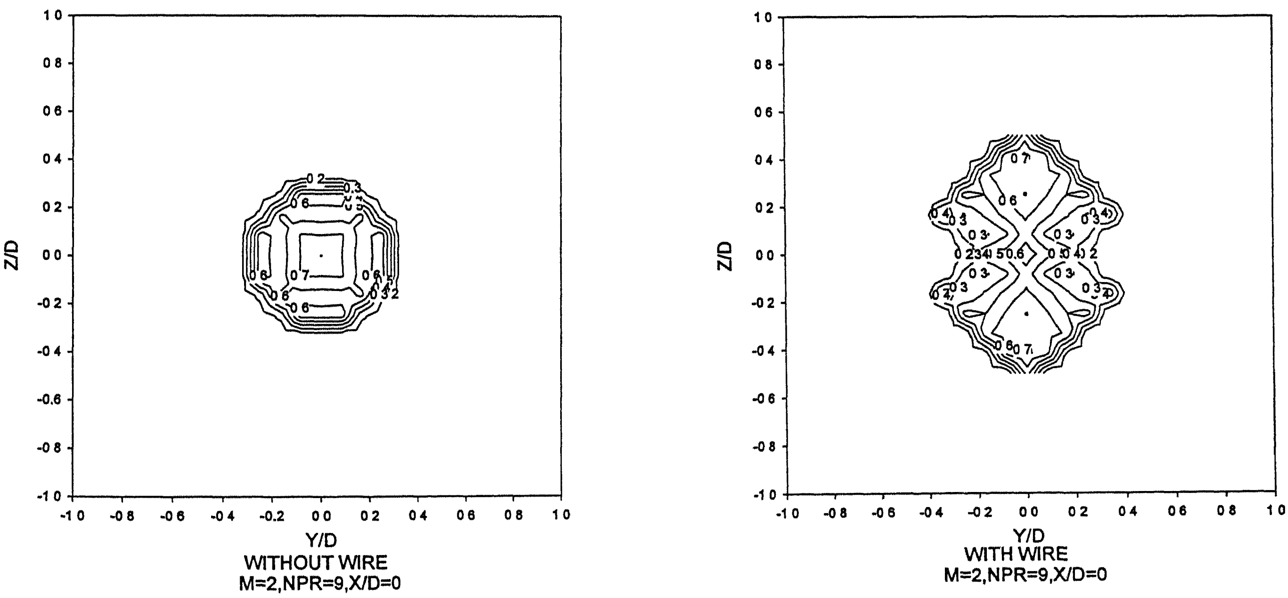


Figure 4.144

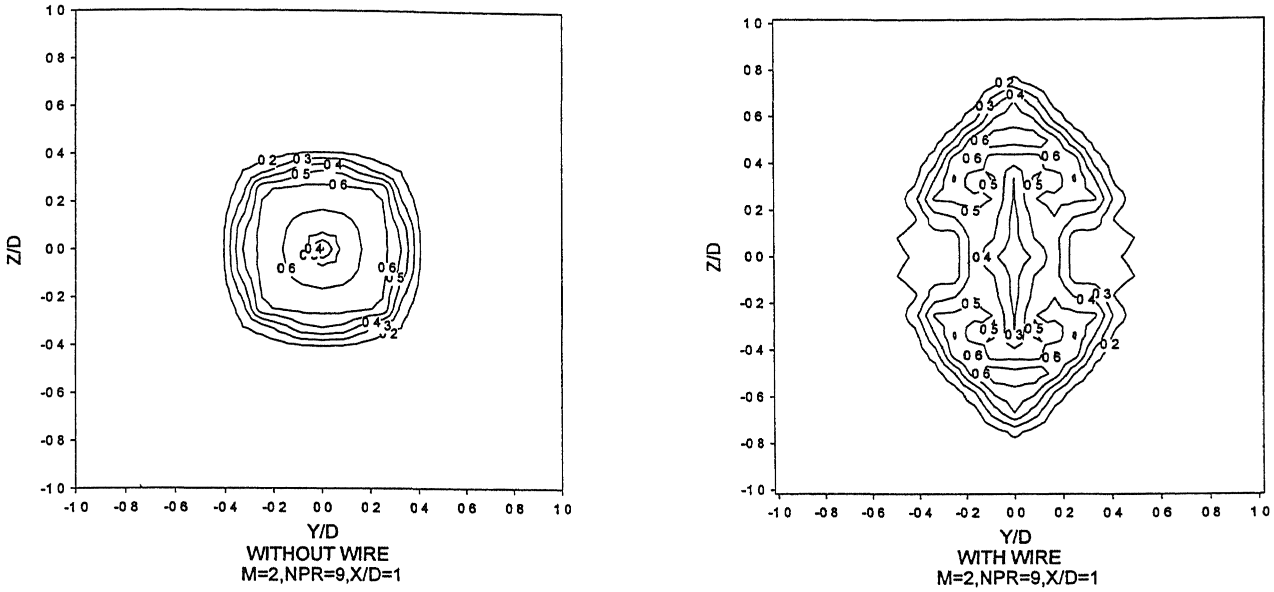


Figure 4.145

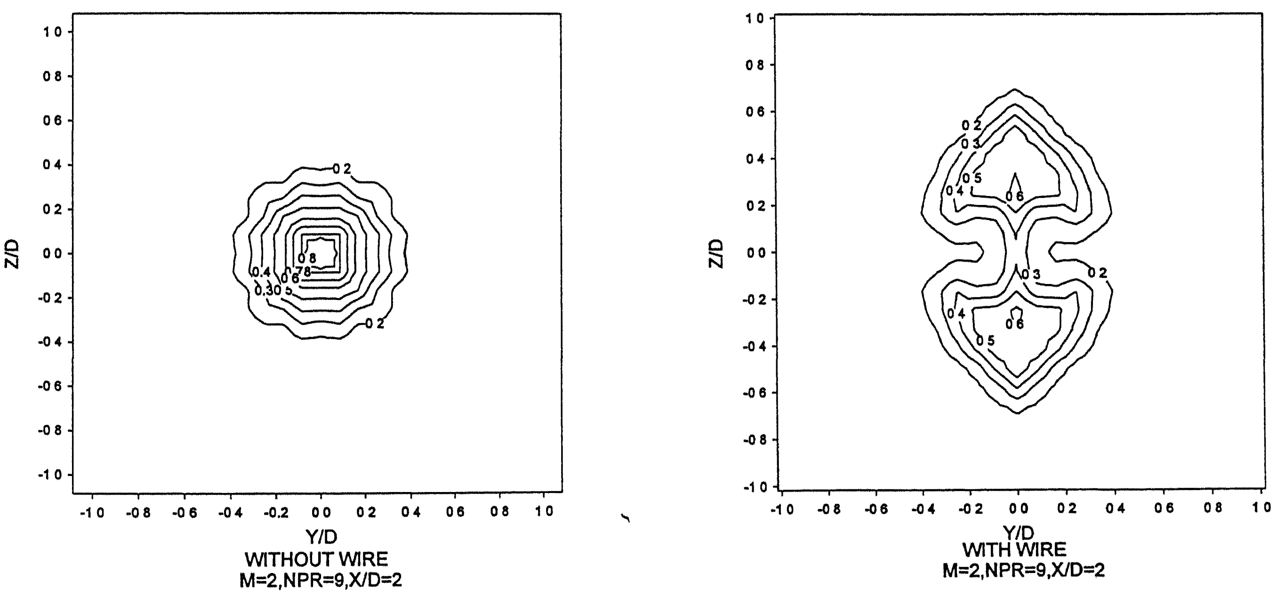


Figure 4.146

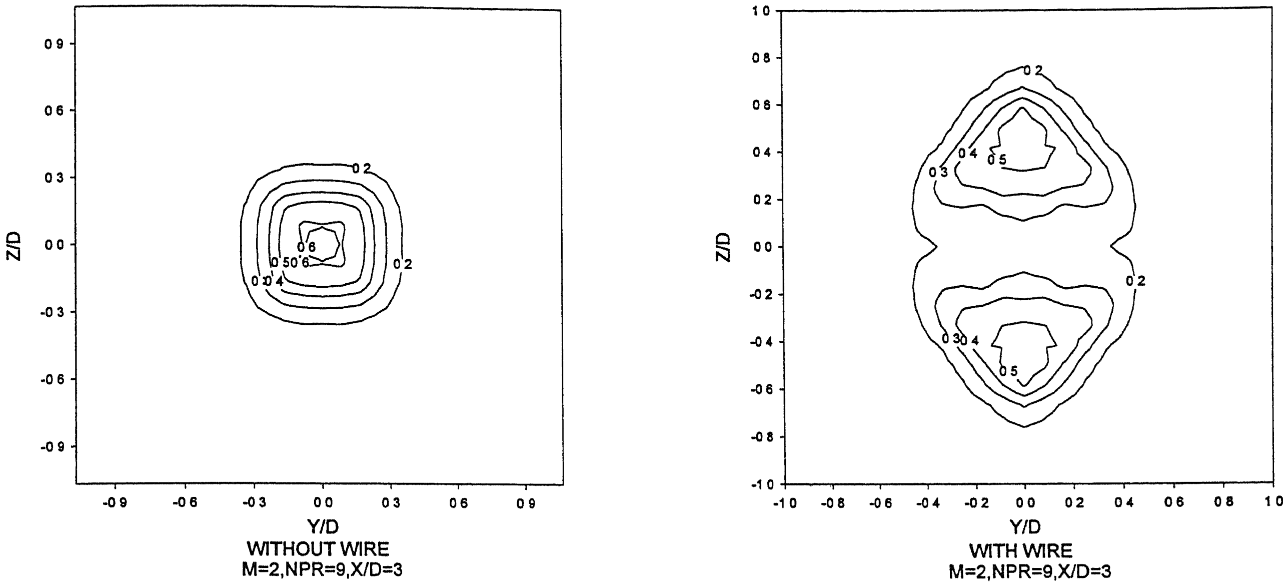


Figure 4.147

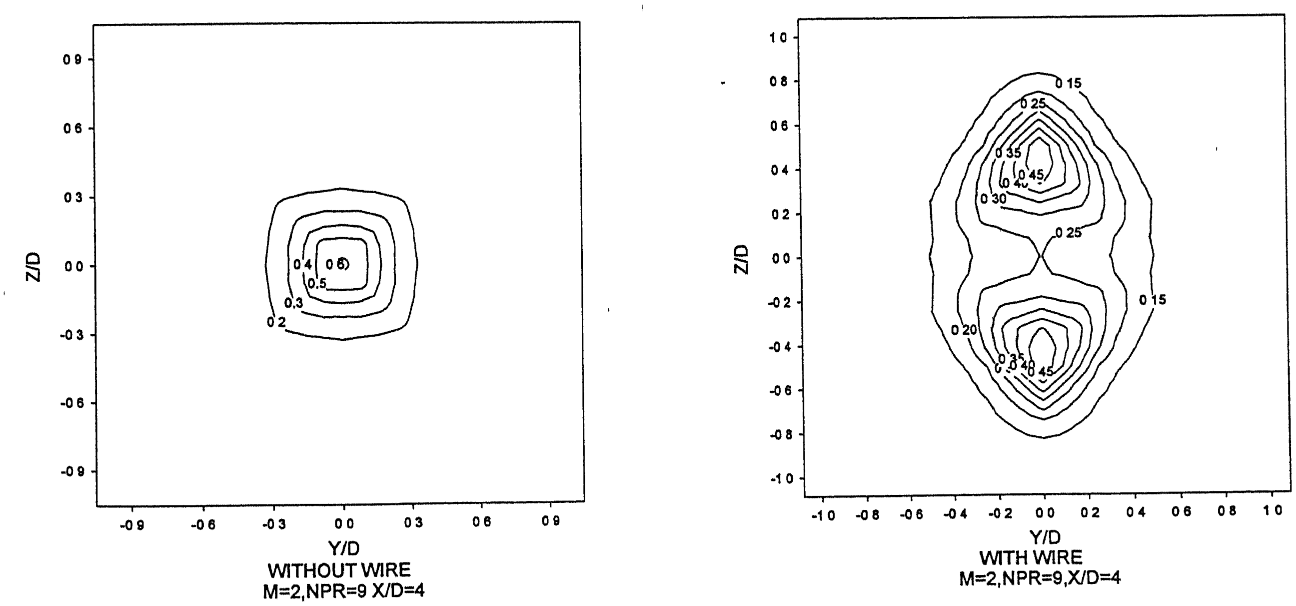


Figure 4.148

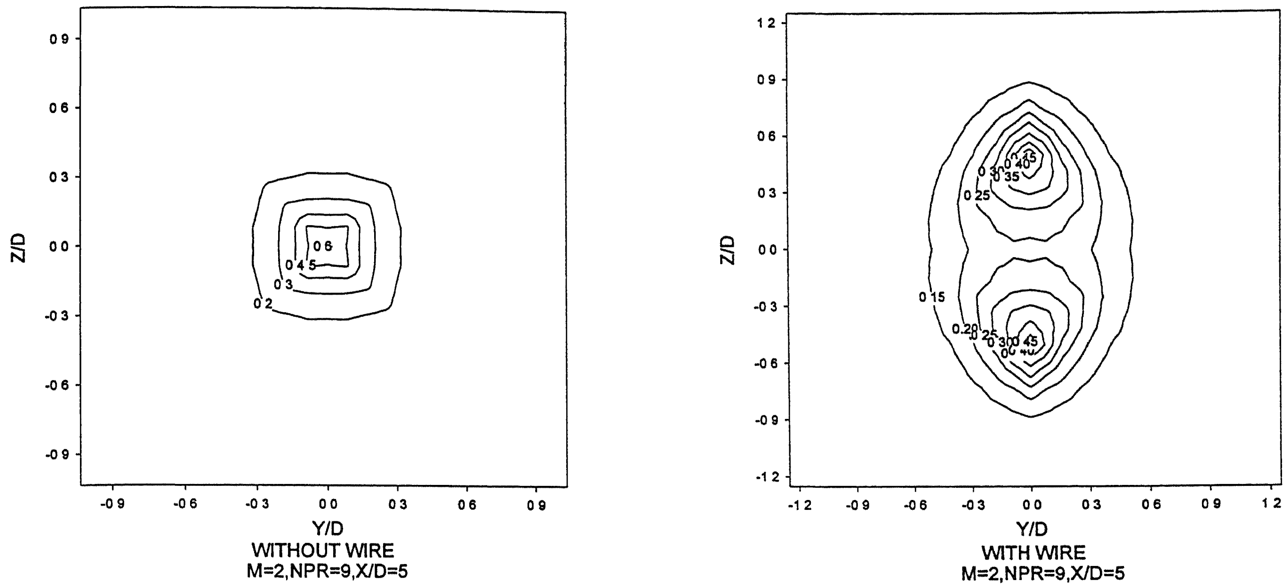


Figure 4.149

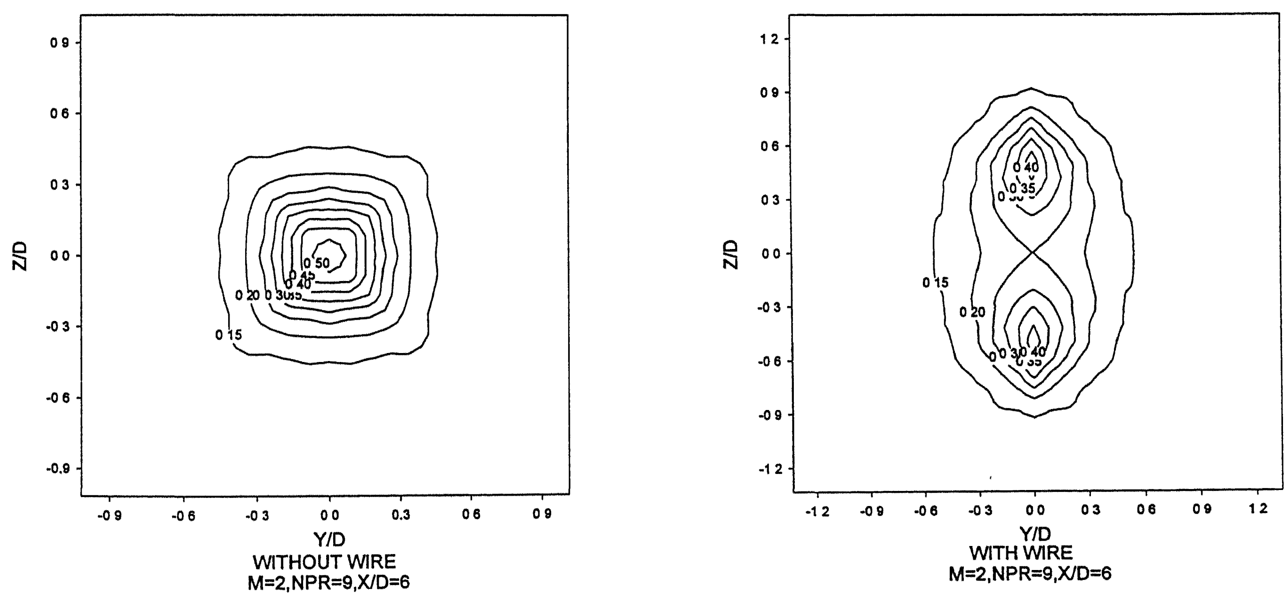


Figure 4.150

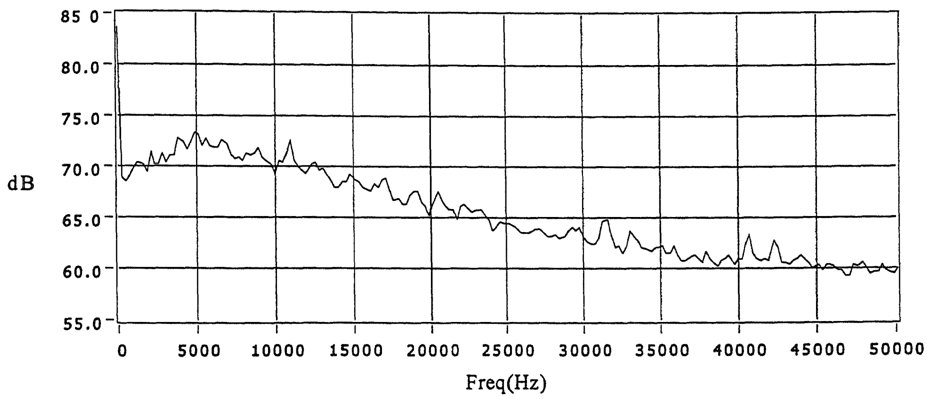


Figure 4.151 Frequency spectrum for M=2, NPR 2, X/D=0, R/D=30
Without wire

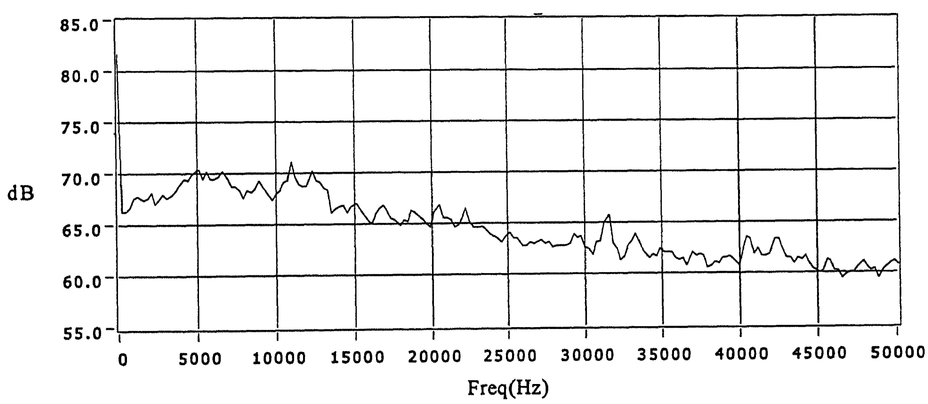


Figure 4.152 Frequency spectrum for M=2, NPR 2, X/D=0, R/D=30
along the wire

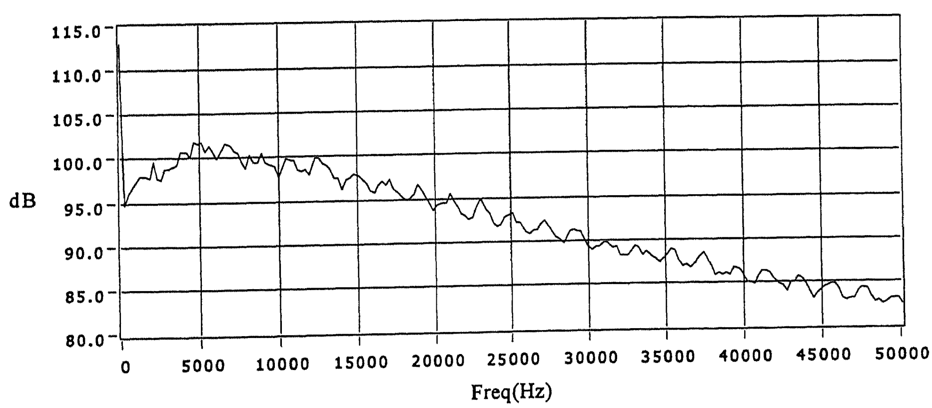


Figure 4.153 Frequency spectrum for M=2, NPR 2, X/D=0, R/D=30
normal to the wire

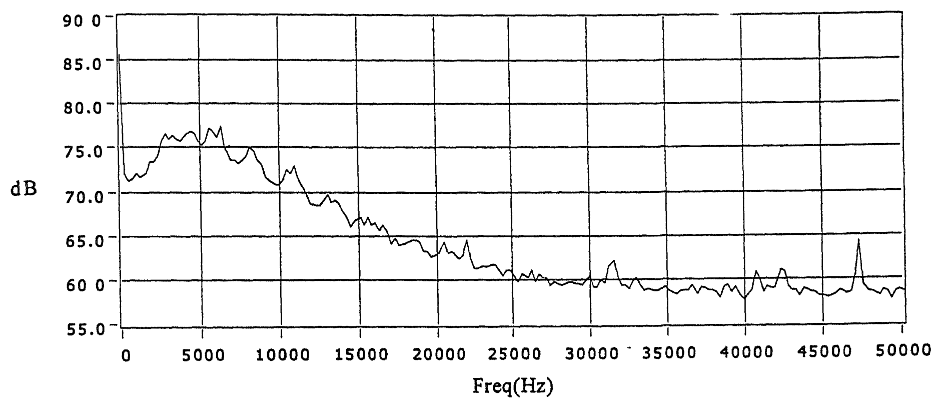


Figure 4.154 Frequency spectrum for M=2, NPR 2, R/D=100, θ =30 deg.
Without wire

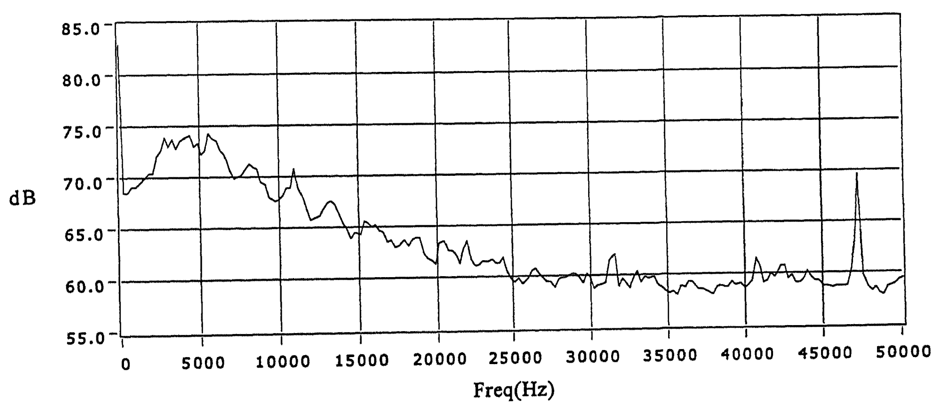


Figure 4.155 Frequency spectrum for M=2, NPR 2, R/D=100, θ =30 deg.
along the wire

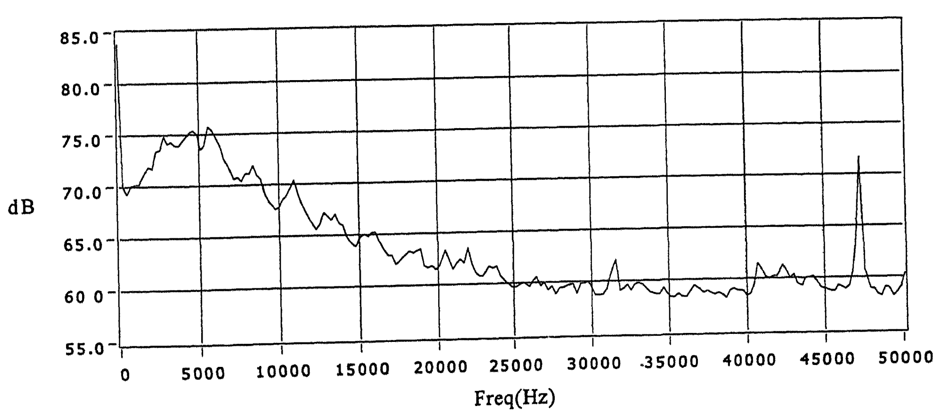


Figure 4.156 Frequency spectrum for M=2, NPR 2, R/D=100, θ =30 deg.
Normal to the wire

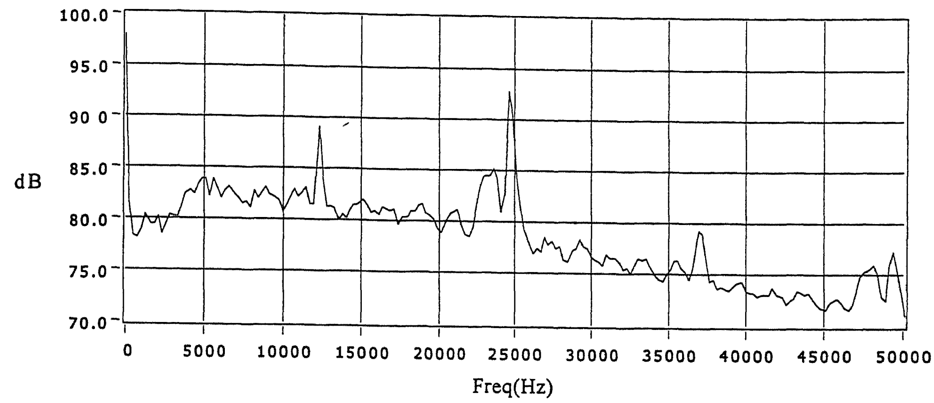


Figure 4.157 Frequency spectrum for M=2, NPR 3, X/D=0, R/D=30
Without wire

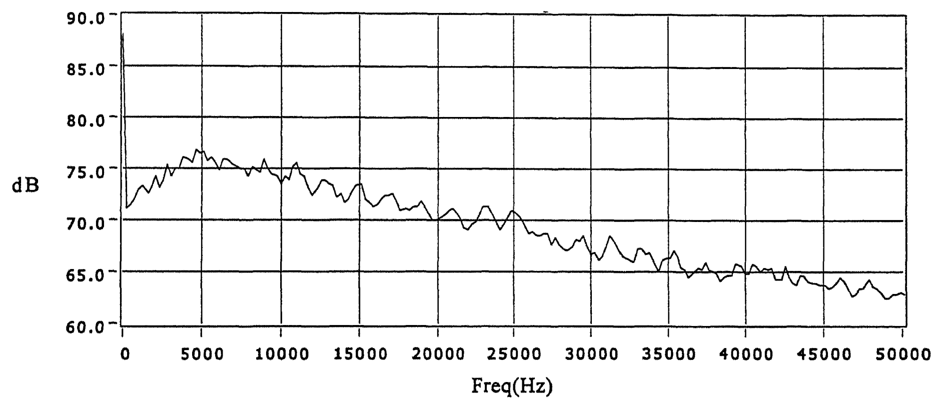


Figure 4.158 Frequency spectrum for M=2, NPR 3, X/D=0, R/D=30
along the wire

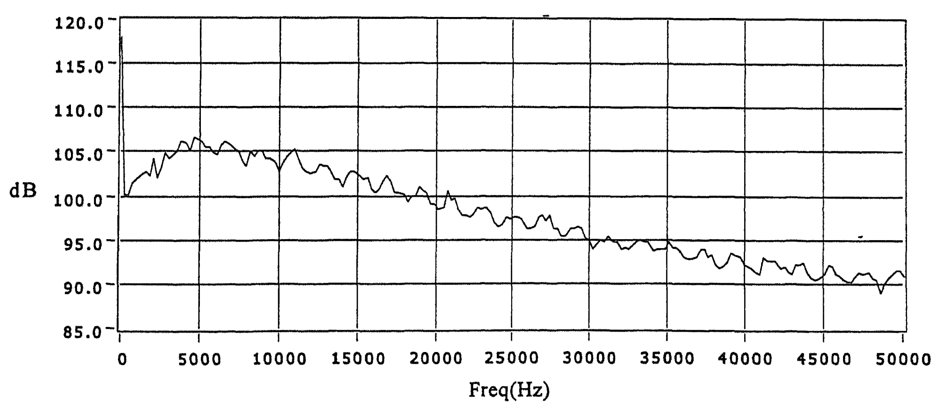


Figure 4.159 Frequency spectrum for M=2, NPR 3, X/D=0, R/D=30
normal to the wire

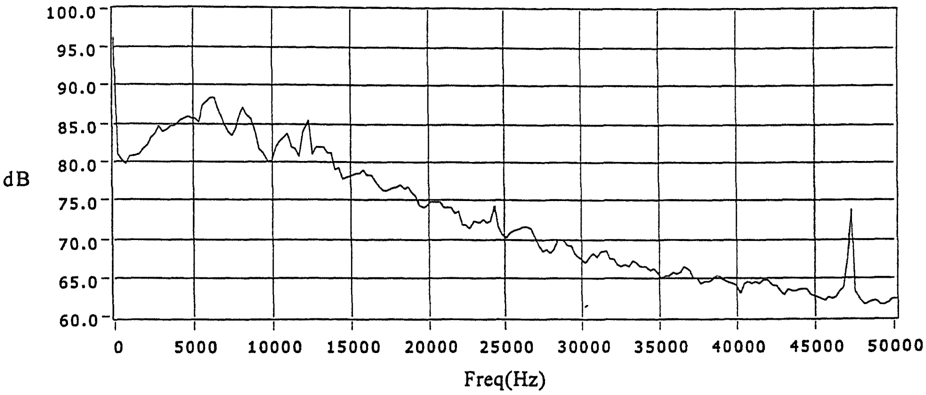


Figure 4.160 Frequency spectrum for M=2, NPR 3, R/D=100, θ =30 deg. Without wire

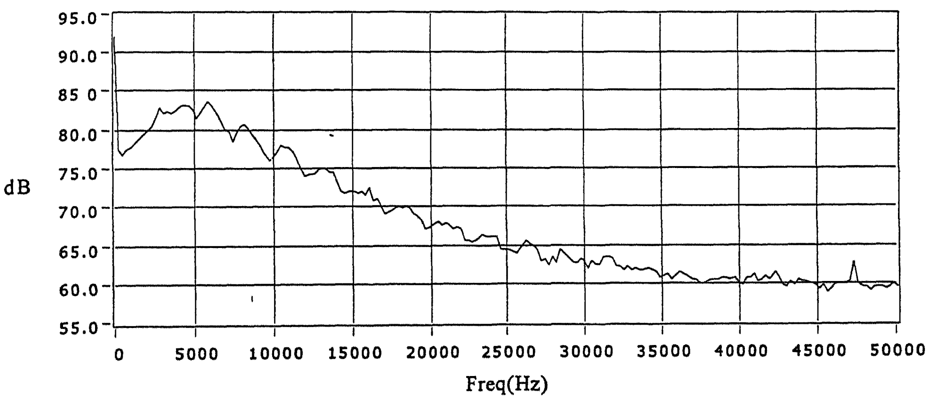


Figure 4.161 Frequency spectrum for M=2, NPR 3, R/D=100, θ =30 deg. along the wire

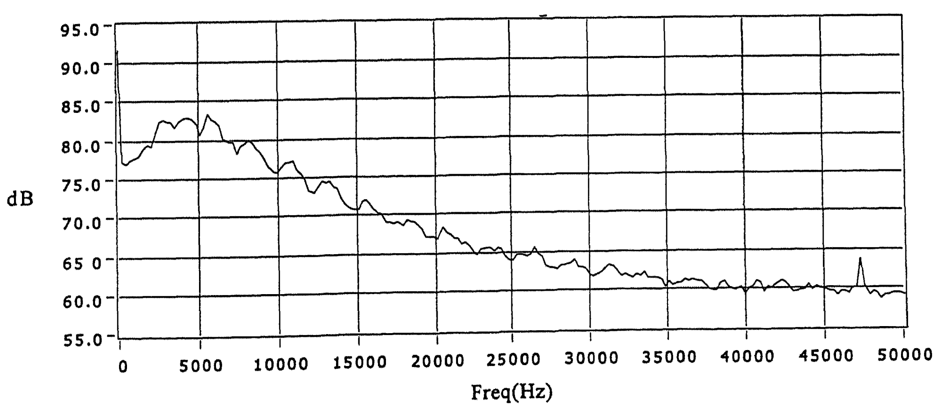


Figure 4.162 Frequency spectrum for M=2, NPR 3, R/D=100, θ =30 deg. Normal to the wire

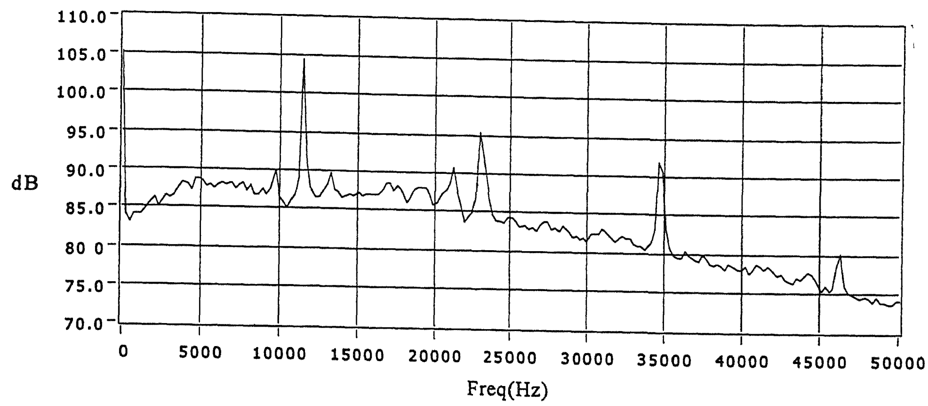


Figure 4.163 Frequency spectrum for M=2, NPR 4, X/D=0, R/D=30
Without wire

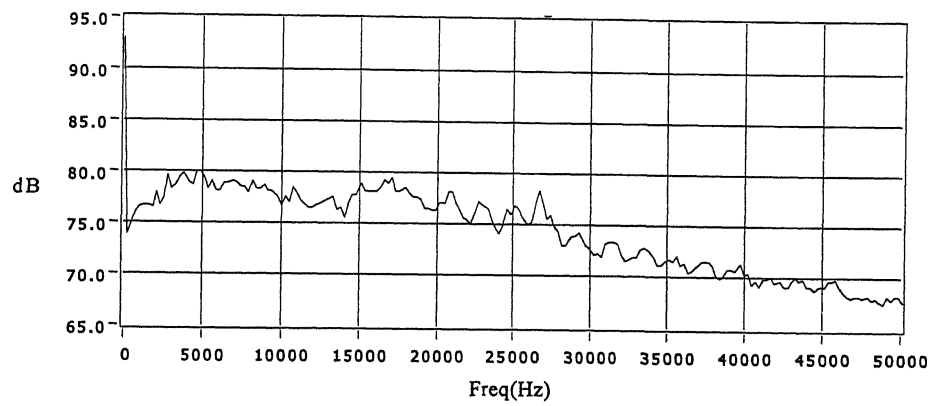


Figure 4.164 Frequency spectrum for M=2, NPR 4, X/D=0, R/D=30
along the wire

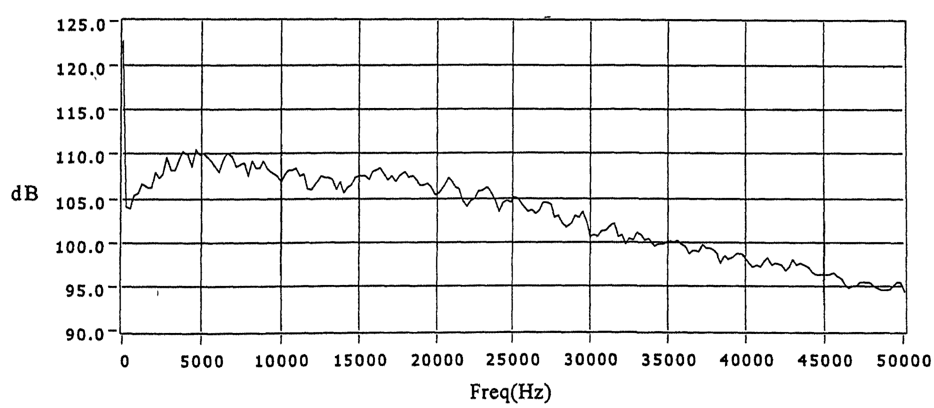


Figure 4.165 Frequency spectrum for M=2, NPR 4, X/D=0, R/D=30
normal to the wire

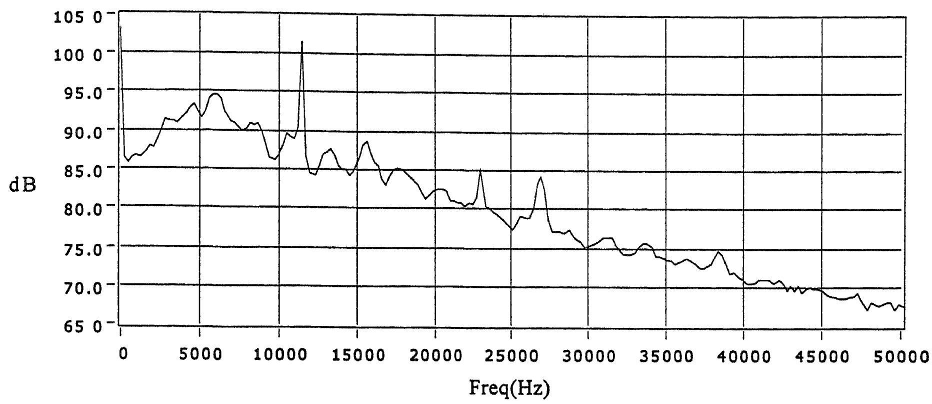


Figure 4.166 Frequency spectrum for M=2, NPR 4, R/D=100, θ =30 deg.
Without wire

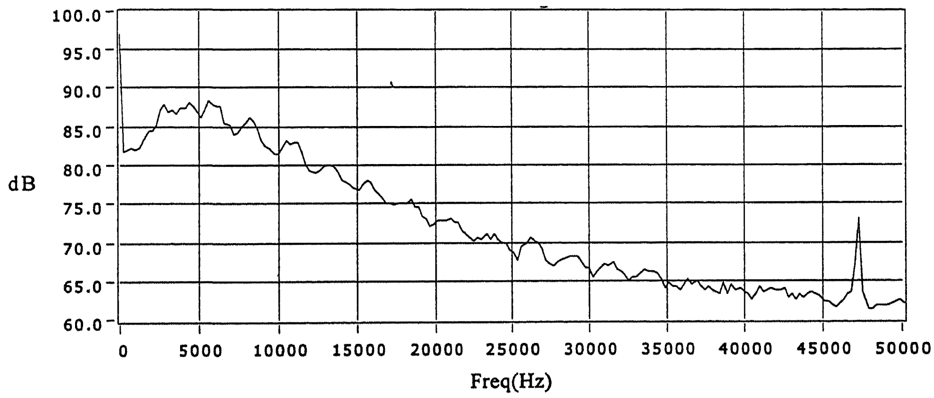


Figure 4.167 Frequency spectrum for M=2, NPR 4, R/D=100, θ =30 deg.
along the wire

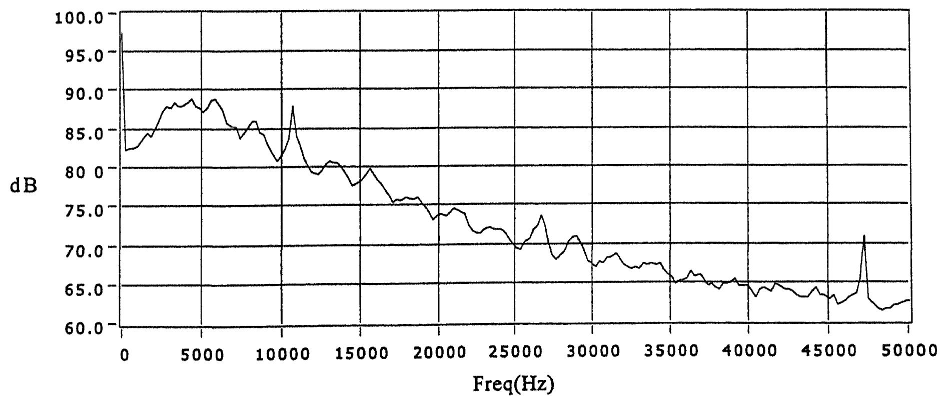


Figure 4.168 Frequency spectrum for M=2, NPR 4, R/D=100, θ =30 deg.
normal to the wire

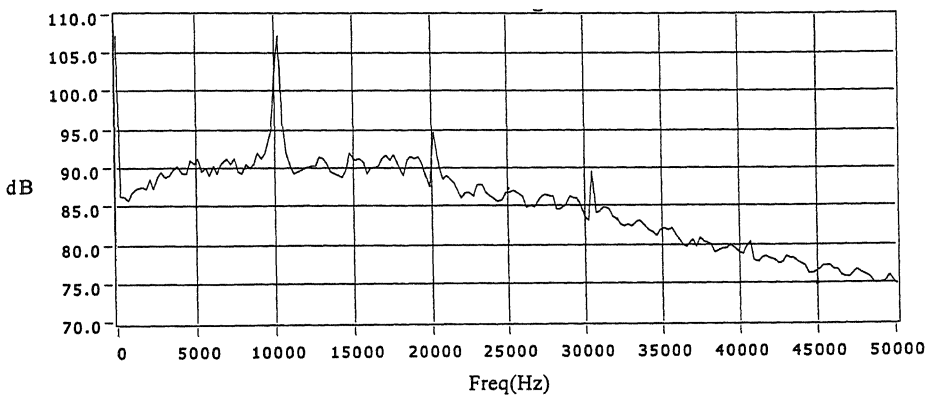


Figure 4.169 Frequency spectrum for M=2, NPR 5, X/D=0, R/D=30
Without wire

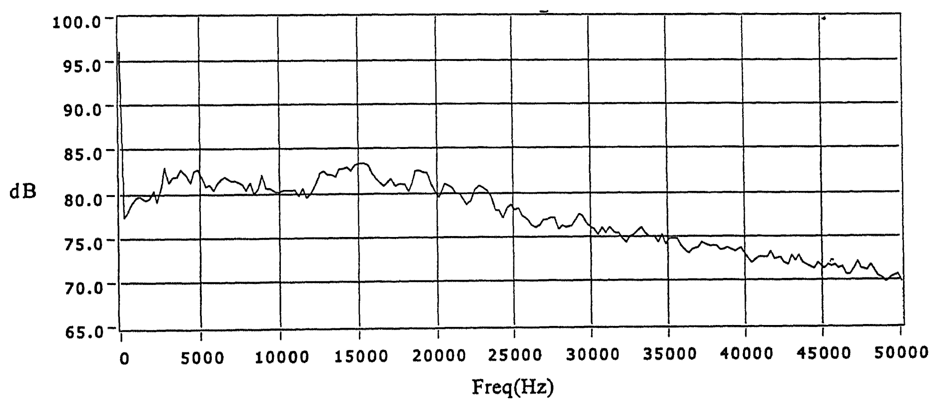


Figure 4.170 Frequency spectrum for M=2, NPR 5, X/D=0, R/D=30
along the wire

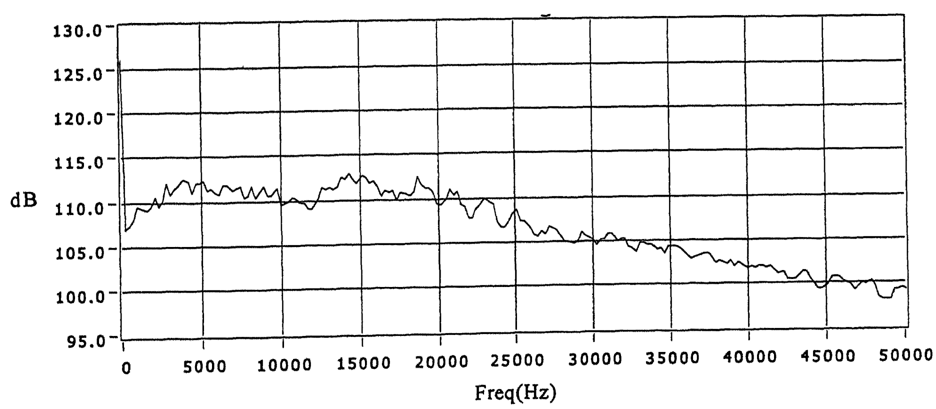


Figure 4.171 Frequency spectrum for M=2, NPR 5, X/D=0, R/D=30
normal to the wire

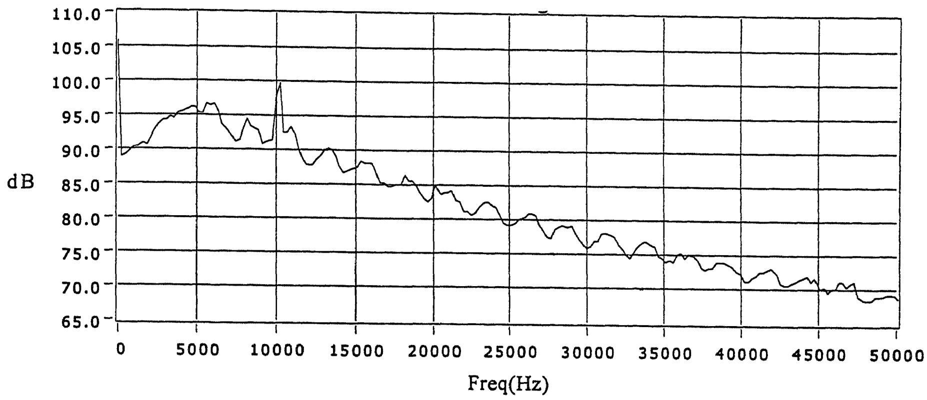


Figure 4.172 Frequency spectrum for M=2, NPR 5, R/D=100, θ =30 deg.
Without wire

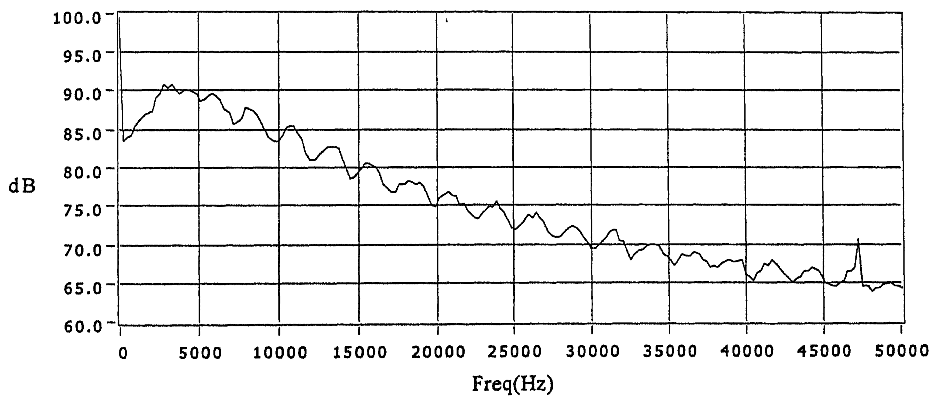


Figure 4.173 Frequency spectrum for M=2, NPR 5, R/D=100, θ =30 deg.
along the wire

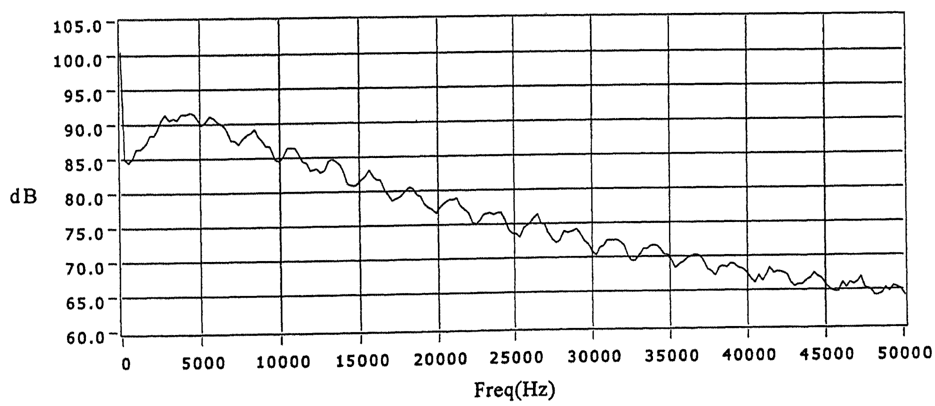


Figure 4.174 Frequency spectrum for M=2, NPR 5, R/D=100, θ =30 deg.
normal to the wire

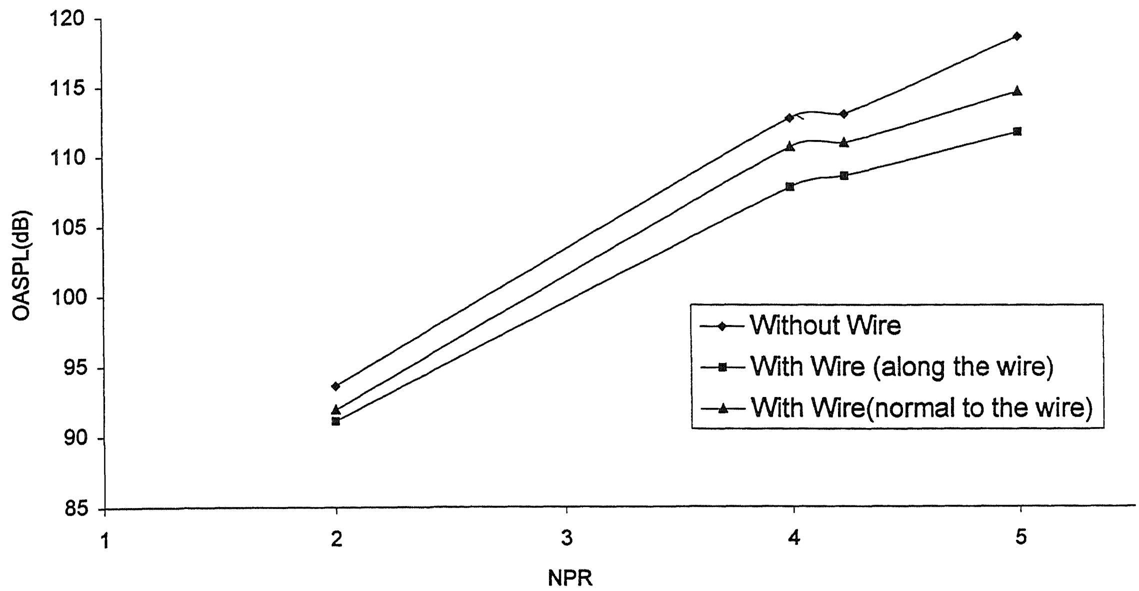


Figure 4.175 Overall Sound Pressure Level (dB) with NPR for M=1.6

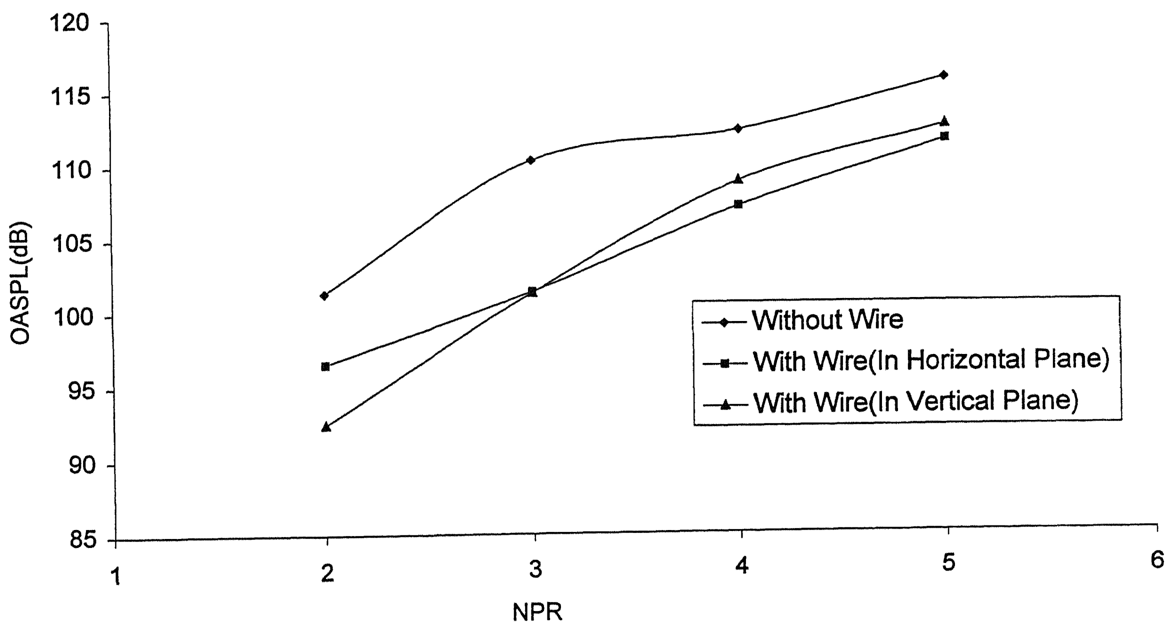


Figure 4.176 Overall Sound Pressure Level (dB) with NPR for M=1.79

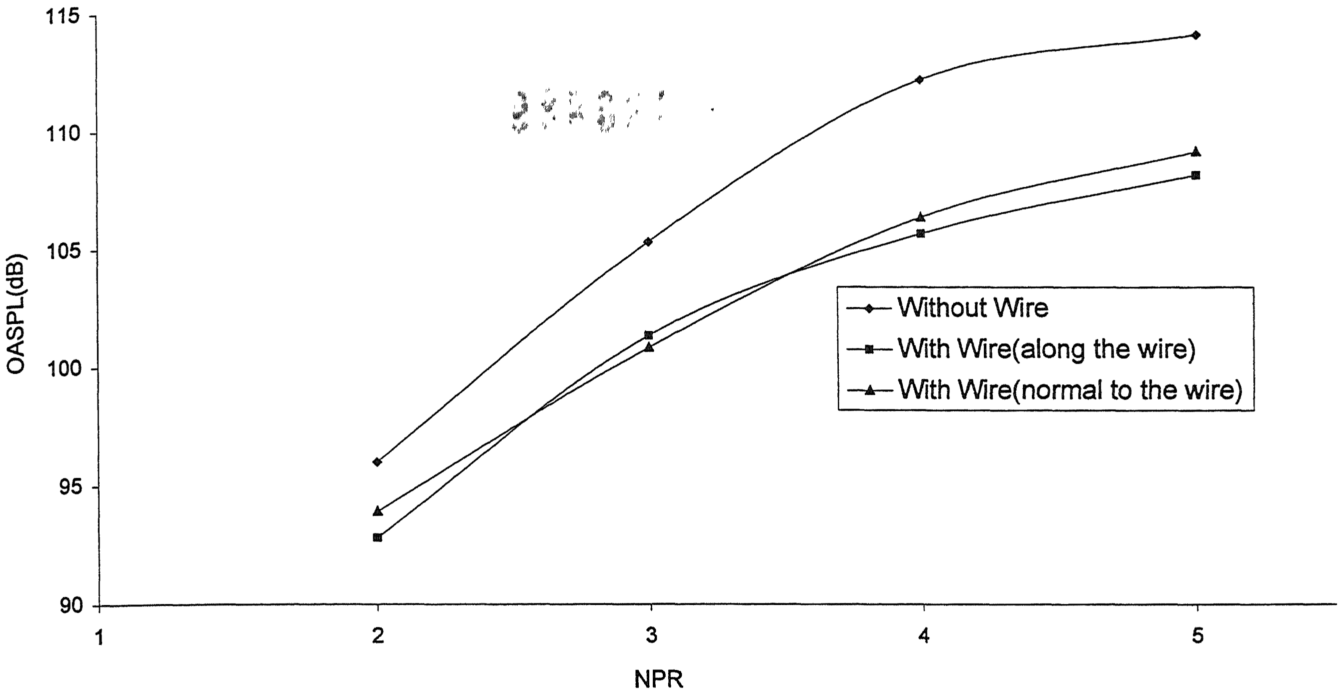


Figure 4.177 Overall Sound Pressure Level (dB) with NPR for M=2